Progress in NMR Spectroscopy, Vol. 24, pp. 159–293, 1992.
Printed in Great Britain.

0079-6565/92 $15.00

STRUCTURAL CHARACTERIZATION OF NONCRYSTALLINE SOLIDS AND GLASSES USING SOLID STATE NMR

HELLMUT ECKERT

Department of Chemistry, University of California, Santa Barbara, CA 93106, U.S.A.

(*Received* 12 *July* 1991)

CONTENTS

1. INTRODUCTION

The glassy state is becoming an increasingly important subject of intellectual fascination, fundamental research, and technology-oriented applications in a wide range of scientific disciplines. Research objectives are quite diverse, including the study of new solid state physics phenomena in the absence of a periodic lattice, the development of new materials for technological applications, and an

understanding of the geological processes occuring in the earth's crust. For the pursuit of any of these objectives, the elucidation of the atomic arrangements that constitute the structure of glasses is often at the very center of the scientific problem studied.

Due to the absence of a periodic lattice, experimental results cannot provide a complete, closed picture of a glass structure. Rather, the depth of information decreases rapidly with distance, and answers to structural questions must be cast in statistical rather than determinate terms. Moreover, these answers are often influenced by the mode of preparation, such as quenching rates, thermal history, and the presence of impurities.

Since the existence of pre-conceived ideas in the area of glass science enhances the danger of biased interpretations of experimental data, measurements of quantities that are directly calculable from first principles are most desirable. The latter objective is rarely achieved, however, without any assumptions. In reality, it is a major advance, if a proposed model proves consistent with results from multi-technique investigations, including structural probes such as X-ray diffraction, neutron diffraction, EXAFS, XPS, infrared and Raman spectroscopy, and solid state NMR. Thus, in the pursuit of glass structure, it is extremely important to use as many techniques as possible. At the same time, it is equally important to exploit each technique to its fullest potential. The present review has been written specifically with the second point in mind. Solid state NMR possesses a number of unique features which, when taken full advantage of, render it an immensely powerful tool for the conceptual description of structural and dynamic disorder in glasses. Since only the local environment of the particular nucleus under study is probed by NMR, this method is especially well-suited for the structural analysis of highly disordered and compositionally very complex systems, where diffraction techniques often fail. The direct proportionality of the signal intensity to the number of contributing nuclei makes NMR the method of choice for stringently quantitative applications, whenever bulk information is required. Compared to several other methods, NMR is element-selective, non-destructive and requires little sample preparation. Most importantly, however, NMR is conspicuous for its interaction-selectivity which is unparalleled by any other technique. By choosing appropriate experimental protocols, we can tailor the internal interaction Hamiltonian such that highly specific information results. Combination of several such experiments can then yield a wealth of complementary information about various aspects of the structural problem under study.

Figure 1 illustrates the dramatic growth in studies of NMR of glasses during the past 10 years. The ever more important role glasses play in materials science and technology has contributed to this growth. Specifically one may think of the new synthesis and processing techniques (splat-cooling, vapor-deposition, and sol–gel technology) that have expanded the range and chemical diversity of glass-forming systems. Virtually in parallel, solid state NMR spectroscopy has evolved as an ever more

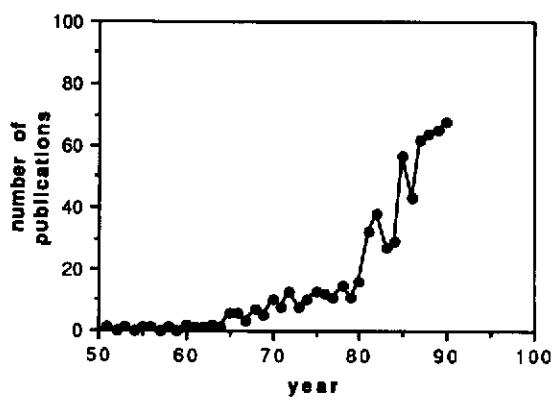

FIG. 1. Number of articles published on the subject of solid state NMR in glasses per year during the period 1950–1990.

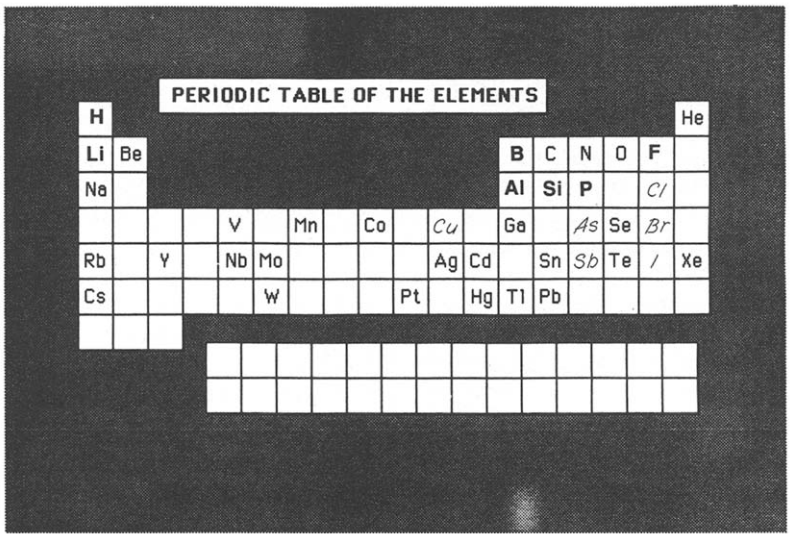

FIG. 2. Elements with suitable nuclear isotopes for solid state NMR studies of glasses. Elements most commonly employed are shown in bold face. Elements not conducive to NMR, but useful for NQR studies of glasses are shown in italics.

exciting research subject in its own right, leading to dramatic advances in resolution, sensitivity, and experimental sophistication. All of these developments have enormously enhanced the analytical and structural significance of solid state NMR during the past 10–20 years, and widened potential ranges of applications, glasses included. As shown in Fig. 2, currently almost half of the nuclei in the Periodic Table lend themselves rather easily to solid state NMR investigation. Virtually all of these nuclei have been studied in the glassy state, and those whose NMR have been especially instrumental for the development of structural concepts, are indicated. The present review attempts to give a broad comprehensive summary of the current state of the field.

1.1. *Historical Background*

Scattered nuclear magnetic resonance measurements on glasses appear in the 1950s literature,[1–4] however, the 1958 study by Silver and Bray, applying ^{11}B NMR to boron–oxide based glasses, was really the first one to provide any insight into glass structure.[5] In the wake of this study, a very detailed and systematic exploration of borate glasses ensued, using ^{11}B (later ^{10}B) NMR in combination with computer-simulation techniques. The experimental arrangement employed in this early work probes the nuclear induction signal in response to a continuously irradiated frequency on resonance. This steady-state technique, usually referred to as "continuous wave (cw)-NMR" requires a linear field (or frequency) sweep for locating the resonance condition. The cw-technique remained the dominant method for lineshape studies well into the 1980s. While it provided detailed information on certain quadrupolar nuclei such as ^{10}B, ^{11}B, and ^{7}Li, cw-NMR studies of other nuclei were generally plagued by low detection sensitivities, saturation effects, and limited chemical shift dispersion due to the use of low field strengths.

A major breakthrough occurred in 1982 with the nearly simultaneous publication of several pulsed, high field Fourier Transform NMR studies,[6–9] using line-narrowing by magic-angle spinning (MAS). The substantial gain in resolution and sensitivity provided by MAS proved critical for the further development of this field. Since then, hundreds of detailed MAS-NMR studies have followed. Today, MAS-NMR and other selective averaging techniques are at the forefront of structural research conducted in the rapidly evolving field of glasses. For reasons detailed below, low-field cw-NMR still

retains decisive advantages for certain ^{11}B NMR investigations. There is, however, little doubt that this niche will eventually vanish due both to the availability of very high field strengths and to the lack of commercially available instrument support for cw spectrometers.

Another important development started in the 1960s, resulting in the characterization of ionic motion in the glassy state by systematic temperature-dependent linewidth studies[10] and temperature- and frequency-dependent relaxation time measurements by pulsed NMR techniques.[11,12] The interpretation of these results and their correlation with temperature and frequency-dependent electrical conductivity measurements has remained an area of active interest and controversy up to the present date.

1.2. *Previous Reviews, and the Focus and Organization of this Review*

Table 1 summarizes the foci of previous reviews that have been written on the topic "NMR studies of glasses". The goal of the present contribution is to give a critical review of the current state of the

TABLE 1. Previous reviews on NMR studies of glasses

Ref.	Year	Authors	Main Topic
23	1960	Bray and Silver	borates
24	1965	Müller-Warmuth	borates
25	1967	Bray	borates
26	1968	Bray	borates
27	1974	Bray	borates
28	1975	Bray	borates
29	1977	Bray	borates
30	1977	Müller-Warmuth	
31	1978	Bray	borates
32	1978	Jellison and Bray	borates
33	1981	Khan and Lüders	metallic glasses
34	1982	Müller-Warmuth and Eckert	NMR and Mössbauer, comprehensive
35	1982	Bray *et al.*	borates
36	1982	Bray *et al.*	borates
37	1982	Bray and Dell	borates
38	1983	Durand and Panissod	metallic glasses
39	1985	Panissod	metallic glasses
40	1985	Bray and Holupka	thermal history
41	1985	Bray	technique-oriented
42	1985	Bray	borates
43	1985	Elliott	silicates
44	1986	Bray and Lui	borates
45	1986	Kirkpatrick *et al.*	silicates
46	1987	Bray	borates, silicates
47	1987	Turner *et al.*	ceramics and glasses, technique-oriented
48	1987	Dubiel	
49	1988	Bray *et al.*	comprehensive
50	1988	Stebbins	motion, dynamics
51	1988	Kirkpatrick	silicates, minerals
52	1988	Marshall *et al.*	
53	1988	Martin	motion, dynamics
54	1988	Dupree	
55	1989	Dupree and Holland	
56	1989	Eckert	chalcogenides
57	1989	Stebbins and Farnan	silicates, liquids
58	1988	Grimmer	comprehensive
59	1990	Elliott	silicates, silicon
60	1990	Stallworth and Bray	comprehensive
61	1991	Bray *et al.*	

literature, with an emphasis on most recent results. This summarizes what has been accomplished, what new kinds of questions have emerged from this knowledge, and which goals have to date proven elusive. To this end, Section 2 of this article will summarize the physicochemical criteria of the glassy state and give a brief introduction into the various structural models developed for the different types of glassy materials. Sections 3 and 4 give a brief review of the necessary theory, in particular in relationship to the study of disordered systems. The treatment will not be mathematically rigorous as excellent monographs on these aspects of solid state NMR are already available.[13-22] Rather, emphasis will be given to the experimental techniques, the manifestations of disorder in the spectroscopic observables, and the corresponding structural interpretations. Then follows a detailed discussion of the results obtained on separate types of glasses. Due to the sheer volume of published work this review is confined to structural inorganic glasses. Other forms of amorphous or glass-like behavior, such as spin-glasses, orientational and quadrupolar glasses are beyond the scope of this review. Likewise, organic glasses, amorphous polymers, fossil fuels, and amorphous surface states will not be covered. Nevertheless, the aim is to give an accurate reflection of the diversity and depth of structural information obtained on glasses, and I apologize in advance for any bias in the selection of the material discussed here in more detail compared to other work.

2. NONCRYSTALLINE SOLIDS AND GLASSES

Materials that lack long-range structural order, and possess a viscosity exceeding 10^{13} Poise are considered noncrystalline (amorphous) solids. The lack of long-range structural order is usually operationally defined by the technique of X-ray diffraction, while the viscosity criterion serves to differentiate between solids and liquids. If the material shows, in addition, the phenomenon of structural relaxation, we speak of a glass.[62-65] Structural relaxation is defined by the existence of a well-defined temperature interval, the "glass-transition region", where, due to the onset of long-range atomic and molecular motion, mechanical and thermodynamic properties become time dependent. The onset of molecular motion manifests itself in a dramatic increase of the heat capacity, which is easily detected by differential scanning calorimetry. Figure 3 shows a typical DSC trace for a glass and

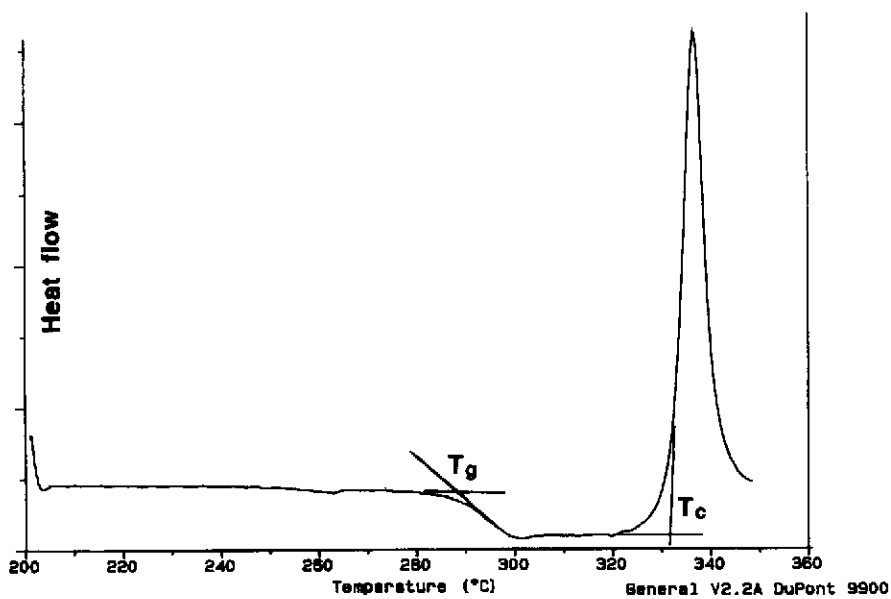

FIG. 3. Typical differential scanning calorimetry (DSC) trace of a glass, revealing glass-transition temperature and recrystallization peak.

illustrates the definition of a glass-transition temperature T_g as the "onset point" associated with the heat capacity change. It is important to realize that, as a result of the structural relaxation phenomenon, T_g depends on the rate with which such thermograms are obtained. For the same reasons, the glass transition temperature can be influenced by the cooling rate with which the glass solidifies, higher cooling rates giving rise to higher T_g values.[62]

The relationship between liquid, supercooled liquid, crystalline solid and glass is illustrated in Fig. 4. Glasses and other noncrystalline solids generally possess excess volume, enthalpy and entropy relative to crystalline compounds with the same composition. Thus, their synthesis necessitates conditions that bypass the establishment of thermodynamic equilibrium, i.e. the nucleation and growth of crystals. Most commonly this is done from the liquid state ("melt-quenching"), which is cooled at a speed such that the temperature interval between T_f, the liquidus temperature, and T_g, the glass transition temperature, is traversed at a rate greater than the nucleation rate. The width of this temperature interval is at a minimum (and hence glass-forming tendency is at a maximum) near the eutectic compositions in the phase diagrams.

Other, less conventional, methods that circumvent nucleation include; (1) evaporation of gaseous materials onto cooled substrates, (2) thermal decomposition of chemical precursors, (3) polymerization of suitable chemical precursors in solution, (4) chemical or electrochemical precipitation from solution, and (5) exposure of crystalline materials to high pressures or neutron irradiation. A review of some newer preparation techniques is given in Ref. 66. Noncrystalline materials not produced from the molten state may or may not meet the more stringent definition of "glass". Thanks to the development of new synthetic methodology and technology, the variety of chemical systems that can be prepared in the noncrystalline or glassy state has expanded considerably during the past two decades. Today it encompasses essentially the entire range of chemical bonding types encountered in solid state chemistry.

As a general rule, the tendency towards minimizing local, rather than global energy is considered the chief driving force for amorphization. On the molecular scale, this goal can be accomplished in a variety of ways. Depending on the particulars of the chemical systems involved, four fundamental models have emerged for a conceptual description of glasses. The *continuous random network model* has been proposed mainly for glasses dominated by heteropolar covalent bonding.[67] It assumes perfect chemical ordering, i.e. the existence of well-defined nearest-neighbor environments, which are comparable to those in analogous crystalline compounds. These local structures are interconnected in

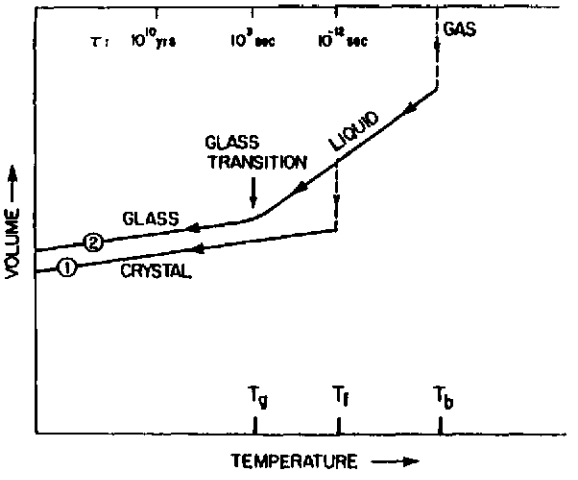

FIG. 4. Volume as a function of temperature, to illustrate the relationship between crystal, glass, and liquid. Reproduced with permission from Ref. 62.

a spatially random fashion via corner-sharing. The lack of periodicity is due to variations in the bond angles and distances to second-nearest neighbors and atoms at even longer distances. Larger structural entities, such as molecular clusters, which would constitute intermediate-range order, are not considered beyond their statistical probability of occurrence. The *random close-packing model* has been proposed for amorphous metals.[68,69] The glass is described as a statistical distribution of atoms, with no regard to establishing any fixed coordination number or local and chemical ordering. In such structures, the important considerations are the packing efficiency (maximally ca. 63.7% compared to 74.05% in a cubic fcc lattice), and, in packings consisting of more than one type of atom, radius ratio and hole filling. A variation of this model, applicable to ionic systems, in particular halide glasses, is the *locally ordered random packing model*. This model follows all the principles of random packing with the important constraint that (energetically unfavorable) homopolar bonds do not form.[70] Amorphous linear organic polymers are described by the *random coil model*, which is not of concern for this review. A fifth model, viewing glasses as a collection of crystals with particle sizes so small that no coherent diffraction occurs ("crystallite model")[71–73] has been ruled out for many glasses based on experimental evidence from radial distribution functions; neverthcless this description may well be applicable to some of the noncrystalline solids not prepared from the molten state.

In approaching a better understanding of the glassy state, the following central structural questions are posed: (1) Does short-range order exist, i.e. can the glass structure be described in terms of reproducible coordination polyhedra? (2) Which atoms are bonded to each other and what are the coordination numbers, bond lengths, and angles in such local environments? (3) How does the short range order compare to that found in crystals? (4) How do the short range environments change as a function of glass composition? (5) Are the coordination polyhedra interlinked in a random fashion, or is there evidence for larger structural groupings ("intermediate-range order") on the 10 -20 Å scale? (6) Is there evidence for either macroscopic phase separation or compositional fluctuations on smaller length scales?

Radial distribution functions (rdf-s) derived from X-ray and neutron diffraction data have played an important role in probing glass structure and in testing the various glass structure hypotheses in specific chemical systems.[70,74] Since, however, the information depends on inter-atomic pair correlations, the situation becomes increasingly complex in multicomponent glasses. For instance, in glasses containing four different atoms, ten different pair correlations contribute to the rdf. In these cases, an element-selective technique such as NMR can provide much deeper insights.

Oxides form by far the most extensively studied group of glasses. The structural description of these systems is heavily influenced by the continuous random network model. In its adaptation to oxide glasses, it distinguishes between network formers (mostly SiO_2, P_2O_5, and B_2O_3), which establish a chemically ordered network of well defined local environments, network modifiers (typically Li_2O, Na_2O, CaO), which are viewed to depolymerize the network by creating non-bridging oxygen atoms, and intermediate oxides (such as Al_2O_3, V_2O_5, TeO_2, MgO), which do not form glasses themselves or in combination with modifiers, but can be incorporated into the network established by a network former. NMR spectroscopy has been used widely to verify these concepts in a quantitative manner and has proven particularly effective in addressing the coordination state of intermediate oxides and in characterizing competitive network modification processes in systems with more than one network former.

As an ever more important aspect in the description of the glassy state, the dynamic aspects of glass structure have moved into the focus of attention. Motional processes of interest in the area of glass science include: low-frequency modes either activated or possibly tunnelling at very low temperatures, atomic diffusion of Li^+, Na^+ or F^-, restricted molecular reorientations around certain symmetry axes, cooperative motion of the extended network above the glass-transition temperature, and chemical exchange processes due to bond-breaking and bond-making in the molten state. NMR spectroscopy provides powerful experimental probes for the characterization of such dynamic phenomena by virtue of variable temperature and multiple-frequency lineshape analysis and by transient pulsed techniques. Such studies have addressed questions regarding the mechanism of ionic conduction in glasses and (in some systems) helped to clarify the structural and dynamical nature of the glass transition.

3. FUNDAMENTALS OF SOLID STATE NMR

3.1. *The NMR Hamiltonian*

All nuclei containing an odd number of either protons or neutrons or both possess angular momentum ("spin" I) and consequently a magnetic moment $\boldsymbol{\mu}$:

$$\boldsymbol{\mu} = \gamma \mathbf{I}. \tag{1}$$

Here γ is a nuclear constant on the order of $10^7\ \mathrm{T}^{-1}\,\mathrm{s}^{-1}$, called the "gyromagnetic ratio". The quantization laws for angular momentum predict the presence of $2I+1$ states, where I is the nuclear spin quantum number. Application of an external magnetic field of magnitude B_0 removes the degeneracy of these states, due to the Zeeman interaction,

$$\mathscr{H}_z = \boldsymbol{\mu} \cdot \mathbf{B}_0 \tag{2}$$

and results in discrete energy levels

$$E_m = -m\gamma\hbar B_{\mathrm{loc}}. \tag{3}$$

B_{loc} is the magnetic field experienced by the nuclei, it comprises the external field B_0 and internal components B_{int} ($\ll B_0$), which arise from internal interactions of the nuclei with their surrounding environments:

$$B_{\mathrm{loc}} = B_0 + B_{\mathrm{int}}. \tag{4}$$

Since these internal fields are intimately related to the structure of the material, their evaluation is of central interest in NMR spectroscopy. To measure the precise energy differences between the magnetic spin states (and hence B_{int}), electromagnetic waves in the radio frequency region (1–600 MHz) are applied, and the frequency at which transitions between the states occur, is measured. At resonance the condition

$$\omega = \gamma B_{\mathrm{loc}} = \gamma(B_0 + B_{\mathrm{int}}) \tag{5}$$

holds. Here $\omega = 2\pi\nu$, and ν (in Hertz) is the frequency of the electromagnetic radiation at which absorption occurs. Table 2 lists, among other pertinent information, the NMR resonance frequencies at a field strength of 7.05 T for most of the nuclei of interest in this review.

In general B_{int} arises from the composite effect of three physically distinct internal interaction mechanisms: (1) magnetic dipole–dipole coupling, (2) magnetic shielding, and (3) for nuclei with spin quantum numbers $>\frac{1}{2}$, nuclear electric quadrupole coupling. Table 3 lists the corresponding interaction Hamiltonians Accordingly, the complete NMR Hamiltonian must be written as:

$$\mathscr{H} = \mathscr{H}_z + \mathscr{H}_{\mathrm{rf}} + \mathscr{H}_{\mathrm{D}} + \mathscr{H}_{\mathrm{CS}} + (\mathscr{H}_{\mathrm{Q}}) \tag{6}$$

($\mathscr{H}_{\mathrm{Q}} = 0$ for spin-1/2 nuclei).

$\mathscr{H}_{\mathrm{rf}}$ describes the interaction of the spins with the periodically fluctuating magnetic component of the radiofrequency field. For a discussion of lineshapes at equilibrium conditions, $\mathscr{H}_{\mathrm{rf}}$ is actually not needed. However, this term is of pivotal importance for understanding pulsed and selective averaging experiments.

The above Hamiltonian is the starting point for discussing the two crucial observables in NMR spectroscopy: (1) energy eigenvalues as measured by resonance frequencies and lineshapes, and (2) relaxation times, reflecting the rates of transitions between different spin states.

3.2. *NMR Lineshape in Solids*

The influence of $\mathscr{H}_{\mathrm{D}}, \mathscr{H}_{\mathrm{CS}}$, (and sometimes $\mathscr{H}_{\mathrm{Q}}$) upon the Zeeman energy levels is minor compared to that of $\mathscr{H}_z$ and hence can be readily calculated by first-order perturbation theory. All of the above interactions are anisotropic. Consequently the energy correction terms arising from the perturbation

TABLE 2. Nuclear magnetic properties, applications and problems encountered in NMR studies of certain isotopes

Nucleus	Spin	Natural abundance (%)	Resonance frequency (MHz)*	Most commonly measured parameter (and experiment)	Typical problems
^{1}H	1/2	100	300.1	δ_{iso} (CRAMPS)	strong dipole-coupling limits resolution
^{2}H	1	0.016	46.07	e^2qQ/h, η (Quad. Echo)	isotopic labelling required, 90° pulses $<2\,\mu$s needed
^{6}Li	1	7.42	44.15	δ_{iso} (MAS)	long T_1, small range of δ_{iso}
^{7}Li	3/2	92.58	116.59	T_1	small range of δ_{iso}, e^2qQ/h
^{9}Be	3/2	100	42.18	δ_{iso} (MAS)	small range of δ_{iso}, e^2qQ/h
^{10}B	3	19.85	32.25	e^2qQ/h, η (cw)	low sensitivity, broad lines
^{11}B	3/2	80.42	96.25	e^2qQ/h, η, N_4 (cw), δ_{iso} (MAS)	small range of δ_{iso}, overlap
^{13}C	1/2	1.11	75.47	δ_{iso} (CPMAS or MAS)	long T_1 in H-free samples quantitation difficult
^{14}N	1	99.63	(21.68)	e^2qQ/h, η (NQR)	low field, broad lines
^{15}N	1/2	0.37	30.41	δ_{iso} (CPMAS or MAS)	isotopic labelling required
^{17}O	5/2	0.037	40.68	e^2qQ/h, η, δ_{iso} (MAS, cw, DOR)	isotopic labelling required
^{19}F	1/2	100	282.32	δ_{iso} (CRAMPS)	strong dipole coupling limits resolution
^{23}Na	3/2	100	79.38	δ_{iso} (MAS, nutation)	lineshape deconvolution; difficult quantitation
^{27}Al	5/2	100	78.20	δ_{iso} (MAS, nutation)	lineshape deconvolution; difficult quantitation
^{29}Si	1/2	4.70	59.70	δ_{iso} (MAS, COSY)	long T_1, labelling often required
^{31}P	1/2	100	121.65	δ_{iso}, M_{2d} (MAS, echo)	interpretation of δ_{iso} unclear
^{45}Sc	9/2	100	72.90	e^2qQ/h, η (NQR)	strong quadrupole coupling
^{51}V	7/2	99.76	78.87	δ_{iso}, δ_{ii}, e^2qQ/h, η, (wideline, MAS, nutation)	lineshape deconvolution
^{63}Cu	3/2	69.09	(79.54)	e^2qQ/h, η (NQR)	strong quadrupole coupling
^{69}Ga	3/2	60.40	72.03	e^2qQ/h, η, δ_{iso} (MAS)	strong quadrupole coupling
^{75}As	3/2	100	(51.38)	e^2qQ/h, η, (NQR)	strong quadrupole coupling
^{77}Se	1/2	7.58	57.20	δ_{iso} (MAS)	long T_1, large csa
^{113}Cd	1/2	12.20	66.71	δ_{iso} (MAS)	long T_1 large csa
^{119}Sn	1/2	8.58	111.85	δ_{iso} (MAS)	long T_1, large csa, wide δ-range
^{125}Te	1/2	7.00	94.79	δ_{iso} (MAS)	long T_1, large csa, wide δ-range
^{133}Cs	9/2	100	39.36	δ_{iso}, e^2qQ/h, η (MAS)	lineshape deconvolution
^{199}Hg	1/2	16.84	53.50	δ_{iso}, δ_{ii} (MAS)	long T_1, large csa, wide δ-range
^{205}Tl	1/2	70.50	173.12	δ_{iso}, δ_{ii} (cw, spin echo)	strong exchange couplings, wide δ-range
^{207}Pb	1/2	22.60	62.79	δ_{iso} (cw, MAS)	long T_1. wide δ-range

* At a field strength of 7.05 T. Parentheses indicate irrelevance for NQR nuclei.

TABLE 3. Interactions in solid state NMR, spectroscopic parameters, and their selective measurement

Interaction	Hamiltonian	Parameters	Selective measurement	Ref.
Dipole–Dipole,		M_{2d} or r_{ij}	90°-t-180° (spin echo decay)	91–93
homonuclear:	$\mathcal{H}=\gamma^2\hbar^2 r_{ij}^{-3}(1-3\cos^2\theta)(3I_z^2-I^2)/2$	Δm_{max} (no. of spins)	multiple quantum NMR	655–657
	(two-spin Hamiltonian)			
	r_{ij} = internuclear distance	r_{ij}	nutation NMR	
	θ = angle (r_{ij}, B_0)	r_{ij}	zero-field NMR	
Dipole–Dipole,		M_{2d} or r_{ij}	90°-t-180° (180°S); SEDOR	94–96
heteronuclear	$\mathcal{H}=\gamma_I\gamma_S\hbar^2 r_{IS}^{-3}(1-3\cos^2\theta)I_zS_z$	r_{IS}	rotary resonance recoupling	98, 99
	(two spin Hamiltonian)	r_{IS}	Rotational Echo Double Resonance (REDOR)	97
	r_{IS} = internuclear distance, θ = angle (r_{IS}, B_0)	T_{CR}	cross-polarization	100
Chemical Shift:	$\mathcal{H}=\gamma\mathbf{I}_z\,\sigma\,B_0$	δ_{11}, δ_{22}, δ_{33}	MAS sideband analysis	86, 87
		δ_{11}, δ_{22}, δ_{33}	2D MAS-NMR	
		δ_{iso}	MAS centerband position	84, 85
Quadrupole:	$\mathcal{H}=(e^2qQ)(3\cos^2\theta-1)(3I_z^2-I^2)/8I(2I-1)$	e^2qQ/h, η	MAS lineshape analysis	88
	(for axial symmetry, $\eta=0$)	(no easy separation)	2-D nutation NMR	103, 104
	θ = angle (eq, B_0)		sideband analysis relating to first-order satellites	

calculation contain an angular dependence, specifying the orientation of a molecular axis system relative to the applied magnetic field direction. (For quadrupolar nuclei, the quantum mechanical treatment depends on the relative magnitude of $\mathscr{H}_Q$ and $\mathscr{H}_z$, see below.) In polycrystalline solids or glasses, the anisotropy of these internal fields in conjunction with their statistical orientation relative to B_0 gives rise to a distribution of resonance frequencies, which is called the "NMR lineshape".

In the following we will discuss in more detail the physical nature of these internal interactions, their influence upon the NMR lineshapes, and what can be learned from their study.

3.2.1. *Chemical Shift Interaction*

3.2.1.1. *Basic interaction.* The chemical shift describes the effect of magnetic electron–nucleus interactions which affect the local field experienced by the nuclei and hence influence their resonance frequencies. Such influences comprise, (a) diamagnetic shielding by closed electronic shells, (b) paramagnetic deshielding by the angular momenta of admixed excited electronic states, (c) shielding or deshielding effects from rapidly fluctuating paramagnetic electron spins, and (d) shielding or deshielding effects due to conduction electrons at the Fermi edge ("Knight shift"). Although these contributions are physically distinct, they are inseparable in the experiment. The chemical shift Hamiltonian, describing the composite effect of these interactions is:

$$\mathscr{H} = \mathbf{I}(1-\sigma)\mathbf{B}_0. \tag{7}$$

Here σ is a second rank tensor, which can be rotated into a coordinate system, the "principal axis system (PAS)" where it has diagonal form, with σ_{xx}, σ_{yy}, and σ_{zz} as the only components. A complete description of the chemical shift tensor includes six parameters, namely the three diagonal components and the three Euler angles that relate the orientation of the PAS to the crystal or molecular axes of the solid considered. In general, such detailed knowledge necessitates orientation-dependent measurements of the resonance frequencies in single crystals. The situation is comparatively simple, if a molecular axis of higher symmetry is present. In this case, the symmetry axis fixes the PAS and only two chemical shift components $\sigma_{||}$ and $\sigma_{\perp}$, parallel and perpendicular to this axis need to be specified.

3.2.1.2. *Effect on the NMR lineshape.* If the NMR lineshape is dominated by the chemical shift anisotropy, the nuclear magnetic resonance frequency depends on the polar and the azimutal angles θ and ϕ of the chemical shift PAS relative to the direction of the magnetic field (see Fig. 5):

$$\nu(\theta, \phi) = \nu_0\{(1-\sigma_{xx})^2\cos^2\phi\sin^2\theta + (1-\sigma_{yy})^2\sin^2\phi\sin^2\theta + (1-\sigma_{zz})^2\cos^2\theta)\}^{1/2}. \tag{8a}$$

For axially symmetric environments, $\sigma_{xx} = \sigma_{yy} = \sigma_{\perp}$, and $\sigma_{zz} = \sigma_{||}$, and hence ν depends only on θ.

$$\nu(\theta) = \nu_0\{1-\sigma_{iso} - \tfrac{1}{3}\Delta\sigma(3\cos^2\theta - 1)\} \tag{8b}$$

Equations (8a and b) include the definitions:

$$\nu_0 = \gamma B_0/2\pi, \tag{8c}$$

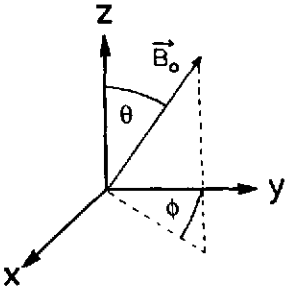

FIG. 5. Polar angles θ and ϕ specifying the magnetic field direction in the chemical shift principal axis system.

$$\sigma_{iso} = \tfrac{1}{3}(\sigma_{xx} + \sigma_{yy} + \sigma_{zz}), \tag{8d}$$

$$\Delta\sigma = |\sigma_{\parallel} - \sigma_{\perp}|. \tag{8e}$$

In a powdered crystalline sample or a glass with no preferred orientation present, the NMR lineshape $g(\nu)$ simply reflects the statistics of θ and ϕ. For spherically symmetric (cubic) environments, all tensor components are equal, and only one sharp, unstructured signal is observed. (Fig. 6a). For the axially symmetric case, the lineshape function is given by:

$$g(\nu) = \tfrac{1}{2}\{[(\nu - \nu_0)/\nu_0] - \sigma_{\perp}\}^{-1/2}(\sigma_{\parallel} - \sigma_{\perp})^{-1/2} \tag{9}$$

(see Fig. 6b). Nuclei in non-axially symmetric environments have lineshapes such as shown in Fig. 6c.[15,18-21] Each point on the lineshape reflects a group of nuclei ("spin packet") for which the principal axis system has the same orientation θ, ϕ relative to the magnetic field direction.

In the absence of reliable absolute chemical shift scales for many nuclei, one usually specifies these components as δ_{11}, δ_{22}, δ_{33} relative to a reference material, defined in ppm according to:

$$\delta_{ii} = (\nu_s - \nu_{ref})/\nu_0. \tag{10}$$

By convention $\delta_{33} > \delta_{22} > \delta_{11}$, and shifts downfield from the reference standard have positive sign.

3.2.1.3. *Structural significance.* Unfortunately, chemical shifts cannot be calculated from first principles. Nevertheless, extensive work on crystallographically well-characterized compounds has established a multitude of empirical and semi-empirical correlations with structural parameters. Judicious application of such databases can therefore render chemical shifts an extremely valuable and reliable source of structural information.

The chemical shift tensor components, which are only available in the solid state, can provide valuable qualitative information about local symmetry. For example, if we observe a lineshape such as that in Fig. 6b we can conclude that a higher local symmetry axis (C_3, C_4, C_6) is present. In glasses and amorphous solids one typically has a distribution of chemical shift parameters. Distribution effects of this kind are accounted for in a heuristic fashion by convoluting the simulated lineshape with a

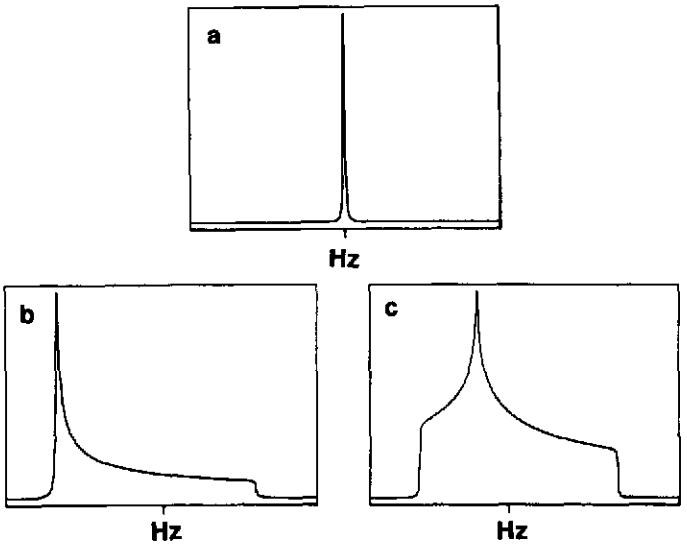

FIG. 6. Typical chemical shift-dominated NMR powder patterns: (a) spherically symmetric chemical shift tensor, (b) axially symmetric chemical shift tensor, and (c) asymmetric chemical shift tensor.

broadening function. In cases where the chemical shift anisotropy is small, this distribution effect may then obscure structured lineshapes.

The isotropic chemical shift

$$\delta_{iso}=\tfrac{1}{3}(\delta_{11}+\delta_{22}+\delta_{33}), \tag{11}$$

is the chief observable in line-narrowing experiments such as magic-angle spinning (MAS) NMR. Like the whole tensor, δ_{iso} depends sensitively on the chemical and electronic environment of the nucleus under study. The influence exerted by structural factors usually follows the hierarchy:

Change in coordination number > nearest neighbor substitution
> next-nearest neighbor substitution.

Substitution effects in higher coordination spheres are generally difficult to identify, and hence usually not considered in the interpretation of chemical shifts. In contrast, changes in nearest- or next-nearest neighbor bond angles are also known to have profound effects on the chemical shifts. While the determination of coordination numbers from chemical shift data (^{29}Si, ^{27}Al, ^{31}P) is generally straightforward, the other chemical shift effects are often of comparable magnitude, and sometimes mutually compensating. Therefore, the interpretation of experimentally observed chemical shift trends in glasses must be done cautiously and in close feedback with known or expected chemical behavior as a function of composition.

3.2.2. *Magnetic Dipole–Dipole Interaction*

3.2.2.1. *Basic interaction.* The magnetic dipole–dipole interaction describes the effect of the local magnetic fields associated with the magnetic moments of surrounding nuclei. Two mechanistic contributions to this effect need to be considered: the "direct" (through-space) coupling and the "indirect" spin–spin coupling transmitted via polarization of bonding electrons. For NMR spectra in solids, the first term is usually dominant. The corresponding Hamiltonian describing the interaction between two spins with gyromagnetic ratios γ_1 and γ_2 and internuclear distance r is given in Table 3. This Hamiltonian can be factored into 6 terms, containing distinct bilinear combinations of the angular momentum operators I_z, I_+, and I_-, respectively.

$$\mathscr{H}_D=\gamma_1\gamma_2\hbar r^{-3}\{\mathscr{A}+\mathscr{B}+\mathscr{C}+\mathscr{D}+\mathscr{E}+\mathscr{F}\} \tag{12}$$

Expressions for these six components are given in the literature. For the discussion of the static NMR spectrum, however, only energy conserving terms need to be retained. These are:

$$\mathscr{A}=(1-3\cos^2\theta)I_{z1}I_{z2} \tag{13}$$

$$\mathscr{B}=-(1-3\cos^2\theta)[I_{+1}I_{-2}+I_{+2}I_{-1}]/4 \tag{14}$$

where θ specifies the angle between the internuclear vector and the magnetic field direction. The term $\mathscr{A}$ describes the classical magnetic dipolar interaction, whereas $\mathscr{B}$ is the quantum-mechanical term associated with coupled transitions ("flip-flop"—term). This latter term is energy-conserving only if the interaction is rendered homogeneous in the presence of strong homonuclear couplings, and hence it contributes to the lineshape only in this case.

3.2.2.2. *Effect on the NMR lineshape.* The second rank tensor characterizing the spatial part of the dipolar two-spin Hamiltonian is always axially symmetric and traceless. This simplifies the mathematical description in the same fashion as previously discussed for the chemical shift anisotropy.

The influence of isolated pairs and clusters of few spins upon the NMR lineshape can be calculated rigorously using first-order perturbation theory. For example, the spectrum shown in Fig. 7a results if the lineshape is dominated by the dipole–dipole coupling between two spins. The problem becomes far more complex, however, when larger numbers of spins are involved. In these cases the lineshape usually resembles the Gaussian function depicted in Fig. 7b. The dipole–dipole coupling is then expressed in terms of a statistical property, the second moment M_{2d}, which is the average mean

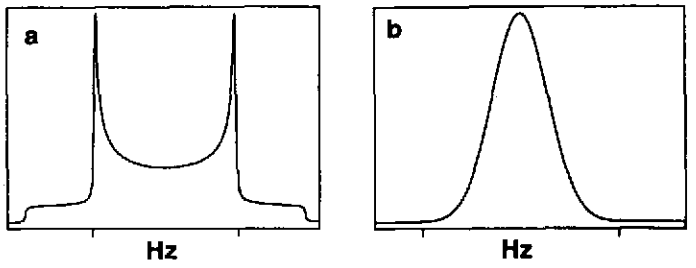

FIG. 7. Typical powder patterns dominated by dipole–dipole couplings: (a) two mutually interacting spins (two-spin system), (b) many-spin system.

squared local field encountered at the nuclei under observation. Experimentally, the dipolar contribution to the second moment is best evaluated by spin-echo spectroscopy (see below).

In the chemically realistic situation, where the lineshape is governed by a large chemical shift anisotropy in addition to weaker multiple dipole–dipole couplings, the lineshape can be simulated as a convolution of powder patterns such as shown in Fig. 6 and a Gaussian broadening function. The case where dipolar and chemical shift interactions are of comparable magnitude requires more explicit analysis.[75]

3.2.2.3. *Structural significance.* Since the dipolar Hamiltonian depends on the internuclear distance, homo- or hetero-dipolar interactions are of strongest structural significance. If well-resolved spectra such as shown in Fig. 7a are observed the internuclear distance r_{ij} is immediately available from the peak to peak distance, expressed in rad/s, $\Delta\omega$:

$$r_{ij} = \{(\tfrac{3}{2})\,(\mu_0/4\pi)\,\gamma^2\hbar/\Delta\omega\}^{1/3} \tag{15}$$

Multi-spin interactions are characterized by the dipolar second moments M_{2d}(in rad^2/s^2), which can be calculated from the structure using van Vleck theory.[76] For a polycrystalline material one obtains:

$$M_{2d} = M_{2Id} + M_{2Sd}, \text{ where} \tag{16}$$

$$M_{2Id} = \tfrac{3}{5}(\mu_0/4\pi)^2\, I(I+1)\gamma^4\hbar^2\, N^{-1}\sum_{i\neq j} r_{ij}^{-6} \tag{16a}$$

$$M_{2Sd} = \tfrac{4}{15}(\mu_0/4\pi)^2\, S(S+1)\,\gamma_I^2\gamma_S^2\,\hbar^2 N^{-1}\sum_{i\neq j} r_{ij}^{-6}. \tag{16b}$$

The first term M_{2Id} is due to the local field arising from resonant nuclei, while the second term M_{2Sd} measures the local field due to non-resonant nuclei S. In both expressions, I and S are the spin quantum number of the resonant and the non-resonant nuclei, respectively, and N is the number of nuclei for which M_{2d} is being calculated. As will be seen below, second moments are of fundamental significance for testing atomic distribution models in disordered materials. Expressions (16) neglect contributions arising from indirect (scalar) spin–spin interactions.

3.2.3. *Nuclear Electric Quadrupole Interaction*

3.2.3.1. *Basic interaction.*[77] Another perturbation on the nuclear magnetic energy levels arises from the interaction of non-spherically symmetric nuclear charge distributions ("nuclear electric quadrupole tensor") with electric field gradients (EFG) generated by asymmetric electron distributions in molecules or lattice sites. The Hamiltonian characterizing this interaction is given in Table 3. This interaction affects only nuclei with $I > \frac{1}{2}$ in non-cubic environments. The anisotropy of the EFG is described by a traceless symmetric tensor, which can be diagonalized to yield the components eq_{zz}, eq_{yy}, and eq_{xx} in a principal axis system. Since according to the Laplace equation

$$\sum_i eq_{ii} = 0,$$

only two principal components are unique. By convention, the quadrupolar interaction is then characterized by two parameters, e^2qQ/h and η. Here eQ is the scalar nuclear electric quadrupole moment, which expresses how much the nuclear charge distribution deviates from spherical symmetry; eq $(=eq_{zz})$ is the electric field gradient along the principal axis, and η, defined as $(eq_{xx}-eq_{yy})/eq_{zz}$, $(0\leqslant\eta\leqslant 1)$, characterizes the deviation of the electric field gradient from cylindrical symmetry. For a complete analysis, the Euler angles specifying the EFG principal axis system relative to the molecular or crystal reference frame need to be specified. Again, the latter is not necessary if the direction of the principal axis is fixed by local symmetry (case $\eta=0$).

3.2.3.2. *Effect on the NMR lineshape.* Depending on its strength compared to the Zeeman interaction, the effect of the nuclear quadrupolar interaction on the solid state NMR spectrum is calculated using either first- or second-order perturbation theory. If $e^2qQ/h < 0.05\ \nu_0$, a first-order perturbation treatment suffices. For an axially symmetric field gradient tensor, the resulting correction terms for the $2I+1$ energy levels are calculated for the various Zeeman states according to:

$$E_m^{(1)}=e^2qQ/h\ (3\cos^2\theta-1)\ (3m^2-I(I+1))/(8I(2I-1)). \tag{17}$$

Figure 8 shows the resulting energy level diagrams and the resulting powder lineshapes for $I=\frac{3}{2}$ and $I=1$, respectively. (Note that the result for $I=1$ is identical to that for the dipolar coupled two-spin-$\frac{1}{2}$ system shown in Fig. 7a.)

For half-integer spins, the central $(\frac{1}{2}\rightarrow -\frac{1}{2})$ transition is, to first-order, unaffected by the quadrupole interaction. In principle, e^2qQ/h and η can be evaluated from the shapes of the satellite transitions, which give rise to powder patterns similar to those shown in Figs 6b and c, because they are governed by the same orientational dependence. In many cases, however, these transitions extend over such a wide spectral region, that they often escape experimental detection. In glasses, the distribution of

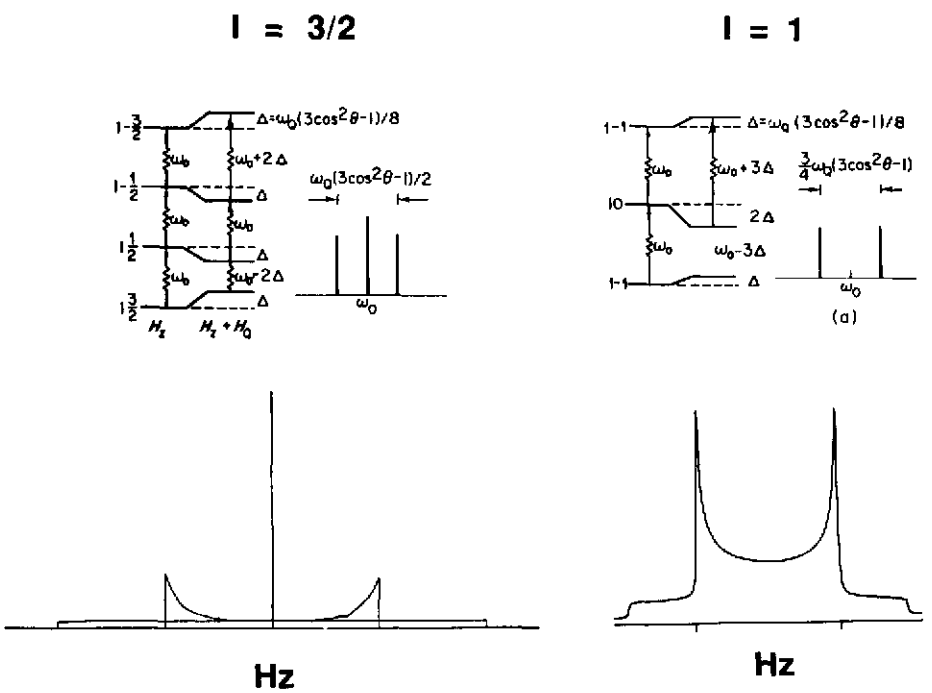

FIG. 8. Energy level diagrams for $I=3/2$ and $I=1$ subject to first-order quadrupolar perturbation, and the resulting lineshapes in single crystals (upper right) and powders (lower part). The upper part of this figure is reproduced with permission from Ref. 15.

nuclear electric quadrupole couplings due to the non-uniformity of sites aggravates the situation further and usually renders the satellite transitions unobservable.

Stronger quadrupolar couplings necessitate treatment by second-order perturbation theory. To second order, the lineshape of the central transition is affected. The energy correction is inversely proportional to the nuclear magnetic resonance frequency, and exhibits a more complicated orientational dependence.

Averaging of the resonance condition over all orientations in a powdered sample results in the structured lineshapes for the central transitions shown in Figs 9a and b for axially and non-axially symmetric EFG tensors. These figures also include the first-derivative spectra, which are usually recorded by low-field cw NMR. Computer-simulation techniques are used to extract e^2qQ/h and η from such spectra. In glasses, however, both of these parameters have to be replaced by distribution functions. It is usually difficult to analyze such lineshapes unambiguously for separate distribution functions of e^2qQ/h and η.

At high fields, the simultaneous influence of anisotropic chemical shift and second-order nuclear electric quadrupole effects is a rather common occurrence. The lineshape then depends not only on the five Hamiltonian parameters previously discussed, but also on the three Euler angles that specify the relative orientation of the chemical shift and the electric field gradient tensor. Simulations of this effect have been published in the literature.[78–80]

3.2.3.3. *Pure quadrupole resonance.* The nuclear electric quadrupole interaction forms the basis of a separate kind of radio frequency spectroscopy, based on the orientational quantization of the nuclei along the internal principal electric field gradient direction. This technique, called nuclear quadrupole resonance, NQR, requires no external magnetic field, but can be otherwise applied to samples using standard NMR technology. Applications to spin-$\frac{3}{2}$ nuclei have had some relevance in the area of glasses. In this case, one measures the quadrupolar resonance frequency:

$$\nu_Q = e^2qQ(1+\eta^2/3)/2h. \tag{18}$$

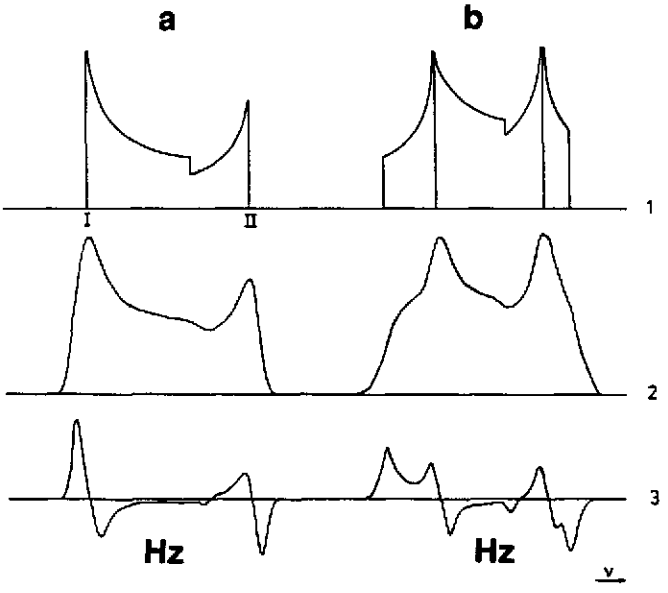

FIG. 9. Central transition lineshapes for half-integer quadrupolar nuclei due to second-order quadrupolar perturbations: (a) axially symmetric EFG, (b) non-axially symmetric EFG. (1) Theoretical powder pattern, (2) lineshape after convolution with a Gaussian broadening function, (3) first derivative of (2), as usually recorded by the cw method.

The advantage of such "zero-field" experiments is that ν_Q does not depend on orientational parameters, and that other interactions can be ignored. NQR experiments on glasses thus provide the ν_Q-distribution directly. Unfortunately, the single observable ν_Q depends on two unknowns. However, it is possible to separate both parameters, e^2qQ/h and η by applying a weak magnetic field, which generates additional energy splittings (Zeeman-perturbed NQR).

3.2.3.4. *Structural significance.* The interpretation of nuclear electric quadrupole parameters suffers from similar restrictions as that of chemical shifts. While electric field gradients are difficult to calculate accurately, useful qualitative and semi-quantitative conclusions are often possible. For instance, if $\eta = 0$ is found, it can be concluded that a unique local symmetry axis is present. Arguments from simple point-charge models and valence bond approaches are often invoked in semiquantitative interpretations.[81] Generally, however, the usefulness of the nuclear electric quadrupole coupling parameters is often limited by the inability of separating e^2qQ/h and η distribution effects, and the failure of these parameters to discriminate between the four- and six-coordinate environments so frequently present in glasses.

3.2.4. *Effects of Atomic or Molecular Motion on Static NMR Lineshapes.* The lineshapes discussed in the preceding sections are caused by local magnetic or electric fields as present in entirely rigid polycrystalline or glassy samples. Atomic and/or molecular motions render these local fields time-dependent. The effect of these motional processes on the NMR spectra depends on their amplitude, inherent timescale and their mechanistic character (periodic, stochastic, correlated), and can be calculated rigorously for many situations.[50,82] Thus, NMR spectroscopy can function as an important spectroscopic tool for the dynamical characterization of solids and glasses.

Due to the fast timescale of lattice vibrations, all lineshapes recorded at room temperature are vibrationally averaged. However, the restricted amplitude of this motion has a rather small influence on the NMR spectra (particularly on chemical shifts and dipole–dipole couplings). The sizeable atomic displacements during the course of molecular reorientations and diffusion processes are a different matter. Such motions are generally treated as stochastic processes and generally described by exponential autocorrelation functions.

$$g(\tau) = \exp - \{\tau/\tau_c\} \tag{19}$$

Here, the correlation time τ_c characterizes how quickly on average an ensemble of molecules lose memory of their coordinates at an earlier time. If τ_c^{-1} is comparable to the frequency ω_{int} of nuclear precession in the local field, the free induction decays, and hence the NMR lineshapes are affected. Since ω_{int} is usually in the kHz region, NMR lineshapes are sensitive to motions with τ_c in the region of 10^{-2}–10^{-5} s. Motions characterized by τ_c substantially smaller than 10^{-5} s lead to a complete averaging of the static NMR lineshape ("motional narrowing"), resulting in exponential free induction decays and simple Lorentzian lineshapes. This is typically the situation in the liquid state, where $\tau_c < 10^{-7}$ s.

3.3. *Spin-Lattice Relaxation*

When an unpolarized sample is introduced into the magnetic field, the orientational quantization and the energy splitting associated with it take immediate effect. Due to this energy splitting, the spin-state population distribution now changes from a uniform one to the familiar Boltzmann distribution at thermal equilibrium, resulting in a macroscopic magnetization along the direction of B_0. This process is called "spin-lattice relaxation". The change in the population distribution lowers the energy of the spin system; it hence involves energy transfer from the spin system to its surroundings (the "lattice"). The attainment of thermal equilibrium can be described by first-order kinetics and characterized by the time constant T_1, called the spin-lattice relaxation time. Microscopically, relaxation is caused by fluctuating magnetic fields from unpaired electrons, conduction electrons, or modulated magnetic dipole–dipole interactions. For nuclei with spin $> \frac{1}{2}$, fluctuating electric field gradients are an efficient source of relaxation. Whichever mechanism dominates, relaxation can be

effected either directly or through spin-diffusion via magnetic dipole–dipole couplings (the B-term in $\mathscr{H}_D$). In solids, the value of T_1 can span a wide range from 10^{-6} s to unmeasurably long values.

Dynamical processes such as atomic or molecular motion result in fluctuating dipolar or quadrupolar interactions, and hence facilitate spin-lattice relaxation.[83] The relaxation efficiency is determined by the overlap between the frequency spectrum of the motional process and the resonance frequency. Simplistically speaking this means that there must be a good match between the energy released from the spin system upon its return to the Boltzmann state and the energy quanta that the lattice is apt to accommodate. This match is described by the spectral density $J(\omega\tau_c)$. Since $J(\omega\tau_c)$ is the Fourier Transform of the correlation function describing the motion, its functional form depends on the mechanism of motion. For an exponential correlation function:

$$J(\omega\tau_c)=\tau_c(1+\omega^2\tau_c^2)^{-1}. \tag{20}$$

A plot of $J(\omega\tau_c)$ as a function of ω is seen in Fig. 10, for the three regimes $\omega_0\tau_c \ll 1$, $\omega_0\tau_c \sim 1$, and $\omega_0\tau_c \gg 1$.

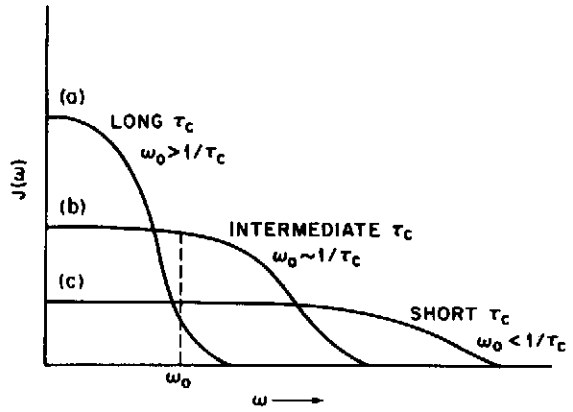

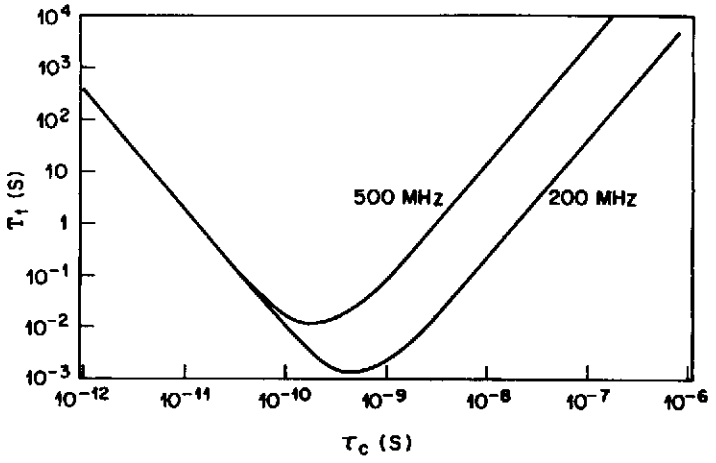

FIG. 10. Top: Frequency dependence of the spectral density function in the extreme narrowing limit ($\omega_o\tau_c \ll 1$), the slow motion limit ($\omega_o\tau_c \gg 1$) and the intermediate region $\omega_o\tau_c \sim 1$. Bottom: Typical dependence of the spin lattice relaxation time T_1 on frequency and correlation time τ_c. Reproduced with permission from Ref. 22.

Considering relaxation by stochastic motion, Bloembergen, Purcell, and Pound (BPP) derived the following general expression for the spin-lattice relaxation rate T_1^{-1}:[83]

$$1/T_1 = C(\tau_c/(1+\omega_0^2\tau_c^2) + 4\tau_c/(1+4\omega_0^2\tau_c^2)). \tag{21a}$$

The constant C depends on which fluctuating interaction (dipolar, quadrupolar, or chemical shift) governs the relaxation process. C can be determined numerically from the Hamiltonian parameters governing the static lineshape in the rigid lattice limit.

In principle, expression (21) allows detailed insights into dynamical processes via temperature- and frequency-dependent measurements of T_1. Applications generally assume an Arrhenius-type relationship between τ_c and temperature:

$$\tau_c = \tau_{c0} \exp^{E_A/RT} \tag{22}$$

where E_A is the activation energy of the motional process dominating the relaxation. For the high-temperature side ($\omega_0\tau_c \ll 1$), eq. (21) simplifies to

$$\ln T_1^{-1} = \ln (5C\tau_{c0}) + E_A/RT. \tag{21b}$$

In the limit of low temperatures ($\omega_0\tau_c \gg 1$), one obtains

$$\ln T_1^{-1} = \ln (8C\omega_0^{-2}\tau_{c0}^{-1}) - E_A/RT. \tag{21c}$$

Thus, symmetrical curves of $\ln T_1^{-1}$ vs inverse temperature are expected, with a maximum at the temperature for which $\omega_0\tau_c = 1$. (Other investigators plot instead $\ln T_1$ vs inverse temperature, yielding a minimum when relaxation is most effective, see Fig. 10, bottom.) In either case, E_A is accessible from both the high- and the low-temperature sides of such plots.

Experimental studies usually comprise detailed temperature- and frequency-dependent measurements of T_1 (see below), from which the activation energy E_A and the pre-exponential factor τ_{c0} can be extracted by computer fitting. In glasses, the large majority of NMR relaxation measurements have concentrated on characterizing ionic diffusion processes. As discussed later, characteristic deviations from "BPP"-behavior are detected, suggesting either distributed correlation times or non-exponential correlation functions.

4. EXPERIMENTAL PULSED NMR

4.1. *Excitation and Detection of Resonances*

In NMR spectroscopy the magnetic component of an applied radiofrequency field stimulates transitions between the nuclear magnetic energy levels. The two most common approaches used to achieve this condition are (1) variation ("sweep") of the external magnetic field under continuous irradiation of a monochromatic frequency ν_0 ("continuous wave"-NMR), and (2) polychromatic excitation of the entire spectrum by short pulses at a carrier frequency ν_0 and a fixed magnetic field strength. Since, during the last 10 years, the second method has become preponderant, only this technique will be discussed in further detail here.

To explain pulse NMR experiments, it is useful to appeal to the classical prediction that the interaction of the nuclear magnetic moments with the magnetic field forces the nuclei to precess around the field direction with the Larmor frequency $\nu_p = (2\pi)^{-1}\gamma B_{loc}$. The macroscopic magnetization, which forms at spin-lattice equilibrium as a result of the Boltzmann distribution, is the target of the pulsed NMR experiment. To measure the NMR spectrum of the sample, this magnetization is converted to a nuclear induction signal. The principle is illustrated with vector diagrams depicted in the "rotating frame", i.e. a coordinate system that rotates with the carrier frequency ν_0 about the magnetic field axis (see Fig. 11). A short (1–10 μs length), intense (100–1000 Watt power) radiofrequency pulse is applied that tips the magnetization into the plane perpendicular to the magnetic field direction ("90° pulse"). The pulse must be applied at a carrier frequency ν_0 in the vicinity of ν_p. Precise resonance is, however, not required, since pulsed excitation is in itself polychromatic. Since samples with multiple sites have a

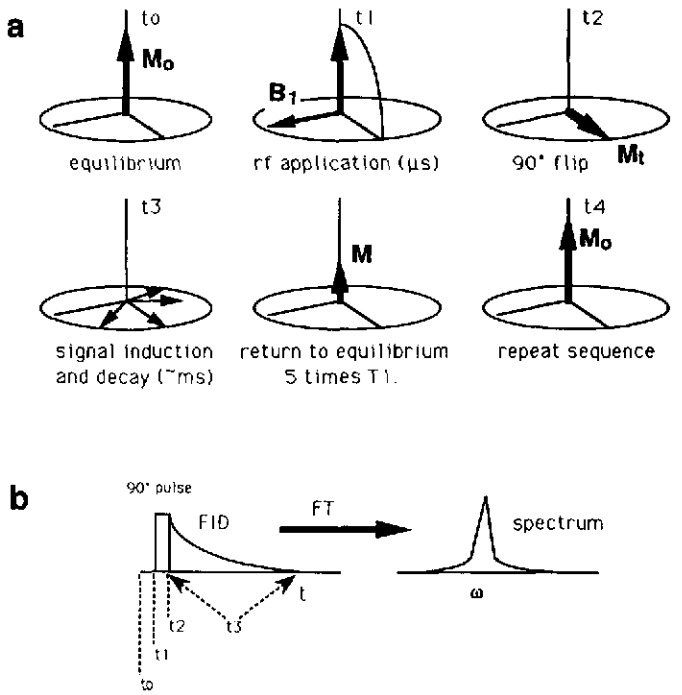

FIG. 11. (a) Detection of NMR signals by pulsed spectroscopy, shown in the rotating coordinate system associated with the oscillating magnetic field component at the applied radio frequency ω_0 at various stages (t_0–t_4) of the experiment: t_0—spin system with magnetization (fat arrow) at equilibrium, t_1—irradiation of the B_1 field orthogonal to the magnetization direction tips the magnetization, t_2—the sytem after a 90° pulse resulting in transverse magnetization M_t, t_3—off-resonance precession and free induction decay in the signal acquisition period following the pulse, t_4—return to spin equilibrium due to spin-lattice relaxation. (b) Timing diagram of the experiment, followed by Fourier transformation.

range of values of ν_p, it is important, however, that the Fourier spectrum of the pulse includes the entire range of such precession frequencies. In polycrystalline solids and glasses the required range is typically 100–200 kHz, which is easily covered by short pulses (ca. 5 μs or less).

In certain cases, site distribution effects or strong quadrupolar interactions generate much wider ranges of resonance frequencies. One then has to resort to traditional cw NMR methods with field sweep (if still available). Alternatively, such broad lines can be mapped out by spin echo spectroscopy under systematic variation of the carrier frequency ν_0. This technique, known as "spin echo mapping" has proven very useful for applications in pulsed nuclear quadrupole resonance of glasses and for measuring the magnetic hyperfine field distributions in amorphous metals. In both applications, the frequency ranges probed can span 100 MHz or more.

Following the 90° flip by the rf excitation pulse, the magnetization precesses with the ν_p components of the nuclei present and induces an a.c. voltage in the detector coil of the NMR probe. This voltage signal decays in time because the magnetization vectors lose their phase-coherence due to their differences in ν_p as well as due to spin–spin interactions. The "free induction decay" signal is amplified, and is mixed in the receiver section of the spectrometer with the carrier frequency ν_0. The resulting signal then oscillates at the difference frequency $\nu_{offset} = |\nu_p - \nu_0|$ and is typically in the audio frequency range (0–200 kHz). If chemically distinct sites are present, this signal is a decaying interferogram ("beating pattern") of several different frequency components. Fourier Transformation of this digitized and stored interferogram then yields the various ν_{offset} (and hence the ν_p) components. Chemical shifts are determined by comparison of ν_{offset} (sample) with that of a chosen standard.

Since the acquired signals are quite weak, signal averaging by repetitive pulsing is usually necessary. A 90° pulse creates a state of equally populated nuclear spin levels. Hence no z-magnetization is present immediately after the pulse, and one must allow for sufficient time for the spin system to relax to its equilibrium state. For quantitative applications, the repetition time must exceed 5 times the longest spin-lattice relaxation time present in the sample.

4.2. *Measurement of Spin-Lattice Relaxation Times*

Two experimental protocols for T_1 measurements are shown in Figs 12a and b. The inversion recovery method 180°-τ-90° (Fig. 12b) measures the re-establishment of longitudinal magnetization at the time t_1 after the magnetization has been inverted by a 180° pulse; T_1 is determined from a series of measurements with different values of t_1, using the relationship

$$I(t_1)=I(0)\,(1-2\exp^{-t_1/T_1}). \tag{23}$$

In the solid state, it is often difficult to provide uniform excitation over the entire spectral region by a 180° pulse. Alternatively, the saturation recovery method $(90°)_n$-t_1-90° (Fig. 12a) can be used. In this case, the re-establishment of the longitudinal relaxation after saturation of the spin system by the 90° pulse-train is given by

$$I(t_1)=I(0)\,(1-\exp^{-t_1/T_1}). \tag{24}$$

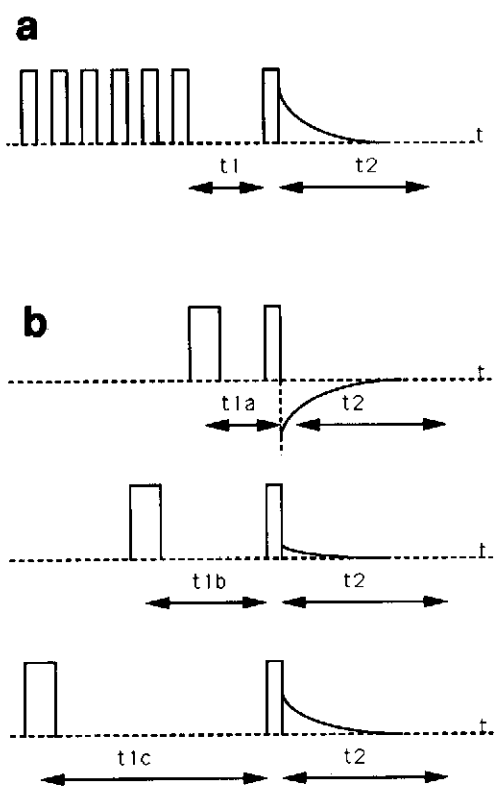

FIG. 12. Measurement of the spin-lattice relaxation time by (a) the saturation recovery $(90°)_n$-t_1-90° method, and (b) the inversion recovery (180°-t_1-90°) method. For the latter, the signal build-up is shown for three evolution times t_{1a-c} elapsing between the preparation pulses and the final 90° detection pulse.

4.3. *Selective Averaging Techniques*

In glasses, spectra as well-defined as those in Figs 6–8 are virtually never observed. This is so, because the lack of long-range order creates always non-singular NMR Hamiltonian parameters that are more appropriately represented by distribution functions. The ultimate goal of the NMR experiment on a glass is to define these distribution functions as precisely as possible and to relate them to structural and geometrical distribution functions. Furthermore, the lineshape of solids is quite generally influenced by the combined effect of several interaction mechanisms, complicating the spectral analysis even further.

To obtain accurate information on the distribution functions of the Hamiltonian parameters in disordered materials and glasses, it is therefore essential to separate the various interactions by selective averaging experiments.

Traditional precursors to such experiments have included field dependent studies, isotopic dilution, and experiments on different isotopes of the same element. More recent approaches utilize sophisticated manipulations in either physical space or spin space to eliminate certain interactions in the Hamiltonian completely while preserving others. Manipulations in spin space take advantage of the fact that the spin-dependent components of the various interaction Hamiltonians differ from each other and hence possess different commutation behavior with the spin Hamiltonian representing the interaction of the nuclei with the oscillating magnetic field stimulating the transitions. Manipulations in physical space modulate the anisotropic components of the spatial part of the internal interaction Hamiltonians and hence serve to separate anisotropic from isotropic interactions. Table 3 summarizes some of the experiments that are more generally applicable. There are many more selective averaging schemes than can be discussed here, some of them very elegant and/or highly sophisticated. However, it appears that to date the relationship between the complexity of the NMR technique and the complexity of the sample has been an inverse one. Therefore the discussion will be limited to some of the simpler, more robust techniques that have had a major impact on glass science applications.

4.3.1. *Magic-Angle Sample Spinning.* Equations 8, 13 and 17 reveal that if the principal axis of the internal interaction tensor has an angle of 54.7° relative to the magnetic field, the term $3\cos^2\theta - 1$ is zero and the anisotropy vanishes. This situation is attained in the liquid state, where due to the rapid molecular motion on the NMR timescale, the orientational average is 54.7° for all molecules present. In the solid state, a similar situation can be accomplished by rotating the sample very rapidly around an axis inclined by this angle ("magic-angle spinning—MAS").[84,85] This manipulation changes the orientation θ in a periodic fashion. During the rotor period, a given spin packet (corresponding to an initial orientation θ_1) traverses a range of θ values as represented by a cone around the orientation $\theta = 54.7°$. While spin packets with different initial orientations (θ_2 etc.) travel on different cones, in all cases the same rotational average is 54.7° for fast rotation. Thus, MAS modulates the anisotropic components of the interaction Hamiltonians and averages the angular dependence of the perturbed Zeeman eigenvalues over the rotation period. At sufficiently fast spinning speeds ν_r such that $\nu_r \gg \Delta\nu$, ($\Delta\nu$ being the linewidth in cycles per second) the only terms that need to be considered in the nuclear spin Hamiltonian are those associated with the isotropic components of the various interactions present. The situation is then essentially the same as in the liquid state, where the traceless dipolar and quadrupolar interactions are completely averaged out by isotropic motion, and sharp resonance lines characterized only by isotropic chemical shifts and scalar spin–spin couplings are observed. In glasses, MAS-NMR lineshapes obtained in this fast-spinning limit are often dominated by distributions of isotropic chemical shifts.

If the condition $\nu_r \geqslant \Delta\nu$ is not achieved (at lower spinning speeds) there may be additional contributions to the MAS-NMR linewidths due to incompletely averaged dipole–dipole couplings. Furthermore, the effect of incompletely averaged heteronuclear dipolar couplings and chemical shift anisotropies will give rise to spinning sidebands appearing at integer multiples of the spinning speed. In crystalline solids it is often possible to extract the anisotropic chemical shift tensor components from such spinning sideband patterns.[86,87] In glasses, these possibilities are more limited. Due to the intrinsically broader MAS-linewidths the need for low spinning speeds (to enhance sideband intensities) often conflicts with the need of observing resolved spinning sideband patterns.

For half-integer nuclei subject to second-order quadrupolar interactions, magic-angle spinning leads to incomplete line-narrowing, because the nuclei are no longer strictly quantized along the magnetic field. In crystalline solids, highly characteristic MAS-NMR lineshapes result, from which e^2qQ/h and η can be extracted via computer-simulations.[88] In glasses, however, MAS-NMR lineshapes of quadrupolar nuclei have little significance, since they are broadened by the distributions of both chemical shift and quadrupole coupling parameters. Two more recent developments exploit (a) incremented angle variation (DAS = dynamic angle spinning), or (b) double rotation (DOR) about two fixed axes with respect to the magnetic field, to eliminate the residual broadening of MAS-NMR spectra due to second-order quadrupolar effects.[89,90] Simple Gaussian or Lorentzian lineshapes are observed, whose resonance location is given by

$$\delta_{exp} = \delta_{iso} + \delta_Q^{(2)}. \tag{25}$$

Here, $\delta_Q^{(2)}$ is the second order quadrupole shift, which is calculated (in ppm) according to:

$$\delta_Q^{(2)} = -3(e^2qQ/h)^2(I(I+1)-\tfrac{3}{4})(1+\eta^2/3)/40I^2(2I-1)^2\nu_0^2. \tag{26}$$

Thus, field-dependent DAS/DOR measurements of δ_{exp} afford both δ_{iso} and the factor $(e^2qQ/h)(1+\eta^2/3)$, and their respective distribution parameters.

4.3.2. *Dipolar Spin-Echo NMR.* The simple spin-echo pulse sequence (90°-t_1-180°, Fig. 13) has proven to be a powerful tool for the selective measurement of homonuclear dipole–dipole couplings.[91–93] Following the initial 90° preparation pulse, the transverse magnetization decays during the evolution period t_1 due to the combined effect of homo- and heteronuclear interactions, as well as chemical shift distribution effects. Application of the 180° pulse at t_1, however, reverses the part of the decay due to all interactions linear in $\mathbf{I}_z$ (i.e. chemical shift anisotropy and heteronuclear dipole couplings), resulting in a spin echo at the time $2t_1$. Thus, the intensity of the spin echo is attenuated only by homonuclear dipole couplings during the evolution time $2t_1$. The evolution time is then systematically incremented, giving rise to an experimental spin echo decay $I(2t_1)/I(0)$. Figure 13 shows the situation for three different values of t_1. For an isolated two-spin system:

$$I(2t_1)/I(0) = \langle \cos a_{ij}t_1 \rangle, \tag{27}$$

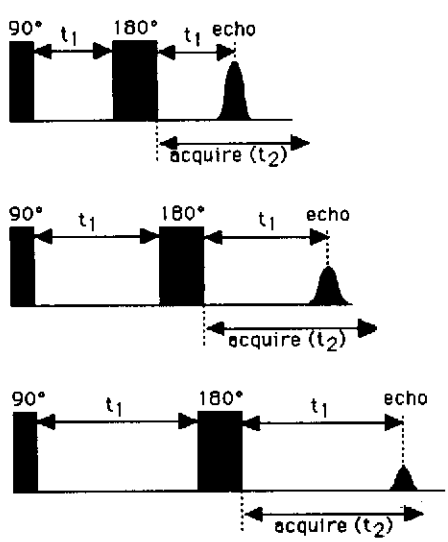

FIG. 13. Spin-echo sequence for measuring homodipolar second moments. Shown are three acquisitions with incremented evolution time t_1, showing decreasing spin echo intensity due to homodipolar interactions. Typically ca. 20 different evolution times are used.

where

$$a_{ij}=(\mu_0/4\pi)\gamma^2\hbar(1-3\cos^2\theta)r_{ij}^{-3} \tag{28}$$

and $\langle\ \rangle$ denotes averaging over all orientations θ.

In the case of multiple pairwise interactions, we must write instead:

$$I(2t_1)/I(0)=\Pi_j\langle\cos a_{ij}t_1\rangle. \tag{29}$$

The dipolar oscillations are damped out, and the resulting decay very often resembles a Gaussian:

$$I(2t_1)/I(0)=\exp-((2t_1)^2\,M_{2d}/2). \tag{30}$$

Equation (30) defines a semilogarithmic plot of normalized echo height vs $(2t_1)^2$, which affords a convenient measurement of the second moment characterizing the homonuclear dipolar interactions. Disordered systems often show dramatic deviations from Gaussian behavior if, due to randomness, a wide distribution of second moments exists. In such cases, eq. (30) must be replaced by

$$I(2t_1)/I(0)=N^{-1}\,\Sigma_i\exp-((2t_1)^2\,M_{2d_i}/2) \tag{31}$$

where the summation goes over i nuclei from 1 to N. In conjunction with eq. (16) this formula allows one to simulate a spin echo decay based on hypothetical atomic distribution models.

The above approach is generally not applicable for the following situations: where (a) the homonuclear dipole interaction is the major defocusing mechanism for the transverse magnetization created by the preparation pulse, hence precluding the formation of a spin echo, or (b) the I nuclei are coupled to non-resonant S-nuclei whose Zeeman eigenstates change during the duration of the experiment. This could happen either due to strong S–S dipolar interactions giving rise to coupled spin-transitions ("flip-flop mechanism") or due to quadrupolar interactions that couple strongly with the lattice, hence producing fast relaxation. In either case, the I–S interaction is not completely refocused. An approximate theory for this situation has been given by Reimer and Duncan.[93] The spin-echo decay $I(2t_1)/I(0)$ of resonant spins I that are dipolarly coupled to non-resonant spins S whose z-components fluctuate with the time constant $T_{2,S}$ is given by:

$$I(2t_1)/I(0)=\exp-\{2(T_{2,S}/T_{2,IS})^2((2t_1/T_{2,S})+(4\exp-(t_1/T_{2,S}))-(\exp-(2t_1/T_{2,S}))-3)\}. \tag{32}$$

Here $(T_{2,IS})^2=1/M_{2,IS}$ characterizes the strength of the heteronuclear I–S dipole–dipole interactions.

Due to these possible interferences, the ability of spin-echo NMR to measure homonuclear second moments accurately in crystalline compounds is somewhat limited. Fortunately, the situation improves in the presence of disorder. Due to the lack of chemical uniformity, invariably a distribution of chemical shifts will be present. At sufficiently high field strengths, such shift distributions then not only ensure the formation of spin echoes, but also uncouple the neighboring heteronuclei from each other and hence quench their flip-flop transitions. Thus, the presence of disorder is of considerable advantage for the measurement of dipole–dipole interactions by spin echo methods.

4.3.3. *Dipolar Spin-Echo Double Resonance Spectroscopy.* Heteronuclear dipolar interactions can be measured selectively by the method of spin-echo double resonance spectroscopy. It was noted in the previous section that the spin echo technique only refocuses the heteronuclear dipolar interaction if the eigenstates of S_z remain constant during the timescale of the experiment. If, on the other hand, we intentionally change the eigenstates of S_z by irradiation with a radiofrequency field on resonance, the spin echo will suffer additional attenuation because now the I–S interaction is no longer refocused. In analogy with the discussion above, this effect forms the basis for a selective measurement of heteronuclear dipolar interactions. The experiment uses a normal spin-echo sequence for the observed nuclei, but now includes a 180° pulse on the S nuclei during the evolution period. Figure 14 shows the pulse sequence. The delay time between the 90° pulse and the 180° (S) pulse is incremented (not shown in this figure), and hence defines the time variable characterizing the spin echo decay as a result of the dipolar I–S interaction. This experiment has been called "spin echo double resonance (SEDOR)".[94–96] The SEDOR decay of the observed nuclei I arises from the combined effect of I–I

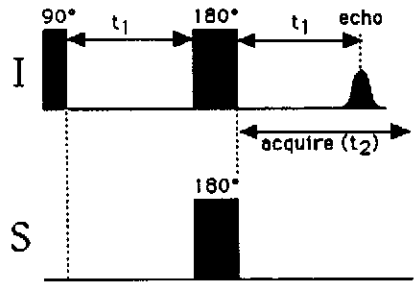

FIG. 14. SEDOR pulse sequence for measuring heterodipolar second moments between observe nucleus I and heteronucleus S.

and I–S interactions:

$$I(2t_1)/I_0 = \Sigma \exp((2t_1)^2 M_{2I-I}/2)\exp((2t_1)^2 M_{2I-S}/2). \tag{33}$$

The contribution due to homonuclear I–I interactions can be studied separately by carrying out a regular spin echo study (with the 180° (S) pulse absent). Thus,

$$I(2t_1)/I_0 = (F(2t_1)/F_0) \cdot \Sigma_i \exp((2t_1)^2 M_{2I-S}/2), \tag{34}$$

where $F(2t_1)/F_0$ is the experimental spin echo decay function measured in the absence of the S pulse.

It is important to realize that SEDOR results can be seriously affected by systematic experimental errors if the 180° (S) pulse is imperfect and/or applied off resonance. In that case, only a fraction of S spins are flipped and hence the I spin echo decays more slowly with $2t_1$ than expected. To account for this experimental artifact, eq. (34) then has to be replaced by

$$I(2t_1)/I_0 = (F(2t_1)/F_0) \cdot ((1-a) + a \cdot \Sigma_i \exp((2t_1)^2 M_{2I-S}/2)), \tag{35}$$

where a ($0 \leqslant a \leqslant 1$) characterizes the fraction of spins actually flipped by the 180°(S) pulse.

Several other techniques have been used to measure heteronuclear interactions. Like the SEDOR technique, they utilize double irradiation, but study the resulting defocusing process on rotational echoes generated by MAS rather than on static spin echoes. These methods, which have been known as REDOR (rotational spin echo double resonance)[97] and RRR (rotary resonance recoupling)[98,99] are able to selectively measure individual heteronuclear dipolar couplings for multiple-peak MAS NMR spectra in crystalline solids. In disordered materials giving rise to MAS-NMR spectra with linewidths governed by wide chemical shift distributions, however, the comparatively small broadening effects caused by the re-introduced heteronuclear dipole–dipole couplings would be impossible to detect. In such cases, the SEDOR technique is the method of choice.

4.3.4. *Cross-Polarization.* A second experiment that is sensitive to heteronuclear dipolar couplings is cross-polarization (CP)[100] (see Fig. 15). This method achieves magnetization transfer (via cross-relaxation) from an abundant-spin system S (usually protons) to the spin system of the observe-nucleus

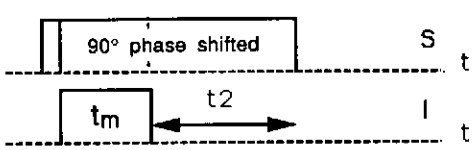

FIG. 15. Pulse sequence for cross-polarization. Following an initial 90° pulse the S magnetization is spin-locked along an applied B_1 field. For the duration of the mixing time t_m a long pulse is supplied to the I spins such that eq. (36) is fulfilled. Following this pulse, acquisition of the transverse I-spin magnetization commences during the acquisition period t_2, while the S-spins are continuously irradiated to provide spin-decoupling.

I whose signal is desired. To accomplish this, the S-spins are first converted into a non-equilibrium state: a 90° preparation pulse is followed by a strong B_1 field in phase with the transverse magnetization which forces the S-spins to precess around the B_1 direction ("spin-locking"). Since $B_1 \ll B_0$, the population difference between the spin states is now too large, and thus there is a driving force for relaxation (and energy exchange). The desired pathway in this technique involves magnetization transfer via cross-relaxation to the I-spin system, i.e. the observe-nuclei. To this end, a radio frequency field is applied at the resonance of the I-spins such that:

$$(\omega_1)_{obs} = (\omega_1)_{abund} \tag{36}$$

for a fixed amount of time t_m on the order of 1–10 ms. Condition (36), known as the "Hartmann–Hahn condition"[101] ensures that the I-spins and the S-spins precess at the same frequency in the rotating frame, hence enabling cross-relaxation via the zero-quantum term in the heteronuclear dipolar Hamiltonian. The rate of magnetization transfer is characterized by the cross-relaxation time T_{CR}, which can be determined by variable contact time experiments. The stronger the dipole coupling, the shorter the cross-relaxation time.

CP experiments have been invaluable for ensuring the observation of signals for rare nuclei, and for indicating spatial proximity on a qualitative basis. It is more difficult to determine M_{2d} values or internuclear distances from CP experiments, because Hartmann–Hahn mismatch and competing spin-lattice relaxation processes in the rotating frame can affect the efficiency of cross-relaxation.

4.3.5. *Chemical Shift Correlation Spectroscopy.* Unlike the techniques discussed above, correlation spectroscopy is not directed at the measurement of selected internal interactions but at uncovering a spatial relationship between sites with different resonance frequencies (chemical shifts). This relationship is detected in the form of coherence transfer that is mediated either by physical diffusion or spin diffusion. For the convenient measurement, two-dimensional pulse sequences are employed. Figure 16 gives two simple examples:[102] Two-dimensional correlated spectroscopy (COSY) employs a two-pulse 90°-t_1-90°-t_2 sequence as shown in Fig. 16a. The evolution time t_1 between the two pulses is

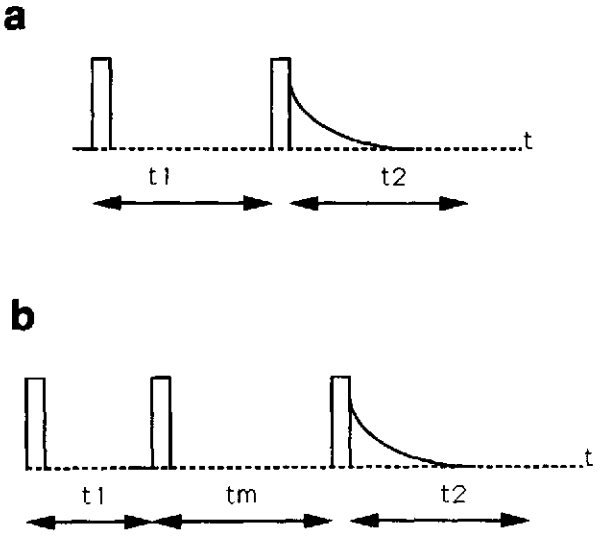

FIG. 16. Two-dimensional coherence transfer spectroscopy. (a) 90°-t_1-90° sequence for homonuclear correlated spectroscopy via scalar spin–spin couplings (COSY). The evolution time t_1 is systematically incremented. (b) 90°-t_1-90°-t_m-90° sequence for homonuclear correlated spectroscopy via chemical exchange or nuclear Overhauser effect (NOESY). The evolution time t_1 is systematically incremented. During the mixing period t_m coherence transfer occurs by virtue of chemical exchange or spin diffusion.

systematically incremented. Following the first 90° pulse the magnetization associated with a specific site characterized by an isotropic chemical shift δ_A precesses in the plane perpendicular to the magnetic field under the influence of its isotropic chemical shift and spin–spin coupling Hamiltonians. Application of the second 90° pulse causes coherence transfer from this site to other sites, whose chemical shifts δ_B are different, if there is indirect spin–spin coupling between both sites δ_A and δ_B. Following the second pulse, part of the magnetization now precesses at the new frequency δ_B at the start of the signal acquisition period t_2. Double Fourier transformation with respect to both t_1 and t_2 dimensions then yields a symmetric correlation plot of chemical shifts. The magnetization components that have taken part in coherence transfer manifest themselves as off-diagonal cross-peaks in this plot. Similar ideas can be implemented for correlating chemical shifts of different types of nuclei. In the solid state, the 2D COSY experiment is generally carried out in combination with MAS. Coherence transfer is accomplished via one- or two-bond indirect spin–spin couplings. Thus, the observation of such a cross-peak at (δ_A, δ_B) in the two-dimensional spectrum then provides positive evidence for spatial through-bond connectivity.

Figure 16b shows a second useful correlation method, the NOESY experiment. This experiment establishes a chronological relationship between sites having different chemical shifts. As such the technique is well-suited to study chemical exchange pathways and equilibria. First, the incremented evolution period t_1 serves to label individual spins by their chemical shifts. During the mixing time t_m the chemical shifts of these spins are altered due to the chemical exchange process under consideration. Thus, during the detection period t_2 part of the magnetization that previously oscillated at δ_A now oscillates at δ_B. This chemical shift correlation manifests itself as a corresponding cross-peak in the two-dimensional double-Fourier transform plot.

4.4. *Quantitative NMR Spectroscopy in Glasses*

One of the greatest advantages of NMR spectroscopy is the strict proportionality of signal intensity to the number of nuclei giving rise to this signal. This property has proven to be immensely useful for the development of quantitative structural concepts describing disordered systems, amorphous materials, and glasses. To maintain the quantitative character of the experiment, however, rigorous protocols have to be adhered to in the execution of the experiments. As a simple test of the chosen experimental conditions, absolute signal intensity measurements of weighed samples with known analytical compositions can be carried out.

Problems distorting the quantitative information available in principle can arise both in the excitation and the detection step. First of all, nuclei in certain chemical environments may not give rise to any NMR signal. This situation can arise, if the nuclear spins are not quantized along a direction near that of the externally applied magnetic field. Examples are nuclei close to paramagnetic electron spins and quadrupolar nuclei interacting with strong electric field gradients. Even if signals are observed for such nuclei, quantitative studies may be difficult or even impossible to perform. Secondly, non-uniform excitation can lead to serious quantitation errors. Nuclei that resonate far away from the carrier frequency experience smaller effective flip angles, resulting in reduced signal intensities, and affecting relative signal areas for spins with different offset frequencies. One can test for such artifacts by reducing the experimental pulse lengths, and by recording the spectra at various different carrier frequencies.

In the following paragraph the most important case, that of half-integer quadrupolar nuclei (such as ^{11}B, ^{23}Na, ^{27}Al, and ^{71}Ga) deserve some special attention. For these nuclei often only the central $\frac{1}{2} \rightarrow -\frac{1}{2}$ transition is observable. The signal intensity then is only 40%, 25.6% and 19% for spin $-\frac{3}{2}, \frac{5}{2}$ and $\frac{7}{2}$ nuclei, respectively, compared to the signal intensity observable for an equal number of nuclei in an isotropic solution. However, the percentage of visible signal may be higher than specified above, if nearby satellite transitions contribute to the integrated area. It also may be lower, if the central transition is strongly broadened by second-order quadrupolar effects. In addition, the quadrupolar interaction influences the excitation behavior for such spins. The precession frequency in the rotating frame (determining the required pulse length for a 90° pulse) depends on whether or not the outer quadrupolar transitions are being excited. This question can be clarified by measurements under

systematic incrementation of the pulse length.[103,104] For the quantitative spectroscopy of quadrupolar nuclei, such "nutation NMR studies" are a mandatory part of the experimental procedure. To avoid lineshape distortions from differing degrees of excitation selectivity in the sample, short flip angles ($<22.5°$) must be used.

Quantitative NMR studies also require that conditions of spin-lattice equilibrium be maintained. This means that the recycle delay between pulses has to be at least 5 times the longest spin-lattice relaxation time present in the sample. Otherwise, the resonances of those nuclei with the longer T_1 values are partially saturated and give rise to reduced intensities. For reasons related to these issues, NMR spectra obtained with the cross-polarization method are usually not quantitative. Here, the signal intensity results from a complicated interplay of cross-relaxation and spin-lattice relaxation processes, and rare-spin nuclei that are too remote from the abundant-spin magnetization reservoir are not detected at all.

Finally, simple one-pulse experiments are affected by the fact that the NMR signal can usually not be detected immediately after the excitation pulse. Due to receiver recovery and probe ringing problems, typically a "dead time" of ca. 10 μs has to elapse before the start of signal acquisition. The signal loss during this deadtime will depend on the rate of the free induction decay, which correlates with the line width of the NMR spectrum. In MAS-NMR spectra of crystalline solids, where the line widths range is 10–100 Hz, the effect is negligible. On the other hand, MAS- and wide line NMR spectra of glasses can be as wide as 10 kHz, in which case 27% of the signal is lost during a 10 μs dead time (assuming exponential decay). Under such conditions, the effect can obviously introduce severe absolute and relative quantitation errors if two lines with substantially different widths are compared. By using a range of delayed acquisition experiments, it is sometimes possible to calibrate the signal loss, but such a procedure still suffers from the fact that the true shape of the FID during the deadtime must be guessed. The deadtime problem can also be circumvented by acquiring the spectrum with a $90°$-τ-$180°$ spin echo method. Variable τ values must be used in order to account for quantitation artifacts due to the irreversible dephasing of magnetization during the evolution time 2τ.

With the above discussion in mind, scepticism is appropriate whenever glass structure models are discussed on the basis of NMR experiments that do not maintain sufficiently rigorous protocols for quantitative signal excitation or detection.

5. SILICATE GLASSES

The great interest in the structure of silicate glasses stems from the importance of these glasses as structural and optical materials compared to other glass-forming systems, and from the pivotal importance of molten silicates in the Earth Sciences.

The first NMR study explicitly addressing the network structure of silicate glasses was carried out by Müller-Warmuth and coworkers using ^{29}Si rapid adiabatic passage and cw wideline NMR;[105] additional compositions in the K_2O–SiO_2 system were later investigated with this technique by Harris and Bray.[106] Meanwhile, the benefits of increased magnetic fields and line-narrowing techniques, first demonstrated in 1982, have led to an explosive development of research activity. Detailed answers have emerged to many questions that are central to an understanding of the glassy state. Such vital questions include, but have not been limited to (1) the Si–O–Si bond angle distribution, (2) the distribution of non-bridging oxygen atoms introduced by network modifiers, (3) the spatial distribution of alkali and alkaline-earth metal cations, (4) the structural role and the distribution of intermediate oxides such as Al_2O_3, (5) anion substitution effects (F, C, N), (6) the speciation and structural role of water, (7) the effect of high pressures, and (8) the influence of sol–gel processing upon the structure of these glasses. A brief summary of these issues is given in Fig. 17.

5.1. *Bond Angle Distribution in Vitreous SiO_2*

In spite of the rapid development of new and unusual glass compositions during the last decade, SiO_2 (silica) remains the archetypical example of a glass-forming material. It has generally been recognized that glassy silica retains the tetrahedral $SiO_{4/2}$ environment present in all of the silica

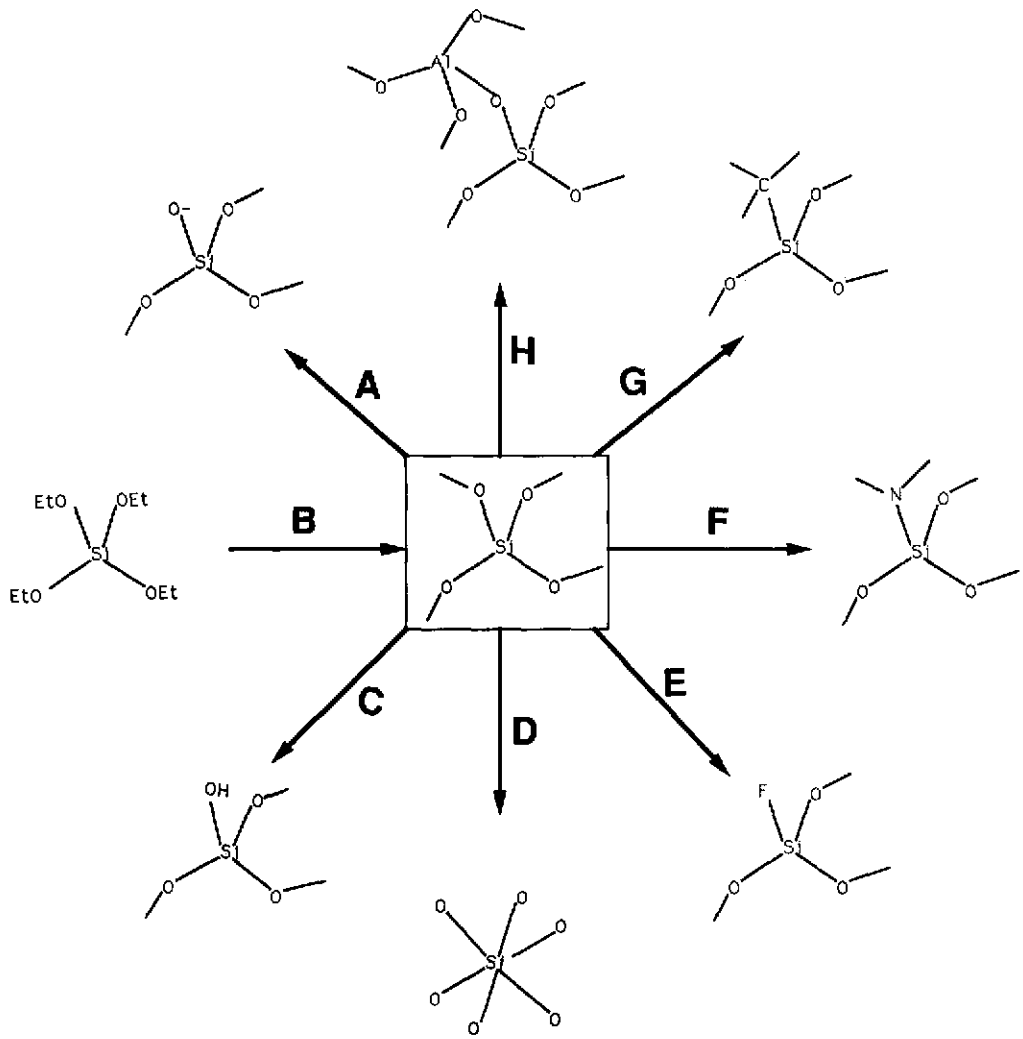

FIG. 17. Issues concerning silica-based glasses that have been addressed by solid state NMR methods: (A) network modification by alkali ions; (B) glass synthesis by the sol–gel method; (C) hydrolysis; (D) coordination change at high pressures or in the presence of P_2O_5 and alkali; (E) nearest neighbor substitution (oxyfluoride glasses); (F) nearest neighbor substitution (oxynitride glasses); (G) nearest-neighbor substitution (oxycarbide glasses); (H) next-nearest neighbor substitution by alumina and other network forming oxides.

ambient-pressure polymorphs. Theoretical calculations show a very broad energy minimum in the Si–O–Si bond angle distribution F_α(Si–O–Si).[107] Glass formation in silicates is generally attributed to an unusually pronounced variability of Si–O–Si bond angles, resulting in the lack of long-range ordering. Therefore, a numerical evaluation of the Si–O–Si bond angle distribution function is the heart of understanding the glassy state in such systems; NMR spectroscopy has made notable contributions to this issue. Figure 18a shows a representative spectrum. A single broad line is seen, whose width is governed by a distribution of chemical shifts. Benchmark studies on crystalline model compounds reveal a systematic correlation between $\delta_{iso}(^{29}Si)$ determined from MAS and α(Si–O–Si).[108] Based on an empirical least squares fit between $\delta_{iso}(^{29}Si)$ and the mean Si–O–Si bond angle, it was initially suggested that these two quantities are linearly correlated. However, on

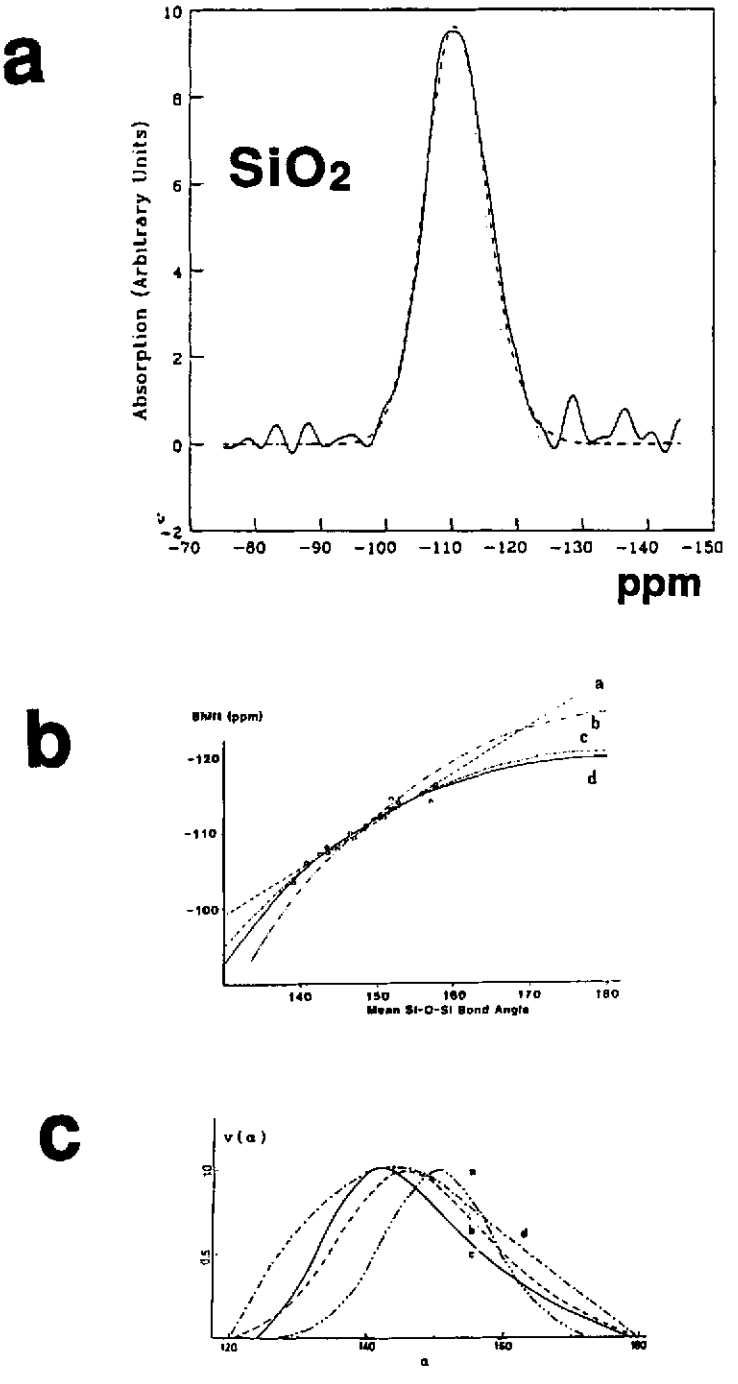

FIG. 18. (a) Experimental ^{29}Si NMR spectrum of SiO_2 glass. Reproduced with permission from Ref. 114. (b) Plots of ^{29}Si NMR chemical shift against mean bond angle using the (a) linear model, (b) point charge model, (c) secant model, and (d) *s*-hybridization model. Experimental data for different silica polymorphs are shown as points. Reproduced with permission from Ref. 113. (c) The deduced bond angle distribution using the (a) linear model, (b) point charge model, (c) secant model and (d) the *x*-ray result by Mozzi and Warren, *J. Appl. Cryst.* **2**, 164 (1969). Reproduced with permission from Ref. 113.

theoretical grounds the paramagnetic component of the ^{29}Si chemical shift is expected to correlate linearly with the degree of *s*-character of the bridging oxygen atoms. Since the latter is calculated by the well-known relationship

$$s = \cos\alpha(\text{Si–O–Si})/(\cos\alpha(\text{Si–O–Si}) - 1), \tag{37}$$

the correlation between chemical shift and bond angle is actually non-linear. A least-squares treatment of the experimental data results in the equation

$$\delta_{iso} = -247.05\, s + 2.19 \tag{38}$$

where *s* denotes the mean *s* hybridization parameter over the four Si–O–Si bonds present for a given site.[109] Analyses based on the Si–O overlap integrals[110,111] and incorporation of point charges arising from second-nearest neighbors[112] lead to essentially similar functional dependences, all of which are shown in Fig. 18b.[113] At the present time, however, none of these models alone can be considered satisfactory, since none of them predict the NMR spectrum of tridymite with sufficient accuracy.[113]

The ^{29}Si MAS-NMR spectrum of vitreous silica yields an approximately Gaussian lineshape centered at -112 ppm with a full width at half height of 11.5 ppm.[114] Minor differences in the experimental results reported by different groups are most likely due to uncontrolled water contents of the samples investigated. These water contents result in variable contributions from OH-bearing silicon species to the lineshape,[114,115] and possibly also influence the bond angle distribution.[116] Under the usual MAS-conditions (3–5 kHz) in samples containing ^{29}Si at natural abundance, the lineshape is entirely governed by a distribution of isotropic chemical shifts. Thus, using expression (38) or one of the correlations shown in Fig. 18b, this shift distribution can be translated into the Si–O–Si bond angle distribution function. Figure. 18c shows the result for the different models.[113] While uncertainty remains as to which of the correlations is most realistic, a common conclusion made from this work is that F_α(Si–O–Si) in glassy silica is narrower than previously deduced from X-ray diffraction[117] and that the most probable Si–O–Si bond angle lies between 142° and 151°. F_α(Si–O–Si) can apparently be modified by exposure to high pressure and to neutron irradiation.[118] Naturally occurring opals seem to have a somewhat narrower bond angle distribution.[119]

Initial attempts at relating ^{17}O wideline NMR data of vitreous silica to bond angle distributions have been reported, albeit with lower accuracy.[120] In principle, ^{17}O NMR would be the more direct probe for addressing this issue. To this end it will be necessary to separate the distributions in e^2qQ, η, and δ_{iso} by wideline, MAS, and DOR studies over a wide range of magnetic field strengths. Also, extensive benchmark studies of crystalline model compounds will be useful.

5.2. *Network Structure of Silicate Glasses*

5.2.1. *Formation of $Si^{(n)}$ Sites and Their Analysis by ^{29}Si NMR.* It is well-known that the incorporation of alkali and alkaline-earth oxides into glassy silica has a profound effect on the thermomechanical behavior of silicate glasses, indicating a depolymerization of the SiO_2 network.[62–65] This experimental result is understood in terms of the traditional network modification model, where each molecular unit of alkaline oxide leads to the breakage of one Si–O–Si bridge, resulting in two non-bridging oxygen atoms. This depolymerization could lead to five distinct silicon microstructures ($Si^{(n)}$ species, also labeled $Q^{(n)}$ species in the literature), all of which are well-known in the crystal chemistry of silicates. These units are defined in Fig. 19, which also summarizes their NMR behavior. Extensive work on such crystalline model compounds has shown that each type of $Si^{(n)}$ units falls within a fairly distinct isotropic ^{29}Si chemical shift range.[121–123] Further distinction can be made by the chemical shift anisotropies: $Si^{(4)}$ and $Si^{(0)}$ species have cubic point symmetry, hence resulting in zero chemical shift anisotropies. In contrast, $Si^{(1)}$ and $Si^{(3)}$ species have axial symmetry, giving rise to powder patterns such as that shown in Fig. 6b, whereas $Si^{(2)}$ is distinguished by a non-axially symmetric chemical shift pattern (Fig. 6c).

Assuming that the $Si^{(n)}$ speciation also exerts the dominant effect on ^{29}Si isotropic chemical shifts in silicate glasses, peak deconvolution of MAS-NMR spectra (Fig. 20b) can be used to quantitate these

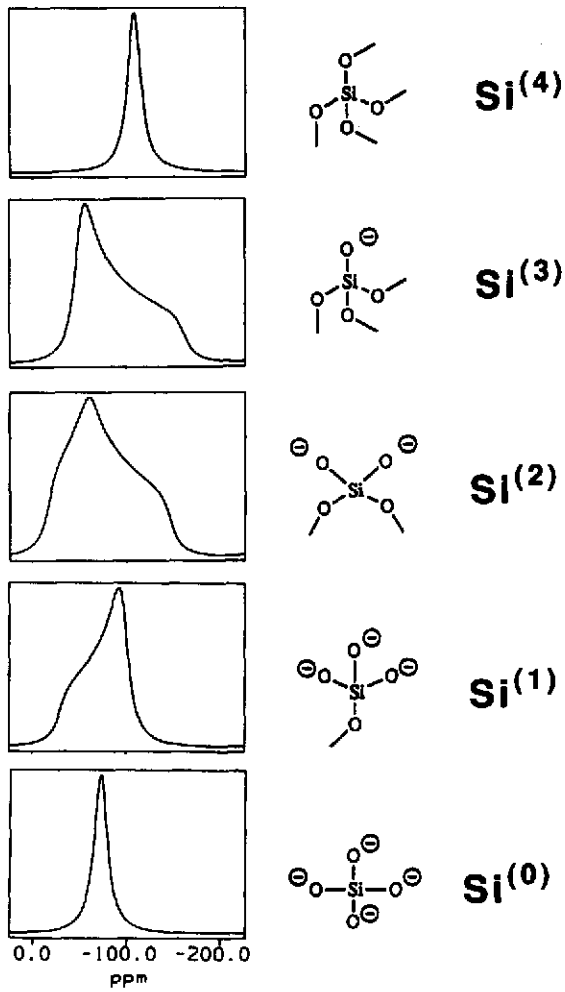

FIG. 19. $Si^{(n)}$ (also labeled $Q^{(n)}$ in the literature) species in alkali silicate glasses and their static chemical shift powder patterns.

species. Generally, Gaussian lineshapes are assumed. Justification for this approach comes from the fact that the species distributions derived in this fashion (with some exceptions) are found to be quantitatively compatible with the amount of non-bridging oxygen introduced with the network modifyer.[124-127]

$Si^{(4)}$ species can be quantitated independently from non-spinning ("wideline") NMR spectra.[128-130] The analysis takes advantage of the fact that, due to the near-zero chemical shift anisotropy, $Si^{(4)}$ species give rise to fairly narrow wideline spectra, in contrast to $Si^{(3)}$ and $Si^{(2)}$ species, which have extended powder patterns due to sizeable chemical shift anisotropies. Figure 20a illustrates the spectral decomposition. Analyses of this kind require that the unobserved FID during the spectrometer dead-time (usually around 10 μs) be taken into consideration. During this deadtime, the FID's due to $Si^{(4)}$, $Si^{(3)}$, $Si^{(2)}$ species decay at different rates due to their differences in line widths, and hence $Si^{(4)}$ species concentrations derived from simple one-pulse experiments tend to be overestimates. More accurate numbers could in principle be obtained from spin-echo Fourier transform experiments.

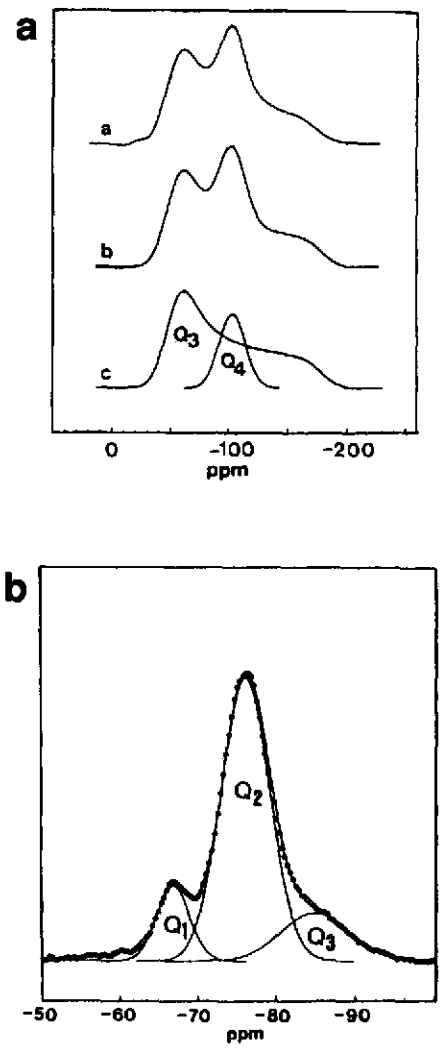

FIG. 20. Quantification of $Si^{(n)}$ structural units by spectral deconvolution. Top: experimental static ^{29}Si spectrum of $K_4Si_5O_{12}$ glass (a) and its deconvolution into individual chemical shift powder patterns associated with the $Si^{(n)}$ units (b) and (c). Bottom: ^{29}Si MAS-NMR spectrum of Na_2SiO_3 glass deconvoluted into Gaussian components. Reproduced with permission from Ref. 141.

5.2.2. *$Si^{(n)}$ Species Distribution and Cation Clustering in Binary Alkaline Silicate Glasses.* Although the ^{29}Si MAS-NMR data in most studies of silicate glasses are generally consistent with the balance of non-bridging oxygen atoms expected from the glass composition, the detailed quantitative distribution of these $Si^{(n)}$ units in alkali silicate glasses has been subject to controversy.[124-141] Some early studies have concluded that this distribution is "binary", i.e. contains a maximum of two $Si^{(n)}$ species, namely those that are present in the stoichiometric crystalline phases closest to the composition of the glass,[124,125] while others have preferred a more statistical distribution.[126] Figure 21 shows a representative dataset for the glass system Na_2O–SiO_2, and contrasts the quantitative predictions made by the two different models. Some of these earlier studies employ inappropriate fitting methods (ignoring spinning sidebands), are hampered by low signal-to-noise ratios, possibly affected by phase separation, and yield results inconsistent with the number of non-bridging oxygen atoms calculated

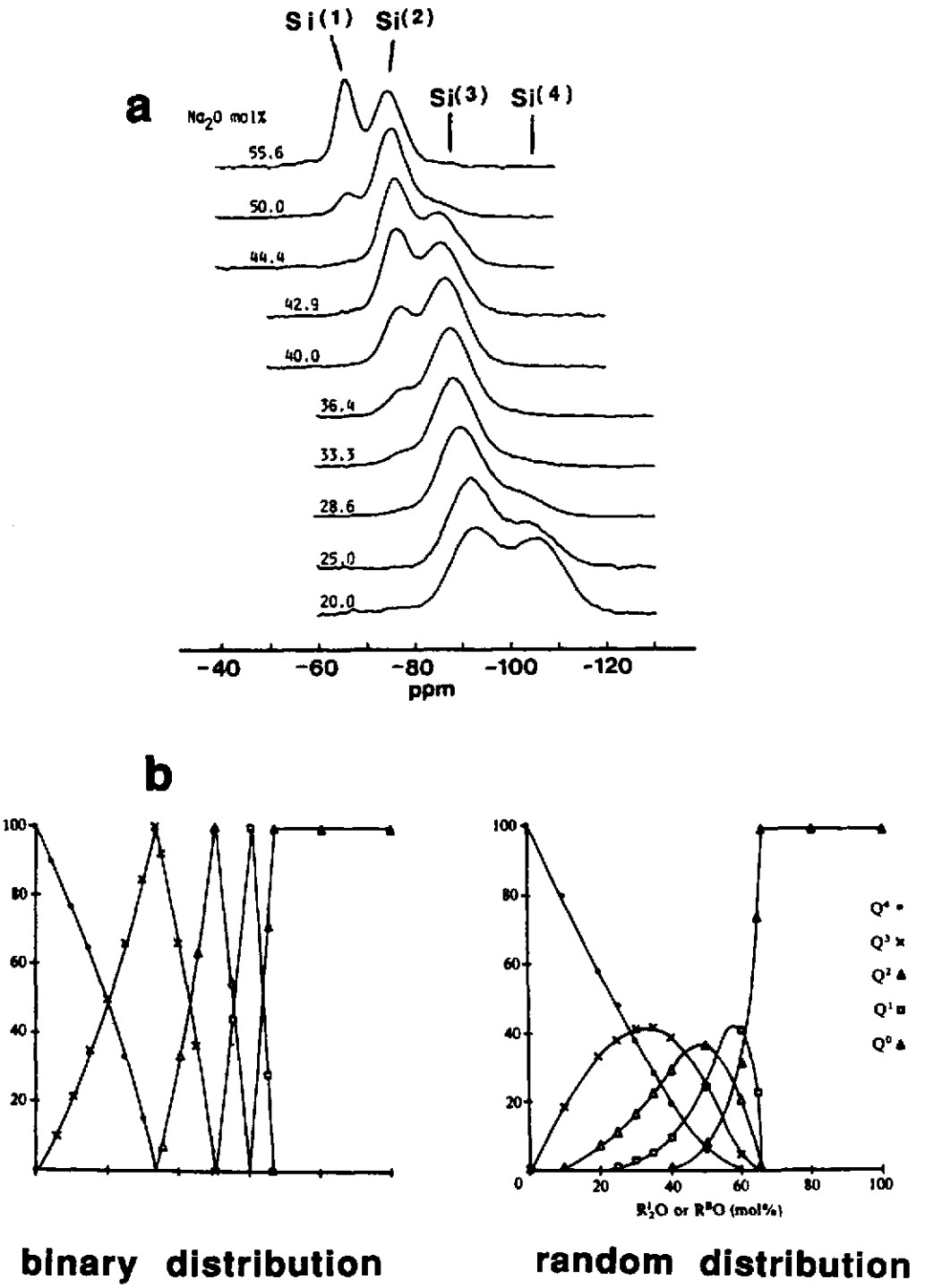

FIG. 21. (a) Compositional dependence of the ^{29}Si MAS-NMR spectra in the glass system Na_2O–SiO_2. Reproduced with permission from Ref. 141. (b) Quantitative predictions of the $Si^{(n)}$ species distributions in the binary and random model. Reproduced with permission from Ref. 144.

from the composition. The experimental results reported in more recent studies[128-141] in most cases detect clear deviations from the binary distribution. All of the more recent studies suggest, however, that the $Si^{(n)}$ distribution is far from random. It must be noted, that these conclusions are based on the fitting of heavily overlapping lines whose detailed shapes are unknown, and could still be severely biased by the commonly made assumption that the MAS-NMR lineshapes are Gaussian. As in the case of amorphous silica, the widths of these peaks are likely to be governed by bond angle distribution effects.[137]

Since the non-bridging oxygen atoms are considered to be in the direct vicinity of the alkali metal cations, the silicon speciation directly reflects the degree of dispersion of the cations in the glass. Maximum cation dispersion would result in a binary distribution, whereas in the case of cation clustering, deviations from this distribution would be expected. The specific effect of the alkali metal ion upon the detailed species distribution has been the subject of several comparative studies on glasses with constant M_2O/SiO_2 ratios. The results are summarized in Table 4. Not surprisingly, there are severe differences between results for identical systems investigated by different groups. Presumably this is due to the differences in the inherent assumptions made for the MAS- or wideline NMR analysis (see discussion above). On the other hand, there is a clear trend when glasses subjected to the same analysis procedure are considered. In general, the higher the cation field strength, the stronger the deviation from the binary distribution. This trend also implies that among the alkali ions, Li^+ has the strongest clustering tendency. In the Li_2O–SiO_2 system, this clustering in fact manifests itself in a tendency towards phase separation at Li_2O contents below 32 mole% Li_2O. Phase separation results in $Si^{(n)}$ lineshapes and average chemical shifts that are independent of the glass composition, and effects of this kind are clearly visible in some of the reported MAS-NMR spectra of the Li_2O–SiO_2 system. It should be pointed out that early, low-field, low-temperature, cw-NMR studies of ^7Li and ^{23}Na appear to provide some evidence of cation clustering in silicate glasses, although this effect is difficult to assess quantitatively due to the multiple contributions to the lineshape.[11,105] In principle, the selective measurement of ^7Li–^7Li dipolar couplings by spin echo spectroscopy should be able to quantify the degree of Li clustering in more precise terms.

The discussion of the $Si^{(n)}$ distribution in silicate melts can be cast in terms of the disproportionation reaction

$$2Si^{(3)} \rightleftarrows Si^{(2)} + Si^{(4)}; \tag{39}$$

characterized by a phenomenological equilibrium constant K,

$$K = [Si^{(4)}][Si^{(2)}]/[Si^{(3)}]^2 \tag{40}$$

which is accessible from the experimentally determined concentrations of each species. From careful analysis of wideline NMR spectra, K is determined to be 0.013 for glassy $Li_2Si_2O_5$.[129] Dupree *et al.*[135] conclude that $K = 0.022$ and 0.008 for $Li_2Si_2O_5$ and $Na_2Si_2O_5$ glasses, respectively. The difference in K again reflects the stronger tendency of the Li^+ cations to cluster, compared to the Na^+ cations. In corroboration of this trend, K is estimated to be close to zero for $K_2Si_2O_5$ glass.[138] A recent re-investigation has confirmed this trend, although the apparent equilibrium constants are generally found to be somewhat higher.[141]

The structural disproportionation of $Si^{(2)}$ and $Si^{(1)}$ species can be discussed in a similar fashion, and a similar trend with regard to the dependence on the counter-cation is observed.[141] Potassium metasilicate glass shows evidence for two $Si^{(2)}$ species, which have been assigned to chain and ring structures. The relevant temperature for these equilibrium constants K is the glass transition temperature T_g, at which all bond-breaking and bond-making processes are frozen in. By varying T_g over a range of 80 K (using different quenching rates) Brandriss and Stebbins showed that for $Na_2Si_2O_5$ glass, K for the reaction (39) increases with increasing temperature. From this temperature dependence, ΔH is estimated as 30 ± 15 kJ/mol.[142] Similar effects are observed in a mixed Na_2O–CaO–silicate glass.

Another aspect of silicate glass structure, recently addressed by NMR, is the connectivity of the $Si^{(n)}$ species. Specifically, the question is whether $Si^{(4)}$, $Si^{(3)}$, and $Si^{(2)}$ species are mainly bound among

TABLE 4. $Si^{(n)}$ speciation of M_2O–SiO_2 glasses with selected compositions

$M_2Si_4O_9$ (20 mol. % M_2O)

Alkali	$Si^{(4)}$	$Si^{(3)}$	$Si^{(2)}$	Ref.	Method	Chem. analysis	Remarks
Li(15.0)	55	45	0	125	MAS	no	low S/N, phase separated?
Li(15.0)	48.5	37	11.9	126	MAS	no	in conflict with O^- balance
Li(17.5)	47	41.1	11.9	126	MAS	no	phase-separated? conflict with O^- balance
Li(20)	37.2	50.4	12.4	126	MAS	no	phase-separated? conflict with O^- balance
Li(22.5)	32.8	63.2	3.9	126	MAS	no	phase-separated?
Li(20)	63	24	13	130	static	no	phase-separated? unusual δ_{iso} for Q^2
Na(15.0)	63	37	0	125	MAS	no	low S/N, fitting method unclear
Na(16.0)	56	43	1	141	MAS	no	
Na(20)	43.5	56.5	0	131	MAS	no	
Na(20)	50	50	0	131	MAS	no	isotopically enriched
Na(19.6)	52	48	0	124	MAS	yes	
Na(20)	48	51	1	140	MAS	yes	
Na(20)	50	48	2	141	MAS	no	
Na(20)	54	40	6	130	static	no	
K(17.2)	55	45	0	138	MAS	yes	
K(20)	57	35	8	130	static	no	
K(20)	33	66	0	131	MAS	no	inconsistent with O^- balance
K(20)	49	51	0	141	MAS	no	
K(22.3)	45	55	0	138	MAS	yes	
Rb(21.5)	47	53	0	135	MAS	yes	
Cs(23.3)	33	67	0	135	MAS	yes	

$M_2Si_2O_5$ (33.3 mol. % M_2O)

Alkali	$Si^{(4)}$	$Si^{(3)}$	$Si^{(2)}$	Ref.	Method	Chem. analysis	Remarks
Li(33.0)	21.9	57.3	14.6	126	MAS	no	
Li(34.0)	26.8	62.2	9.2	126	MAS	no	
Li(32.9)	10.2	79.6	8.2	134	static	yes	
Li(33.3)	14.5	71	14.5	130	static	no	
Li(33.3)		100		125	MAS	no	incorrect from spectrum inspection
Li(33.4)	22.6	55.8	21.6	133	MAS	yes	
Li(33.3)	22	63	15	141	MAS	no	
Li(33.3)	11.5	77	11.5	129	static	no	
Li(33.3)	8	81	11	127	MAS	no	
Na(30)	7	88	5	140	MAS	yes	
Na(33.3)	11	79	10	141	MAS	no	
Na(33.3)	8	84	8	127	MAS	no	
Na(33.3)	7.5	85	7.5	130	static	no	
Na(33.3)		100		125	MAS	no	
Na(33.3)		100		124	MAS	yes	
Na(33.3)	6.4	87.2	6.4	129	static	no	
Na(34.2)	7.2	85.6	7.2	128	static	yes	
Na(33.5)	17.4	61.7	20.9	133	MAS	yes	
K(33.3)	5.5	89	5.5	130	static	no	
K(33.0)		100		138	MAS	yes	
K(33.3)	7	86	7	141	MAS	no	
Rb(33.3)	3	94	3	130	static	no	
Cs(31.3)	9	91		135	MAS	yes	

themselves, thus forming "island-like" domains, or whether there is a sizeable fraction of interconnected $Si^{(n)}$ species. The observation that the chemical shift for a given $Si^{(n)}$ species depends on the composition of the glass argues against island formation.[124,139,140] More direct evidence comes from 2D COSY studies[143] on Na_2SiO_3 and $Na_2Si_4O_9$ glass, both enriched in ^{29}Si. The results, shown in Fig. 22, clearly confirm the existence of $Si^{(3)}$–$Si^{(4)}$ and $Si^{(2)}$–$Si^{(3)}$ cross-connectivities, although their quantitative extent is difficult to determine with this method. Significantly, the cross-peaks do not coincide exactly with the chemical shifts of the peak maxima seen in the regular 1D MAS spectra. Rather, the presence of a direct connection to a site with different n appears to shift the more polymerized sites further upfield, and the less polymerized sites further downfield compared to the peak positions of the unperturbed sites. It is not clear, whether inductive next-nearest neighbor effects or differences in the Si–O–Si bond angle distribution are responsible for this effect.

5.2.3. *$Si^{(n)}$ Species Distribution and Cation Clustering in Alkaline Earth Silicate Glasses and Related Systems.* Several attempts to extend the ^{29}Si MAS NMR analysis to the speciation of microstructures in alkaline earth silicate glasses have met with only limited success.[127,131] No clear site resolution is obtained, indicating that the spread of chemical shifts due to bond angle variations is comparable to the effect of the nonbridging oxygen. It was noted that there is a systematic trend for the ^{29}Si MAS-NMR linewidth to decrease with increasing size of the alkaline earth metal ion, but there is little hope that an unambiguous structural interpretation for this effect will be found.

Better site resolution is accomplished for lead silicate glasses.[7,45,144–146] This glass system forms over an exceptionally wide compositional region, extending to 70 mol.% PbO. The use of ^{29}Si static NMR is clearly inadequate in this case,[145] but MAS-NMR data can be explained consistently in terms of a $Si^{(n)}$ distribution that is very close to statistical.[144] This behavior contrasts sharply with that of the alkali metal ions. While Dupree *et al.* conclude that glasses containing 65 and 70 mol.% PbO contain mostly $Si^{(0)}$ units,[144] as expected from the stoichiometry, Kirkpatrick and coworkers cite Pb_2SiO_4 glass (66.6 mol.% PbO) as an interesting example of a $Si^{(n)}$ speciation that differs from the expectation based merely on stoichiometry.[45] Several crystalline Pb_2SiO_4 polymorphs are known, none of which has $Si^{(0)}$ sites, in spite of the orthosilicate composition. Comparisons of ^{17}O and ^{29}Si

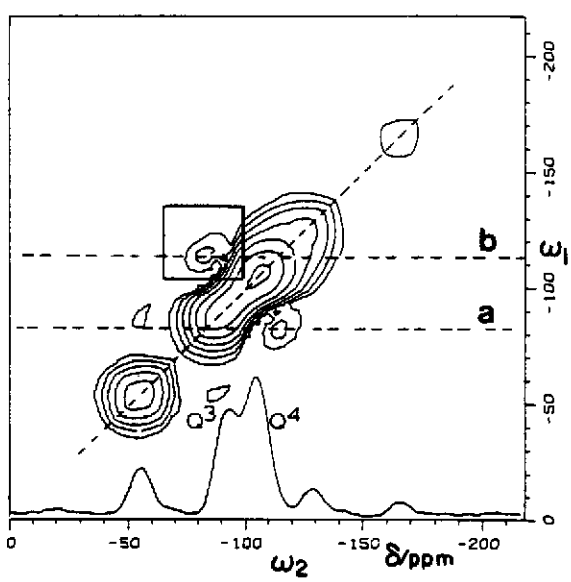

FIG. 22. Two dimensional ^{29}Si COSY spectroscopy of a glass with composition $Na_2Si_4O_9$. The $Si^{(3)}$–$Si^{(4)}$ connectivities are revealed by the existence of cross-peaks. Reproduced with permission from Ref. 143.

MAS-NMR data with those on crystalline model compounds[146] strongly suggest that the structure of the glass resembles that of the low-temperature polymorph, which contains dimeric $Si^{(1)}$ environments. This, in turn, implies that the glass must contain Pb–O–Pb bonds. Older ^{207}Pb chemical shift data on this glass system seem indeed to confirm this interpretation.[147]

5.3. *The Structure of Aluminosilicate Glasses*

Among all oxide glass systems studied, aluminosilicate glasses are perhaps those with the greatest geological significance as well as the most commonly used ones in daily life. Al_2O_3 is known as an "intermediate oxide"; incapable of forming glasses by itself or in combination with modifyer oxides, it can be introduced into glass-forming systems in great quantity. Introduction of Al_2O_3 into alkali silicate glasses enhances their thermal, mechanical and chemical stability to considerable extent, resulting in widespread practical applications. While this effect signifies that aluminum adopts a network-former role in these glasses, direct evidence for this idea had been lacking before the advent of NMR. Other questions, such as the effect of Al on the silicon speciation, and its possible role as a network modifying cation at certain compositions are still matters of considerable controversy. Not surprisingly, therefore, there has been tremendous activity in the structural exploration of these glasses, including an abundance of solid state NMR studies.

5.3.1. *Approaches, Promises and Limitations of MAS NMR in Aluminosilicate Glasses.* The structure of aluminosilicate glasses can be discussed in terms of 15 different $Si_m^{(n)}$ units, corresponding to SiO_4 tetrahedra with all possible permutations of n bridging oxygen atoms and m Al next-nearest-neighbors ($m \leqslant n$). Studies of crystalline model compounds show that the presence of Al next-nearest-neighbors has a strong effect on $\delta_{iso}(^{29}Si)$. Likewise, Fig. 23 illustrates that the ^{29}Si chemical shift of aluminosilicate glasses shows a distinctive dependence on the Si/(Si + Al) ratio.[51] What is unfortunate for the investigation of aluminosilicate glasses, however, is that changes in m as well as in n by one unit result in up or downfield shift effects of comparable magnitude, generally resulting in poorly resolved spectra whose interpretation is highly ambiguous. Because resolved peaks are generally not observed,

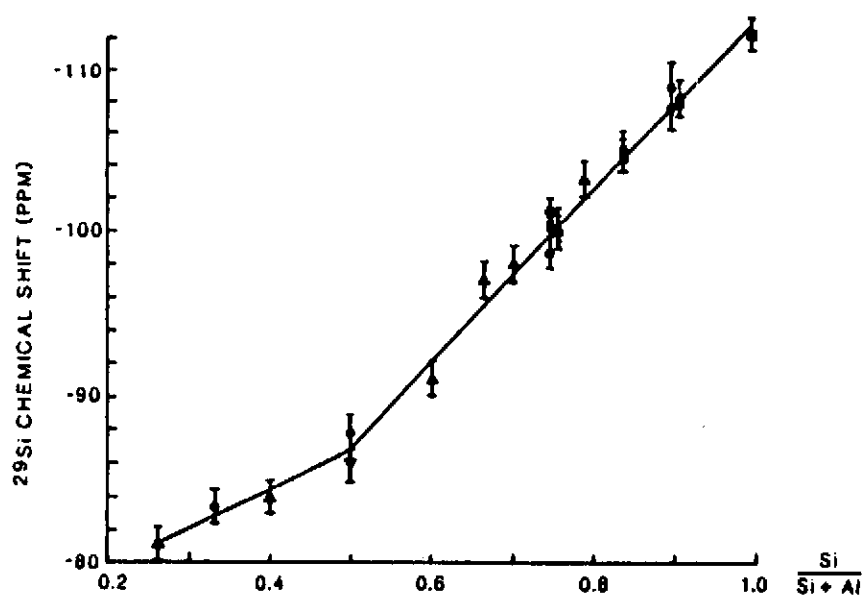

FIG. 23. Effect of aluminium next-nearest neighbor substitution in aluminosilicate glasses on the ^{29}Si chemical shift. The plot shows a correlation of $\delta_{iso}(^{29}Si)$ with the ratio Si/(Si + Al). Reproduced with permission from Ref. 51.

investigators have resorted to the use of the linewidths as indicators of the extent to which distributions in n and m are present. Due to the arbitrary way in which the linewidth is defined (full width at half height) and due to the multiple contributions to them, the conclusions based on such analyses must be treated with caution. It remains to be seen whether the use of more sophisticated statistical approaches, recently proposed for the spectral analysis of aluminosilicate glasses,[148,149] prove any more successful.

Due to the above-mentioned problems with ^{29}Si NMR, investigators have turned to the ^{27}Al resonance for additional information. ^{27}Al MAS-NMR offers a fairly easy chemical shift distinction between four-coordinate Al (Al^{IV}, 40 ppm $\leqslant \delta_{iso} \leqslant$ 80 ppm) and six-coordinate Al (Al^{VI}, -20 ppm $\leqslant \delta_{iso} \leqslant 20$ ppm). Recently, however, the picture has been complicated by the identification of five-coordinated Al sites (Al^{V}) with intermediate chemical shift properties and strong second-order shift contributions. Furthermore, complications intrinsic to NMR studies of half-integer quadrupolar nuclei make it difficult to obtain rigorous quantitative information about site populations: the signal arising from strongly distorted Al sites (of any coordination number) may go undetected, due to the inability of MAS to narrow second-order quadrupolar powder patterns beyond a certain width. This difficulty requires careful spin counting studies on weighed samples, using suitable standards. Since it is difficult to find defect-free solids, often liquid samples are employed as quantitation standards. Results of experiments of this kind have been reported in the literature. Using an unspecified method, Hallas *et al.* report that only a fraction of Al is being detected in their studies of sodium aluminosilicate glasses.[150] In contrast, Kirkpatrick and co-workers conclude on the basis of FID back-extrapolation studies on static samples that their ^{27}Al spectra of alkaline-earth aluminosilicate glasses are quantitative.[151] The latter conclusion rests, however, on the assumption that the unobserved free induction decay during the receiver dead-time after the pulse (40 μs in their experiments) has the form of an exponential. More extensive protocols, such as discussed in Section 4 may be required to settle this question. As a general rule such tests are crucial if quantitative information is sought from the NMR of nuclei subject to second-order quadrupolar perturbations.

5.3.2. *Silicon Site Speciation and the Coordination of Aluminium in Aluminosilicate Glasses.* The NMR data of aluminosilicate glasses appear generally consistent with a glass model in which the addition of aluminium to a binary alkali or alkaline-earth silicate glass successively increases the degree of polymerization, reducing the number of non-bridging oxygen atoms.[152] This occurs via formation of $AlO_{4/2}$ units which attract the positively charged cations. For advancing a structural discussion, it is useful to divide the glass into various compositional regions. Denoting the M_2O (or MO)/Al_2O_3 ratio as x and the Al_2O_3/SiO_2 ratio as y, these four regions are:

(1): $x=1$, and $y<0.5$;
(2): $x>1$, and $y<0.5$;
(3): $x>1$, and $y>0.5$;
(4): $x<1$, y assuming any value.

A detailed MAS NMR study of glasses in the system $CaO-Al_2O_3-SiO_2$ has been interpreted in these terms.[152] Glasses in region (1) are thought to form fully polymerized networks of $Si_m^{(4)}$ units, containing all of the Al in the form of $AlO_{4/2}$ - tetrahedra. In corroboration, ^{27}Al MAS-NMR studies show that all of the detected aluminium is four-coordinated.[152] Furthermore, a uniform ^{29}Si average chemical shift trend appears to reflect the statistics of Si/Al next-nearest neighbors. Likewise, a good correlation is found between $\delta_{iso}(^{29}Si)$ and $\delta(^{27}Al)$. The interpretation of $\delta(^{27}Al)$ is ambiguous, however, due to a contribution from the second order quadrupolar shift.

Glasses in region (2), where the modifier content exceeds the Al_2O_3 content, contain non-bridging oxygen atoms, i.e. $Si_m^{(3,2,1,0)}$ units, in addition to the $Si_m^{(4)}$ units, but otherwise unaltered Al environments. Again ^{27}Al MAS detects only Al^{IV}. All of the data in regions (1) and (2) are considered to be consistent with the Al–O–Al avoidance principle (Loewenstein's rule[153]). It must be admitted, however, that for glasses within this compositional domain NMR has done little more here than provide additional support to previously existing views.

The structure of glasses with Al_2O_3/SiO_2 ratios ≥ 0.5 (region 3) is of special interest, since due to their stoichiometry, they cannot follow the above structural model while adhering to the aluminium avoidance principle. Engelhardt *et al.* postulate that such glasses contain extra-framework aluminium in addition to Al^{IV}, which they claim is unobservable in their spectra due to strong quadrupolar couplings (and possibly wide distributions thereof) in highly distorted environments.[152] Specifically they suggest a $Si_4^{(4)} + Si_3^{(3)}$ distribution for the geologically important glass of composition $CaAl_2SiO_6$. This interpretation conflicts with the more ordered model of Kirkpatrick *et al.* who invoked exclusively $Si_4^{(4)}$ units, and a glass structure analogous to crystalline $CaAl_2SiO_6$.[151] As mentioned above, these authors also claimed that all of the aluminium is being detected in their experiments. More experimental and quantitative work is needed to clarify the structural role of aluminium in this region.

An interesting situation arises in glasses with $CaO:Al_2O_3$ ratios less than one (region 4). Due to charge balance constraints, the "excess" aluminium cannot be present in the form of AlO_4^- units. Two possibilities exist: (a) Al^{3+} might act as a network modifier and hence depolymerize the silicate network, leading to the appearance of $Si^{(n)}$ units with $n<4$; or (b) Al participates in the formation of neutral units such as $Al(AlO_2)_3$ species or "triclusters".[154] Based on ^{29}Si NMR data, which do not reveal an increase in the amount of non-bridging oxygen species, Engelhardt *et al.* favor the second alternative.[152] The ^{27}Al MAS-NMR spectra of the glasses with the highest excess in aluminium show a new, six-coordinated, type of Al species, in addition to the tetrahedral site. This behavior is nicely consistent with some early cw ^{27}Al NMR data on $K_2O/Al_2O_3/SiO_2$ glasses, which show dramatic linebroadening effects (albeit no site resolution) when the K_2O/Al_2O_3 ratio drops below 1.[155,156] The exact details of the Al environments in this compositional region are still not clear, however.

Notwithstanding the methodological difficulties and constraints mentioned above, aluminosilicate glasses have been the subject of numerous other NMR studies.[157–169] Table 4 summarizes the chief conclusions from this work, illustrating that important qualitative information is often available from a detailed inspection of the compositional dependences.

Recently, roller-quenching techniques and sol–gel methodology have made possible the preparation of modifier-free binary Al_2O_3–SiO_2 glasses.[170–172] The quenched material is phase separated, whereas the sol–gel derived material appears to be single-phase. This difference manifests itself in the ^{29}Si MAS-NMR spectra, which suggest stronger Al–O–Si connectivity in the dehydrated gel material. The ^{27}Al MAS-NMR spectra (see Fig. 24) are fairly complex and reveal the presence of Al^{IV}, Al^{V}, and Al^{VI}. Upon heat-treatment above 950°C the samples convert to mullite ($Al_6Si_2O_{13}$). A detailed structural interpretation of these effects must await a reliable relative quantitation of these species. Considerable interest has also been devoted to the structural characterization of amorphous aluminosilicate gels, which are important catalytic materials. NMR studies show that these materials have basically disordered and disrupted zeolite-like atomic arrangements, containing both Al^{IV} and

TABLE 5. Chief conclusions made from NMR studies of aluminosilicate glass systems

System	Ref.	Main conclusion
Na_2O–Al_2O_3–SiO_2	150	only Al^{IV} detected
Na_2O–Al_2O_3–SiO_2	168	thermal history effects
CaO–Al_2O_3–SiO_2	152	some Al^{VI} for $Al_2O_3/CaO>1$
$CaO(MgO)$–Al_2O_3–SiO_2	157	only Al^{IV} detected
$CaO(M_2O)$–Al_2O_3–SiO_2	158, 159	alkali metal influences δ_{iso}
$NaAlSi_3O_8$–$NaBSi_3O_8$	160	only Al^{IV} detected
$CaMgSi_2O_6$–$NaAlSi_3O_8$	165	Al increases degree of Si-polymerization
$MAlSi_3O_8$ (M = K, Na, Ca)	167	systematic linewidth changes
$NaAlSi_3O_8$–$CaAl_2Si_2O_8$	161	tentative Si speciations
$Na(K)AlSi_3O_8$–SiO_2	166	all glasses fully polymerized
$CaMgSi_2O_6$–$CaAl_2SiO_6$	151	Al increases degree of Si-polymerization;
$CaAl_2Si_2O_6$–$CaMgSiO_6$–Mg_2SiO_4	162	all Al detected and in AlO_4^- coordination
$Na_3Al_2Si_4O_{12}F$ etc.	169b	some Al^{V} and Al^{VI}
$(Al_2O_3)_x$–$(SiO_2)_{1-x}$	170, 171	Al^{IV}, Al^{V}, Al^{VI} present simultaneously

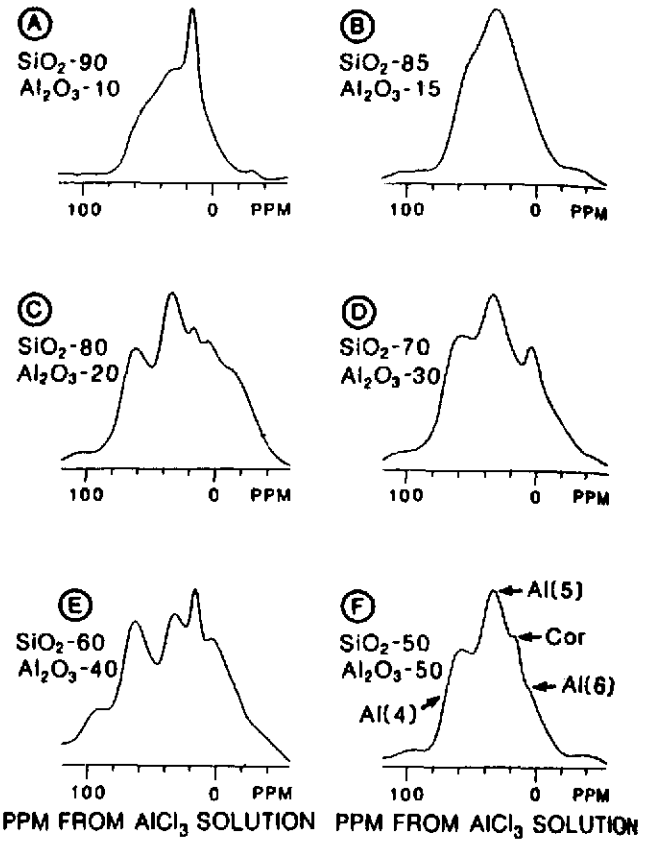

FIG. 24. ^{27}Al MAS-NMR spectra of melt-quenched binary SiO_2–Al_2O_3 glasses. Reproduced with permission from Ref. 170.

Al^{VI} species to variable extents.[173–176] Site resolution in this case is accomplished best by 2D nutation NMR.[177]

5.4. *Anion Substitution in Silicate Glasses*

Partial replacement of oxygen by fluoride, nitride, or carbide ions influences both the optical and mechanical properties of silicate glasses. A number of NMR studies have been carried out to study the influence on the structural properties.[133,178,179,181,182,185–187] In an exemplary application of dipolar ^{19}F spin echo spectroscopy, Duncan *et al.* studied the atomic distribution of small amounts of fluoride in glassy silica.[178] In principle, the incorporation of fluorine could generate $SiO_{3/2}F$, $SiO_{2/2}F_2$, $SiO_{1/2}F_3$, and SiF_4 coordination environments, which are easily distinguishable on the basis of the homonuclear ^{19}F–^{19}F dipolar coupling. Dipolar spin echo spectroscopy of a glass containing 1.03 wt% F reveals that only the first two units are present. The $SiO_{2/2}F_2$ units, which contain two closely spaced fluorine atoms are responsible for the fast decay at short evolution times ($2t_1 < 0.2$ ms), whereas the less strongly coupled F atoms in the $SiO_{3/2}F$ units give rise to a much slower spin echo decay at longer evolution times. The experimentally determined spin echo decay data are compared with simulations based on the three different ^{19}F–^{19}F pair radial distribution functions depicted in Fig. 25a. This comparison (Fig. 25b) reveals that the fraction of $SiO_{2/2}F_2$ units is substantially enhanced over the statistical probability. Most recently, the location of fluoride in jadeite glasses was

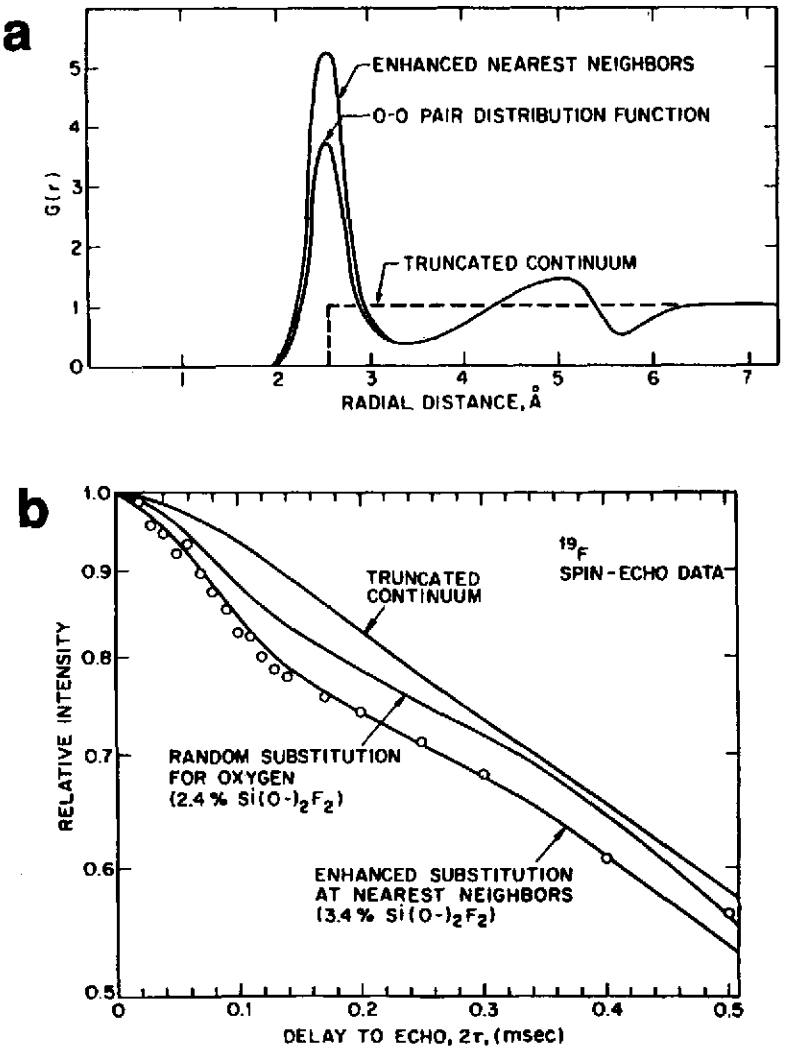

FIG. 25. (a) Hypothetical radial distribution functions $G(r)$ for ^{19}F–^{19}F pairs in amorphous SiO_2. The O–O pair distribution function is based on a molecular dynamics simulation. (b) Experimental ^{19}F spin echo decay functions and comparison with decay predicted by the three radial distribution functions in (a). Reproduced with permission from Ref. 178.

studied by ^{19}F–^{27}Al CPMAS NMR.[169b] The results confirm that the fluoride ions bind selectively to Al atoms, and convert them partially into Al^{V} and Al^{VI} species.

Nitridation of silicate glasses is known to result in desirable thermo-mechanical properties such as increased glass transition temperatures, viscosity, hardness and a reduction in the thermal expansion coefficient.[180] These effects are generally attributed to the partial substitution of bridging oxygen by bridging nitrogen atoms, which results in a higher degree of polymerization of the glass. Si–N bonds are easily detected by ^{29}Si MAS-NMR, as coordination of silicon to nitrogen causes the ^{29}Si resonance to move downfield. This effect can be exploited to estimate the average number of Si–N bonds. In nitrided aluminosilicate glasses, N shows a distinct preference for Si over Al.[182] Unfortunately, the limited spectroscopic resolution precludes further quantitative interpretations.[133,181,182]

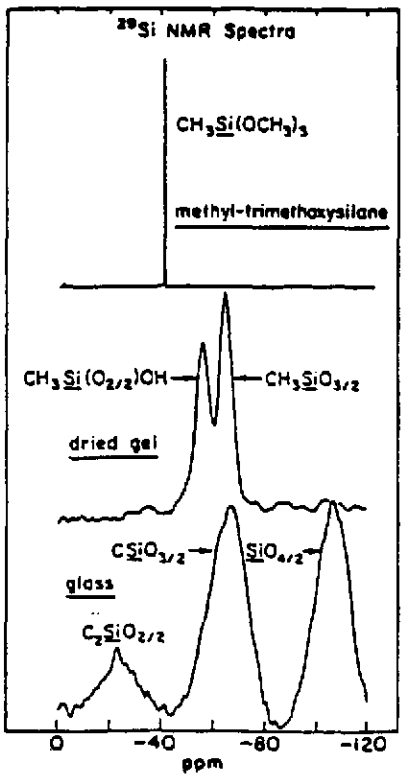

FIG. 26. ^{29}Si NMR spectra of oxycarbide glass and precursor: top: methyltrimethyloxysilane, middle: dry gel, bottom: final glassy product. Reproduced with permission from Ref. 187.

Recently, there has been substantial interest in the synthesis and characterization of silicon oxycarbide glasses.[183,184] These materials can be synthesized via sol–gel routes from precursors containing silicon–carbon bonds, followed by high-temperature treatment. This treatment results in extremely hard materials of interest for ceramic fiber applications. ^{29}Si MAS-NMR has been instrumental in showing that materials prepared in this fashion have a silicon oxycarbide structure with mixed $SiO_{4-n}C_n$ local environments and are not segregated amorphous SiO_2/carbon mixtures.[185–187] Figure 26 shows typical ^{29}Si NMR spectra obtained for the precursor, the dried gel and the glassy material, illustrating excellent chemical shift resolution between the various $SiO_{4-n}C_n$ microenvironments.[187]

5.5. *Silicate Glass and Melt Structure at High Temperatures*

As discussed in Section 2, an important feature of glassy materials as contrasted to other crystalline or amorphous solids is the phenomenon of structural relaxation. The property is a consequence of long range molecular mobility activated above the glass transition temperature T_g. Studies of NMR lineshapes and relaxation parameters provide excellent ways of studying dynamical properties of glasses on a wide range of timescales. Very slow atomic motions (timescale ~ 1s) are sensitively detected by 1D or 2D chemical shift exchange spectroscopy. NMR lineshape parameters are affected by motions with correlation times in the ms region, whereas the spin-lattice relaxation times are most sensitive to motions on the timescale of nuclear precession periods, i.e. 10^{-8} s.

Due to the fundamental geological importance of silicate melts, a number of high-temperature *in situ* studies have been carried out,[188–192] all of which have shown that for all practical purposes, the

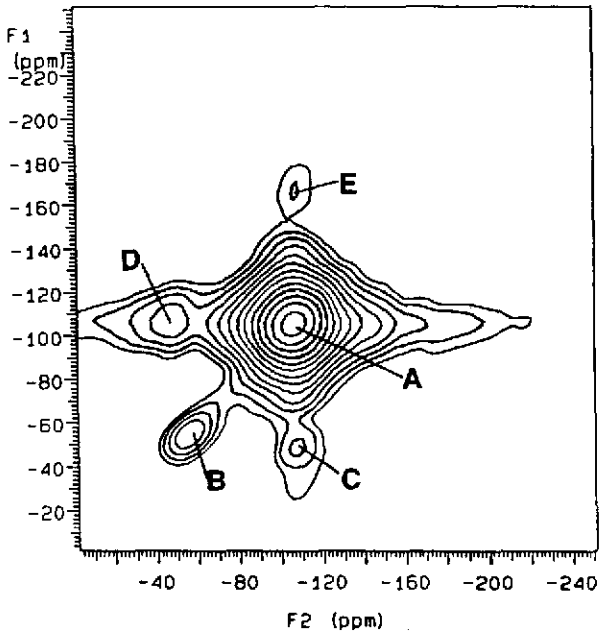

FIG. 27. Contour plot of the 2D chemical exchange ^{29}Si NMR spectrum of $K_2Si_4O_9$ glass at 571° C. The cross-peaks C and D reveal that the $Si^{(4)}$ and $Si^{(3)}$ species are in chemical exchange with each other. Feature E possibly reflects a five-coordinated silicon species (Si^{V}) in equilibrium with $Si^{(4)}$. Reproduced with permission from Ref. 188.

network structure of silicate glasses below T_g can be viewed as rigid. 2D ^{29}Si chemical exchange spectroscopy has shown that in glassy $K_2Si_4O_9$ the glass transition at 500°C is probably associated with a slow $Si^{(4)} \rightleftarrows Si^{(3)}$ site exchange process.[188] Figure 27 shows a typical result, obtained at 571°C. Site exchange manifests itself as a cross-peak (−106 ppm, −55 ppm) corresponding to the peak maxima of the static powder patterns of $Si^{(4)}$ and $Si^{(3)}$, respectively. The $Si^{(4)} \rightleftarrows Si^{(3)}$ site exchange process is very slow at this temperature, and thus has no effect on the static NMR lineshapes. Nevertheless these results establish, for the first time by NMR, a direct link between the glass transition and the Si–O bond breaking/bond making processes resulting in chemical exchange phenomena. This finding explains the NMR-established fact,[193] that fibers quenched during rapid shearing of liquids produce no local alignment. Since the Si–O bonds are so labile at temperatures as low as T_g, shearing cannot produce cooperative flow in this case or in other oxide glasses.[193]

Figure 28 shows that the $Si^{(3)}$ and $Si^{(4)}$ powder patterns persist up to 200°C above T_g. Above 700°C, the static NMR spectra of the $Si^{(3)}$ and $Si^{(4)}$ species are affected simultaneously by this site exchange process and by motional averaging of the chemical shift anisotropy and dipole–dipole couplings. When the temperature exceeds 1000°C, the lifetime of individual silicate tetrahedra becomes very short on the NMR timescale, resulting in chemical-shift averaged, sharp "liquid-like" lines. Although the resulting effect on the lineshape is rather complex, it is possible to simulate the chemical exchange effect and derive approximate exchange rates at different temperatures (see Fig. 28).[189a] The Arrhenius plot of exchange rate versus temperatures yields an activation energy of 179.4 ± 5.4 kJ/mole. Furthermore, from back-extrapolation of this line it is predicted that the exchange rate at T_g amounts to ca. 9 Hz.[189a] Results obtained for $Q^{(2)} \rightarrow Q^{(1)}$ site exchange in lithium silicate glasses with high lithium contents have led to similar conclusions.[189a]

Valuable information about molecular motional processes has also been obtained from T_1 measurements.[190–192] Generally, the temperature dependence of ^{29}Si T_1 in silicate glasses reveals a distinct discontinuity at T_g, whereas the T_1 of a mobile cation (such as ^{23}Na) is affected to a much lesser extent. These results provide supporting evidence for the central role of silicon motion in the

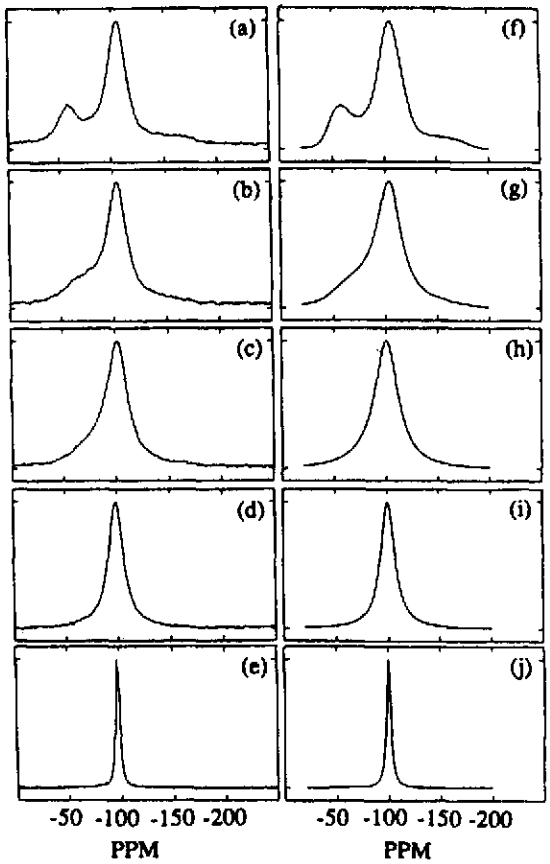

FIG. 28. Variable temperature ^{29}Si NMR spectra of $K_2Si_4O_9$ glass (a–e) and corresponding simulations (f–j) based on chemical exchange between $Si^{(3)}$ and $Si^{(4)}$ units. Temperatures and exchange rates are: (a) 697°C, (b) 774°C, (c) 800°C, (d) 847°C, (e) 997°C, (f) 2000 Hz, (g) 10,000 Hz, (h) 25,000 Hz, (i) 50,000 Hz, (j) 500,000 Hz. Reproduced with permission from Ref. 189a.

interpretation of the glass transition. The quantitative interpretation of the T_1^{-1} vs T curves at high temperatures in terms of molecular mechanisms and relaxation processes is rather complex and not yet fully understood.

5.6. *Silicate Glass and Melt Structure at High Pressures*

The structural behavior of silicate melts at high pressures is of central importance for the understanding of many geological processes occurring in the Earth's interior. Elevated pressure can affect the Si–O–Si bond angle distribution function, $Si^{(n)}$ speciation equilibria in silicate melts, and the silicon coordination number. As discussed below, ^{29}Si MAS-NMR has made important contributions to the quantitative elucidation of such pressure effects, hence considerably advancing the current state of knowledge.

Upon exposure to elevated temperature and pressure (50 kBar, 600°C) amorphous silica undergoes substantial densification (16%).[194] A 2.5 ppm downfield shift is observed in the ^{29}Si MAS-NMR peak maximum.[195] Consistent with X-ray diffraction work[196] this effect is interpreted in terms of a 5° shift in the Si–O–Si bond angle distribution function towards smaller values. This result is in qualitative agreement with previous MO calculations by Ross and Meagher.[197] However, assuming that correlation (37) still holds at elevated pressure, the NMR data would suggest that densification occurs

with no change in the width of Si–O–Si bond angle distribution function. This result conflicts both with theoretical predictions as well as with X-ray diffraction data.

While ambient-pressure silicates show silicon invariably in four-coordination, crystalline silicates formed in the Earth's interior at 500 km depth (where pressures are in the GPa range) have predominantly six-coordinated Silicon (Si^{VI}). Indeed, molecular dynamics simulations predict a transition of silicate melts from Si^{IV} to Si^{VI} at pressures in the GPa range.[198] Data on crystalline reference compounds show that the chemical shift range (−190 to −210 ppm) of Si^{VI} is quite distinct from Si^{IV}.[199–201]

Very recently, Stebbins and coworkers have identified small peaks in this chemical shift range in binary sodium and potassium silicate glasses quenched from 1500°C at high pressures and decompressed at room temperature.[202–204] They also observed a pronounced change in the Si^{IV} speciation present in these glasses, indicating a shift of the $Si^{(3)}$ disproportionation equilibrium (39) to the right side, and a new peak at −150 ppm.[202–204] The latter resonance is assigned to five-coordinated silicon (Si^{V}), an unprecedented species in the crystal chemistry of silicates (to this author's knowledge). Figure 29 illustrates nicely the gradual emergence of Si^{VI} and Si^{V} in $Na_2Si_4O_9$ glass as the pressure is increased.[202]

In a similar fashion, Al has been reported to convert to six-coordination in albite glass at 6–8 GPa and 1650–2000°C.[205] However, Stebbins and Sykes[206] could not reproduce this result. Also there appears to be no coordination change for silicon in this pressure range.

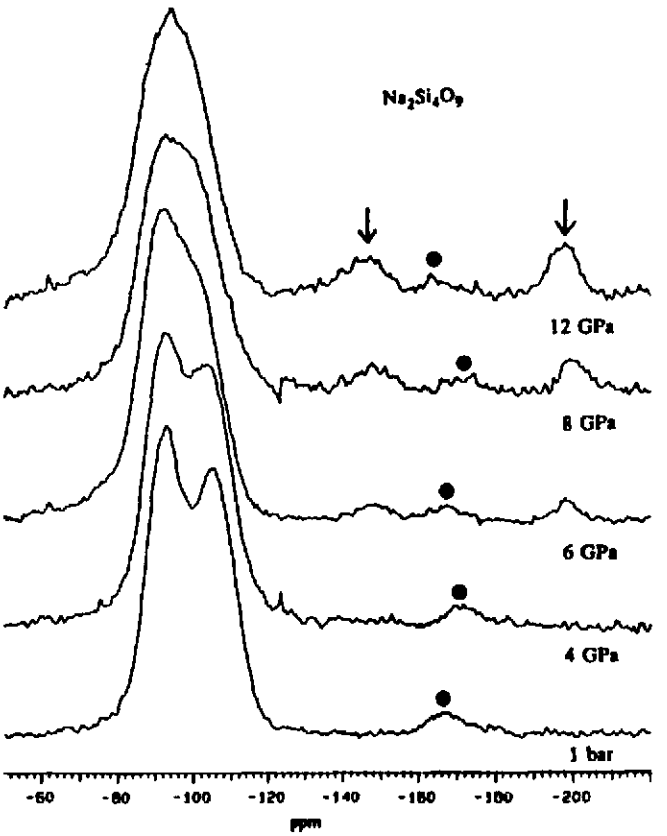

FIG. 29. ^{29}Si MAS-NMR spectra of glassy $Na_2Si_4O_9$ samples quenched from high temperatures and different pressures (listed in the figure) and decompressed at room temperature. The formation of Si^{V} and Si^{VI} indicated by the gradual emergence of peaks at −150 and −210 ppm (indicated by arrows) as the pressure is increased. Reproduced with permission from Ref. 202.

5.7. *The Interaction of Water with Silicate Melts and Glasses*

Silicate melts are known to dissolve considerable amounts of water at elevated temperatures and pressures. The nature and the structural properties of this water in the resulting hydrous glasses have received considerable attention in both geology and materials science.[207] From the standpoint of geology, water plays a crucial role in modifying phase equilibria and physical properties of magmas; hence much effort has been devoted to determining the concentration and chemical speciation of water in volcanic glasses and synthetic analogues of magmas.[208,209] From a materials science standpoint, the presence of even minute amounts of water has a dramatic effect on physical properties such as bulk modulus, melt viscosity, ionic conductivity and the optical absorption characteristics of glasses, hence influencing possible ranges of technological applications.[207] The latter is especially significant in view of the hydrous environments encountered in modern sol–gel processing techniques for silicate glasses (see below).

5.7.1. *Structural Characteristics of the Hydrous Species*

5.7.1.1. *The speciation of water.* Many previous experimental studies[207] suggest that water acts to depolymerize the silicate network, according to the reaction:

$$\text{Si–O–Si} + \text{H}_2\text{O} \rightarrow 2\,\text{Si–OH}. \tag{41}$$

Recent studies of infrared-overtone and combination bands indicate, however, that water in silicate glasses is present both in the form of OH groups, and as molecular water species.[208,209] This result is confirmed by ^{1}H wideline NMR spectra which appear to be superpositions of a broad Pake doublet attributed to H_2O, and a sharper Gaussian component assigned to OH groups.[210–214] Thus, eq. (41) has to be viewed as a chemical equilibrium. The determination of the equilibrium constant necessitates a separate quantification of OH and H_2O species. Other, more detailed, questions of interest include: (a) the strength of its interaction with the network oxygen atoms (O–H···O bond lengths); (b) the spatial distribution of OH and H_2O species in the network, (random or clustered), and (c) the motional properties of water molecules in glasses.

The relative amounts of OH and molecular H_2O species have been determined by ^{1}H MAS-NMR for a series of albitic glasses with water contents ranging from 0.5 to 8 wt% H_2O.[218,219] The left side of Fig. 30 shows typical experimental ^{1}H MAS-NMR spectra. Parallel studies were carried out on the model compounds tremolite and analcite as models for structurally isolated OH and H_2O groups, respectively (see Fig. 30, top). The spectra indicate that at the spinning speed employed (around 8 kHz), the OH groups give rise only to a strong centerband, because all the interactions affecting the static spectrum of the OH groups are effectively averaged by MAS. In contrast, 8 kHz MAS is unable to average the strong intramolecular dipolar interaction between the H atoms in the water molecule, resulting in a well defined spinning sideband pattern for this species. The OH/H_2O ratio can then be determined from the intensity of the sidebands relative to the centerband. A typical comparison between experimental and simulated sideband intensities is shown in Fig. 30, right side.

The main problem generally encountered in ^{1}H magic-angle spinning NMR is the strength of the homogeneous dipolar interactions among protons, which make it difficult to achieve significant line-narrowing at technically feasible spinning speeds. Thus, the well-resolved sideband patterns of Fig. 30 might seem surprising at first sight. However, in samples with a low hydrogen content, where the hydrous species are relatively isolated from one another, inhomogeneous line broadening mechanisms dominate. Specifically, theory predicts that the homonuclear dipolar interaction within an isolated pair of two spins is inhomogeneous, hence resulting in well-defined spinning sideband patterns upon MAS. This prediction has been verified experimentally on a number of crystalline hydrates.[220,222] Nevertheless, in the application of ^{1}H MAS-NMR to hydrous glasses, the use of spinning speeds $\geqslant 8$ kHz is crucial, since the effects of secondary ^{1}H–^{1}H dipole–dipole couplings and of the chemical shift anisotropy upon the spinning sideband intensities are eliminated only under fast-spinning conditions.

Figure 31 summarizes the resulting NMR-derived water speciation for various aluminosilicate glasses.[218,219] At low overall water contents, most of the hydrous species are present in the form of

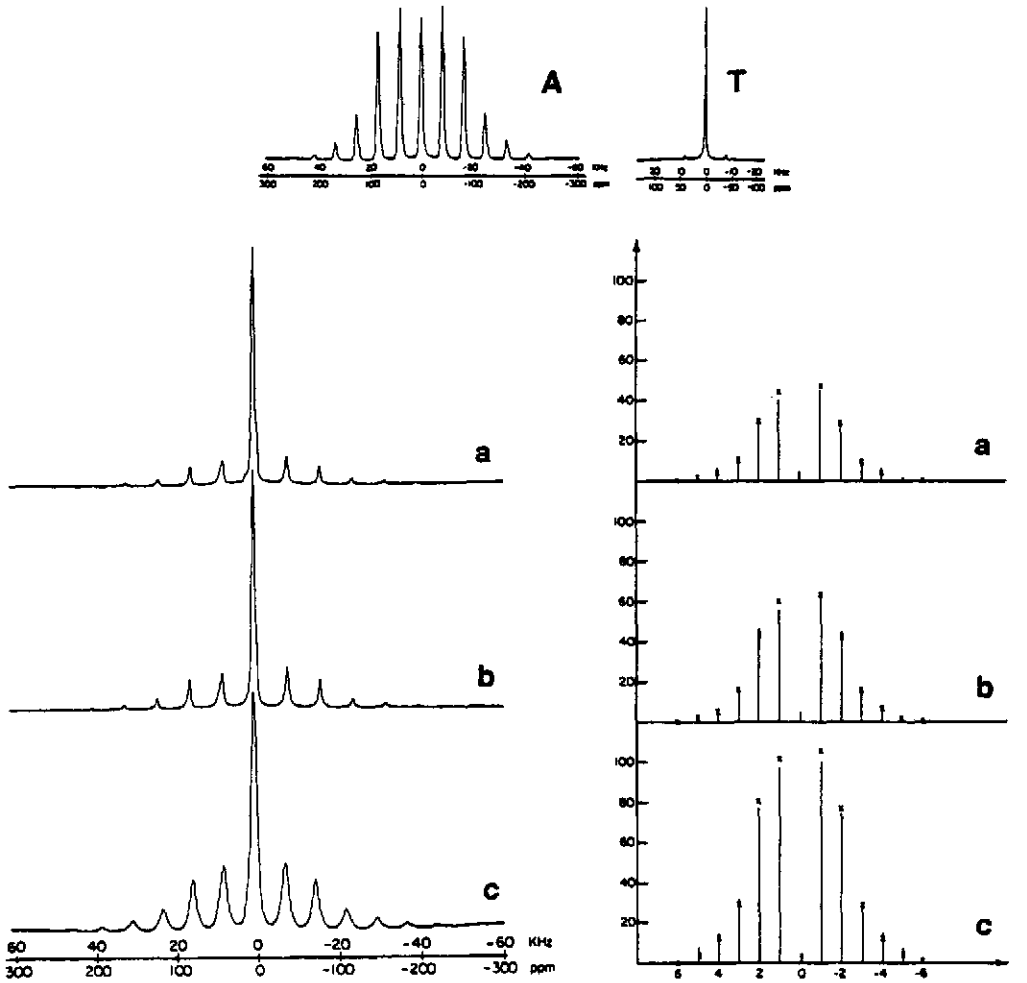

FIG. 30. ^1H high-speed MAS-NMR studies of hydrous silicate glasses. Left side: experimental spectra at 8 kHz spinning speed. Top: experimental spectra obtained on tremolite (T; model for structurally isolated OH groups) and analcite (A; model for structurally isolated H_2O groups). Right side: spinning sideband peak heights (in arbitrary units) for the same glasses. Solid lines are experimental results, crosses are heights predicted by additive superposition of the experimental spectra of analcite and tremolite, in a ratio such that identical heights for the centerbands (not shown here) result. Results for the following glasses are shown: (a) orthoclase glass, containing 1.5 wt% H_2O; (b) orthoclase glass containing 2.7 wt% H_2O, and (c) anorthite–silica–wollastonite glass containing 7.9 wt% H_2O. Reproduced from Ref. 219.

OH groups. This behavior is consistent with previous measurements on glasses with very low water contents.[215–217] As the water concentration increases, the OH species concentrations level off at 2–3 wt% H_2O, and the concentration of molecular water species increases steeply. The observed behavior agrees well with IR spectroscopic results, which are consistent with an equilibrium constant of ~0.2 characterizing the above reaction.[208,209] The overall intensity profile of the sideband pattern in the glasses reveals further that the OH and H_2O units are randomly distributed and not clustered.[218,219]

5.7.1.2. *Hydrogen bond strength characteristics.* Another question of interest is the strength of the interaction between the hydrous species and the silica network, i.e. the hydrogen bond strength

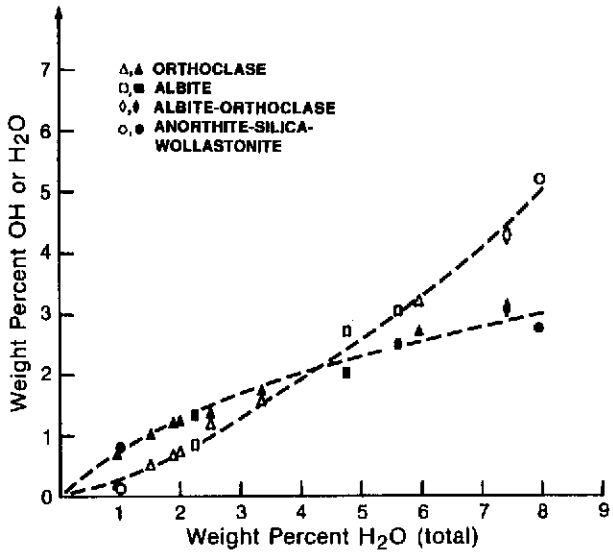

FIG. 31. Speciation of water in various silicate glasses. The different symbols indicate different glass compositions. Open symbols relate to H_2O contents, filled symbols to OH contents. The wt% is reported in terms of the amount of H_2O that would be released from the sample on heating. Reproduced from Ref. 219.

characteristics. Theoretical studies indicate that the ^1H chemical shift should be very sensitive to hydrogen bonding effects.[223] As a convenient measure of the hydrogen bonding strength, one may take the O–H···O distance of the hydrogen bond. A linear least-squares regression analysis of the ^1H chemical shift database on crystalline model compounds[219–222] yields:[219]

$$\delta_{iso}(\text{ppm}) = 79.05 - 25.5\,\text{d(O–H}\cdots\text{O) (Å)}. \tag{42}$$

This correlation allows us to estimate average hydrogen-bonding lengths in a variety of water-bearing silicate glasses. In albitic glasses the distribution is more-or-less uniformly centered around d(O–H···O) of 2.9 Å.[218,219] This result has been confirmed independently by measurements of the average ^2H quadrupolar coupling constant of D_2O-bearing glasses on the basis of a similar empirical correlation with O–D···O distances.[224] ^1H MAS-NMR spectra obtained on hydrous alkali silicate glasses reveal a decidedly bimodal behavior including rather short (2.6 Å) and longer (2.9 Å) distances.[225] The appearance of short H-bonds is believed to be due to strong coordination of OH groups to the non-bridging oxygen atoms in these glasses.

The location of the OH species in silica has been addressed more specifically by ^{29}Si CPMAS NMR.[226] Since cross-polarization requires the presence of ^1H–^{29}Si dipole couplings, only those silicon atoms that are near a hydrogen atom can be detected this way. This principle affords a selective amplification of the signal due to Si–OH groups. The spectra obtained are consistent with a model in which the reaction of water with the silica melt results mostly in Si–OH and only few $Si(OH)_2$ units. In sharp contrast, CPMAS NMR studies fail to detect any Si–OH groups in albite glasses. In a major departure from previous thinking, the authors hence suggest that reaction (41) is not applicable to this network.[227] The presence of water was found to perturb the ^{23}Na resonance quite strongly, indicating that there are significant OH···Na interactions.[227] Unfortunately, the spectroscopically observed effects do not lend themselves easily to a quantifiable result such as an average sodium–proton distance. It should be pointed out that the presence of strong alkali metal–proton interactions in glasses is not unprecedented. Effects of this kind were noted first by Müller-Warmuth and coworkers based on a detailed analysis of the heteronuclear contributions to the ^1H second moments in binary alkali silicate glasses with different modifier cations.[216]

5.7.1.3. *Motional properties.* Information about the motional properties of molecular water in silicate glasses has come predominantly from ^{2}H NMR of rhyolitic glasses obtained by autoclaving melts at 850°C with D_2O.[224] ^{2}H NMR lineshapes and spin-lattice relaxation times are extremely sensitive to motional effects. Figure 32a shows a typical ^{2}H NMR spectrum of a D_2O-containing silicate glass. This lineshape can be decomposed into two distinct contributions, b and c, which are shown in Fig. 32 together with corresponding simulations (d and e). Species b and c are characterized by a two-orders of magnitude difference in spin-lattice relaxation times. The spectrum of the rapidly relaxing component can be observed selectively by using very small recycle delays (10 ms). Its lineshape is characteristic of the motionally averaged powder pattern resulting from D_2O molecules undergoing two-fold rotations about their bisector axes at rates rapid compared to the NMR timescale (10^{-5} s). The lineshape of c, on the other hand, is typical of a rigid O–D deuterium species, with a close-to-axially symmetric quadrupole interaction tensor. The separation of D_2O and OD species on the basis of differences in T_1 is possible here (in contrast to glasses containing regular water) because the ^{2}H

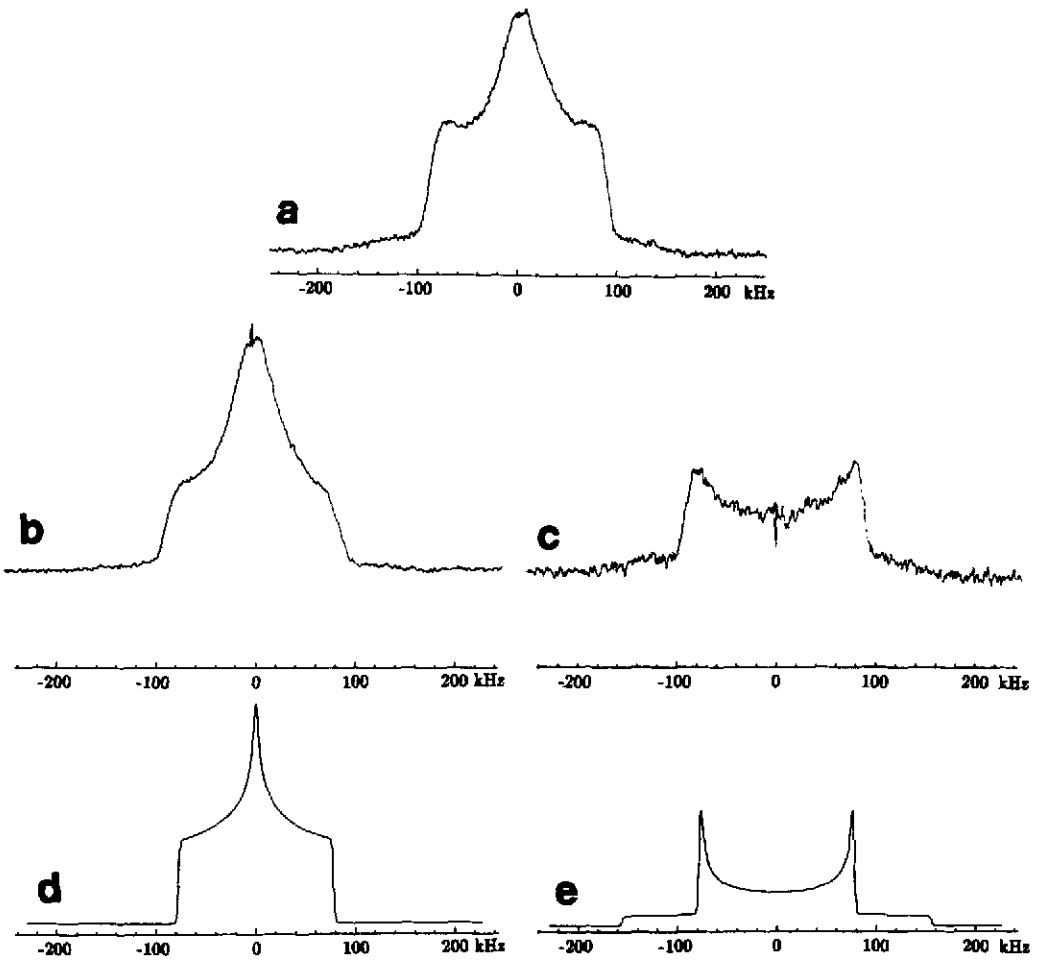

FIG. 32. ^{2}H NMR spectra at 76.8 MHz of rhyolitic glass containing 4.89 wt% D_2O. (a) Fully-relaxed spectrum; (b) partially saturated spectrum, resulting in selective detection of the D_2O species; (c) difference spectrum, assigned to the OD groups; (d) simulated spectrum for a D_2O molecule undergoing 180° flips; (e) simulated spectrum for a rigid OD species. Reproduced from Ref. 224.

quadrupolar interaction results in strong inhomogeneous broadening effects suppressing the spin diffusion mechanism.

5.7.2. *Interaction of Glasses with Water at Low Temperatures.* Structural effects of water have also been noticed at low interaction temperatures in the glassy, as opposed to the molten state. Hydrothermal leaching experiments carried out on a sodium aluminosilicate glass show pH dependent cation exchange, depolymerization, and water incorporation effects presumed to occur via a dissolution–reprecipitation mechanism.[228,229] The original ^{23}Na lineshape is strongly perturbed indicating the formation of a hydration shell surrounding this ion.

5.8. *Network Structure and Hydrogen Environments in Sol–Gel Prepared Glasses and Amorphous Silicas*

The "sol–gel" process used in the synthesis of oxide glasses is based upon the hydrolysis of a suitable monomeric precursor species. This hydrolysis product forms a colloidal solution ("sol") that undergoes polymerization ("gellation") upon standing. This heavily hydrated "gel" is then thoroughly dried and heated to remove residual water, resulting in further densification and eventually in bulk glassy material.[230] For silica-based glasses, the standard precursor is tetraethylorthosilicate (TEOS). The sol–gel process can be summarized by the following reaction schemes:

$$\text{hydrolysis:} \qquad Si(OEt)_4 + 4H_2O \rightarrow Si(OH)_4 + 4EtOH, \tag{43a}$$

$$\text{condensation:} \qquad n\,Si(OH)_4 \rightarrow [SiO_x(OH)_{4-2x}]_n + xn\,H_2O \tag{43b}$$

$$\text{dehydration:} \qquad [SiO_x(OH)_{4-2x}]_n \rightarrow n\,\text{“}SiO_2\text{”} + n\,(4-2x)/2\,H_2O. \tag{43c}$$

For the purpose of glass synthesis this process is appealing for several reasons. Since the low-temperature mode of synthesis avoids the molten state, it bypasses existing thermodynamic constraints. Therefore, it is often possible by copolymerization of suitable precursor species to prepare homogeneous glasses for systems that would show liquid–liquid phase separation in the melt. In certain cases, the sol–gel technique succeeds in extending the glass-forming region, hence making the synthesis of glasses possible that cannot otherwise be prepared. Finally, perhaps the most important advantage is the opportunity for the synthetic chemist to control the entire process, and concomitantly the structure and properties of the final product, by fine-tuning a large number of experimental parameters at each individual stage of the reaction. It is therefore not surprising that, since its inception, the low-temperature synthesis of silicate and other oxidic glasses by sol–gel chemistry has been the subject of intense research.

Of course, the processes summarized in eqs (43a–c) proceed via many steps. Substitution of OEt by OH occurs one moiety at a time, and the polymerization of the resulting $Si^{(0)}$ species yields more highly condensed $Si^{(n)}$ species, i.e. $Si^{(1)}$ (end groups), $Si^{(2)}$ (middle groups), $Si^{(3)}$ (2D-branching groups), and $Si^{(4)}$ (3D-branching groups). These species are in perfect analogy to those introduced in Section 5.1, except that they are terminated by OH rather than O^-.

Nuclear magnetic resonance has proven to be an excellent method for monitoring each stage of the reaction. Since the hydrolysis and the initial stages of polymerization of the hydrolysis products occur in homogeneous solution, they can easily be followed by standard liquid-state ^{29}Si NMR. A plethora of solution-state NMR studies have concerned themselves with the kinetics of the hydrolysis and polymerization stages, with the identification and quantification of molecular intermediates, and the effect of experimental parameters (pH, temperature, chemical additives, etc). Figure 33 summarizes the assignments for TEOS hydrolysis and condensation products. For TEOS hydrolysis, there is a monotonic chemical shift trend with increasing degree of OH substitution. Furthermore, dimeric species occur in a separate chemical shift region, while the various $Si^{(n)}$ sites present in the polymerization products are again nicely separated. The solution-state line widths of these peaks are much broader, due to a combination of increased spin–spin relaxation rates and chemical shift distribution effects. The numerous NMR applications investigating the mechanisms of hydrolysis and condensation in the liquid state are beyond the scope of this review, and the reader is instead directed to several key references.[231–238]

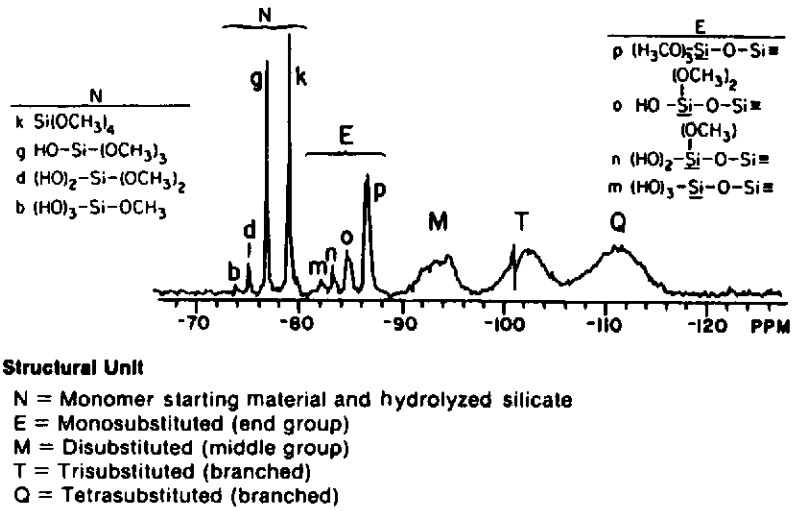

FIG. 33. Typical ^{29}Si solution state NMR spectrum of a TEOS hydrolysate/condensate. The various species are labeled in the figure. Reproduced with permission from Ref. 232.

The dehydration step (43c) converts the heavily hydrous silica gel to a bulk glass. Important issues at this stage are the structural identification and quantification of the various hydrogen environments present, the structural evolution of the silica framework (or whichever glassformer is studied), and the residual water content in the final glass. Incidentally, these questions are the same as those asked for the structural characterization of the well-known amorphous silica gels. Due to this similarity, and because the philosophy of the NMR application is essentially the same, the results on silica gels and sol–gel glasses will now be discussed together.

5.8.1. *Identification and Quantification of the Hydrous Environments.* $^{29}Si-^{1}H$ CPMAS has been of great utility for the selective detection of Si–OH groups. Figure 34, top, demonstrates that ^{29}Si chemical shifts generally differentiate quite well between $SiO_{4/2}$, $Si(OH)O_{3/2}$, and $Si(OH)_2O_{2/2}$ species (peaks A, B, and C, respectively). The peak assignments are based on the different cross-polarization dynamics of the silanol groups compared to those of Si atoms more removed from hydrogen. To illustrate this effect, Fig. 34, bottom, shows variable contact-time experiments obtained on a sample of silica gel.[239] CPMAS experiments with a contact time on the order of ca. 5 ms will lead to the selective enhancement of Si–OH resonances relative to other silicon atoms. While the CPMAS spectra do not lend themselves easily to quantification, this can be accomplished by ^{29}Si MAS-NMR one-pulse experiments. Though rigorously quantifiable, these spectra are usually much less-well resolved, due to the dominance of $Si^{(4)}$ groups. In practice, one therefore carries out both experiments. The CPMAS studies are used to characterize the $\equiv SiOH$ and $=Si(OH)_2$ groups by unambiguous lineshape parameters, which are then used for peak fitting in the less-resolved single-pulse spectra.

In the same fashion, $^{17}O-^{1}H$ CP enables the selective detection of the silanol oxygen.[240] The NMR parameters of this species are found to be clearly different from those of the bulk SiO_2 resonance. However, as in many applications of quadrupolar nuclei, it appears difficult to carry out this separation in a quantitative manner.

Complementary information has come from high resolution proton NMR, obtained either by fast magic-angle spinning, multiple pulse line-narrowing, or a combination of both. This technique permits the distinction of molecular H_2O, isolated SiOH groups and H-bonded SiOH groups. The assignment is carried out by combined dipolar dephasing and chemical exchange spectroscopy experiments.[241] Furthermore ^{1}H NMR spectroscopy is useful for detecting residual organic matter in the glasses.[242,243]

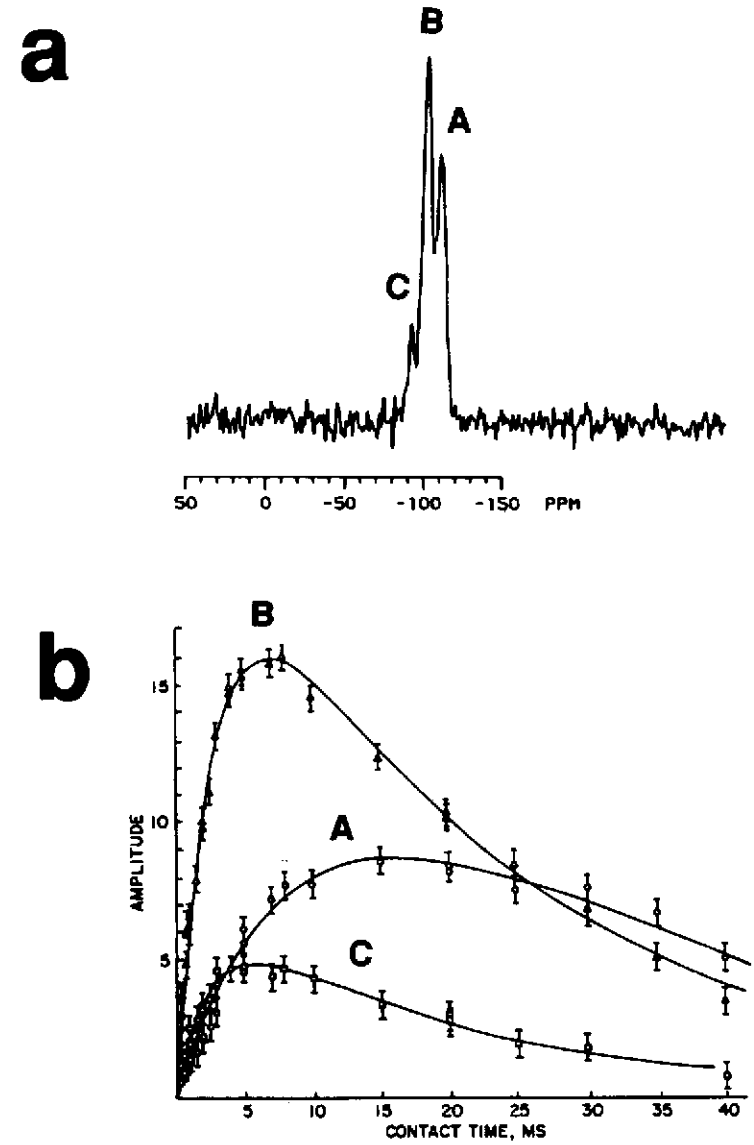

FIG. 34. (a) ^{29}Si CPMAS spectrum of a silica gel sample. (b) Plot of ^{29}Si signal amplitudes measured by variable contact time experiments on silica gel. (A) Peak attributed to regular $Si^{(4)}$ units. (B) Peak attributed to Si–OH (Si^{3}) groups. (C) Peak attributed to $Si(OH)_2$ ($Si^{(2)}$) groups. Note that the different cross-polarization dynamics enable one to enhance selectively resonances due to OH-bonded silicon atoms. Reproduced with permission from Ref. 239.

The influence of experimental conditions on the network structure and the fate of residual hydrous species during the various stages of the gel–glass transition have been studied in detail by Vega and Scherer.[244] Figure 35 shows the aging process for a gel over a period of several months. The spectra show three peaks, assigned to $Si^{(2)}$, $Si^{(3)}$ and $Si^{(4)}$ species. The peak ratio of these species changes remarkably little upon aging and syneresis, indicating that the polymerization is to a large degree arrested at the gellation stage. The peak deconvolution on the final glass samples attained after prolonged aging shows $Si^{(4)}$ and $Si^{(3)}$ in roughly equal proportions and a small amount ($< 5\%$) of $Si^{(2)}$

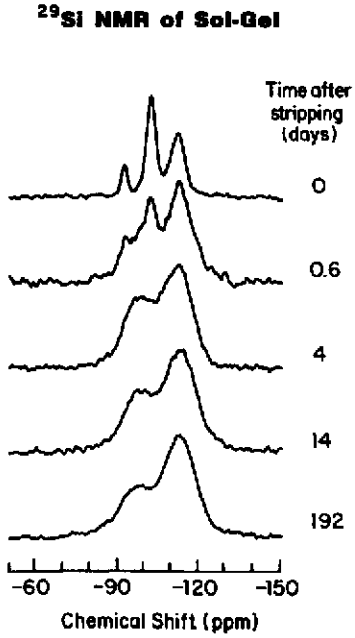

FIG. 35. ^{29}Si NMR spectra of a static sample of an aging gel that was kept in a closed vial at room temperature after refluxing for 3 h and stripping to 1.1 g/cm^3 as a function of aging time. The molar composition of the parent solution was TEOS/H_2O/ethanol/HCl = 1/16/4/0.01. Reproduced with permission from Ref. 244.

species. This corresponds to a final OH content of 0.5–0.6 units per silicon. Independently performed proton spin-counting experiments reveal that after prolonged drying and aging near room-temperature an ultimate H/Si ratio between 0.5 and 0.9 is attained. At the low end, this number is nicely consistent with the ^{29}Si peak analysis, whereas at the high end the deviation is due to a small amount of free molecular H_2O.

Information about the hydroxyl dynamics is available from an inspection of the ^{1}H free induction decays (Fig. 36). Two signals are present: a rapidly decaying ("solid-like") signal with an apparent T_2 of ca. 40 μs and a liquid-like species with an apparent $T_2 > 150$ μs. The solid-like signal arises from rigid Si–OH groups. It represents the exclusive signal contribution at H/Si ratios of less than 1.0. At higher hydrogen contents, the liquid-like component appears and becomes the only contribution above H/Si 1.5, at which point all the protons from Si–OH groups and molecular water constitute one liquid state, with the hydrogen atoms exchanging rapidly between free water and bound silanol groups. In the intermediate range of hydrogen content ($1.0 \leqslant H/Si \leqslant 1.5$) this exchange takes place only in those regions of the sample where the local water content is sufficiently high. Figure 37 shows representative ^{1}H and ^{29}Si MAS-NMR spectra for a series of gels at different stages of hydration. The liquid-like component dominates the spectrum at H/Si ratios of above 1.0, and gradually broadens and shifts from ca. 5.0 ppm towards 2.0 ppm at lower proton contents. The 2.0 ppm peak is accompanied by a wide spinning sideband pattern (not shown), which originates from strong H–H dipolar interactions, indicating pairing or clustering. Two additional sharp signals at 3.0 and 1.0 ppm are attributed to isolated Si–OH groups involved in different degrees of hydrogen bonding. Overall the hydrogen species observed are remarkably similar in nature to the hydrous species observed on amorphous silica surfaces.

5.8.2. *Network Structure of Sol–Gel Derived Silicas and Silicate Glasses.* Most of the work in this area has concentrated on sol–gel derived silicas. The ^{29}Si MAS-NMR spectra shown in Figs 35 and 37 (from the study by Vega and Scherer) bear important information on the network structure.[244,245]

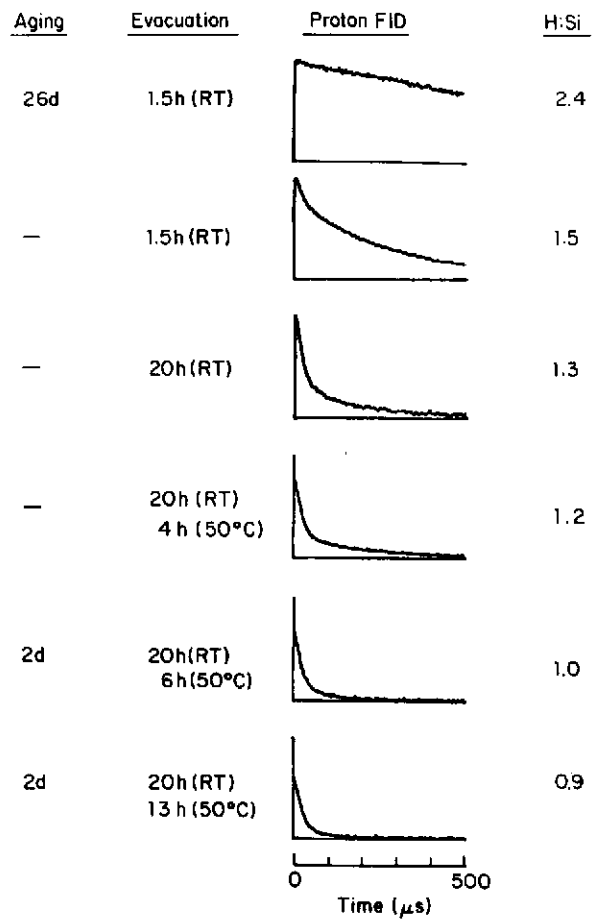

FIG. 36. ^1H free induction decays for static samples of gels that were given the indicated drying treatments. The first column indicates whether and for how long the stripped sol–gels were aged, the second column shows the periods of exposure to vacuum at room temperature and 50°C. Note the systematic variation of the shape with H/Si ratio (last column), but the lack of correlation with the drying schedule. The molar composition of the parent solution was $TEOS/H_2O/ethanol/HCl = 1/16/4/0.01$. Reproduced with permission from Ref. 244.

Evidently, the $Si^{(n)}$ speciation remains constant at this stage of dehydration ($H:Si < 2.0$). The $Si^{(n)}$ peaks are clearly resolved at H/Si ratios above 1.5 and below 0.8, respectively, but rather poor resolution is observed inbetween. To reduce the hydrogen content any further, high-temperature treatment is necessary.[246,115,116] The NMR spectra reveal that samples heated above 950°C are essentially devoid of hydrogen.[115,116] During this process, some subtle lineshape changes are observed for the $Si^{(4)}$ species at intermediate stages (500–600°C), and have been tentatively attributed to changes in the Si–O–Si bond angle distribution.[115,116] However, the bond angle distribution in the final glass is identical to that in fused silica glass.[246,115,116]

The ^{29}Si MAS and CPMAS approach has been extended further to TEOS-based multifunctional sol–gel materials,[247] SiO_2–TiO_2–ZrO_2 copolymerizates,[248] vitreous precursors to sphene ($CaTiSiO_5$) glass ceramics[249] and binary B_2O_3–SiO_2 glasses.[250,251] For the latter system, it was concluded that virtually no mixed B–O–Si linkages occur in the polymerized gel at room temperature. Upon heating these samples, certain changes are observed in the ^{11}B spectra, including an increase in the fraction of tetrahedral boron atoms (B_4). This behavior was interpreted to signify B–O–Si bond

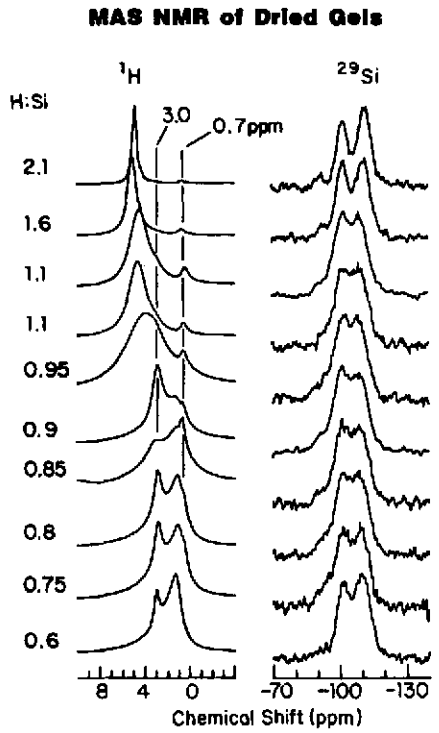

FIG. 37. ^{1}H and ^{29}Si MAS-NMR spectra of gels dried to various residual moisture levels. The various H/Si ratios are indicated along side each spectrum. The molar composition of the parent solution was TEOS/H_2O/ethanol/HCl = 1/16/4/0.01. Reproduced with permission from Ref. 244.

formation, although the NMR spectra are unable to specify the extent to which this occurs. Finally, ^{29}Si and ^{7}Li MAS-NMR have been used to measure the site speciation $Si^{(n)}$ in binary Li_2O–SiO_2 glasses prepared by the sol–gel method.[252–254] Apart from the effect of residual H present, the site speciation is found to be otherwise similar to that seen in compositionally analogous glasses cooled from the melt.[252]

6. BORATE GLASSES

Although alkali borate glasses have less wide-spread practical importance than silica-based glasses, they have attracted substantial interest from a fundamental point of view: (1) the continuous random network hypothesis appears to be not applicable here, and (2) ^{11}B solid state NMR is a particularly powerful structural probe. Using ^{11}B and ^{10}B NMR, Bray and his coworkers have provided extremely detailed insights into the structure of borate glasses. Since their work has been discussed extensively in previous reviews (see Table 1), only a condensed summary of the main findings will be given here.

6.1. *Short and Intermediate Range Order in Glassy B_2O_3*

One of the fundamental issues regarding glassy B_2O_3 is the question of whether and to what extent is its structure based on six-membered boroxol ($B_3O_3O_{3/2}$) rings. This hypothesis, initially based on density and viscosity data,[255,256] implies that the glass is characterized by substantial intermediate range order and hence violates Zachariasen's continuous random network concept. Substantial support for the boroxol hypothesis has come from the observation of a strong, highly polarized Raman band at 808 cm^{-1}, which can be assigned unambiguously to the symmetric boroxol breathing

mode.[257] Subsequent work has shown, however, that this mode is strongly over-emphasized in the Raman spectrum, due to an extremely large transition probability.[258] Although NMR data are still unable to offer unambiguous quantitative answers to the question of boroxol ring occurrence, substantial progress has been made. The chief conclusion from much of the early work[259–262] was that, due to the presence of second order quadrupolar broadening, boron is coordinated to three oxygen atoms (B^{III} species). Furthermore, detailed analyses revealed that there had to be either a non-zero asymmetry parameter or a distribution of quadrupole coupling constants and/or asymmetry parameters. This ambiguity could be resolved later with the help of ^{10}B NMR data, which, in contrast to ^{11}B NMR, also discriminates between distribution effects of e^2qQ/h and η, respectively.[263] Thus, Jellison *et al.* succeeded in fitting both the ^{10}B and the ^{11}B NMR lineshapes of glassy B_2O_3 to a consistent set of Gaussian distribution functions for both e^2qQ/h and η, respectively. A few mutually contradictory semi-quantitative approaches have been used to interpret these distribution effects in structural terms.[264,265]

Additional evidence for the existence of boroxol groups comes from the observation that the ^{17}O NMR lineshapes can be fitted in a satisfactory manner to two distinct oxygen sites, with e^2qQ/h (η) values corresponding to 4.69 MHz (0.58) (site 1) and 5.75 MHz (0.4) (site 2).[263] Site 1 might correspond to O atoms within the boroxol rings (B–O–B angle 120°), whereas site 2 might correspond to O atoms linking two boroxol rings and having a substantially wider B–O–B angle. While these fits are probably not unique, it is worth noting that *ab initio* calculations on $H_2B\,OBH_2$ have indeed indicated that the quadrupolar parameters for both sites should be similar.[266,267]

If the structure of glassy B_2O_3 is entirely composed of boroxol rings, a (site 1/site 2) ratio of 2 is expected. On the other hand, Jellison *et al.* found that this ratio lies in the vicinity of 1.2,[263] which is compatible with a model where 83% of the boron atoms are within boroxol rings. Recently ^{11}B pure NQR studies on glassy B_2O_3 have indeed confirmed the presence of two distinct boron sites. Two resonances are detected, characterized by average quadrupolar frequencies ν_Q of 1358 and 1305 kHz, respectively.[268–270] In excellent agreement with the ^{17}O NMR fits, the ratio of these boron sites is estimated to be 85:15, assuming that the observed NQR peak intensities reflect site populations. It remains now to be shown whether the e^2qQ/h and η distributions extractable from these NQR data are compatible with the ^{10}B and ^{11}B NMR lineshapes reported in earlier studies.

6.2. *Network Structure in Binary Alkali Borate Glasses and Related Systems*

6.2.1. *Boron Short Range Order and its Analysis via ^{11}B NMR.* Introduction of alkali oxide into glassy B_2O_3 results in the formation of four-coordinated BO_4 (B^{IV}) units as well as three-coordinated boron atoms bonded to non-bridging oxygen ($B^{III(0-2)}$). The ability of boron to increase its coordination number from three to four results from its Lewis acid character. In these B^{IV} units the charge formally resides on the B atom, but is in reality delocalized over the entire BO_4 unit, whereas in the $B^{III(0-3)}$ units the negative charges are localized on oxygen atoms. In an abundance of detailed experimental studies, NMR spectroscopy has proven its unique suitability for determining the speciation of these units in a quantitatively accurate manner.

Since ^{11}B is a quadrupolar nucleus ($I=\frac{3}{2}$), its static lineshape is affected by nuclear electric quadrupolar interactions (both first- and second-order perturbations), as well as by chemical shift anisotropy and distribution effects. Even at very low fields, the highly symmetric B^{IV} units are affected only by first-order effects, resulting in a sharp central $\frac{1}{2}\rightarrow-\frac{1}{2}$ transition. In contrast, the central transition lineshapes for all the B^{III} species in three-coordinate environments are strongly affected by second-order quadrupolar effects. The lineshapes for three-coordinate boron atoms with zero or three non-bridging oxygen atoms ($B^{III(0)}$ and $B^{III(3)}$ species) are characterized by a quadrupole coupling constant around 2.7 MHz with a small asymmetry parameter, due to approximate D_{3h} local symmetry. We will refer to both of these units as symmetric three-coordinate (B^{III_s}) units. The lineshapes of the B^{III} species with one or two non-bridging oxygen atoms ($B^{III(1)}$ and $B^{III(2)}$ species) are characterized by e^2qQ/h around 2.6 MHz and η of ca. 0.6; these species will be called asymmetric three-coordinate (B^{III_a}) units. Figure 38 shows typical lineshapes (in the first derivative mode as usually

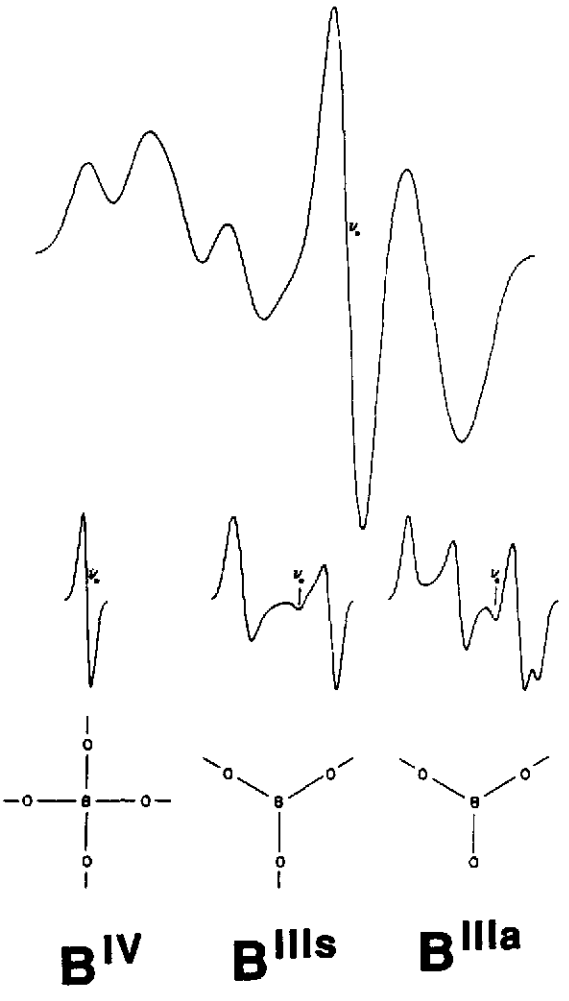

FIG. 38. Typical low-field ^{11}B NMR derivative spectra of a glass in the system Li_2O–B_2O_3, and its deconvolution into B^{IV}, B^{IIIs}, and B^{IIIa} units. This figure also summarizes the terminology used in the text. Reproduced with permission from Ref. 42.

recorded and presented in the literature) and shows the units expected along with the terminology used here.

While the qualitative assignment summarized in Fig. 38 and the peak deconvolution are straightforward, the quantitative interpretation of quadrupole coupling constants and asymmetry parameters is still uncertain. Thus the analysis has concentrated on the quantitative deconvolution of experimental lineshapes in terms of the fractional contributions N_4, N_{3s}, and N_{3a}, using standard computer-fitting methods.[272–273] A typical example is shown in Fig. 39. Simpler spectral decomposition procedures as used in some of the earlier ^{11}B NMR work are likely to be less accurate. Specifically they tend to overestimate N_4 if a significant fraction of B^{IIIa} species are present, since these units give rise to intensity in the same spectral region near the central resonance frequency. Interestingly, for N_4 determinations, static low-field cw NMR has so far proven to be superior to pulsed, high field methods. At low field strengths, chemical shift distribution effects are minimized, whereas second-order quadrupolar broadening effects are maximized, resulting in optimum spectroscopic resolution between the individual lineshape components in Fig. 38. If the field strength is increased, the spectra associated with

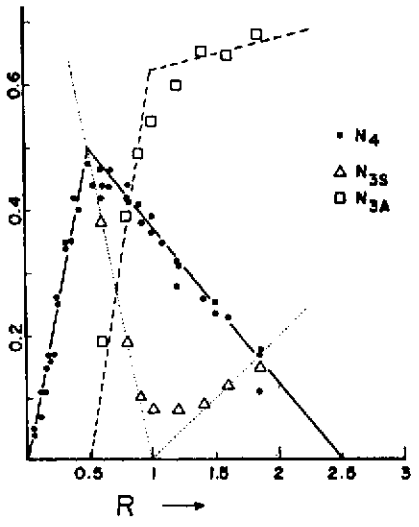

FIG. 39. Quantitative boron speciation in the system Li_2O–B_2O_3, as obtained with lineshape deconvolution as a function of R = mole Li_2O/mole B_2O_3. Reproduced with permission from Ref. 303.

the B^{III} species (dominated by the quadrupolar interaction) get narrower, whereas those associated with the B^{IV} species (dominated by chemical shift distribution) broaden. At field strengths above 8T, both components have merged into an essentially inseparable composite lineshape. Even if the high field is combined with MAS, the achievable resolution is limited due to the inability of MAS to effectively narrow lineshapes affected by second order quadrupolar effects, except potentially at the highest field strengths currently available.[330]

A series of papers have challenged the lineshape deconvolution procedures in terms of discrete spectroscopic sites. These authors argue that similar ^{11}B lineshapes could also result if the distribution of quadrupolar coupling constants were not bimodal as generally assumed, but much wider and much less regular.[274–277] If this were indeed true, the structural insights obtained by ^{11}B NMR would be severely limited. The premises of this alternative view have been debated in Ref. 278. Overall, the observation of well-defined quadrupolar satellites (measured by the dispersion technique)[279] and of well-resolved ^{10}B NMR spectra in alkali borate glasses[280] argue strongly against such ideas. Furthermore, recent pure ^{11}B NQR results obtained by Lee, Gravina and Bray clearly show that the distribution of ^{11}B quadrupole coupling constants in borate glasses is quite narrow.[268–270] Besides refuting the arguments raised above, the latter work also illustrates that the various boron sites present in crystalline and glassy borates can be distinguished sensitively on the basis of their nuclear electric quadrupole coupling.

6.2.2. *Binary Alkali Borate Glasses.* Table 6 summarizes the published ^{11}B NMR determinations of N_4 for binary alkali borate glasses and other systems.[281–330] The compositional dependence of N_4 in alkali borate glasses is characterized by the following observations: At low alkali oxide content (<0.33 mol.%), $N_4 = R = [\text{mol.\% } M_2O]/[\text{mol.\% } B_2O_3]$. In this compositional region, each molecular unit of alkali oxide is used nearly quantitatively to convert two boron atoms from three- to four-coordination. N_4 reaches a maximum near $R = 0.5$ (33 mol.% alkali oxide), while at higher alkali oxide contents N_4 decreases again, approaching zero at R near 2. Remarkably, the N_4 maximum can be correlated with relative extrema in many of the thermal and mechanical properties of borate glasses.[331] In particular, N_4 and T_g appear to be closely related.[332,333] Planar $BO_{3/2}$ groups result in essentially two-dimensional bonding. The tetrahedral B^{IV} units can be thought of cross-linking two-dimensional $BO_{3/2}$-based layers, thus favoring an increase in T_g. In contrast, $B^{III(0-2)}$ units containing non-bridging oxygen decrease the polymerization, thus lowering T_g.

TABLE 6. N_4 analysis in binary and ternary borate glasses

Additive	References
Li_2O	282, 288, 301, 303, 322
Na_2O	282, 288, 292, 294, 322, 330
K_2O	281, 282, 292, 319, 322, 327
Rb_2O	282, 322
Cs_2O	282, 293
NaF, KF	285, 291
MgO	302
CaO	286
SrO	292, 295
BaO	289
Ag_2O	297
Tl_2O	290
ZnO	316
CdO	449
SnO	27
PbO	147, 283
Bi_2O_3	284
GeO_2	296
TeO_2	307
V_2O_5	323
Li_2O–M_2O	322
Li_2O–Ag_2O	312
Li_2O–Li_2SO_4	326
Ag_2O–AgI	310, 325
Na_2O–MgO	298
K_2O–CuO	311
Na_2O–CuO	313
Na_2O–Al_2O_3	300
CaO–Al_2O_3	286
BaO–Al_2O_3	320
PbO–Al_2O_3	315
Li_2O–TeO_2	317
Li_2O–V_2O_5	318
Na_2O–V_2O_5	299, 328, 329
Na_2O–MoO_3	313
PbO–Fe_2O_3	314
V_2O_5–Al_2O_3	323

Figure 39 shows the concentrations of B^{IV}, B^{III_a}, and B^{III_s} units in the system Li_2O/B_2O_3.[303] Especially at low alkali oxide contents (R values) these distributions are found to be strongly non-statistical, indicating a high preference for certain structural units within limited compositional ranges. For instance, species with non-bridging oxygen atoms are essentially absent below $R=0.5$. It is for this reason, that the structural speciation of borate glasses is often expressed in the form of simple reaction equations, illustrating the transformation of a given structural unit by additional modifier oxide into another, usually more highly charged one.

While early studies noted no significant influence of the alkali ion on the boron speciation,[282] newer results using improved lineshape deconvolution procedures suggests that there is a specific cation effect:[322] Above $R=0.5$, N_4 decreases in the order Li→Na→K→Rb→Cs at any given R-value, indicating that $B^{III(1)}$ and $B^{III(2)}$ species compete more and more effectively with B^{IV} species, as the size of the alkali ion is increased. Even more interesting, mixed alkali glasses with a given R value show a systematic depression of N_4, much below the average value of the pure binary glasses.[322] This finding appears to be a manifestation of the so-called mixed alkali effect, which is thought to constitute a preferential pairing of unlike cations.[334,335] Evidently such pairing is energetically more favorable if the charges are localized on single oxygen atoms, and hence the formation of units with non-bridging

oxygen atoms is favored. All of these systematics are also in excellent agreement with the experimentally observed T_g behavior. In contrast, there appears to be no evidence for mixed cation effects in $(Ag_2O, Li_2O)B_2O_3$ glasses.[312]

6.2.3. *Boron Conversion in Systems Related to Alkali Borate Glasses.* The study of alkali borate glasses has been extended to a number of related systems based on monovalent network modifiers. KF has principally the same influence as alkali oxide,[285,291] resulting in the formation of tetrahedral BO_3F and BO_2F_2 groups. The latter give rise to very characteristic lineshapes given by the simultaneous effect of strong quadrupolar and heteronuclear dipole–dipole interactions.[336] Thallium borate glasses have been reported to show unusually high N_4 at low R values. To explain these results, one has to invoke the formation of three-coordinated oxygen.[290] This system should be re-examined in view of subsequent investigations by neutron diffraction and Raman spectroscopy, which have failed to detect any three-coordinate oxygen atoms.[337] The structural speciation of boron in silver borate glasses is closely related to the behavior in alkali borate glasses.[297] Silver borate glasses doped with AgI have recently attracted substantial interest for solid electrolyte applications, and have thus been widely studied. For glasses with $R \leqslant 1$ it was found that the addition of AgI to a silver borate glass with fixed R value does not change N_4, resulting in the conclusion that AgI is dispersed within the interstices of the network and not structurally active.[310] In glasses with higher Ag_2O contents, the addition of large amounts of AgI tends to lower N_4.[325] Most likely the AgI indirectly influences the melt equilibria determining the balance of B_4 and B_{3a} species. In contrast, lithium sulfate additive tends to increase N_4 at a given R-value,[226] hence suggesting that the sulfate ions are structurally active.

Divalent oxides act as modifiers in the borate network in a similar way as monovalent oxides: by and large the $N_4 = R$ rule is followed at low R values, whereas at higher metal oxide concentrations N_4 decreases due to the formation of non-bridging oxygen. At certain compositions, in the systems $SrO–B_2O_3$,[295] $PbO–B_2O_3$,[283] and $ZnO–B_2O_3$[316] the structures of the glasses deviate from those of stoichiometrically analogous crystalline compounds. This finding is a rare one for oxide glasses. In CuO- and MoO_3-containing glasses, N_4 seems to depend strongly on the glassmaking temperature, although the effect may be difficult to evaluate in view of the paramagnetism of Cu^{2+}.[306,313] Paramagnetic effects on the ^{11}B and ^{207}Pb NMR spectra have been studied in further detail by Bucholtz and Bray in the $PbO–Fe_2O_3–B_2O_3$ system.[314]

In the systems $MgO–Na_2O–B_2O_3$,[298] $PbO–B_2O_3$,[283] and $B_2O_3–Tl_2O$[290] changes in the boron conversion rate at higher R values have not been interpreted in terms the B^{IV}/B^{IIIa} balance, but in terms of the ability of the metal oxide additive of becoming part of the network rather than contributing to its transformation. According to this interpretation, the added metal ion forms its own $MO_4^{(n-4)}$ units (n being the charge of the metal cation). This behavior appears to be generally correlated with a markedly reduced number of B^{IIIa} species as compared to alkali borate glasses at comparable compositions. Qualitative evidence for the contention that the cations gain network forming ability has come from the observation of certain chemical shift trends observed for the nuclear magnetic resonances of metal ions (specifically ^{207}Pb and ^{205}Tl) that are introduced into the network.[283,290,338]

Trivalent oxides act as network modifiers and boron conversion agents only in exceptional cases, such as Bi_2O_3.[284] Mostly, however, such glass constituents are intermediate oxides, which gain network forming capability in the borate network. This structural feature of borate glasses is discussed further in Section 6.3.

6.2.4. *Intermediate Range Order in Alkali Borate Glasses.* Beyond the issue of nearest-neighbor environments, a key question has been the existence of intermediate-range order in borate glasses. The latter view was advanced by Krogh-Moe, who observed that the vibrational spectra of borate glasses can be interpreted in terms of the typical intermediate-range environments present in crystalline borates.[339] According to this interpretation, the structure of borate glasses consists mostly of well-defined ring structures, (see Fig. 40), and their populations can be assumed to follow simple lever rule predictions. Obviously, this view contradicts the crn model of Zachariasen. A number of NMR studies have been undertaken to test such ideas. These studies have exploited the fact that the wideline NMR

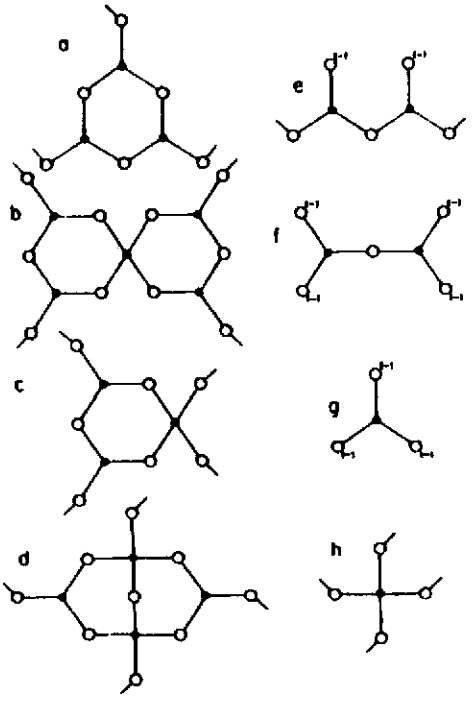

FIG. 40. Intermediate-range order structural units proposed for glassy B_2O_3 and alkali borate glasses. (a) Boroxol rings; (b) pentaborate groups; (c) triborate groups; (d) tetraborate groups; also called diborate groups; (e) metaborate groups; (f) pyroborate groups; (g) orthoborate groups; (h) loose BO_4 groups.

lineshapes of the less abundant isotope, ^{10}B, ($I=3$) reveal substantially more detail than ^{11}B NMR lineshapes. The observed ^{10}B spectra usually comprise the two central ($0\rightarrow -1$) and ($1\rightarrow 0$) transitions, which also allow a separate assessment of e^2qQ/h and η distributions. In a series of papers, Bray and coworkers have analyzed such lineshapes in terms of a total of nine individual components, characterized by unique quadrupolar Hamiltonian parameters subject to Gaussian distribution functions.[280,340–343] These components are identified with the B^{IV} and B^{III} sites of the structures shown in Fig. 40, primarily on the basis of the compositional dependence of their population. The lineshape fitting is then done in compliance with a number of constraints imposed by the stoichiometry R, the B^{IV}/B^{III} ratio of certain sites, and the value N_4 measured independently by ^{11}B NMR. Based on these assumptions the authors find that only for $R<0.4$ is the distribution of microstructures consistent with simple lever rule predictions in the Krogh-Moe model, whereas at higher alkaline oxide contents the population distribution shows substantial deviations from this model. It is conceiveable, however, that a variety of other models fit equally well. Additional support for the Krogh-Moe model could come from ^{10}B NMR measurements of crystalline model compounds. Such studies could impose additional constraints on the quadrupolar Hamiltonian parameters chosen for the various B^{III} and B^{IV} sites in the glasses, and thereby limit the number of adjustable variables.

6.3. *Network Modification of Borate Glasses by Intermediate Oxides*

6.3.1. *Alkali and Alkaline-Earth Aluminoborate Glasses.* Incorporation of Al_2O_3 into alkali and alkaline earth borate glasses at constant R leads to a reduction in N_4.[286,300] This observation is qualitatively consistent with the partial consumption of modifier oxide to convert the Al present to four-coordinated $AlO_{4/2}^-$ (Al^{IV}) units, at the expense of the boron conversion process. It was noted early on, however, that not all of the aluminium can exist in this coordination, since even at a ratio

$M_{(2)}O/Al_2O_3$ of unity a sizeable amount of four-coordinated boron is detected. Subsequent high-field ^{27}Al MAS-NMR studies indeed confirm the presence of six-coordinated aluminium (Al^{IV}) over a wide compositional range.[344-348] These results are fundamentally different from the situation in aluminosilicate glasses, where Al^{VI} is usually never detected unless the $M_{(2)}O/Al_2O_3$ molar ratio is below unity. While in aluminosilicate glasses the formation of Al^{IV} takes precedence over any other network conversion process, in aluminoborate glasses Al and B appear to compete for the modifier oxide on a more equal footing. The final balance between both conversion processes also seems to depend on the counter-cation. Na and K favor aluminium conversion, whereas boron conversion is more preferred with Li and Pb, thus resulting in a larger fraction of Al^{VI} in the glass structure.[346,348] Unfortunately, absolute intensity measurements with a $NaAlO_2$ standard indicate that only ca. 25% of the Al atoms are detected. Presumably, the majority of the Al atoms are not observable due to extreme quadrupolar broadening resulting from highly distorted environments.[345] This difficulty precludes a more quantitative interpretation of these results.

6.3.2. *Related Systems.* The study of intermediate oxide effects on the boron conversion process has been extended to glass systems containing MoO_3,[313] V_2O_5,[299,318,328,329] and TeO_2.[307] While the binary TeO_2–B_2O_3 system has glass-forming ability, it has a high tendency to phase-separate, except within the region of 6–25 mol.% B_2O_3.[349] ^{11}B NMR indicates that these glasses contain a substantial fraction of B^{IV} units. This effect suggests that the tellurium coordination numbers are altered as well,[307] a possibility that should be tested by ^{125}Te MAS-NMR. Harris and Bray investigated a large series of glasses in the ternary system B_2O_3–TeO_2–Li_2O.[317] The development of structural models based on the N_4 measurements is complicated here by the fact that both TeO_2 and alkali oxide function as sources of four-coordinated boron. By extrapolation, the fraction $N_4(R=0)$ due to TeO_2 was determined to be;

$$N_4(R=0)=0.46\,K \text{ for } K\leqslant 0.5 \tag{44a}$$

$$N_4(R=0)=0.09\,K+0.19 \text{ for } K\geqslant 0.5 \tag{44b}$$

$$(K=\text{mol.\%}\,TeO_2/\text{mol.\%}\,B_2O_3).$$

These expressions are in fact well-compatible with the N_4 values published for the three binary glasses by Göring *et al.*[307]

Harris and Bray also investigated ternary B_2O_3–TeO_2–Al_2O_3 glasses.[317] The presence of Al_2O_3 tends to reduce the fraction of four coordinated boron, presumably because some of the oxygen introduced into the glassy network is now directed towards the aluminium network. These results are in close analogy to the situation found in calcium aluminoborate glasses.[286]

Recently, borovanadate glasses have attracted some interest.[318,323,328,329] While in pure binary B_2O_3–V_2O_5 glasses only B^{III} is detected, the simultaneous introduction of Al_2O_3 has been reported to produce some B^{IV}. At the same time, the situation is complicated by partial reduction of vanadium to the quadrivalent state. N_4 measurements of ternary alkali borovanadate glasses reveal that the alkaline oxide is used for both boron and vanadium conversion.[299]

GeO_2 forms homogeneous glasses with B_2O_3 over a wide composition range. ^{11}B NMR studies indicate the absence of B^{IV} units in these glasses.[296] The formation of a mixed B–O–Ge network is suggested by a systematic compositional trend in the ^{11}B nuclear electric quadrupole coupling constant. Recently Dickinson *et al.* published preliminary multinuclear MAS-NMR results on the achetypical three-network-former system SiO_2–B_2O_3–P_2O_5.[351] These glasses also contain some hydrogen, as evidenced by mass spectrometric analysis. CP-experiments on these glasses establish that this hydrogen is only associated with phosphorus atoms. Furthermore, P is believed to promote $B_3 \rightarrow B_4$ conversion, giving rise to BPO_4-like groups, and ^{29}Si MAS-data suggest substantial silicon–boron interactions.

6.4. *Further NMR Studies of B_2O_3 and Borate Glasses*

Elevated pressure has relatively little effect on the structure of B_2O_3.[352] Water functions as a network modifier in B_2O_3 converting B^{III} to B^{IV}-OH units.[353a,b] Rigid-lattice ^7Li linewidths and

second moments have been measured.[11,12,354] In the limit of low lithium contents (below $R=0.5$) these second moments appear to be much too large compared to a statistical distribution, and independent of the lithium content. Assuming that these second moments are dominated by ^7Li–^7Li interactions, the conclusion has been offered that there is substantial cation clustering.[12,354] On the other hand, due to the coulombic interaction between Li^+ ions and the negatively charged BO_4^- units, strong ^{11}B–^7Li dipole–dipole couplings are expected. As discussed previously, the experimental $M_2(^7Li)$ values at low lithium contents can be accounted for if an average B–Li distance of 1.8Å is assumed.[34]

Several authors have used ^{11}B NMR to study the structural depolymerization of glassy B_2O_3 and alkali borate glasses at elevated temperatures.[310,355–358] Room temperature measurements on alkali borate glasses with different quenching histories suggest that N_4 decreases with increasing temperature.[357] This seems to be corroborated by the most recent high-temperature ^{11}B NMR measurements. Surprisingly, however, N_4 appears to decrease even at temperatures below T_g.[358]

An additional area of interest has been the study of low-temperature spin-lattice relaxation phenomena, which appear to be connected with low-frequency phonon-like modes in the glassy state. Due to the existence of these modes, quadrupolar nuclei (in particular ^{11}B and ^7Li) have several orders of magnitude shorter spin-lattice relaxation times in glasses as compared to crystalline solids at low temperatures. Various phenomenological models have been proposed to explain this behavior. These models involve either bridging oxygen atom tunnelling between two potential wells[359,362] or low-frequency phonon-like modes characteristic of the glassy state.[360,361]

7. PHOSPHATE GLASSES

Phosphate glasses have been known for a long time as laboratory curiosities with few specialized applications. Recently, however, these systems have gained considerable interest in connection with the development of fast ionic conductors,[364,365] new optical lens materials and of glasses with nonlinear optical properties.[366–368]

7.1. *Network Structure in Binary and Pseudobinary Phosphate Glasses*

Due to its extreme hygroscopicity, pure glassy P_2O_5 is very difficult to synthesize. Presumably this is the reason that no NMR results have appeared in the literature until very recently. The ^{31}P MAS-NMR spectrum is characterized by a single wide spinning sideband pattern revealing an axially symmetric chemical shift tensor. The central resonance (−55 ppm) lies within the range of values observed for the three crystalline P_2O_5 polymorphs.[369]

In contrast to glassy P_2O_5, binary and ternary alkali, silver and thallium phosphate glasses are readily prepared. The structure of these glasses is generally described in terms of corner-shared coordination polyhedra with local symmetry close to tetrahedral. Depending on the oxide/P_2O_5 ratio, four distinct types of local phosphorus environments are then formed, which are depicted in Fig. 41.[370] In analogy to the nomenclature for silicate glasses, these units are labeled $P^{(n)}$ ($0 \leqslant n \leqslant 3$), where n is the number of bridging oxygen atoms. Each of these microstructures is characterized by a distinct ^{31}P isotropic chemical shift range. Furthermore, Fig. 41 illustrates that ^{31}P anisotropic chemical shift tensor components distinguish equally well between these structural units. Olyschläger and Müller-Warmuth were the first to develop a comprehensive chemical shift scale for crystalline and glassy phosphates in terms of the $P^{(n)}$ speciation.[371] These results were later confirmed by high-field NMR studies, which in combination with MAS also resulted in more precise chemical shift information.[372–376] The ^{31}P chemical shift anisotropies for $P^{(3)}$, $P^{(2)}$ and $P^{(1)}$ units are quite large, resulting in intense spinning sidebands for typical ^{31}P MAS-NMR spectra of phosphate glasses. While these sidebands slightly complicate the quantitative analysis of the NMR spectra, their presence further facilitates structural assignments.

As for silicate glasses, the quantitative $P^{(n)}$ speciation is of intrinsic interest for an understanding of phosphate glasses. Again the question is whether the binary or a random model are more suitable.

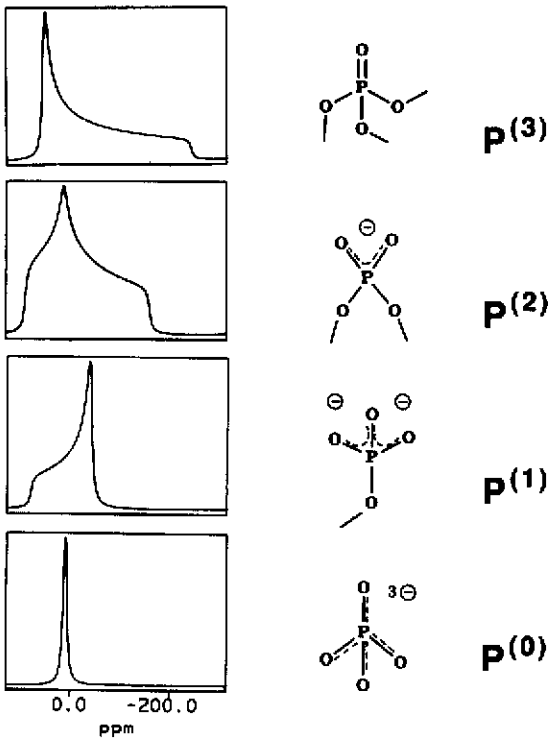

FIG. 41. Distinguishable short range order arrangements in phosphate glasses, and their static ^{31}P NMR lineshapes expected. This figure also summarizes the terminology used in the text.

Since the chemical shift separation for the $P^{(n)}$ units is significantly better than for the $Si^{(n)}$ species in silicate glasses, the quantitative analysis of the ^{31}P spectra should be a rather straightforward matter. Unfortunately, however, the quantitation is complicated by the fact that, due to their hygroscopic nature, binary alkali phosphate glasses usually contain water, which by itself acts as a network modifier. Thus, the water content of the glass has to be known exactly, before any conclusions on the distribution of non-bridging oxygen species can be drawn. This determination can, in principle, be made by ^{1}H NMR.[377,378] Although a number of studies with informational content on the issue of the $P^{(n)}$ site distribution in phosphate glasses have appeared in the literature,[373,379–381] it was not until the study of Brow *et al.*[382] that some definite knowledge on this question was obtained. Taking the water content into consideration, the detailed quantitative data presented for the Na_2O–P_2O_5–H_2O system strongly favor the binary model in phosphate glasses. Representative spectra and a summary of their quantitative analysis are shown in Figs 42a, b. The binary model is also substantiated in the fast ionic conductors based on Ag_2O–AgI–P_2O_5 glasses, which show excellent chemical shift resolution for the $P^{(n)}$ species.[383] The results of that study are in partial conflict with the findings of Rao and coworkers, who suggest that the addition of AgI facilitates a disproportionation of pyrophosphate units into *meta* and *ortho*phosphate.[384] Additional experimentation will be necessary to resolve this problem. As found to be true quite generally in such ionically conductive systems, the AgI component does not participate in the network modification, but appears to be dispersed throughout the glass structure, thereby facilitating silver ionic conduction.

7.2. *Anion Substitution in Phosphate Glasses*

Nitridation is known to increase the hydrolytic stability of alkali phosphate glasses considerably. ^{31}P and ^{15}N NMR have been used in an attempt to gain an understanding of this effect on a structural

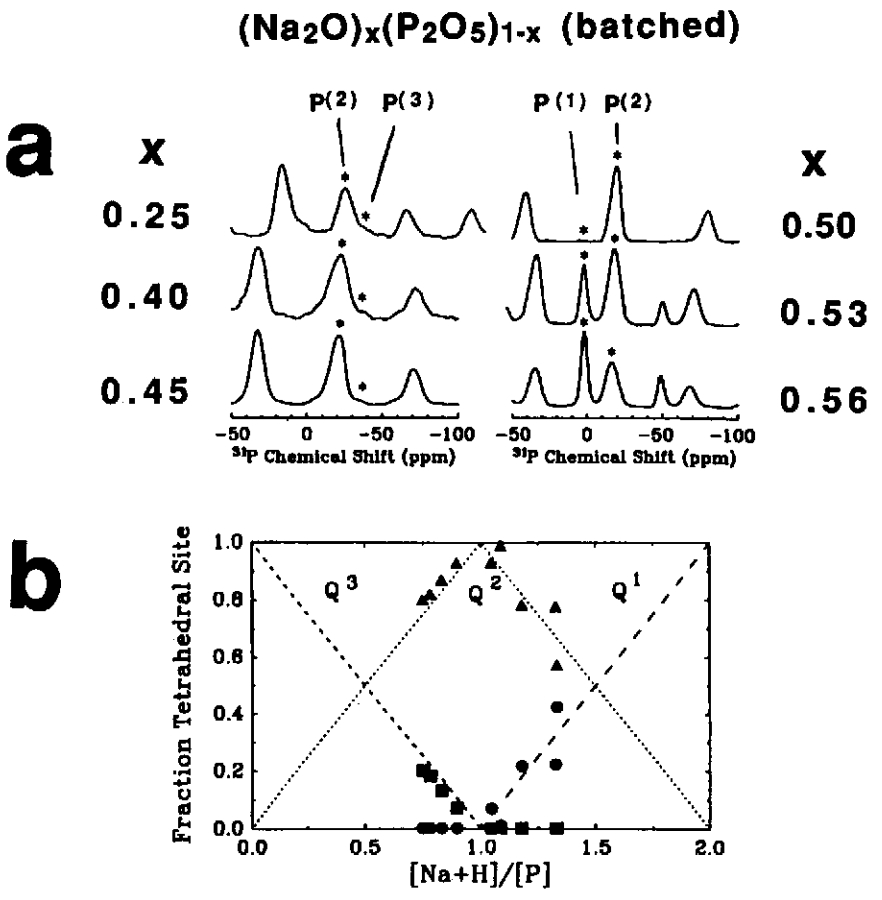

FIG. 42. (a) Typical ^{31}P MAS-NMR spectra of sodium phosphate glasses with the Na_2O/P_2O_5 compositions, x indicated. MAS-NMR centerbands are indicated in the figure. Reproduced with permission from Ref. 382. (b) $P^{(n)}$ speciation (denoted $Q^{(n)}$ in the figure) as a function of composition, taking into account the measured H_2O content of these glasses. Dashed lines show the species concentrations expected from the binary model. $P^{(1)}$, $P^{(2)}$, and $P^{(3)}$ species concentrations are denoted by circles, triangles and squares, respectively. Reproduced with permission from Ref. 382.

basis.[385] The ^{31}P MAS NMR spectra show partially resolved peaks assigned to PO_4, PO_3N and PO_2N_2 units, since each substitution of O for N results in a downfield shift increment of approximately 10 ppm. The spectral areas of these units as a function of nitrogen content show similar trends to those expected from probability arguments. ^{15}N NMR spectra, obtained on isotopically enriched samples invariably show two resonances at 90 and 60 ppm, respectively. The relative ratios of these peaks appear not to depend on the composition in any systematic manner. Only the 60 ppm resonance shows spinning sidebands at spinning speeds around 5 kHz, hence suggesting that both nitrogen species have substantially different chemical shift anisotropies. Based on this fact and model compound studies, the two peaks at 60 and 90 ppm are assigned to sp^2 and sp^3 hybridized N atoms, respectively. Overall the results of this study suggest that nitrogen replaces oxygen in the phosphate glass network both in the form of P–N=P and P–N–P nearest neighbor arrangements.

These results support the interpretation that nitrogen cross-links the structure, but not as efficiently as does a cationic glass constituent such as Al^{3+}.

Recently, preliminary results have been presented on the technologically interesting fluorophosphate systems.[386–391] Introduction of fluoride into phosphate glasses is known to depolymerize the

network, resulting in the conversion of $P^{(2)}$ into $P^{(1)}$ and PO_3F units. However, in the quantitative analysis of this effect, NMR has contributed relatively little new knowledge. Although this conversion process has also been studied by ^{31}P and ^{19}F NMR in several complex glasses, simple cw-NMR or ^{31}P MAS-spectra are not sufficiently informative due to the lack of chemical shift resolution. Clearly, more selective approaches, involving ^{31}P–^{19}F double resonance and other, more sophisticated experiments are desirable to clarify the structure of these interesting glasses.

7.3. *Coordination of Other Glass Constituents in Phosphate Glasses*

Further NMR studies of phosphate glasses have addressed the coordination and chemical bonding properties of other glass constituents. For instance, ^{7}Li second moments, measured by the cw technique, indicate that the lithium–lithium interactions in phosphate glasses are significantly weaker than in silicate glasses with comparable Li contents.[371] This result suggests that the Li ions are in a state of wider dispersion in phosphate glasses. Other examples of older, previously reviewed applications include: ^{51}V and ^{31}P NMR investigations of V_2O_5–P_2O_5 glasses,[392–395] the effect of composition and temperature on the ^{205}Tl resonance in Tl–phosphate glasses,[396,397] and the coordination of aluminium in the systems CaO–Al_2O_3–P_2O_5[398,399] and Na_2O–Al_2O_3–P_2O_5.[400] In contrast to aluminosilicate glasses, aluminophosphate glasses appear to contain large fractions of the aluminium in six-coordinated environments.

8. OXIDE GLASS COFORMER SYSTEMS

8.1. *The Structure of Phosphosilicate Glasses*

Phosphorus is an important component of many synthetic and natural glasses and can have a significant effect on their crystallization and thermodynamic behavior.[401] Like SiO_2, P_2O_5 is a network former, and will, in the molten state, react with network modifiers under formation of non-bridging oxygen attached to P. The structure of coformer systems containing both SiO_2 and P_2O_5 is thus characterized by the competition of both glassforming constituents for the modifier oxide. The quantitative consequences of this effect have been recently studied in ternary P_2O_5–SiO_2–M_2O glasses (M = Li, Na, K).[402–406] Figure 43 shows representative ^{29}Si MAS-NMR results, illustrating the effect of small amounts of P_2O_5 present in lithium disilicate melts (the Li_2O/SiO_2 is kept fixed to 0.5, resulting in an average $Si^{(3)}$ speciation). Note the gradual replacement of the $Si^{(3)}$ resonance by the $Si^{(4)}$ resonance as the P content is increased. These data reveal a repolymerization of the silicate network. At the same time, the P_2O_5 network is depolymerized: For lithium disilicate glasses, ^{31}P MAS-NMR identifies mostly PO_4^{3-} ($P^{(0)}$) species, consistent with the melt reaction:

$$3SiO_{3/2}O^- + P(O)O_{3/2} \rightarrow PO_4^{3-} + 3SiO_{4/2}. \tag{45a}$$

In contrast, $Na_2Si_2O_5$ and $K_2Si_2O_5$ glasses show dominant formation of dimeric pyrophosphate ($P_2O_7^{4-}$, $P^{(1)}$) groups, indicating the reaction

$$4SiO_{3/2}O^- + 2P(O)O_{3/2} \rightarrow P_2O_7^{4-} + 4SiO_{4/2}. \tag{45b}$$

The $P^{(1)}$ groups become more and more dominant with increasing size of the alkali ion and with increasing P_2O_5 content. Considering both reaction modes, the $Si^{(4)}/Si^{(3)}$ ratio in a glass $rM_2O/sSiO_2/pP_2P_5$ is calculated from the expression:

$$Si^{(4)}/Si^{(3)} = (1 - 3r - p(1 - 2(3m + 2n))/(2r - 2p(3m + 2n))), \tag{46}$$

where m and n, the fractions of $P^{(0)}$ and $P^{(1)}$ groups, $(m + n = 1)$ are determined experimentally from the ^{31}P NMR spectra. This model, which assumes the absence of any P–O–Si linkages, was found to be in reasonable agreement with the experimentally determined $Si^{(n)}$ speciation. Evidently, small concentrations (up to 11 mol.%) of P_2O_5 compete extremely effectively for the modifier oxide, acting essentially as scavengers. Similar effects have been observed for alkaline-earth silicate glasses of composition $MSiO_3$ (M = Mg, Ca, Sr, Ba).[302]

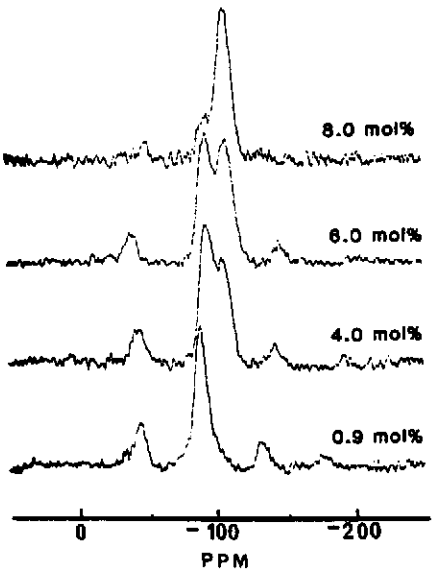

FIG. 43. Influence of P_2O_5 on the ^{29}Si MAS-NMR spectra of lithium phosphosilicate glasses with composition $Na_2O/2SiO_2/pP_2O_5$. Reproduced with permission from Ref. 405.

Due to the limited content of alkali metal ions in the disilicate compositions investigated, reactions (45a and b) are only applicable up to $p=0.33$ and 0.5, respectively. Indeed, the ^{29}Si and ^{31}P MAS-NMR spectra shown in Fig. 44a reveal that beyond a threshold value of $p=0.37$ the structure of P_2O_5 containing sodium disilicate glasses is fundamentally different. Within $0.37<p<1.0$, metaphosphate units ($P^{(2)}$) are the only P-containing structural units present, consistent with the reaction

$$Si^{(3)} + P^{(3)} \rightarrow Si^{(4)} + P^{(2)}. \tag{45c}$$

The modifier oxide not associated with the $P^{(2)}$ units again controls the $Si^{(4)}/Si^{(3)}$ balance. This is confirmed by a systematic ^{29}Si chemical shift trend observed in this concentration range. (Presumably due to a distribution of Si–O–Si and Si–O–P bonds, no separate $Si^{(n)}$ peaks are observable here.) Consistent with the modifier oxide content, the NMR spectra reveal that for $p=1.0$, the glass contains only $Si^{(4)}$ and metaphosphate ($P^{(2)}$) units.

For $p>1.0$, the NMR spectra reveal the formation of SiP_2O_7-like regions in the glass, containing only bridging P atoms and six-coordinated silicon with chemical shifts close to those of the crystalline material. The fraction of Si^{VI} in the glass increases with p, up to 40% at $p=4$. 2D ^{29}Si COSY studies have failed to reveal appreciable concentrations of two-bond connectivities between Si^{IV} and Si^{VI}, hence confirming the idea of SiP_2O_7-like islands.[143] Figure 44b shows that the fraction of Si^{VI} at a fixed SiO_2/P_2O_5 ratio increases with increasing metal ion content r. Binary SiO_2–P_2O_5 glasses contain mostly Si^{IV},[407,408] although small amounts Si^{VI} have also been reported at certain compositions. Thus, the presence of modifier oxide favors the formation of six-coordinated silicon in silicophosphate glasses. Glasses quenched at different rates have markedly different T_g values and Si^{VI}/Si^{IV} ratios. Partial substitution of P_2O_5 by Al_2O_3 reduces the Si^{VI} content and leads to formation of Al^{VI}.[406] Overall, it appears that the structure of Na_2O–SiO_2–P_2O_5 glasses is controlled by the formation of certain phosphorus units that are energetically favorable in specific concentration regimes, to which the Si speciation accommodates.

Binary P_2O_5–SiO_2 glasses are of considerable technological importance, since the incorporation of small amounts of P_2O_5 and Al_2O_3 into glassy SiO_2 can be used to tailor the refractive indices of optical waveguides.[409] The ^{31}P NMR spectra of such binary SiO_2–P_2O_5 glasses reveal axially symmetric chemical shift tensors, consistent with the presence of $O=PO_{3/2}$ ($P^{(3)}$) groups (see Fig. 45a). Figure 45b

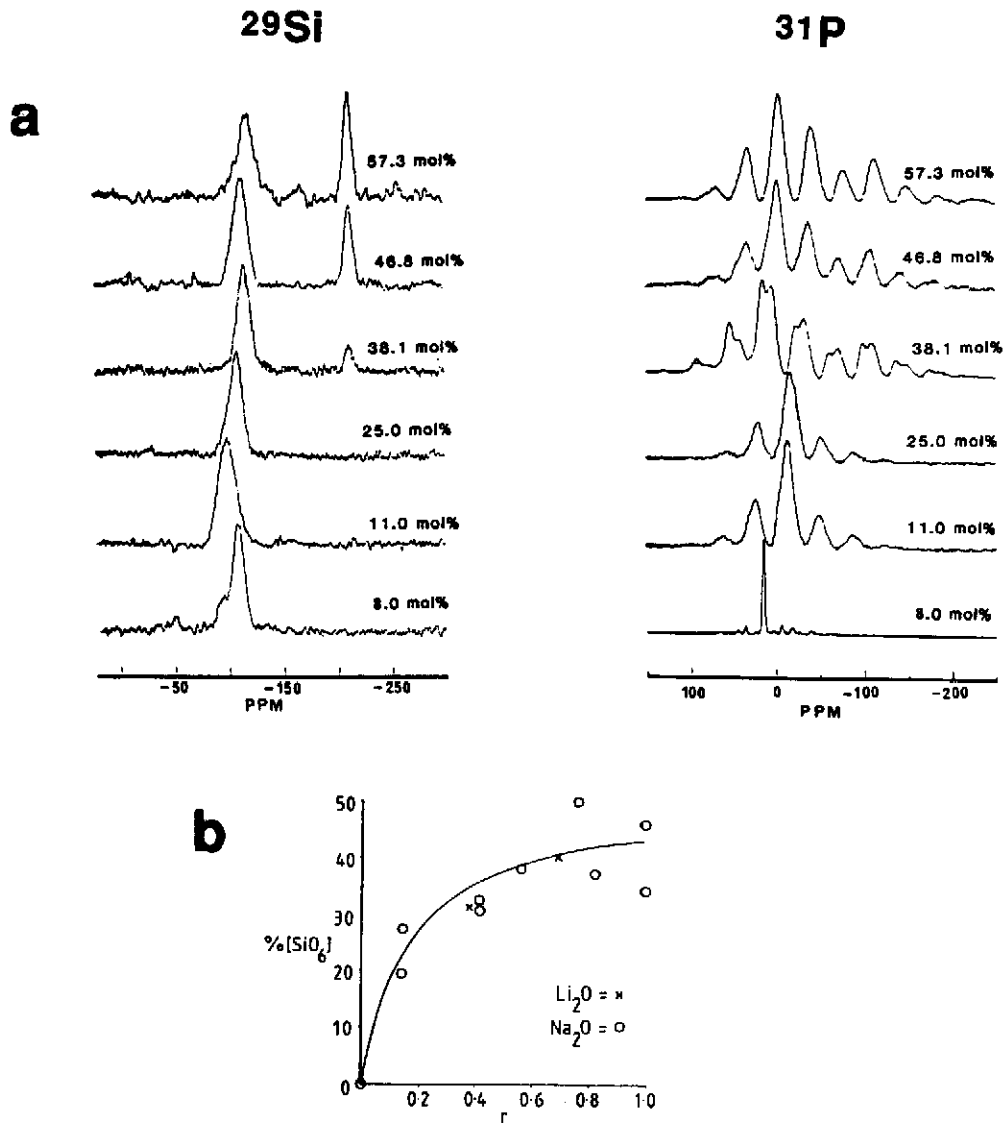

FIG. 44. (a) ^{29}Si and ^{31}P MAS-NMR spectra of sodium disilicate glasses containing the amounts of P_2O_5 shown against each spectrum. Note the formation of Si^{VI} at high P_2O_5 concentrations. Reproduced with permission from Ref. 406. (b) Observed fraction of Si^{VI} in glasses of composition rM_2O–$2SiO_2$–$3P_2O_5$ as a function of r ($0 \leqslant r \leqslant 1$). Reproduced with permission from Ref. 406.

illustrates typical results from ^{31}P dipolar spin-echo experiments. The experimental data agree with a model in which the phosphorus groups are distributed in a more-or-less statistical fashion, and are not clustered.[409] Ternary SiO_2–P_2O_5–Al_2O_3 glasses show more symmetrical $AlPO_4$-like sites.[410]

8.2. *The Structure of Borophosphate Glasses*

Both ^{31}P MAS-NMR[411–413] and ^{11}B wideline NMR[414–418] have been utilized to study the competitive network coformer effect in borophosphate glasses. ^{11}B NMR generally shows that the

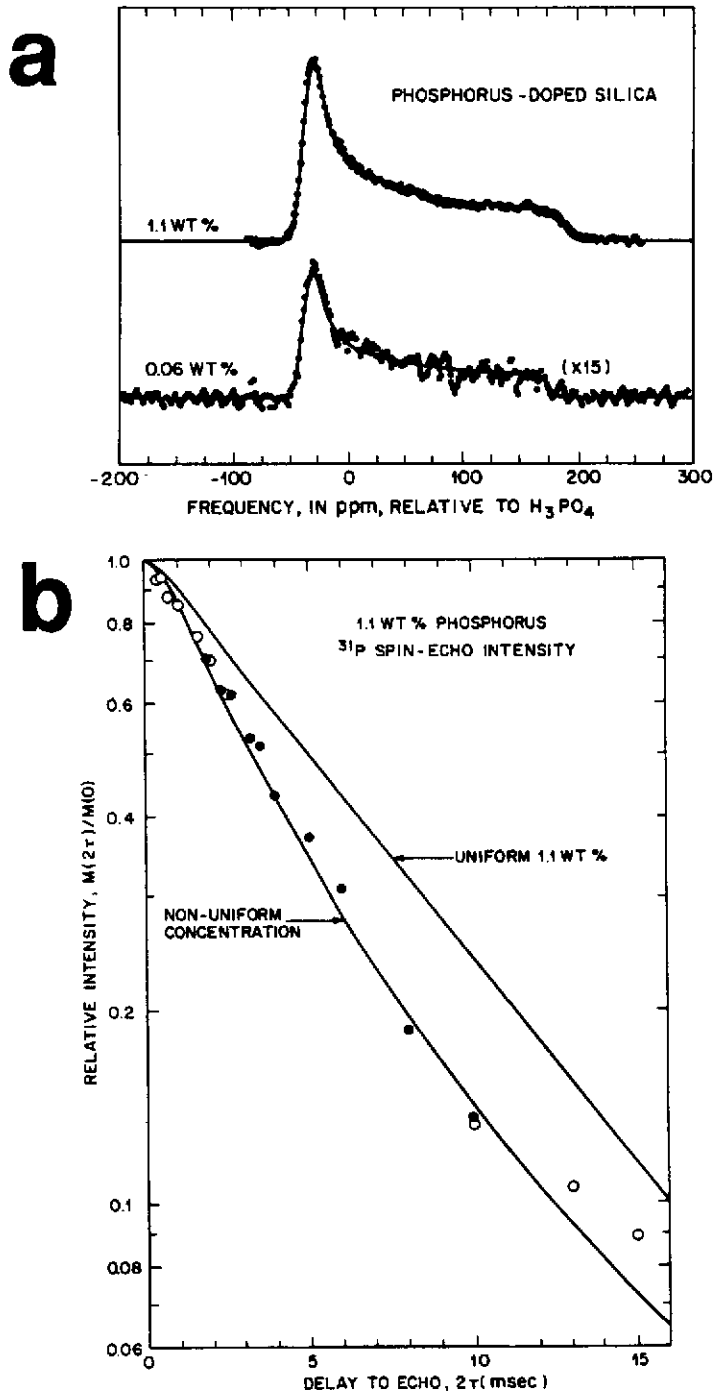

FIG. 45. ^{31}P NMR results obtained for P_2O_5-doped silica. (a) Static ^{31}P spectrum as a-function of doping level. (b) Spin-echo decay experiments on the sample containing 1.1 wt% P. Closed and open circles represent results from two independent data sets. The experimental data are compared with a uniform and a random distribution of P atoms. Reproduced with permission from Ref. 409.

introduction of P_2O_5 into binary alkali borate glasses increases N_4. Furthermore, the presence of phosphorus in the glass markedly alters the dependence of N_4 on R, and is best described by the relation:

$$N_4 = 0.5\,\alpha R + \beta, \tag{47}$$

where α and β depend on the ratio $K = [P_2O_5]/[B_2O_3]$.[416]

This result means that there are at least two fundamentally different types of BO_4 units in the glass structure: those formed as a consequence of the interaction of B_2O_3 with alkali oxide and those formed as a consequence of the interaction of B_2O_3 with P_2O_5. The latter are suggested to be $B(OP)_4^-$ units, well-known to exist in crystalline BPO_4.

The most important contribution to our current knowledge of the structure of borophosphate glasses has come from the excellent study of Villa *et al.*[413] The various phosphorus environments that are expected in these glasses will be denoted as $P_m^{(n)}$, where n is the number of bridging oxygen atoms and m is the number of next-nearest B neighbors ($m \leqslant n$). Thus, we expect a total of 10 distinct units, namely $P^{(0)}$, $P_0^{(1)}$, $P_1^{(1)}$, $P_0^{(2)}$, $P_1^{(2)}$, $P_2^{(2)}$, $P_0^{(3)}$, $P_1^{(3)}$, $P_2^{(3)}$, $P_3^{(3)}$. An additional possibility is the formation of a "BPO_4" unit, $P_4^{(4)}$, known to exist in crystalline borophosphate. Chemical shift assignments for these units, as far as they exist, have come from detailed compositionally dependent MAS-NMR studies on a wide range of glasses in the systems $Li_2O \cdot z[(B_2O_3)_y(P_2O_5)_{1-y}]$ and $Ag_2O \cdot z[(B_2O_3)_y(P_2O_5)_{1-y}]$. The results on the lithium-based glasses are somewhat affected by reduced resolution[412,413] and potential phase separation problems, but the silver-based glasses have resulted in exceptionally detailed information. Figure 46a shows typical spectra and corresponding peak assignments. From these studies, the following picture has emerged: In the ultraphosphate region ($z > 1$), substitution of P_2O_5 by small amounts of B_2O_3 leads to the immediate "disproportionation" of $P^{(3)}$ units ($P^{(3)}$ units connected to boron are concluded to be unstable) into $P_4^{(4)}$ and $P_1^{(2)}$ units. As y is increased, the $P_4^{(4)}$ units are depolymerized under successive formation of $P_1^{(2)}$, $P_2^{(2)}$, and (at high y values) $P_1^{(1)}$ units. Similar effects are incurred in the *meta*- and pyrophosphate region. The NMR data can be interpreted comprehensively by calculating the average charge of the PO_4 tetrahedron

$$Q = \sum i(P^{(3-i)}), \tag{48}$$

with $i = -1$, 0, 1, 2, and 3 for $P^{(4)}$, $P^{(3)}$, $P^{(2)}$, $P^{(1)}$, and $P^{(0)}$ units, respectively. Q can be obtained by measuring the fractional contributions ($P^{(n)}$) ($n = 3 - i$) via peak deconvolution of the assigned spectra. Figure 46b summarizes the results, illustrating that B substitution generally leads to an increase of Q, i.e. a decrease in the average number of bridging oxygens per P atom. These results clearly argue against an "equal partition model" which would leave the average state of polymerization constant and independent of y. Instead, the results favor a distribution of the network modifier such that the charge on the phosphorus units is systematically increased. This result is again reminiscent of the "scavenging" effect observed for phosphorus in silicate glasses (see above). For low y values, the results are quantitatively consistent with the notion that the phosphorus charge is actually maximized, whereas for y-values > 0.5 a compromise between equal partition and charge maximization is attained. It is in this compositional region that dopant components (LiCl, AgI) that are added to increase the ionic conductivity, are also found to have a pronounced influence on the glass structure, by generally favoring charge maximization for the P atoms. The pronounced effect of AgI and LiCl dopants in the present system is exceptional, and contrasts with their structural inertness in many other glass systems. Most likely this is a kinetic effect, however, and does not involve direct participation of the halide ions in the phosphorus coordination environments.

It would be of interest to compare the conclusion from the ^{31}P MAS-NMR data regarding the maximization of the phosphorus charge with the ^{11}B NMR data of Yun and Bray.[416] Even if we assume that the different counter-cations used in both studies do not affect the behavior, the primary difficulty lies in the fact that the low-field cw ^{11}B technique cannot differentiate between the four-coordinate B atoms arising from the borate–phosphate interaction and those arising from the borate–alkali oxide interaction. It is therefore not possible to quantitate the fraction of modified

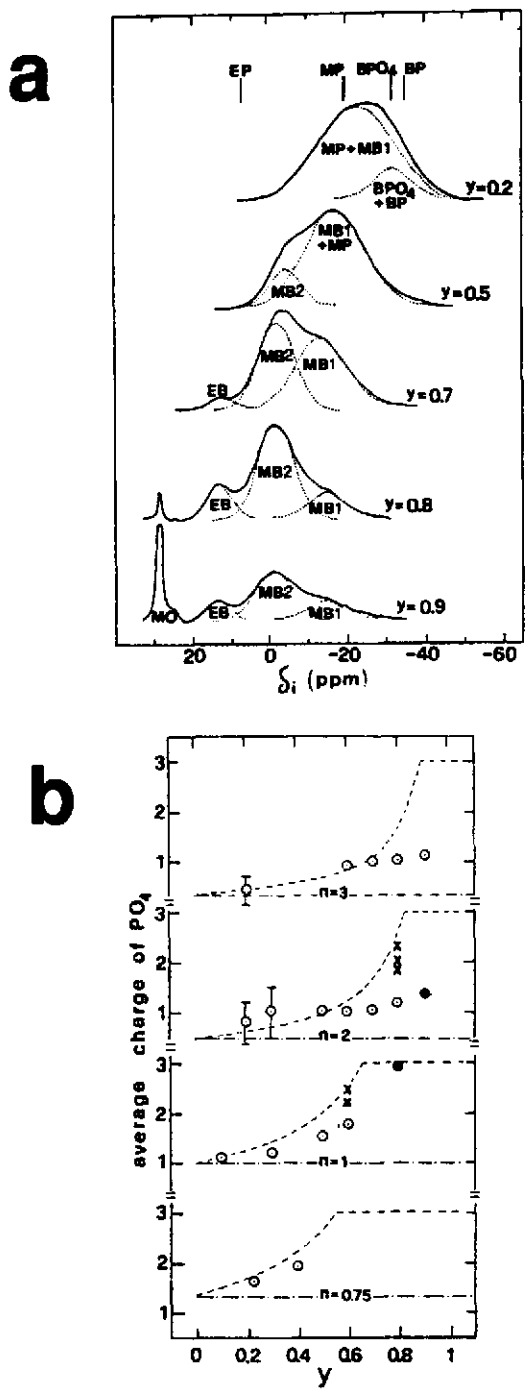

FIG. 46. ^{31}P MAS-NMR results obtained on silver borophosphate glasses. (a) Glasses in the system $Ag_2O \times 2(B_2O_3)_y(P_2O_5)_{1-y}$. The terminology used by the authors translates into the terminology used here in the following manner: $MO = P^{(0)}$, $EB = P_1^{(1)}$, $EP = P_0^{(1)}$, $MB2 = P_2^{(2)}$, $MB1 = P_1^{(2)}$, $MP = P^{(2)}$, $BP = P^{(3)}$, $BPO_4 = P_4^{(4)}$. (b) Average negative charge of phosphate units in silver borophosphate glasses of composition $Ag_2O \times n(B_2O_3)_y(P_2O_5)_{1-y}$ as a function of n and y. Open circles, filled circles, and x refer to glasses, partially crystallized samples, and glasses doped with AgI, respectively. The dashed–dotted line represents an equal partition of non-bridging oxygen atoms between the borate and the phosphate networks, whereas the dashed curves correspond to a model in which the average charge on phosphorus is maximized. Reproduced with permission from Ref. 413.

boron. This question awaits an answer from ^{11}B MAS-NMR studies at high fields, which might be able to resolve separate peaks for both types of tetrahedral boron atoms.

8.3. *The Structure of Borosilicate Glasses*

Because of their widespread practical applications, borosilicate glasses have attracted great interest for fundamental structural studies including solid state NMR investigations. To date, the majority of knowledge has been derived from low-field cw ^{11}B NMR spectra,[419-444] which are analyzed in terms of B^{III}, B^{III_s}, and B^{III_a} species along the lines of Fig. 38. More recently, these studies have been complemented by ^{17}O and ^{29}Si MAS-NMR work.[445] While the ^{29}Si NMR spectra are broad and unresolved, the resonance center permits a qualitative estimate of the $Si^{(n)}$ species containing non-bridging oxygen atoms. A promising complementary method recently introduced by Kirkpatrick and coworkers is high-field ^{17}O wideline or MAS NMR.[445] Even at the highest available field strengths the static lineshapes are governed by second-order quadrupolar broadening, giving rise to spectra such as shown in Fig. 9. As illustrated in Fig. 47, ^{17}O NMR is uniquely suited for differentiating between various oxygen sites in borosilicate glasses. The assignments made in Fig. 47 are based on model compounds and the expectations from the earlier ^{11}B NMR work, regarding compositional dependences.

Early on, elaborate reaction schemes were developed in order to explain the compositional dependence of N_4, N_{3a}, and N_{3s} measured by ^{11}B NMR and these descriptions have evolved considerably over time. As stated by Dell *et al.*[433] it is important to realize that these reaction schemes

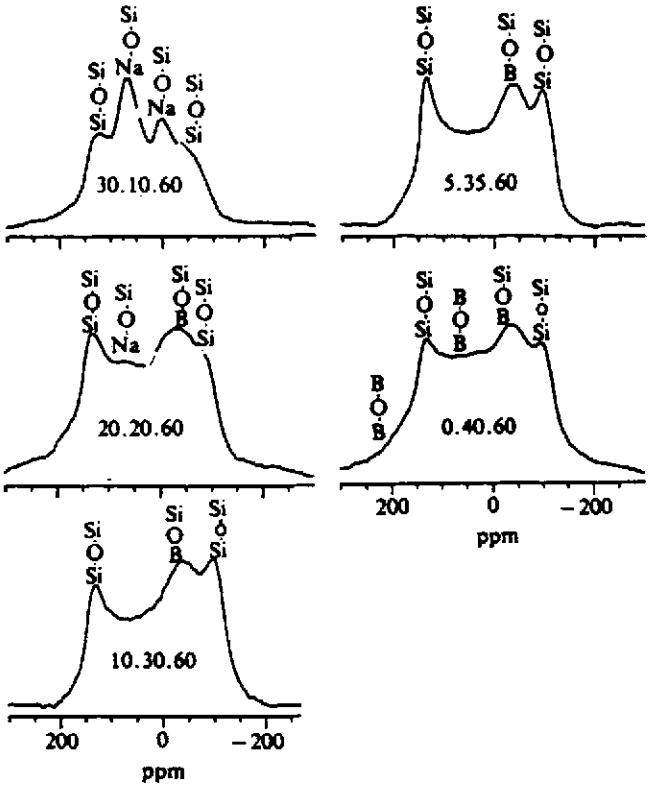

FIG. 47. ^{17}O NMR spectra of static samples and assignments in sodium borosilicate glasses. The numerals indicate molar percentages of Na_2O, B_2O_3, and SiO_2, respectively. Reproduced with permission from Ref. 445.

should not be taken in the literal sense, but simply as a way of picturing the (highly non-statistical) species distributions as a function of composition.

In general, for glasses of the general composition $xNa_2O \cdot yB_2O_3 \cdot zSiO_2$, the boron speciation can be discussed separately within four distinct compositional regimes, characterized by the quantities $R = x/y$ and $K = z/y$. Again, this choice in the description is necessarily a simplification of the multitude of mutually dependent equilibria in the molten state, and the transitions from one regime to the next are not to be viewed as discontinuous.[433]

Region I: ($R \leqslant 0.5$); In this region, the boron speciation is identical to that found in binary borate glasses, regardless of silica content. Only B^{III_a} and B^{IV} units are present. Likewise ^{29}Si MAS-NMR spectra are identical with those of glassy SiO_2, and Si–O–Na linkages appear to be absent in the ^{17}O NMR spectra.[444,5] These NMR results thus suggest that in region I the borosilicate glasses are essentially mixtures of alkali borate glasses and vitreous silica. Indeed, borosilicate glasses in this compositional region are known for their tendency to phase-separate.

Region II: ($0.5 \leqslant R \leqslant R_{max} = 0.5 + K/16$). In this region, the boron speciation in alkali borosilicate glasses starts to deviate from that of binary alkali borate glasses. Specifically, N_4 continues to increase with R, up to a limiting value depending on K. The interpretation of this result invokes the formation of reedmergnerite ($NaB(OSi)_4$) units ($R = 1$; $K = 8$). This suggestion is supported by the chemical shift of the sharp ^{11}B NMR line, which lies close to that of reedmergnerite.[450] It is assumed that all of the silicon present is involved in these units. Furthermore, for $0.5 < R < R_{max} = 0.5 + K/16$ all of the alkaline oxide added to the network is assumed to contribute to the formation of these species, and non-bridging oxygen bonded to boron (B^{III_a} units) is not present. Therefore, in this compositional region the

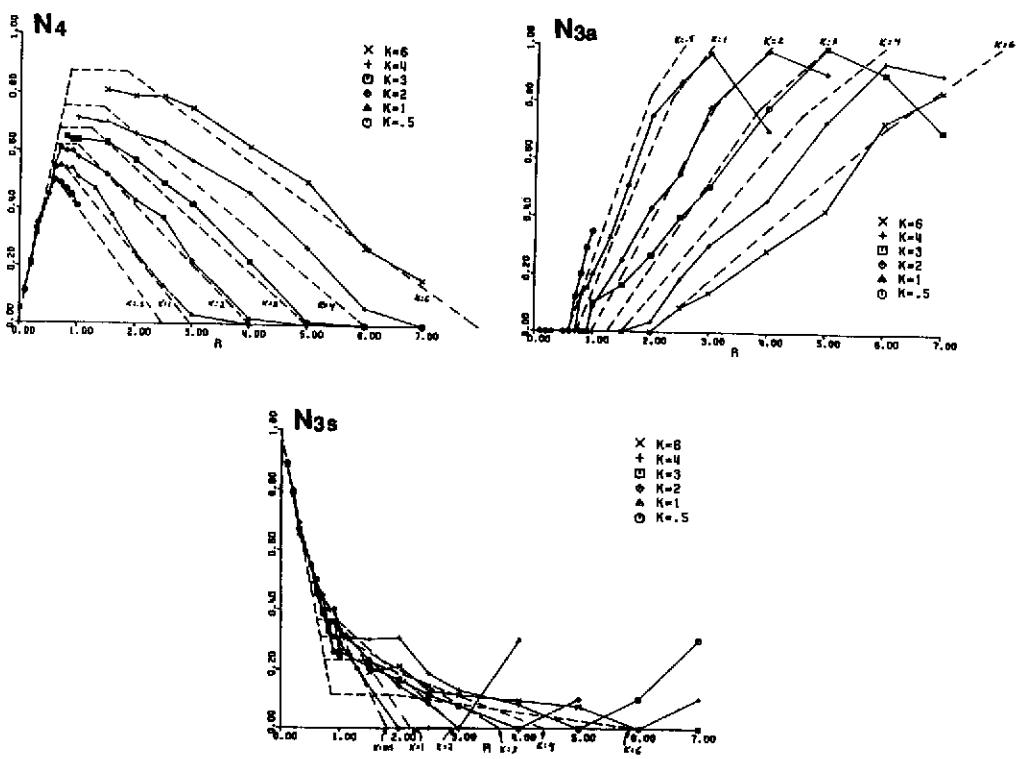

FIG. 48. Compositional dependence of N_4, N_{3a}, and N_{3s} in sodium borosilicate glasses, as a function of R = mol.% Na_2O/mol.%B_2O_3 and K = mol.%SiO_2/mol.%B_2O_3. Reproduced with permission from Ref. 433.

total concentration of tetrahedral boron is still equal to the sodium content in the glass. Complementary evidence for this idea has been given by ^{17}O and ^{29}Si NMR, although these experiments are less definitive due to poor resolution.[445]

Region III: $R_{max} < R < R_{D1} = 0.5 + K/4$. In this region, the glass contains silicate units with non-bridging oxygen atoms. It is assumed that little further boron conversion takes place here, and N_4 remains approximately constant. This idea, originally conceived from the interpretation of ^{11}B-N_4 data is strongly supported by ^{29}Si MAS, which shows a systematic downfield shift in accordance with the formation of $Si^{(4-n)}$ species.[445]

Region IV: $R > R_{D1}$: In this region, the B^{IV} species are successively converted to B^{IIIa} species, thus leading to a decrease of N_4. The alkali ions are partitioned more or less equally among the borate and silicate networks, respectively.

Within each compositional region, a separate set of relations is used to describe the quantities N_4 and N_{3a} as a function of R and K. These expressions, which are derived in Ref. 433, are depicted in Fig. 48, along with experimental results for the glass system Na_2O–B_2O_3–SiO_2. Similar models have been proposed for lithium borosilicate glasses. Furthermore, a number of borosilicate and germanate glasses with divalent cations have been published. For PbO–B_2O_3–SiO_2[447,448] CdO–B_2O_3–SiO_2,[449] and CdO–B_2O_3–GeO_2 glasses[446] the N_4 balance differs substantially from the situation in the alkali borosilicates. This is primarily due to two reasons: (a) the number of B^{IIIa} species bonded to non-bridging oxygen atoms is small, and (b) at higher concentration the divalent oxide gains the ability to participate in the network formation. Qualitative evidence for the latter is given by ^{113}Cd and ^{207}Pb chemical shift trends.[447,449] For cadmium borogermanate glasses, the NMR results are consistent with an equal sharing of the modifier between the borate and the germanate networks.

9. OTHER IONIC GLASS SYSTEMS

9.1. *Gallium Oxide Based Glasses*

In contrast to Al_2O_3, the heavier homologue Ga_2O_3 is able to form glasses in combination with alkali oxides. A particularly wide region of glass formation is encountered in the system Ga_2O_3–Cs_2O. Zhong and Bray have studied the ^{71}Ga and ^{69}Ga resonances of such glasses at a field strength of 7T.[451] Based on model compound studies, they conclude that ^{71}Ga, the isotope with the smaller quadrupole moment, provides reasonably good chemical shift separation between four and six-coordinated Ga atoms. The relative Ga(4)/Ga(6) peak ratio was shown to increase systematically with increasing Cs content. The question of whether all of the gallium present is actually detected, still needs to be examined.

9.2. *Tellurium Oxide Based Glasses*

TeO_2-based glasses show potential promise in the area of solid electrolytes and infrared optics. NMR investigations of such systems are at a very early stage. Preliminary ^{125}Te NMR measurements of simple alkali tellurite glasses show rather broad signals with limited informational content.[452] In the systems LiF–TeO_2 and Li_2O–TeO_2, ^7Li and ^{19}F second moments have been extracted from wideline NMR spectra and interpreted in terms of possible atomic distribution models.[453] It is not clear, however, whether the wideline spectra are entirely dominated by dipolar effects, as assumed in the analysis.

9.3. *Halide Glasses*

The structure of BeF_2 glass is very analogous to that of silica glass, consisting of corner-sharing BeF_4 tetrahedra. To date, only low-field cw ^{19}F and ^9Be NMR studies have been reported on BeF_2-based glasses.[454–457] The F atoms appear to be somewhat mobile at room temperature, resulting in a

reduced ^{19}F second moment. In addition to a broad ^{9}Be signal, an "anomalous" ^{9}Be resonance is detected, with a much sharper line width than predicted from the Be–F distances from eq. (16b).[455] Since this line cannot be attributed to the effect of fluoride diffusion (it stays sharp down to 77 K), the authors ascribe it to the presence of reduced berryllium clusters in the glass. Alternatively, the sharp line could be a rare example of the self-decoupling phenomenon, previously observed in compounds with presumably similar spin dynamics (KF and AgF).[458,459] According to this interpretation, the ^{19}F–^{9}Be dipolar interaction is averaged out by very rapid ^{19}F–^{19}F flip-flops.

Addition of NaF to glassy BeF_2 increases the strength of the nuclear electric quadrupole coupling, as detected by second-order effects on the ^{9}Be resonance at very low-fields. While the authors take this as evidence for some 5-coordinated Be, introduction of a non-bridging F atom is expected to have a similar effect. High-field NMR work still remains to be done in order to elucidate the detailed effect of network modifiers on the structure of glassy BeF_2.

Pronounced glassforming tendency is found in many phase diagrams involving heavy metal fluorides such as LaF_3 and ZrF_4 and mixed systems.[460] These "halide" glasses are an interesting new class of solid state materials with promising applications for infrared windows and solid electrolytes. Although NMR spectroscopy has been widely applied to elucidate the diffusive behavior of the mobile fluoride ions in these systems (see section 12), to date few substantial structural insights have been obtained. The ^{19}F NMR lineshape is dominated by very strong homonuclear dipole–dipole coupling among the ^{19}F spins.[461] In view of the multicomponent character of these glasses one expects to find a number of chemically distinct fluoride species. Repeated experimental claims to this effect[462,463] require further examination by high-field, high resolution solid state NMR. This task necessitates either MAS at spinning frequencies in excess of the dipolar line width (> 20 kHz) or in combination with special multiple-pulse sequences. Neither of these experimentally demanding applications have been reported so far on these relatively novel materials.

9.4. *Other Glass Systems*

^{27}Al MAS-NMR studies of amorphous alumina films generated via anodic oxidation reveal the presence of Al^{IV}, Al^{V}, and Al^{VI}.[464] Amorphous SiO shows two signals at -67 and -109 ppm, which are attributed to a-Si- and a-SiO_2-like environments, respectively. The quantitative evaluation of these results is difficult, because only ca. 50% of the expected signal intensity is seen. In connection with ESR spin counting studies, the authors conclude that nearby unpaired electron spins render a significant fraction of the silicon nuclei unobservable.[465]

10. NON-OXIDE CHALCOGENIDE GLASSES

Non-oxide chalcogenide glasses based on the sulfides, selenides, and tellurides of Main Group III–V elements are a promising new class of solid state materials, with intriguing possibilities for applications as low-frequency waveguides, fibers, and solid electrolytes.[466] In the past two decades, much work has been devoted to the phase diagrams, regions of glass formation and the thermodynamic and physicochemical properties of these systems. It has been much more recently that, driven by the search for structural guidelines to optimize materials properties, the atomic arrangements of these systems have been subject to direct spectroscopic investigation. During the course of such studies a number of unusual structural features have been uncovered that are challenging the applicability of existing glass structure hypotheses, and bear great intrinsic interest for a better understanding of glass formation in covalent systems. These features have included valence alternation pairs,[467] new types of micro-environments not known in analogous crystalline compounds[468,469] and cluster entities with a high degree of intermediate range order.[470] Since, however, many of the spectroscopic techniques used are not inherently quantitative and tend to emphasize ordered environments, there is currently a great need for new experimental probes that can test the existing structural hypotheses in a more stringent manner. Solid state NMR appears to be an excellent method of choice, particularly in view of the many contributions this technique has made to fundamental knowledge in the oxide glass area. Indeed, a

number of cw NMR applications to chalcogenide glasses have been published since the early 1970s.[471-495] A more detailed discussion of these early works can be found in Ref. 34. While much of these initial NMR applications broke new ground, the inability of low-field cw NMR techniques to provide sufficiently specific structural information, and the lack of a database for crystalline model compounds was a clear handicap in these early studies. It has been much more recently, that, with the application of selective averaging techniques, the considerable potential of modern solid state NMR techniques has become much more apparent.

In general, the types of chalcogenide glasses currently under investigation can be grouped into two classes: (a) binary and ternary III–V chalcogenides, and (b) network former/network modifier systems, which are based on stoichiometric main group III–V chalcogenides and stoichiometric sulfides of electropositive cations. In the following these groups will be discussed separately.

10.1. *Atomic Distribution and Site Speciation in Binary and Ternary III, IV, and V Chalcogenides*

This group comprises the glassy alloys of main group III–V elements with sulfur and selenium. A characteristic feature of these glasses, which distinguishes them from compositionally analogous oxidic systems, is their pronounced tolerance towards deviations from stoichiometry. In binary systems, the region of glass formation typically extends from the pure chalcogen well beyond the stoichiometry of the binary compound known in the crystalline state. Incorporation of a third constituent often enlarges the region of glass formation considerably. Currently, the interest in these systems focuses mainly on their potential uses in infrared optics. The air- and moisture-sensitivity and the low glass transition temperatures of many systems, however, have remained substantial challenges that need to be overcome by the development of new materials.

10.1.1. *Binary Boron Chalcogenide Glasses.* In analogy to B_2O_3, samples with the nominal compositions B_2S_3 and B_2Se_3 can be prepared in the glassy state. A number of NMR studies of glassy B_2S_3 have been published in the literature.[355,496-498] As discussed in Ref. 499 studies employing commercial B_2S_3 without further purification are suspect due to the doubtful chemical composition of this material. The production of research-quality samples necessitates either very elaborate clean-up procedures or synthesis from the elements under carefully controlled experimental conditions.[498,499] The ^{11}B cw wideline NMR spectrum of glassy B_2S_3 produced in this fashion confirms that the glass structure is based on trigonal $BS_{3/2}$ units. The lineshape can be fitted to a much narrower EFG distribution than that of B_2O_3, hence suggesting a lesser degree of disorder.[498] In contrast, the corresponding B–Se glasses show no evidence of analogous $BSe_{3/2}$ units. Instead, the composition "B_2Se_3" appears to disproportionate into BSe_2 and a yellowish amorphous selenide B_xSe ($x \leqslant 1$). BSe_2 prepared in this fashion has a polymeric structure containing a selenium–selenium bond (see Ref. 500). Strong internuclear dipole–dipole interactions detected by NMR indicate that the B_xSe phase must contain boron–boron bonds.[498] The dramatic differences between the B–S and the B–Se systems reveal the increasingly efficient competition of homo-atomic (B–B and Se–Se) versus heteroatomic (B–Se) bond formation as the size of the chalcogen atoms is increased. Binary boron tellurides are not even known.[501]

10.1.2. *Binary Silicon Chalcogenide Glasses.* In contrast to SiO_2, the heavier silicon chalcogenides SiS_2 and $SiSe_2$ can only be converted to the glassy state by rapid melt-quenching. Extensive infrared and Raman spectroscopic studies carried out on these glasses have revealed the presence of $SiX_{4/2}$ tetrahedra interconnected by edge-sharing.[502-504] Such edge-sharing units are well-recognized structural features in the crystal chemistry of silicon sulfides and selenides.[500] However, in the glassy state they constitute a violation of the traditional Zachariasen network model, which explicitly excludes any connectivities different from corner-sharing. While vibrational spectroscopy is limited to the qualitative aspect, further quantitation can be obtained by solid state NMR.[505-508] Figure 49 compares the MAS-NMR spectra of glassy SiO_2[114] with those obtained on glassy SiS_2 and $SiSe_2$.[505-507] Note that, in contrast to the SiO_2 spectrum, the spectra of the latter two glasses show multiple peaks. This finding suggests that the bond angle distribution functions in glassy SiS_2 and

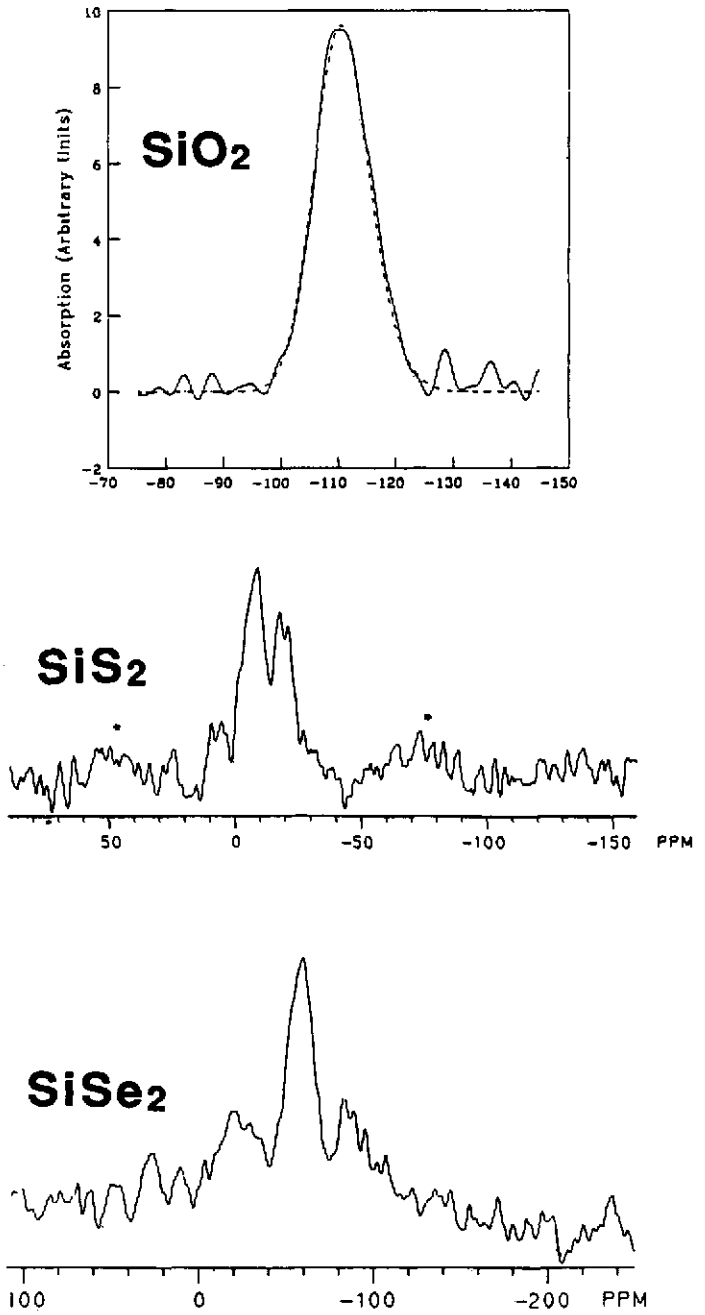

FIG. 49. ^{29}Si MAS-NMR spectra of glassy SiO_2, SiS_2, and $SiSe_2$. The SiO_2 spectrum is reproduced from Ref. 114.

$SiSe_2$ are non-monotonic and contain distinct maxima and minima. The three broad maxima observed in the NMR spectra can be assigned[505] to silicon tetrahedra sharing edges with no, one or two adjacent tetrahedral units $E^{(0)}$, $E^{(1)}$, and $E^{(2)}$, respectively. These units are shown below (Scheme 1).

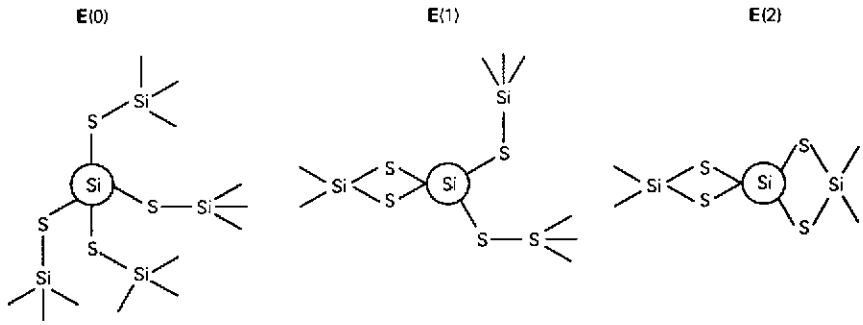

SCHEME I.

Evidently, the individual $E^{(n)}$ species have sufficiently different average Si–S–Si bond angles, that discrete resonances can be observed. Compared with the situation in silicates, the relationship between $\delta_{iso}(^{29}Si)$ and average bond angles $\langle\alpha\rangle$ appears to be reversed here, with smaller angles yielding more upfield shifts. This reversal arises from the combined effect of multiple electronic factors contributing to the measured chemical shift value. It serves to illustrate the inherent difficulties one confronts when relating chemical shifts to structural properties.

The quantitative ratio $E^{(0)}:E^{(1)}:E^{(2)}$ is roughly 1:2:1 both in glassy SiS_2 and glassy $SiSe_2$.[505–507] Note that the observation of $E^{(2)}$ units implies the presence of a $[SiSe_2]_n$ chain of at least three silicon atoms. At the present time it is not possible, however, to answer the question of the distribution of chain lengths and the connectivity of the $E^{(n)}$ species. Studies of Si–X glasses with higher chalcogen contents show different behavior for the sulfides and selenides. Si–S glasses tend to phase separate, hence yielding a compositionally independent $E^{(n)}$ distribution.[508] In contrast, Si–Se glasses with higher Se contents show an increase of the $E^{(0)}$ component, whereas the $E^{(2)}$ component is essentially absent.[506] The same result is obtained in mixed $SiSe_2$–P_2Se_5 glasses, indicating a more continuous distribution of silicon microstructures, including the presence of Si–Se–Se and Si–Se–P linkages. The inapplicability of a segregation model in the Si–Se system is also consistent with evidence from vibrational spectroscopy.[509]

10.1.3. *Phosphorus Chalcogenide Glasses*

10.1.3.1. *The system P–Se.* The system phosphorus–selenium is characterized by a pronounced tendency towards vitrification. Glasses are formed over a wide compositional region, from 0–52 and 62–80 mol.% P. There is a marked change in the compositional dependence of thermal and mechanical properties near 40 at% P. In part due to mutually contradictory phase diagrams, the structural organization of these glasses has been subject to a great deal of speculation and controversy.[510–516] Extensive spectroscopic investigations have been carried out,[517–519] but it has been only very recently that modern solid state NMR techniques have been employed.[520–525] Figure 50 shows some possible short-range order environments that might be present. NMR experiments on crystalline model compounds show that three- and four-coordinate P atoms have distinct chemical shift ranges. For three-coordinate P atoms, however, it is not possible on the basis of chemical shifts to identify the number of P or Se nearest neighbors.[521]

Figure 51a shows representative ^{31}P MAS-NMR spectra of binary P–Se glasses.[521] Very fast spinning is an essential prerequisite for achieving site resolution in these systems, since the linewidths are rather large due to wide chemical shift distributions. Thus, it is only at spinning speeds of 12–14 kHz that the sidebands are sufficiently decreased in intensity and far enough removed from the centerbands, to make the analysis reliable. In accordance with the model compound work, the two peaks in the vicinity of 130 and 10 ppm are assigned to three and four-coordinate P (P^{III} and P^{IV}),

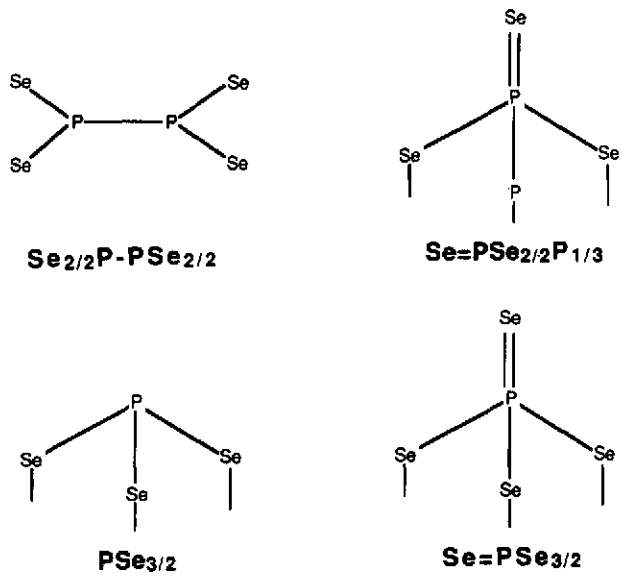

FIG. 50. Possible short-range order environments in P–Se glasses.

respectively. Note the systematic depletion of P^{IV} units at higher P contents as expected from equilibrium considerations.

Figure 51b shows the mole fraction of four-coordinated P atoms $[P^{IV}] = N_4\{P\}$ as a function of composition. Here $\{P\}$ is the total mole fraction of P present and N_4 is the fraction of four-coordinated P atoms. The quantitative phosphorus speciation in the region of low phosphorus contents (up to 30 at%) can be nicely explained in terms of a melt-equilibrium model:

$$PSe_{3/2} + Se \rightleftarrows Se{=}PSe_{3/2} \tag{49}$$

assuming an equilibrium constant around 0.8 at.$^{-1}$

Within the compositional region from 30 to 50 at%P ^{31}P MAS-NMR spectra show only small differences. Above 47.5 mol.% P, the MAS-NMR spectra reveal molecular P_4Se_3 units, which are dispersed within the glassy matrix.

The statistics of P–P versus P–Se bonding have been addressed by dipolar spin-echo spectroscopy.[522–525] Ultimately this issue raises the question of how the phosphorus atoms are distributed in space. Three such possible distributions, corresponding to (a) uniform (b) clustered, and (c) random arrangements are shown in Fig. 52. Obviously these three arrangements produce significantly different internuclear distance distributions. Via eq. (16), these distance distributions yield different theoretical M_{2d} values, which are then compared with experimental data from spin-echo NMR (see eq. 31).

Figure 52 shows the results of experimental spin-echo NMR studies and computer-simulations, illustrating the comparison between calculated and experimental M_{2d} values for the three different distribution models. Clearly the experimental data are incompatible with either uniform, clustered or random arrangements. Qualitatively, these results indicate that P–P bond formation does occur over a wide range of compositions, however, to a distinctly lesser extent than statistically probable. More quantitative information is obtained from a detailed analysis of the overall spin echo decay function. As revealed by the simulations in Fig. 53, the spin echo decays for P atoms coordinated to selenium only and the decays for P atoms with a phosphorus nearest neighbor are distinctly different. One can then vary the fraction of P-bonded P atoms in the simulations until a satisfactory agreement with the experimental data is obtained.[524] Typical results are shown in Fig. 54. The simulations reveal that P–P bonds contribute to the glass structure above 25 at%P.

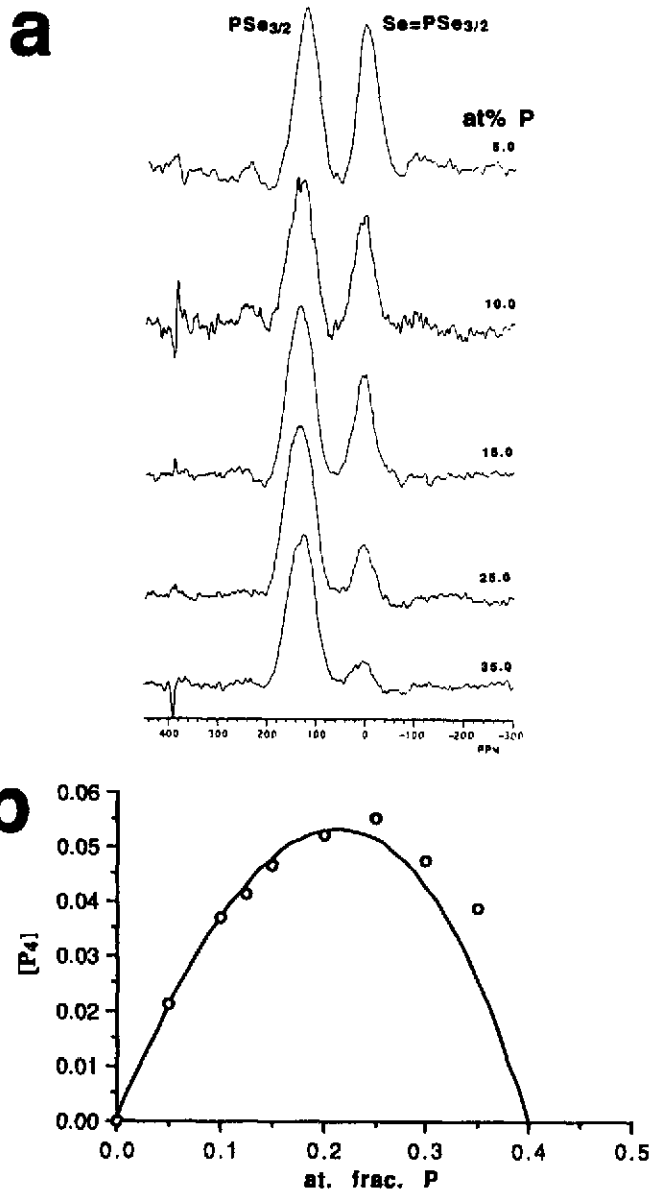

FIG. 51. (a) Representative ^{31}P MAS-NMR spectra of binary P–Se glasses. Reproduced from Ref. 521. (b) Mole fraction of four-coordinated P atoms present in P–Se glasses, as a function of composition. This number is calculated as $[P^{IV}] = N_4\{P\}$, where N_4 is the fraction of P atoms that are four-coordinated and $\{P\}$ is the atomic fraction of phosphorus present in the glass. The solid curve is calculated according to an assumed equilibrium $PSe_{3/2} + Se \rightleftarrows Se = PSe_{3/2}$ with an equilibrium constant of 0.8 at. fraction^{-1}.

The combined analysis of ^{31}P spin-echo and MAS-NMR results yields the final phosphorus speciation of Fig. 55.[524] There is a definite preference towards formation of P–Se rather than P–P bonds. Likewise P–Se bonds are greatly favored over Se–Se bonds, although the latter can be found over the entire glass-forming region. While there exists a distinct driving force for the formation of $PSe_{3/2}$ groups, the reaction of these units with excess Se to form $Se{=}PSe_{3/2}$ groups is much less favored.

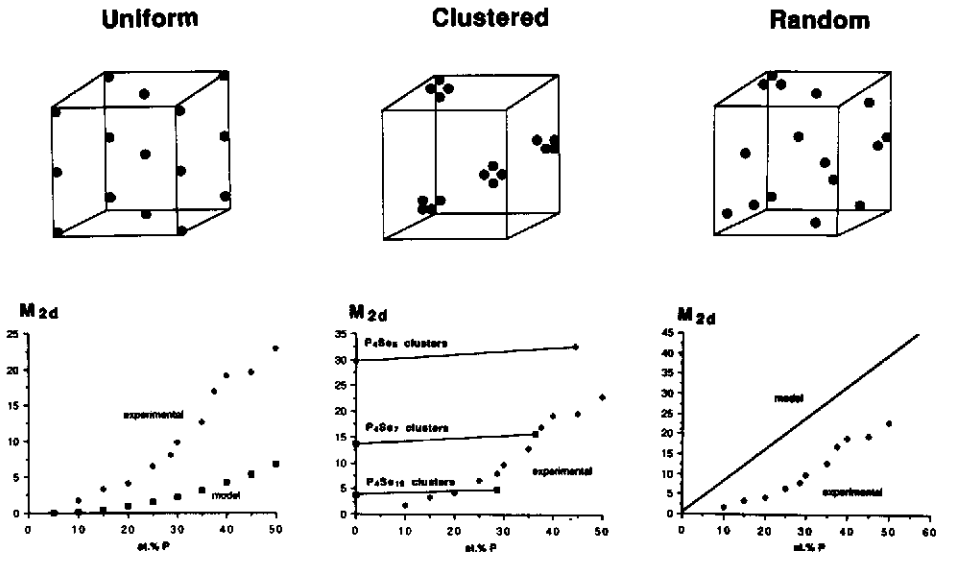

FIG. 52. Possible atomic distribution models for P-atoms in phosphorus–selenium glasses and other chalcogenide systems and their test against the compositional dependence of the ^{31}P second moments.

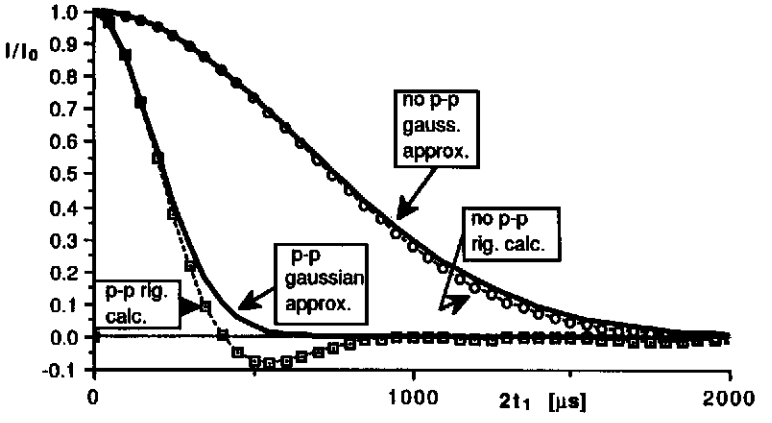

FIG. 53. Computer simulations of spin-echo decays for phosphorus atoms bonded to one P, and for phosphorus atoms not bonded to P in a P–Se glass containing 40 at%P randomly distributed beyond the first coordination sphere. Included are the results of a rigorous calculation as well as a Gaussian approximation.

The multitude of structural units present at each composition tends to disfavor nucleation processes that would eventually lead to crystallization. This chemical disorder qualitatively explains the high tendency for glass formation in the P–Se system and the great resistance of these glasses to recrystallization.

It is interesting to explore the relationship of the microstructural speciation shown in Fig. 55 with the compositional dependence of T_g. No unusual features or speciation discontinuities are visible around 40 at% P. Most likely, the T_g increase is not a short-range order effect, but rather a percolation phenomenon,[526] related to a depletion of longer Se_n chain units. Indeed, application of the percolation concept to P–Se glasses predicts the rigidity percolation threshold right at 40 at% P.[524]

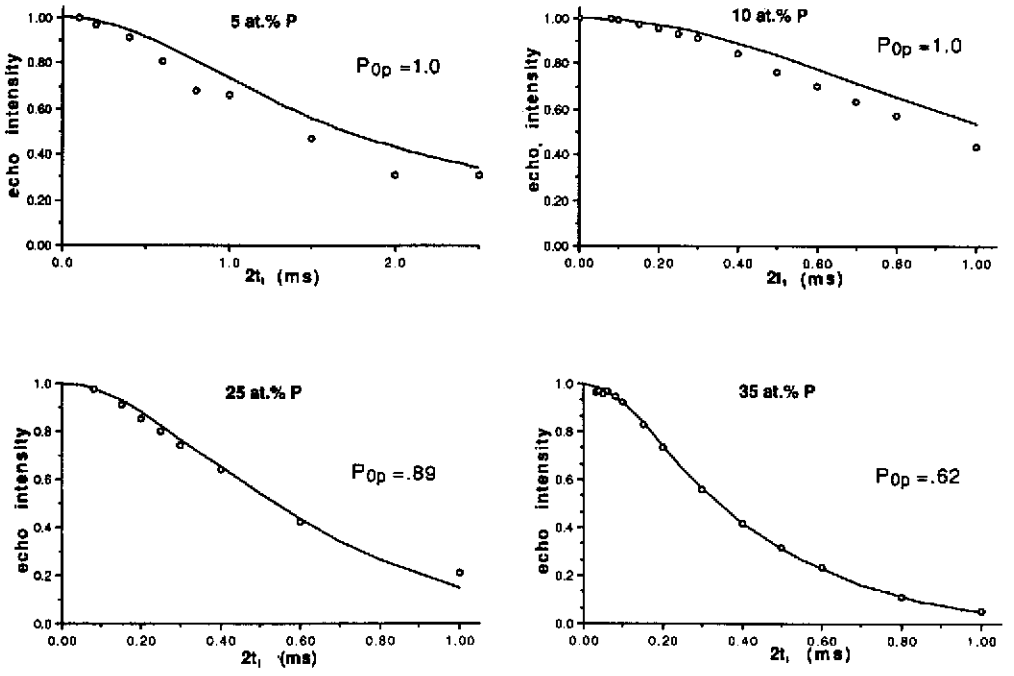

FIG. 54. Experimental (points) and calculated (curves) spin echo decays for P–Se glasses, using the fraction of P-bonded phosphorus atoms. Note the systematic deviation of the experimental ^{31}P spin echo decays of P–Se glasses with low P contents from the calculated decays assuming a random P distribution with no P–P bonding. Reproduced from Ref. 524.

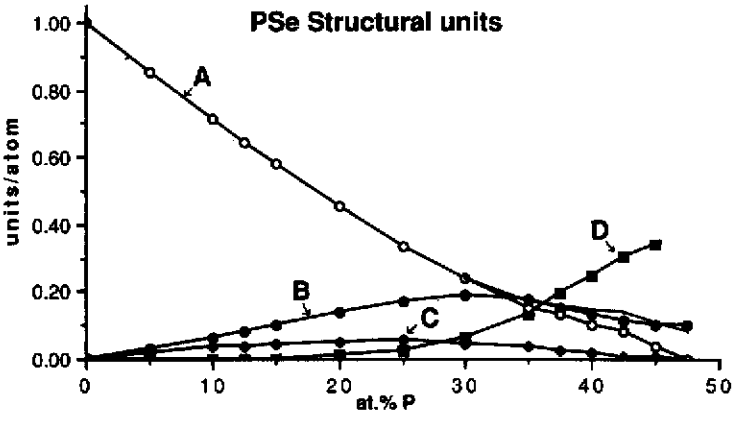

FIG. 55. Site speciation in P–Se glasses, as deduced from the combined analysis of spin-echo and MAS-NMR investigations. A: Se–Se bonds, B: $PSe_{3/2}$ units, C: $Se=PSe_{3/2}$ units, D: P–P bonded units. Reproduced from Ref. 524.

While both the MAS-NMR and spin-echo data disagree with the cluster model as portrayed in Ref. 517, at low P concentrations the ^{31}P spin echo intensities deviate significantly from the simulations based on random P distribution and no P–P bonding, as shown in Fig. 54. This result could signify a more subtle intermediate-range ordering phenomenon, where the formation of P–Se–P linkages is favored to some degree. The situation is sketched schematically in Fig. 56. Evidently, the P distribution

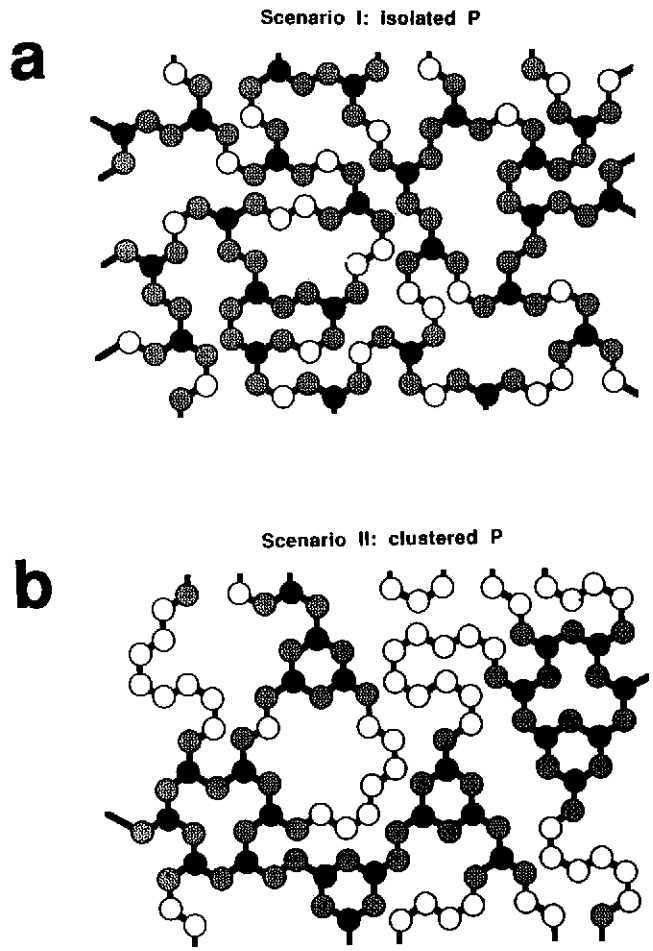

FIG. 56. Two possible scenarios on the P-distribution in P–Se glasses with low P contents: (a) random distribution of P atoms: (b) partial clustering, resulting in an enhanced probability of P–Se–P bridges. Black circles: P atoms, grey circles: P-bonded Se atoms, white circles: Se-bonded Se atoms.

looks more like that in part (b) rather than part (a) of this figure. This question can be investigated by studying the ^{31}P–^{77}Se dipole–dipole couplings with the SEDOR technique.[525] Figure 57 shows the echo intensity as a function of dipolar evolution time. Part A of this figure shows that even in the absence of the ^{31}P pulse, the ^{77}Se spin echo decays slowly with $2t_1$ (open squares). This behavior is attributed to the effect of ^{77}Se–^{77}Se interactions. In contrast, when the ^{31}P pulse is present, the SEDOR decay (filled squares) has two distinct components: a short-term component due to Se-atoms directly bonded to P, (and hence decaying rapidly because of the strong ^{31}P–^{77}Se dipole coupling), and a long-term component due to Se atoms not directly bonded to P. For the long-term component, the ^{31}P–^{77}Se interaction is insignificant, and the time behavior matches closely that of the regular ^{77}Se spin echo decay (i.e. in the absence of the ^{31}P pulse) observed for the entire Se population. Extrapolation of this long time behavior to zero time yields Se_{se}, the percentage of Se atoms not directly bonded to P. Furthermore, subtraction of the long-term spin echo decay function from the entire set of data affords the decay function of the P-bonded Se atoms selectively. As shown in the simulations Fig. 57, part B, these decay functions differ substantially between a Se species bonded to one and only one P atom and a Se species, which forms a P–Se–P linkage. The experimental data show intermediate behavior between the two extreme scenarios of Fig. 56.

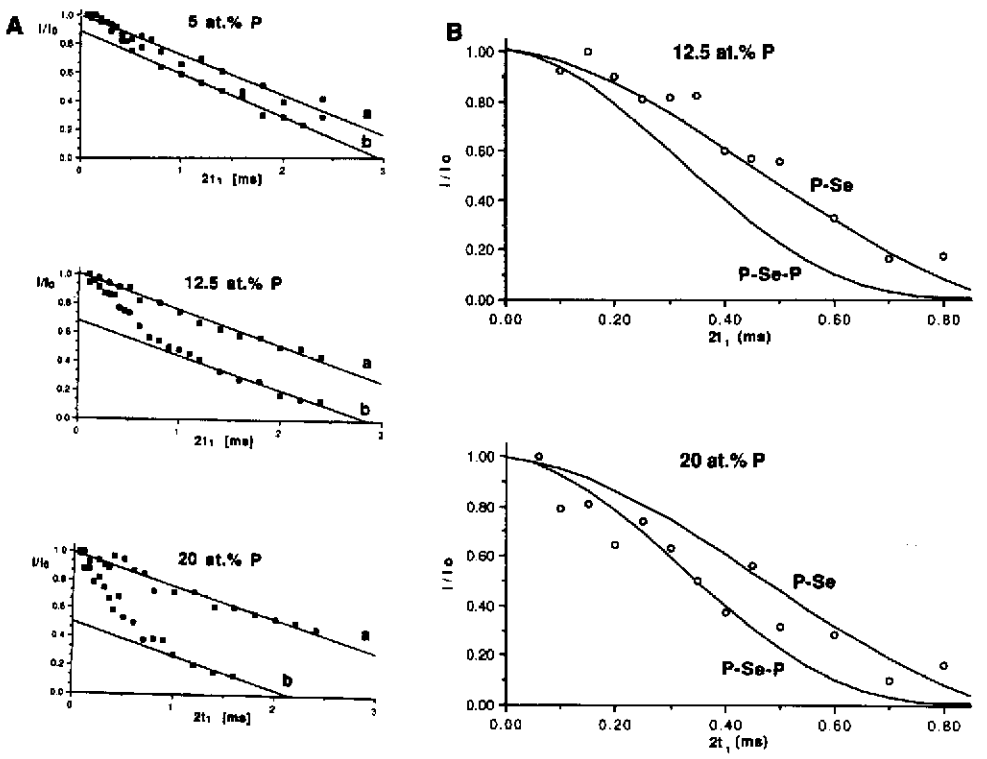

FIG. 57. ^{31}P–^{77}Se spin echo double resonance (SEDOR) NMR results for P–Se glasses with low phosphorus contents. (A) Normalized ^{77}Se spin echo intensities as a function of evolution time $2t_1$ (a) without and (b) with application of the ^{31}P pulse. The straight lines are linear least squares fits to the whole data of curve a and to the long-time behavior of curve b, respectively. (B) Dipolar decay curves of the P-bonded Se atoms, obtained via SEDOR difference analysis. Top: glass containing 12.5 at% P. Bottom: glass containing 20 at% P. The solid curves show the simulated decay within the region 0 ms $\leq 2t_1 \leq 0.85$ ms for isolated P–Se bonds and P–Se–P bridges, respectively.

10.1.3.2. *Ternary P–Se based systems.* Introduction of a third glass constituent such as germanium, arsenic, or tellurium into P–Se based glasses has a profound influence on the thermal and chemical stability. Extensive ^{31}P MAS-NMR studies have been carried out to elucidate the structural effect of such compositional modifications. Partial substitution of P by As within the compositional series $[P_xAs_{1-x}]_{1-y}Se_y$ leads to a systematic increase in N_4.[527] In view of the well-documented fact that in the binary As–Se system the glass structure is dominated by $AsSe_{3/2}$ groups and no tetrahedral $Se{=}AsSe_{3/2}$ units exist, the equilibrium description eq. (49) can be expanded by assuming As to substitute only for $PSe_{3/2}$ groups:

$$RSe_{3/2} + Se \rightleftarrows Se{=}RSe_{3/2}, \tag{50}$$

where R = P, As.

The data in Fig. 58 suggest that the basic structure of P–Se glasses is essentially retained upon successive substitution of P by As up to substitution levels of $x = 0.5$. Evidently the compositional perturbation caused by replacing P with the exclusively three-coordinated As is counterbalanced by changes in the phosphorus speciation such that the overall fraction of four-coordinated pnictogen atoms remains approximately constant. It is only for higher As contents that $[R^{IV}]$ is noticeably decreased, although still distinctly higher than expected from an interpolation between the data in the system P–Se and As–Se ($[R^{IV}] = 0$ for the latter system at all compositions). This result implies non-

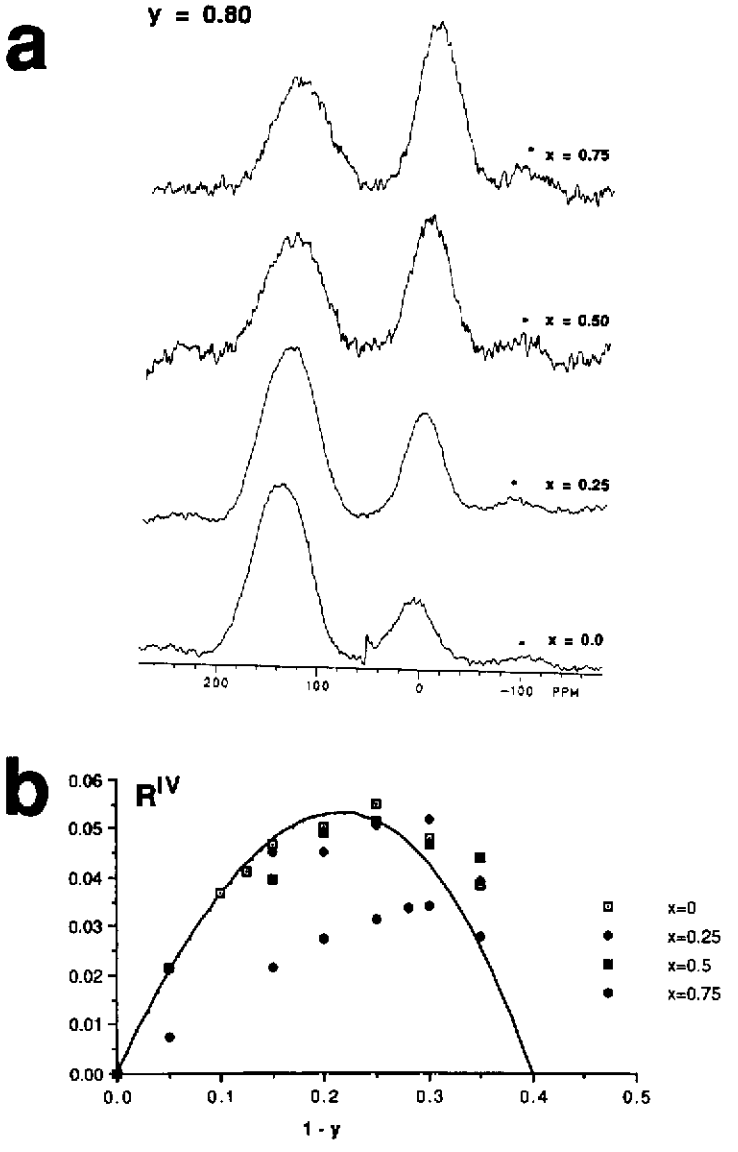

FIG. 58. (a) Typical ^{31}P MAS-NMR spectra for glasses of the system $(P_{1-x}As_x)_{20}Se_{80}$. (b) The total molar fraction $[R^{IV}]$ of $Se=PSe_{3/2}$ units in $(P_{1-x}As_x)_{1-y}$ glasses as a function of x and y. The experimental data are compared with the predicted behavior for the equilibrium $RSe_{3/2}+Se \rightleftarrows Se=RSe_{3/2}$ with an equilibrium constant K of 0.8 mole fraction^{-1}. Note the uniform behavior for $0 \leqslant x \leqslant 0.5$.

statistical ordering, indicating that the formation of four-coordinated species in these glasses is energetically relevant. It also reveals, indirectly, that the site speciations of P and As are different.

In contrast to the effect of As substitution for P, preliminary studies indicate that the substitution of Se by Te decreases N_4.[528] An explanation can be found if one assumes that phosphorus–tellurium bonds are absent, and that tellurium forms its own microdomains or substitutes only within the Se_x chains and rings in these glasses. Support for this assumption also comes from the crystallization behavior, which shows the formation of crystalline tellurium upon annealing above T_g. Overall, the

results suggest that Se and Te are both structurally and thermodynamically inequivalent in these glasses.

10.1.3.3. *The System P–S.* The phosphorus–sulfur system forms glasses with compositions ranging from 0 to 25 mol.% P. The structure of these glasses has been studied by combined dipolar spin echo and MAS-NMR spectroscopy,[529] as well as liquid state NMR carried out on extracts.[529-531] MAS-NMR data show that at low P contents the spectra are dominated by a broad resonance at 112 ppm. The static and magic angle spinning spectra for this resonance reveal a wide chemical shift anisotropy pattern characteristic of an axially symmetric shift tensor. The comparison with δ_{ii} values for a number of crystalline phosphorus sulfides[529,532-536] strongly suggests that the peak at 112 ppm reflects a $S=PS_{3/2}$ group and not a $PS_{3/2}$ group.

For P contents above 15 at% P additional sharper resonances at 51 and 57 ppm become increasingly intense and finally dominate the spectrum at 25 at%. These peaks indicate the presence of molecular P_4S_{10} and P_4S_9 "cluster" units in the glass structure and signify that the distribution of P atoms is non-statistical.

Spin-echo echo experiments confirm these segregation effects.[529] Figure 59 shows the compositional dependence of M_{2d}, as compared with M_{2d} values calculated, (a) for both uniform and P_4S_{10} cluster models, and (b) for a random distribution of P atoms, excluding the formation of P–P bonds. The significantly higher values of M_{2d} measured in the experiment throughout the entire region of glass-formation indicate an increased propensity of P–S–P bond formation. The preferred formation of such linkages leads to the formation of molecular clusters at higher P contents, and culminates in the crystallization of P_4S_{10} at the glassforming border.

10.1.4. *Arsenic Chalcogenide Glasses.* Glassy As_2S_3 and As_2Se_3 are probably the most widely-studied chalcogenide glasses. Unfortunately, their investigation by NMR methods has been hampered by the unfavorable properties of the nuclear isotopes ^{77}Se and ^{75}As. ^{77}Se has long T_1 values and gives rise to very broad spectra due to large csa and shift distributions and hence, the structural significance of ^{77}Se NMR in glasses has been limited.[474,475,478] ^{75}As possesses such a strong nuclear electric quadrupole moment, that the nuclear spin is usually quantized along the direction of the principal component of

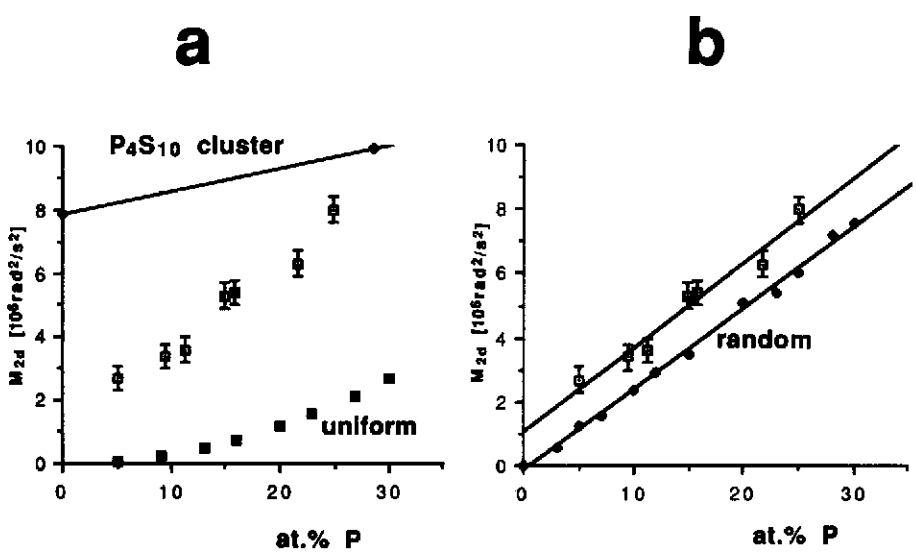

FIG. 59. Experimental dipolar ^{31}P second moments, M_{2d} (open squares) in Phosphorus–Sulfur glasses, and comparison with the values calculated from various models: (a) uniform distribution and P_4S_{10} clusters, and (b) a random distribution excluding P–P bonds (filled symbols). Reproduced from Ref. 529.

the electrostatic field gradient tensor rather than the externally applied magnetic field. In these systems, it has been possible, however, to conduct pure[537-541] or Zeeman-perturbed[473] nuclear quadrupole resonance experiments. This approach has proved to be very successful in the investigation of binary and ternary arsenic chalcogenide glasses. Although the NQR spectra in the glasses are quite broad due to the distribution of local environments, the average nuclear electric quadrupole frequencies of $AsX_{3/2}$ coordination environments and As–As-bonded microstructures are sufficiently different to permit facile site resolution in arsenic chalcogenide glasses.

All the available experimental evidence indicates that binary arsenic chalcogenide glasses possess a much higher degree of chemical ordering than the homologous P–Se glasses.[524] Specifically, the structure of glasses containing 40% As (corresponding to the stoichiometric composition As_2S_3 or As_2Se_3) appears to be completely dominated by $AsX_{3/2}$ groups (X = S, Se), giving rise to single peaks near 78 and 58 MHz for the sulfide and selenide systems, respectively. At these compositions and at lower arsenic contents, no significant amounts of either As–As-bonded or $X=AsX_{3/2}$ groups are present. As the arsenic content increases such that it exceeds that of the stoichiometric compositions As_2S_3 and As_2Se_3, new structures containing As–As bonds must be formed. These new structural units yield new NQR peaks at 90 and 80 MHz, for the sulfide and the selenide glasses, respectively. The fractional areas of these new peaks are quantitatively consistent with the reaction

$$4AsSe_{3/2} + 2As \rightarrow 3Se_{2/2}As\text{–}AsSe_{2/2} \tag{51}$$

hence suggesting that predominantly species with one As–As bond are formed. The same process occurs in ternary glasses with the stoichiometry $Cu_x(As_{2/5}X_{3/5})_{1-x}$. Because of the tendency of Cu to adopt four-coordination by selenium, the As environment is depleted in selenium, resulting in the formation of As-bonded arsenic atoms, as seen in Fig. 60a. The fraction b of the As–As bonded structures is predicted to be[540]

$$b=2.5x(1-x)^{-1}. \tag{52}$$

As shown in Fig. 60b, the NQR results are quantitatively consistent with this prediction. Although it is also possible to detect ^{63}Cu NMR signals in these systems, their structural significance is limited by strong second order quadrupolar broadening and distribution effects.[541]

10.2. *Site Speciation in Network Former/Network Modifier Systems*

These types of chalcogenide glasses are compositionally analogous to the usual oxide glass systems discussed above, differing from the latter merely in the replacement of oxygen by sulfur or selenium. Experimental studies have concentrated on Li_2S containing glasses based on B_2S_3, SiS_2, and P_2S_5, which are formed by rapid quenching techniques. Although these materials are solid electrolytes with high room temperature ionic conductivities (10^{-2} S/cm), wide spread applications of these glasses as components in lithium batteries have been limited, perhaps due to their instability in moist air, their recrystallization above T_g, and their reactivity towards lithium metal anodes. The development of new materials with improved thermal and chemical stabilities and maintaining their ionic conductivity is an area of active research, and requires support by structural investigations.[542] In this context, a salient question is how far the compositional analogy between these glasses and binary alkali borate, silicate, and phosphate glasses translates into structural analogy.

10.2.1. *Network Modification in Boron Chalcogenide Glasses.* Like its oxide analogue, glassy B_2S_3 is known to accommodate network modifiers such as Li_2S, although fast quenching (ice–water) of small samples is necessary to preserve the glassy state. Confirmed regions of glass-formation are: $(Tl_2S)_x(B_2S_3)_{1-x}$ ($0 \leqslant x \leqslant 0.75$) and $(Li_2S)_x(B_2S_3)_{1-x}$ ($0.5 \leqslant x \leqslant 0.7$). Both Na_2S and Li_2S, as well as Tl_2S generate four-coordinated boron atoms,[544-547] the quantitative compositional dependence being in rough analogy to the behavior of alkali oxide modifiers in alkali borate glasses (see Section 6). Figure 61 shows typical ^{11}B MAS-NMR spectra of the binary Li_2S–B_2S_3 glass system at a field strength of 11.7 T.[548] Although three- and four- coordinated B atoms are well separated on the ^{11}B chemical shift scale, the quantification is still complicated by the spinning sideband contributions,

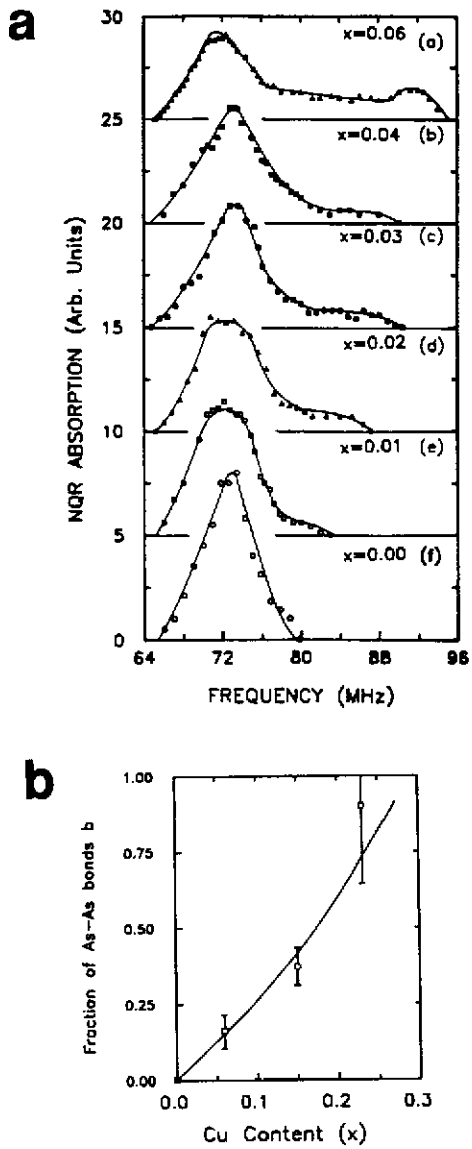

FIG. 60. (a) ^{75}As NQR lineshapes for glasses in the system $Cu_x(As_{0.4}S_{0.6})_{1-x}$ as a function of x. (b) Fraction of As sites containing one As–As bond, b, as a function of x in glasses with composition $Cu_x(As_{0.4}S_{0.6})_{1-x}$ (open squares) and in $Cu_x(As_{0.4}Se_{0.6})_{1-x}$ (open circles). The solid curve corresponds to the behavior predicted according to eq. (52). Reproduced with permission from Ref. 540.

which lead to undesirable spectral overlap. To suppress these sidebands, spinning speeds of ca. 15 kHz would be required. Nevertheless, the successive decrease of N_4 with increasing Li_2S content is clearly evident, and qualitatively consistent with an earlier cw NMR study of this effect.[544]

10.2.2. *Network Modification in Alkali Thiosilicate Glasses.* Glasses in the system $(Li_2S)_x$–$(SiS_2)_{1-x}$ ($0.4 \leqslant x \leqslant 0.6$) are prepared by heating the starting materials in vitreous carbon crucibles to approx. 850°C, followed by rapid quenching in liquid nitrogen.[549,550] The region of glass-formation can be extended further (to x values as low as 0.20) by using roller-quenching methods.[551] In view of the

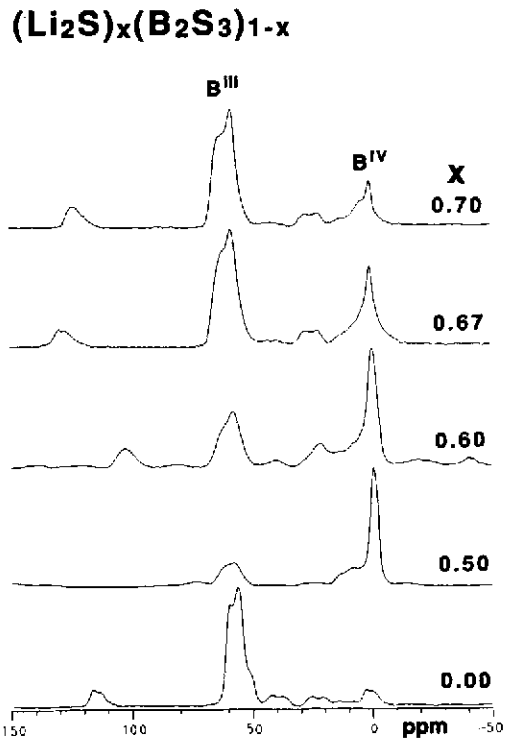

FIG. 61. ^{11}B MAS NMR spectra at 11.7 T in the binary glass system $(Li_2S)_x(B_2S_3)_{1-x}$

compositional analogy of these glasses to binary alkali silicate systems, the question arises as to whether the well-accepted network modification model discussed above for the silicate glasses is also applicable for the sulfide analogs. Data from Raman spectroscopy do indeed suggest that Li_2S acts as a network modifier much in the same fashion as Li_2O in oxide glasses, creating non-bridging sulfur atoms.[551] However, Raman spectroscopy is unable to offer conclusions on the quantitative aspects of this network transformation and the role of the edge-sharing units in this process.

Comprehensive ^{29}Si MAS-NMR studies of SiS_2–Li_2S glasses and crystalline model compounds reveal that the ^{29}Si chemical shifts are dominated by the $E^{(n)}$ rather than the $Si^{(n)}(Q^{(n)})$ specification; this means also that the number of non-bridging sulfur atoms produces only minor chemical shift changes for a given $E^{(n)}$ species.[552,553] It is therefore not possible to quantitate the number of non-bridging sulfur atoms. The NMR spectra show, however, that introduction of Li_2S into glassy SiS_2 initially reduces the extent of edge-sharing markedly, and the $E^{(2)}$ species have disappeared for the composition $x = 0.30$. Figure 62 illustrates the network modification scheme developed on the basis of the NMR data. This model reveals that, implicitly, the destruction of edge-sharing units by Li_2S (represented by diagonal arrows) will result in the formation of non-bridging sulfur atoms. In the compositional region where the most stable glasses form ($0.38 < x < 0.6$) the $E^{(n)}$ distribution remains approximately constant, with a $E^{(0)}/E^{(1)}$ ratio of ca. 2.5 : 1. Glasses prepared by ampule quenching and by the faster twin-roller quenching method show almost identical T_g values and $E^{(n)}$ speciations. Finally, preliminary studies carried out on the system Na_2S–SiS_2 reveal the same principles as discussed above, although the fraction of edge-sharing units appears to be consistently higher.[554]

10.2.3. *Network Modification in the System Li_2S–P_2S_5.* The high ionic conductivity of glasses in the system $(Li_2S)_x$–$(P_2S_5)_{1-x}$ has already come to commercial utilization. Initially, the region of glass formation was reported to be rather narrow,[555] but subsequent studies have shown that rapid

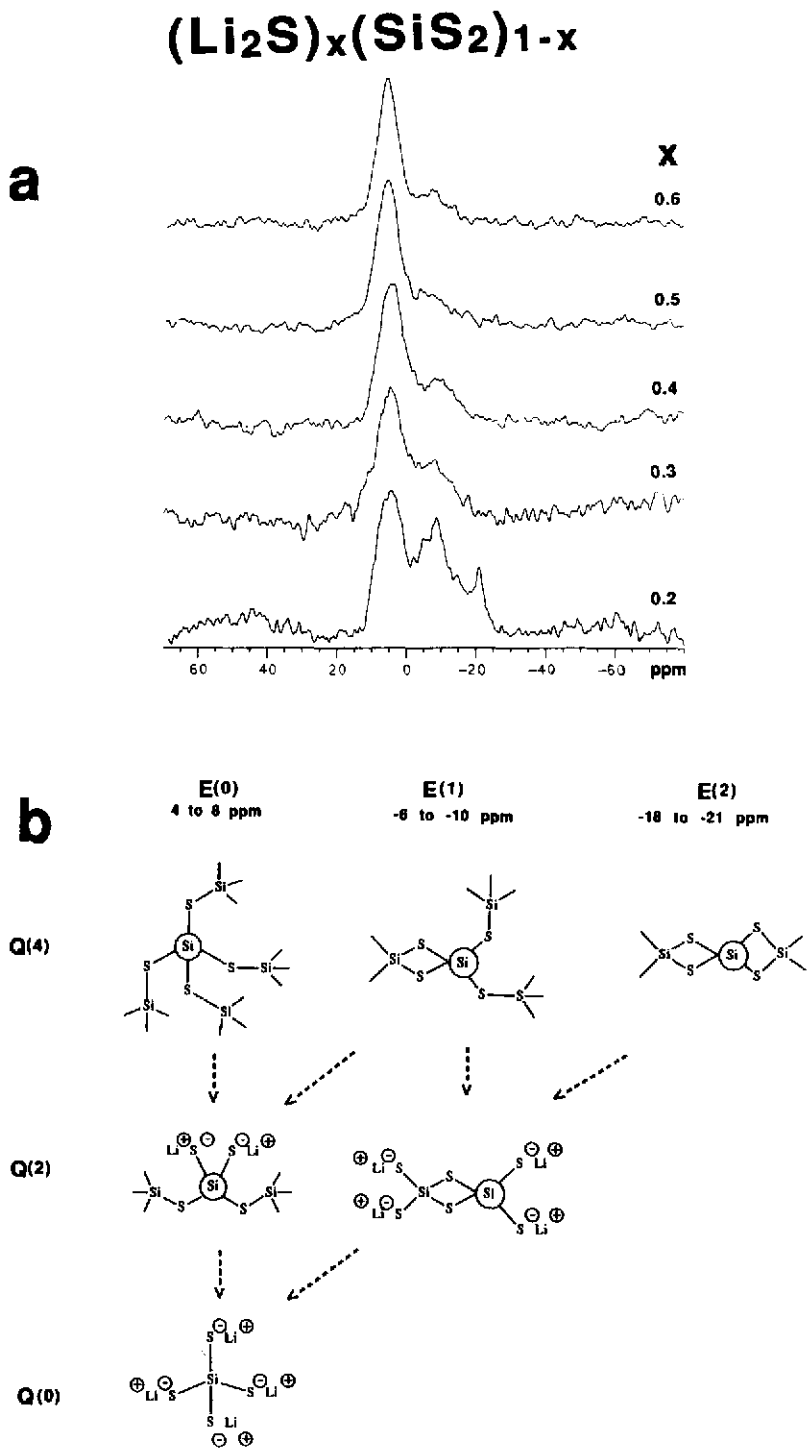

FIG. 62. ^{29}Si MAS-NMR spectra (a) and structural interpretation (b) for glasses in the system $(Li_2S)_x(SiS_2)_{1-x}$. Reproduced from Ref. 553.

quenching of samples sealed in quartz ampules affords glasses within the compositional range $0.5 \leqslant x \leqslant 0.7$.[556] The glass transition temperature increases with increasing Li_2S content, reflecting the change of the molecularly organized P_2S_5 glass to a material held together more strongly by ionic forces. There are four binary compounds with stoichiometries $LiPS_3$ ($x=0.5$), $Li_4P_2S_6$ ($x=0.66$), Li_3PS_4 ($x=0.75$), and Li_7PS_6 ($x=0.875$) which have been crystallographically characterized.

^{31}P MAS-NMR studies carried out on the whole range of glassy materials are shown in Fig. 63a.[557] Within the entire glassforming region, large chemical shift differences between crystalline

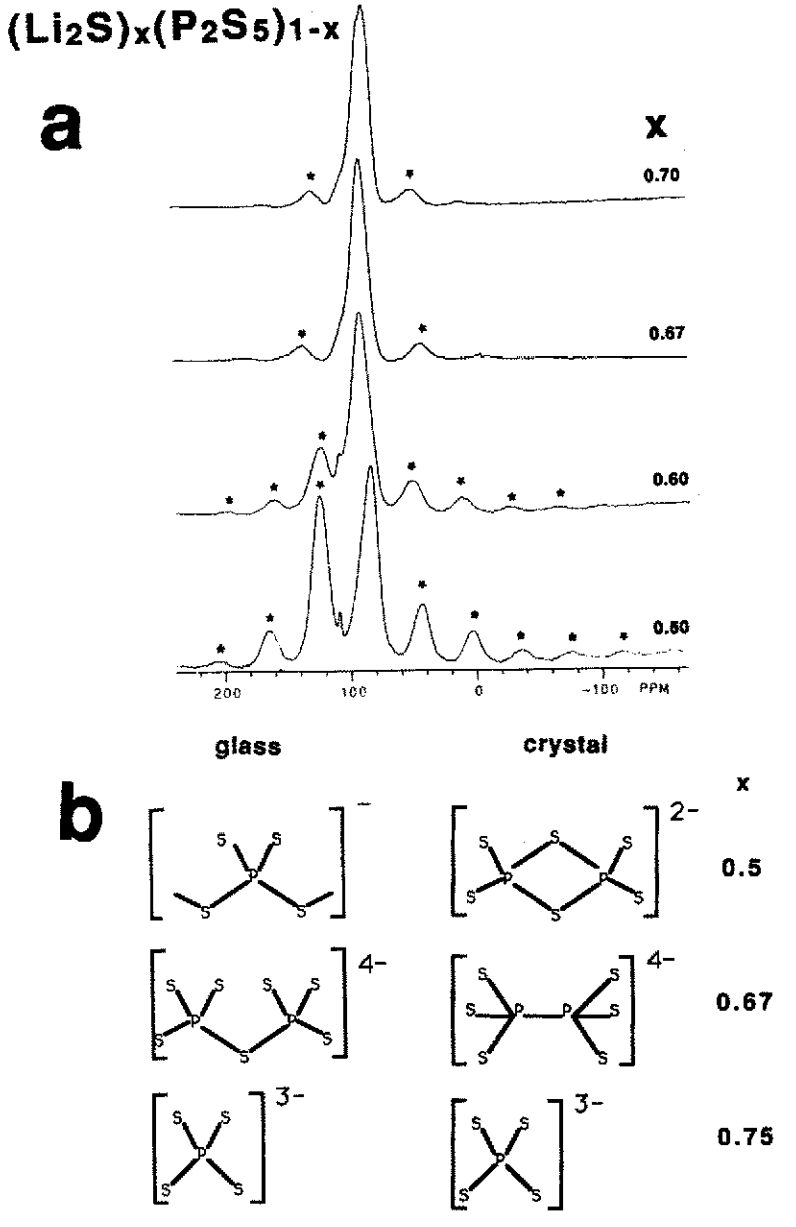

FIG. 63. ^{31}P MAS-NMR spectra (a) and structural interpretations (b) for glasses in the system $(Li_2S)_x(P_2S_5)_{1-x}$. Reproduced from Ref. 557.

and glassy phases are observed at most compositions.[557] Figure 63b suggests a tentative interpretation of the results obtained. In the glasses, the chemical shift anisotropies measured from the observed spinning sideband patterns follow similar systematic compositional dependences as observed previously for phosphate glasses. For this reason, the structural environments present in the glassy state are thought to resemble those present in phosphate glasses. For example in $(Li_2S)_{0.5}(P_2S_5)_{0.5}$ glass, a MAS-NMR pattern with numerous spinning sidebands is observed, revealing a large chemical shift anisotropy with a non-zero asymmetry parameter. In conjunction with model compound work undertaken on phosphates, this spectrum is assigned to the non-axially symmetric $P^{(2)}$ units expected at this stoichiometry. Likewise, the well-defined spectrum observed for $(Li_2S)_{0.67}(P_2S_5)_{0.33}$ glass is assigned to the dimeric $P^{(1)}$ units expected for this stoichiometry. The spinning sideband intensities are much weaker here, reflecting a significantly lower chemical shift anisotropy. The spectrum at the intermediate composition $x=0.40$ is easily explained in terms of a superposition of $P^{(1)}$ and $P^{(2)}$ contributions. Note that in view of the limited chemical shift difference (ca. 8 ppm) and the relatively broad lines the respective centerbands are actually not resolved from each other and the main distinction is afforded by the spinning sideband intensity patterns.

In contrast to the situation in the glassy states there appears to be no close structural correspondence between lithium phosphorus oxides and sulfides in their crystalline forms. In particular, glass with $x=0.66$ ($Li_4P_2S_7$) disproportionates on crystallization, according to

$$Li_4P_2S_7(\text{glass}) \rightarrow Li_4P_2S_6(\text{cryst.}) + S. \tag{53}$$

Thus, it appears that the pyro-thiophosphate unit can only be preserved in the glassy state. A close inspection of the spectra in Fig. 63a reveals that the decomposition occurs, in fact, also to a limited degree ($<10\%$) in the glassy state, as suggested by the downfield shoulder near 105 ppm. Overall, however, the structural differences between the crystalline and the glassy states in this system are quite pronounced, and this seems to be a quite general characteristic for pseudobinary network former/network modifier glasses based on chalcogenides.

10.2.4. *Competitive Network Modification in Chalcogenide Glasses.* Recently, pseudo-ternary lithium sulfide based glasses generated from mixed network former systems have been shown to have certain distinct advantages over simple pseudobinary systems in their electrochemical behavior. For example, addition of P_2S_5 as a third component to Li_2S–SiS_2 glasses results in a marked improvement of the stability of these glasses against Li anode material in battery systems.[558] The detailed structural origins of the stabilizing action of such coformers is not known, but may be related to the formation of three-component structural units in these glasses. Certainly, modern solid state NMR techniques are expected to provide some answers on a structural basis. In addition, the issue of how the two networks compete for the Li_2S modifier species is an interesting fundamental one that has provided important insights into the structural principles operative in oxide systems (see Section 8). In this connection, a series of experiments has been undertaken, addressing the effect of second network former constituents such as SiS_2, B_2S_3, and Al_2S_3 on the structure of $(Li_2S)_x$–$(P_2S_5)_{1-x}$ based glasses. The results can be summarized as follows.

(1) *Effect of SiS_2*—^{31}P MAS-NMR measurements have been carried out in the system $(Li_2S)_{0.6}[(SiS_2)_{1-y}(P_2S_5)_y]_{0.4}$. For $y=1.0$, the spectrum reveals a superposition of $P^{(1)}$ and $P^{(2)}$ units. With the successive introduction of SiS_2, the $P^{(2)}$ units are destroyed, and a monotonic shift in the peak maximum is observed, reflecting the gradual replacement of P–S–P by P–S–Li and/or P–S–Si linkages. Thus, the NMR spectra suggest that, as the result of the competition of the network formers for Li_2S, the average number of nonbridging S atoms around P is increased in the pseudo-ternary glass system.[559] This behavior is reminiscent of the alkali metal scavenging effect of phosphorus in alkali phosphosilicate glasses. In sharp contrast to the oxide system, however, Li_2S–P_2S_5–SiS_2 glasses show no evidence for six-coordinated silicon.

(2) *Effect of Al_2S_3*—Figure 64 shows ^{31}P MAS NMR spectra of a series of glassy and crystallized samples in the system $(Li_2S)_{0.67}[(P_2S_5)_{1-y}(Al_2S_3)_y]_{0.33}$.[560] The spectra suggest that the presence of Al_2S_3 favors to some extent the disproportionation reaction (53) in the glassy state. Furthermore,

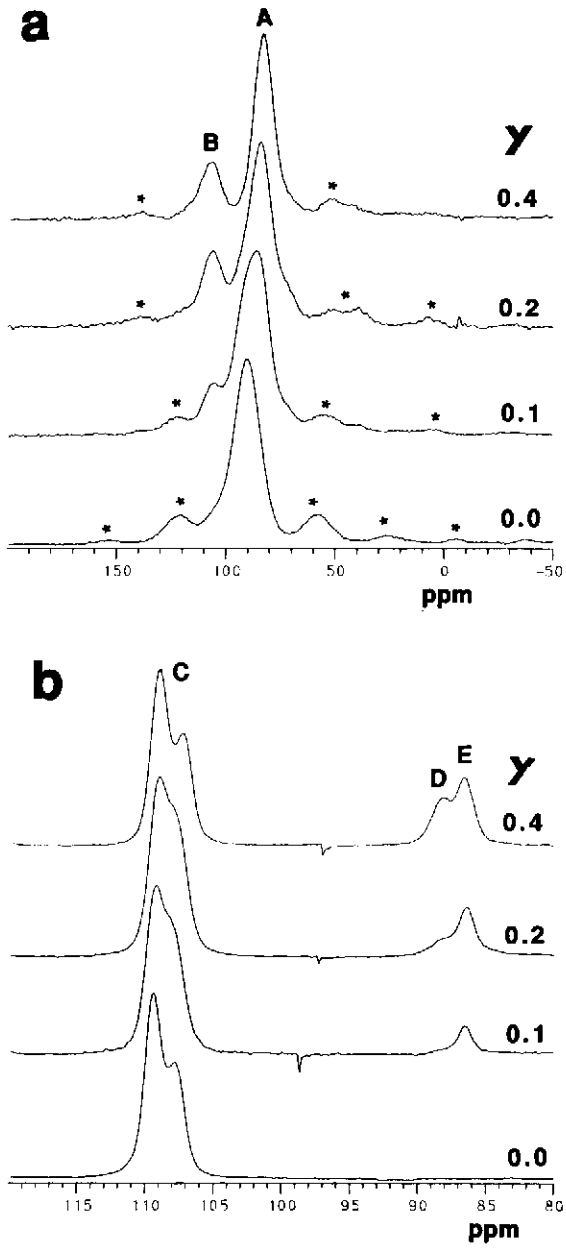

FIG. 64. ^{31}P MAS-NMR spectra of (a) glasses and (b) crystallized samples in the system $(Li_2S)_{0.67}[(P_2S_5)_{1-y}(Al_2S_3)_y]_{0.33}$. The value of y is indicated in the figure. Assignments are (A) $P_2S_7^{4-}$ and PS_4^{3-} groups; (B) $P_2S_6^{4-}$ groups; (C) cryst $Li_4P_2S_6$; (D) cryst. Li_3PS_4; (E) cryst. Li_7PS_6. Reproduced from Ref. 560.

changes in line widths and peak positions seem to indicate that Al_2S_3 also influences the $P^{(n)}$ speciation. More definite information on this matter comes from the spectra of crystallized samples, which reveal $Li_4P_2S_6$, Li_3PS_4, and Li_7PS_6, respectively. Crystallization of the first phase can be correlated to the presence of $P^{(1)}$ units in the glassy state, whereas the other two phases must originate from $P^{(0)}$ units. The results clearly indicate that the presence of Al_2S_3 in the glass increases the average number of

nonbridging S atoms around phosphorus. Bearing in mind that $(Li_2S)_{0.67}(Al_2S_3)_{0.33}$ would nominally be an $Al^{(3)}$ species, the network former competition can be characterized by the process:

$$Al^{(3)} + P^{(1)} \rightarrow Al^{(4)} + P^{(0)}. \quad (54)$$

This scheme is consistent with the well-known tendency of aluminium to avoid non-bridging oxygen species in aluminosilicate glasses.

(3) *Effect of B_2S_3*—Similar studies have been carried out with glasses in the system $(Li_2S)_{0.67}[(P_2S_5)_{1-y}(B_2S_3)_y]_{0.33}$.[546] This system tends to phase separate and does not form a continuous series of glasses. Combined measurements of $N_4(^{11}B)$, $M_{2d}(^{31}P)$, and $\delta_{iso}(^{31}P)$ suggest that glasses with $y \geqslant 0.7$ phase separate into a binary Li_2S–B_2S_3 glass with a lower network modifier/network former ratio than 0.67:0.33, and a mixed $Li_2S/P_2S_5/B_2S_3$ glass with a higher network modifier/network former ratio than 0.67/0.33. The phosphorus environment in this second glass phase is independent of composition and most likely a $P^{(0)}$ (PS_4^{3-}) unit. Thus a common thread for all competitive network former systems studied so far is the tendency of phosphorus to maximize its number of non-bridging chalcogen atoms (i.e. minimize the number n in the $P^{(n)}$ notation). This phenomenon compares well with the "alkali metal scavenging" effect of phosphorus in the alkali borophosphate glasses (Section 9.2).

11. IONIC DIFFUSION STUDIES OF GLASSY SOLID ELECTROLYTES

Besides providing information on the structure of the rigid glass network, NMR spectroscopy also offers the opportunity of studying dynamic behavior in glasses on a variety of experimental time scales. NMR lineshapes and relaxation times have proved to be very sensitive to the effects of ionic diffusion in glasses. This has been an area of very intense research effort, the ultimate goal being a deeper understanding of the detailed mechanism of ionic transport in glasses. There are a number of important, partly inter-related questions to be answered: Does the "weak electrolyte theory",[561] formulated on the basis of thermodynamic data, have physical reality? Do the ions move in a correlated manner, as implied by Funke's jump relaxation model,[562] or is the motion stochastic? Has the non-Debyean relaxation behavior so often observed for the electrical conductivity and other transport properties in glasses[563] an intrinsic theoretical foundation or is it merely an artifact of the disordered state?

There has been an abundance of experimental studies, mainly devoted to the effect of ionic motion on static NMR interaction parameters and spin-lattice relaxation behavior. Broadly, three principal areas can be distinguished: (a) fluoride conducting ZrF_4-based glasses,[564–576] (b) amorphous Ag solid electrolytes (mostly the system AgI–Ag_2O–B_2O_3),[577–585] and (c) Li^+-containing solid electrolytes, including silicate, borate, phosphate, chalcogenide and fluoride-based glasses.[586–601] There have also been a few studies of other mobile ions such as sodium,[602,603] cesium,[604] and thallium.[605] Since, however, the principle of application is essentially the same in all of these systems, no distinction will be made here.

11.1. *Temperature-Dependent NMR Lineshape Studies*

Figure 65 illustrates some typical experimental results from temperature dependent ^{19}F and ^{7}Li static wideline NMR spectroscopy in ionically conductive glasses. As the temperature is increased, the thermally activated ionic motion modulates the anisotropic static interactions (magnetic dipole–dipole couplings, nuclear electric quadrupole couplings). As a result, one typically observes for these nuclei a continuous decrease in the line width and a lineshape change from Gaussian to Lorentzian. Other systems (especially in the case of F^- motion) show the emergence of a relatively sharp line, which grows at the expense of the original broad line as the temperature is increased. According to Resing,[606] such is the expected behavior if a wide distribution of correlation times is present. The two regimes of τ_c corresponding to the motional narrowing situation and the rigid lattice behavior, respectively, are separated by a cut-off correlation time τ_{cc}. As the temperature increases, this mobility window is shifting, hence resulting in all of the experimental observations.

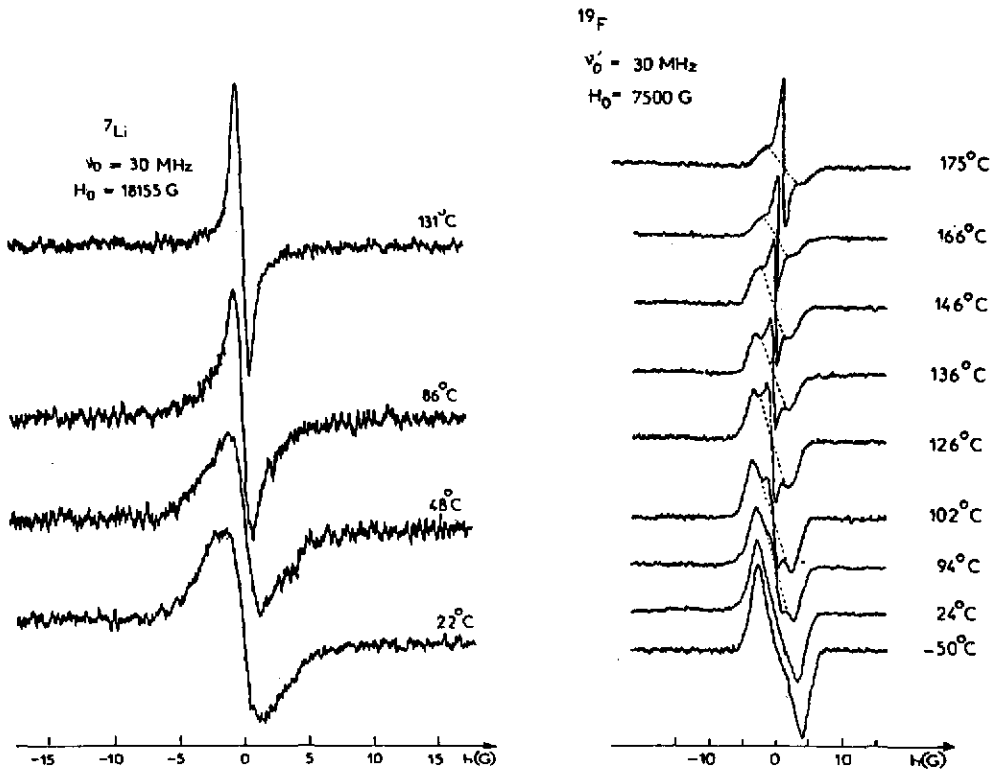

FIG. 65. Effect of ionic motion on the ^{19}F and ^{7}Li static lineshape derivatives in $(LiF)_{0.6}(BaF_2)_{0.1}(ThF_4)_{0.2}(ZrF_4)_{0.1}$, typical glassy solid electrolyte. The behavior shown here is representative of most of the glasses investigated in this field. Reproduced with permission from Ref. 568.

There have been several phenomenological attempts to relate the motional narrowing effects to temperature dependent correlation times, but in general their physical justification has remained uncertain. Indepth discussions of these approaches and critical comparisons are given in Refs 607 and 608. At present, a theory describing the detailed lineshape changes over the entire temperature region in agreement with experimental results in glasses is still lacking. In part, this unsatisfactory situation arises from the fact that static lineshapes are influenced by more than one basic interaction. In the case of ^{7}Li, for instance, the static lineshape includes contributions from ^{7}Li–^{7}Li dipole–dipole couplings, heterodipolar couplings to other nuclei (such as ^{11}B and ^{31}P) in the glass, and nuclear electric quadrupole couplings. Furthermore, due to site variations in glasses, all of the corresponding Hamiltonian parameters are subject to distribution effects. Finally, when motion is activated, different ions are expected to experience different dynamics.

In spite of the complexity of this situation, temperature-dependent wideline NMR spectra are useful for qualitative purposes and can serve as a fast screening method for examining the suitability of certain glass composition for solid electrolyte applications. While the electrical conductivity (σ) depends on both the carrier concentration (n) and mobility μ ($\sigma = ne\mu$) the temperature dependent NMR data address explicitly the question of ionic mobility. A few important conclusions from such studies (generally consistent with detailed a.c. and d.c. electrical conductivity measurements) are the following: (1) The Li^+ mobility of lithium-based glassy electrolytes generally increases with increasing lithium content, particularly when additional lithium is added in the form of halide. This lithium halide appears to be widely dispersed in the glass structure and there is no evidence by NMR for the formation of separate microdomains. (2) Lithium sulfide-based glasses have much higher ionic

mobilities than their corresponding oxide counterparts. (3) The mobility of fluoride ions in ZrF_4 based glasses increases with the content of network modifiers such as BaF_2 and LiF. (4) Both Li^+ and F^- are mobile in such glasses.

11.2. *Temperature-Dependent Spin-Lattice Relaxation Time Studies*

A large number of spin-lattice relaxation studies have been carried out, with the goal of providing further insights into the mechanistic aspects of ionic transport in glassy solid electrolytes. The bulk of the experimental T_1 measurements have been on ^{7}Li in lithium-conducting glasses. A complete data set constitutes a measurement over a wide temperature range at atleast two different nuclear magnetic resonance frequencies; an example is shown in Fig. 66. When interpreting such a data set, it is at first necessary to identify which internal interaction dominates the spin-lattice relaxation rate. For ^{7}Li the relaxation appears to be dominated by fluctuating magnetic homonuclear dipole–dipole interactions. The magnetization recoveries measured upon saturation or inversion are generally found to be exponential, as expected. Only a single T_1 is measurable, indicating that strong ^{7}Li–^{7}Li dipole–dipole interactions cause efficient spin diffusion. The situation is different in the case of the ^{8}Li β-radiation detected NMR studies, where the absence of spin diffusion results in a relaxation time manifold. Here, each lithium ion has its own, individual T_1 value, and this manifests itself in non-exponential magnetization decays.[589–591]

Silver conducting glasses (particularly in the system $AgI–Ag_2O–B_2O_3$) have been studied by both ^{109}Ag and ^{11}B spin-lattice relaxation times. For ^{109}Ag, the relaxation mechanism is caused by chemical shift fluctuations, resulting in exponential magnetization recoveries. In contrast, the ^{11}B relaxation is caused by electric field gradient fluctuations due to the diffusive behavior of the Ag^+ ions. This relaxation mechanism is outside of the realm of BPP theory in the limit of slow motion ($\omega_0\tau_c > 1$). For a spin 3/2 nucleus, two quadrupolar spin-lattice relaxation rates, a_1 and a_2 are defined in the slow

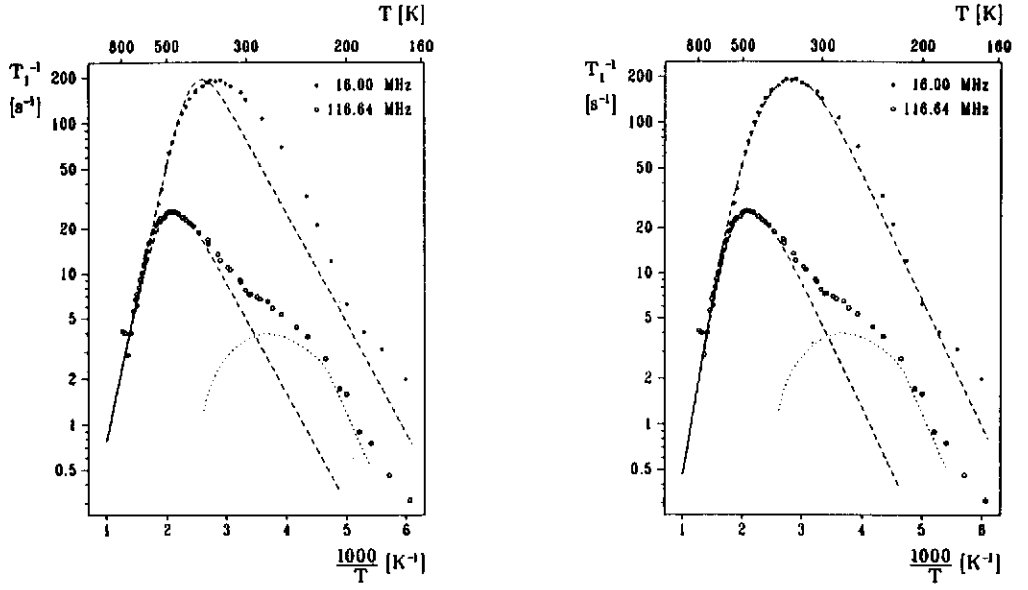

FIG. 66. Temperature and frequency dependent ^{7}Li spin lattice relaxation rate of a glass with composition $54B_2S_3$–$34Li_2S$–24LiI. Left side: comparison with theoretical fit to BPP theory assuming a Cole–Davidson distribution of correlation times. Right side: comparison with theoretical fit to Funke's jump relaxation model. Note that only the latter model describes the frequency dependence correctly. Reproduced with permission from Ref. 600.

motion limit:

$$\frac{M_z^{(t)}-M_0}{M_z^{(0)}-M_0}=\frac{4}{5}\exp^{-\{a_1 t\}}+\frac{1}{5}\exp^{-\{a_2 t\}},$$

where, $a_1 \sim T(2\omega_0)$ $a_2 \sim T(\omega_0)$,

This situation results in non-exponential magnetization recovery, as long as all of the transitions are being excited by the radio frequency pulse. As the temperature decreases, a point is reached where $\omega_Q \tau_c > 1$. In this regime, the static spectrum is split into the three separate transitions shown for $I=\frac{3}{2}$ in Fig. 8. If the quadrupolar interaction is sufficiently strong, the two outer transitions can then no longer be excited by the radio frequency pulse. As a consequence, the effective 90° pulse length is shortened to one-half of its original value. In this limit, the magnetization recovery will resume once again exponential character, and only T_1 for the central $\frac{1}{2} \rightarrow -\frac{1}{2}$ transition will be measured. Complications of this kind must be kept in mind when executing and interpreting temperature dependent T_1 measurements of nuclei with larger quadrupole moments (^{11}B, ^{23}Na, ^{27}Al).

All relaxation time measurements carried out so far on ionically conductive glasses have shown a common pattern of grossly BPP-deviant behavior. (1) The $1/T_1$ vs T^{-1} curves are asymmetric, with a much smaller slope in the low-temperature regime than in the high-temperature regime. (2) The frequency dependence of T_1^{-1} in the low-temperature regime is closer to ω_0^{-1} than to ω_0^{-2}. (3) The activation energy extracted from the low-temperature slope is significantly smaller than the value determined from d.c. electrical conductivity measurements. (4) The prefactor τ_{c0} in eq. (22) assumes unrealistically small values.

Substantial effort has gone into attempts to modify expression (21a) to yield better agreement with experimental T_1 data.[608,609] A frequently used approach is to replace the correlation time τ_c in eq. (22) by a distribution function. The use of the Cole–Davidson function has been quite successful in this regard, although the physical meaning of this distribution function is not clear. Alternatively, the data can be fitted very well, if the exponential correlation function (19) is replaced by the stretched exponential, the Kohlrausch–Williams–Watts function[563]

$$g(\tau)=\exp\{-\tau/\tau_c\}^{\beta} \quad (\beta<1). \tag{55}$$

Equation (55) implies non-Debyean relaxation behavior. This is quite common in amorphous systems; for instance the KWW-function also explains successfully the frequency dependence of the a.c. conductivity in amorphous solid electrolytes. It was first pointed out by Ngai, that the BPP-deviant behavior and the non-Debye behavior of the electrical conductivity have a common origin.[610] An explicit discussion of this issue is given by Angell and Martin,[611] who argue that the low apparent value of the activation energy as determined from the low-temperature slope of T_1 vs T^{-1} data compared to the value from d.c. conductivity is a direct consequence of non-Debyean relaxation. Figure 67 illustrates the principle. The left side of this figure shows a typical plot of temperature and frequency dependence for a solid electrolyte. While at low frequencies there is virtually no frequency dependence of the a.c. and d.c. conductivities over a wide range of temperatures, this is not the case in the frequency range around 10^7–10^8 Hz, where the NMR experiment is usually undertaken. The frequency dependence is steeper at low temperatures, where the structural relaxation tends to lag behind the rapidly oscillating a.c. field. The result of this temperature-dependent behavior at each fixed frequency is plotted on the right side. At low temperatures, the slope of σ as a function of T^{-1} at a fixed frequency decreases with increasing (fixed) frequencies, manifesting itself in an apparently lower activation energy. In contrast, no appreciable frequency dependence of the conductivity exists in the high temperature region where all the curves on the right side of Fig. 67 have joined.

According to the above explanation, the activation energy extracted with eq. (21b) from the high temperature side of the relaxation maximum should be in good agreement with that from d.c. conductivity data. Unfortunately, however, this region is seldom reached experimentally, because it often lies beyond the glass-transition temperature. Thus, for most glasses a relaxation rate maximum is not observed, since at temperatures above T_g other types of relaxation mechanisms contribute to ^{7}Li–T_1, and, furthermore, crystallization may occur.

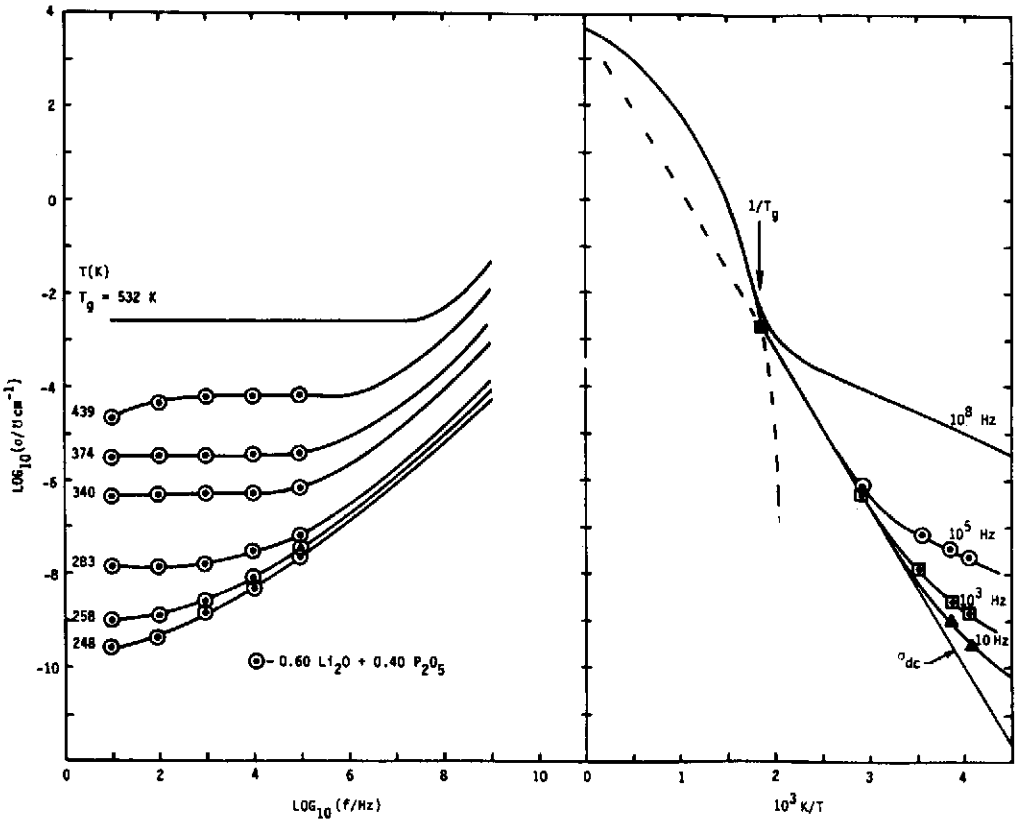

FIG. 67. Temperature and frequency dependent a.c. conductivity in glassy $(Li_2O)_{0.6}(P_2O_5)_{0.4}$, showing frequency dependent activation energy in the a.c. regime, and expected behavior at an NMR frequency of 10^8 Hz. Note that the apparent slope of σ vs inverse temperature depends on the frequency of the measurement. Reproduced with permission from Ref. 611.

The explanation by Angell and Martin immediately suggests a number of experiments for verification: a.c. conductivity measurements in the 10^7–10^8 Hz region for a direct comparison with the NMR data, and NMR relaxation time measurements at low effective magnetic fields. The latter is possible, for instance, via T_1-measurements in rotating frame ($T_{1\rho}$), which provide for an inherent timescale of 10^3–10^5 Hz. It must be borne in mind, however, that conductivity relaxation on the one hand and nuclear magnetic spin-lattice relaxation on the other are of intrinsically different nature. Conductivity relaxation occurs in response to a periodically oscillating a.c. field, whereas NMR spin-lattice relaxation is not a process driven by an externally applied field. Rather, the applied radiofrequency merely defines the window of observation for motional processes occurring on the timescale of the nuclear precession period. It is therefore, in this author's opinion, not obvious that the activation energies from both experiments (even when carried out at identical frequencies) should necessarily agree.

While the KWW function thus provides a common formalism to explain the experimental results relating to the frequency dependent conductivity behavior, the temperature-dependent linewidth, as well as the T_1- relaxation behavior of solid electrolytes, the deeper meaning behind it still remains to be understood. Recently, Funke has presented an appealing jump-relaxation model, based on correlated rather than stochastic ionic motion.[562,612–614] According to this model, the mutual repulsive interaction between the mobile ions causes a jump diffusion consisting of correlated forward–backward hopping sequences. Funke also showed that this model results in KWW behavior[615] and

can be used to fit frequency dependent spin-lattice relaxation NMR data in a quantitatively satisfactory manner (see for example Fig. 66).[562b, 600] A conceptually similar approach derives from Ngai's "coupling model", combined with a previously developed two-level-system (TLS) formalism for spin-relaxation.[616] The TLS model was originally developed to describe experimental results indicating a very weak frequency dependence of the spin-lattice relaxation rate T_1^{-1} in glasses at low temperatures:

$$T_1^{-1} \sim \omega_0^{-m} (0.8 > m > 0.5). \tag{56}$$

Somewhat surprisingly, in glasses with low alkali metal contents (such as $(Li_2O)_{0.25}(B_2O_3)_{0.75}$ and others with comparable cation concentrations) this peculiar frequency dependence seems not to be restricted to low temperatures. Rather, the spin-lattice relaxation of mobile nuclei (such as ^7Li, ^{23}Na) in these glasses is described rather well by the expressions[602]

$$\begin{aligned} T_1^{-1} &\sim T^{1+\gamma}\omega_0^{-m} \qquad (T < 100\,\mathrm{K},\ 0 \leqslant \gamma \leqslant 0.3) \quad 0.5 \leqslant m \leqslant 0.8 \\ &\exp(-E/kT)\omega_0^{-m} \quad (T \geqslant 300\,\mathrm{K}) \qquad\qquad 0.5 \leqslant m \leqslant 0.8. \end{aligned} \tag{57}$$

Based on these findings, the authors suggest that the TLS model may be applicable over a wide temperature range. Ngai's model then predicts a universal relationship between the two activation energies derived from conductivity and NMR measurements:[602, 603]

$$E_a(\mathrm{NMR}) = \beta E_a\ (\mathrm{conductivity}), \tag{58}$$

where β is the Kohlrausch–Williams–Watts exponent.

Recent ^{23}Na T_1 and conductivity measurements have verified this expression experimentally for a range of Na_2O–GeO_2 glasses.[603] Thus, E_a (conductivity) can simply be obtained from E_a(NMR) and β is obtained from a.c. conductivity measurements.

Both in the jump–relaxation and the coupling model the parameter β characterizes the degree to which the cation motion is correlated. For $\beta = 1$ the motion is completely random, while for $\beta = 0$ the motion is completely correlated. The degree of correlation will depend on both ion–ion interactions and the single ion potential, both of which are subject to distribution effects in glasses. As the alkali concentration of a glass is increased, the average proximity of the ions increases and the well-depth decreases, resulting in mutually reinforcing effects on the degree of correlation. Qualitatively, this prediction is borne out by experiment. For example, in various alkali germanate glasses, β decreases markedly with increasing alkali concentration particularly at very low alkali concentrations. This dependence is not monotonic, however, and there is a striking, somewhat unsatisfactory, prevalence of β-values around 0.5–0.6 over a wide range of compositions.[603] Possibly such behavior might reflect cation clustering or sub-microscopic phase segregation phenomena occurring in glasses with these compositions.

In view of these new developments it appears that NMR-spin-lattice relaxation data may have substantial potential to advance our understanding of ionic transport mechanisms in amorphous solid electrolytes. Challenges for the future include: quantitative verification of KWW/jump–relaxation behavior on a wider range of solid electrolytes, a deeper quantitative understanding of the fractional exponent β in terms of structural properties, and the development of more quantitative theories for the motional narrowing effect seen in the temperature-dependent NMR lineshapes.

12. AMORPHOUS HYDROGENATED SILICON FILMS AND RELATED SYSTEMS

12.1. *Amorphous Hydrogenated Silicon*

Amorphous hydrogenated silicon (a-Si:H) films are technologically interesting materials for a variety of applications in solar cells and thin-film transistors. These materials are prepared by glow discharge or by plasma-enhanced chemical vapor deposition (PECVD) of silanes on heated substrates. In the past there has been considerable interest in these materials because of their potential applications, resulting in many research programs aimed at elucidating their structure–property relationships.[617] A large number of NMR studies have been published, including several providing

textbook examples illustrative of the immense power of selective NMR techniques. The work carried out has centered on three principal topics: (1) the geometrical structure of the silicon network and the silicon speciations, (2) the spatial distribution and chemical nature of the hydrogen atoms, and (3) the atomic distribution and geometrical inter-relationship of substituents or dopants (B, C, Ge, N, F, and P) added to modify the electronic properties of these materials.

12.1.1. *Silicon Speciation and Bond Angle Distributions in Hydrogenated Amorphous Silicon.* $^{29}Si-^{1}H$ CPMAS NMR studies of hydrogenated amorphous silicon films show very broad (50–70 ppm) unresolved lineshapes bearing little structural information. The reported peak positions differ substantially between the various studies.[618–621] The explanation for these variations lies in the fact that these lineshapes are comprised of several distinct components, whose contributions are sample-dependent. The most convincing argument comes from a study of the cross-polarization dynamics, which suggests the presence of three species.[622] Since these samples are known from IR spectroscopy to contain both Si–H and SiH_2 groupings in addition to Si-only bonded silicon atoms, interpretational attempts were initially made in terms of such distinct sites. Later work has shown that this view is too simplistic and suggests that the ^{29}Si CPMAS spectra can best be interpreted in conjunction with wideline ^{1}H NMR spectra. As discussed in more detail below, the ^{1}H NMR spectra of a-Si:H samples are composed of a broad and a narrow line respectively. The broad line is assigned to hydrogen atoms within a cluster ("CL") region where the protons are densely clustered, hence resulting in strong dipolar band broadening. The sharp line is attributed to a dilute ("DI") region with a low proton concentration, and hence moderately weak dipolar coupling. Both regions are spatially distinct, and their relative abundances depend on the overall hydrogen content and the sample preparation conditions. Hayashi *et al.* were the first to discover that the ^{1}H and the ^{29}Si NMR spectra of a-Si:H samples are closely correlated.[623–625] Si atoms within the DI region resonate near -40 ppm, whereas Si atoms in the CL region resonate near -80 ppm. The average ^{29}Si chemical shift reflects the relative occurrences of DI and CL regions. Experimental spectra and a schematic of this correlation are shown in Fig. 68.

The origin of the large chemical shift difference between Si atoms within the CL and DI regions is not clear;[625] likewise a good explanation has not been given for the large downfield shift of the ^{29}Si MAS peak for a-Si relative to crystalline Si (-40 vs -80 ppm).[626,627]

The width for the ^{29}Si peak is partly due to the simultaneous presence of DI and CL regions, and partly due to bond angle distribution effects. Thus, if bond angle distribution effects are to be studied, samples must be carefully selected: one region (CL or DI) should predominate and all other experimental parameters need to be held constant. This has been done by Gerstein and coworkers, who observed that in hydrogen-depleted a-Si samples annealed to various temperatures, the peak width correlates with the bond angle distribution width determined independently by radial distribution function (RDF) measurements. The results obtained in this study suggest that with increasing annealing temperature, increasing bond angle order is obtained, resulting in partial crystallization above 600°C.[626,627]

Amorphous, hydrogen-free silicon is of great fundamental interest as a possible model for a tetrahedrally-bonded continuous random network. Several theoretical approaches for modelling such networks have been published, and found to be in excellent agreement with experimental RDF results.[628–633] The most elegant modelling approach used starts from the crystalline silicon (c-Si) lattice and amorphizes this lattice by introducing random bond switches.[631–633] This process of bond switching newly introduces five- and seven-membered rings, at the expense of the 6- and 8-membered rings (the only ones present in c-Si). The resulting ring statistics and rms bond angle distributions depend on the number of such bond switching defects. In addition to characterizing the overall rms bond angle distribution (which is ca. 11° according to RDF studies) detailed *local* information about such ring size distributions and bond switches would be highly desirable. At the present time, the complexity of the ^{29}Si NMR lineshape in a-Si, the impossibility of calculating chemical shifts with the required accuracy, and the lack of a suitable data base on crystalline model compounds make it rather difficult to assess the potential of ^{29}Si NMR to provide such topological information in a-Si materials.

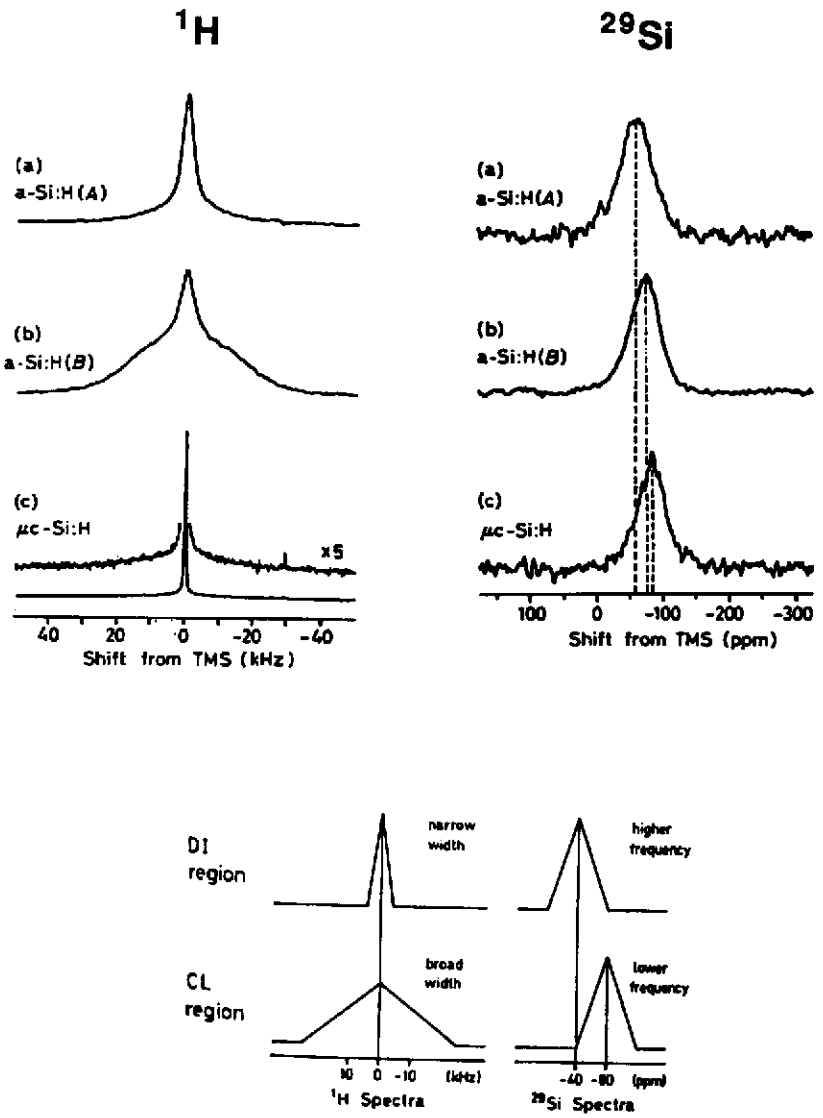

FIG. 68. ^{1}H and ^{29}Si NMR results for a-Si:H samples. Top: experimental results for two amorphous samples with different H/Si ratios: sample A: atomic ratio H/Si = 0.16. Sample B: atomic ratio H/Si = 0.40. Results for a partially crystalline sample (μc-Si : H) are also included. Bottom: schematics of the correlation between ^{1}H DI/CL ratio and ^{29}Si chemical shift. Reproduced with permission from Refs 623 and 625.

12.1.2. *Hydrogen Environments in Amorphous Hydrogenated Silicon.* When a-Si is prepared via plasma decomposition of SiH_4 or Si_2H_6, residual hydrogen from the molecular precursor is incorporated into its structure. This hydrogen plays the important role of removing the defect states in the band gap, reducing their concentration by four orders of magnitude. As a result, the Fermi level of a-Si can be controlled by dopants, hence giving a-Si all the important properties of a useful semiconductor. Due to this beneficial effect of hydrogen on the electrical properties of amorphous silicon materials, there has been a tremendous interest in its chemical speciation and atomic distribution within the amorphous matrix. During the past ten years, a significant amount of

knowledge on this topic has come from ^1H and ^2H NMR lineshape, spin-echo, and spin-lattice relaxation experiments.

12.1.2.1. *The spatial distribution of hydrogen.* Quite generally, the NMR studies of amorphous hydrogenated silicon samples reveal that the hydrogen distribution is quite inhomogeneous, even for device-quality material (which contains typically 8–20 at% H).[634–684] There are regions with isolated Si–H bonds (DI), giving rise to ^1H NMR spectra that are quite sharp ($\Delta\nu_{1/2} \sim 3$–4 kHz), due to fairly weak ^1H–^1H dipole–dipole couplings. In addition, the observation of a broad lineshape component ($\Delta\nu_{1/2} \sim 25$ kHz) is indicative of regions with hydrogen clustering (CL). Most pulsed FT studies devoted to the quantitative determination of the CL/DI ratio will tend to produce underestimates, if the results have not been corrected for the faster decay of the broad lineshape component during the spectrometer deadtime. In spite of these caveats, it can be concluded from these studies that the CL/DI ratio generally increases with increasing hydrogen content, and that it can be influenced further by a number of experimental parameters (concentration of silane in the gas phase, substrate temperature, film thickness, type of silane and diluent gas used, presence of dopants, deposition rate, annealing temperature, homogeneous chemical vapor vs rf plasma deposition).[639–648] These studies support the general picture that up to 5 at% H the DI phase is dominant, whereas any additional hydrogen atoms contribute mostly to the CL phase. Phosphorus doping reduces the DI/CL ratio, even when the overall hydrogen content remains constant.

The contention that the DI and CL regions are spatially distinct is confirmed by hole-burning[639] and solid echo experiments.[638] Two-dimensional cross-polarization experiments show, however, that both types of hydrogen interact equally strongly with the silicon,[653] and thus both must arise from silicon-bonded atoms.

The CL phase is thought to contain both Si–H as well as SiH_2 groups. Although the ^1H NMR spectrum of SiH_2 species is expected to be a Pake doublet as shown in Fig. 7a, such a pattern is actually never observed experimentally, because the lineshape is broadened out by dipolar interactions with other nearby hydrogen atoms in this phase. Nevertheless, Boyce succeeded in detecting two-spin behavior typical of SiH_2 groups in the free induction decay of certain a-Si–H samples, hence providing, for the first time, direct evidence for SiH_2 groups.[652]

Information concerning the more specific arrangements in the CL phase has come from multiple-quantum NMR.[654–656] This technique uses specifically designed pulse sequences to force the nuclear spins to interact collectively via their dipole–dipole couplings. This results in a coherent superposition of states with differences in magnetic quantum numbers Δm larger than the usually allowed $\Delta m = 1$ transition. The preparation time required to build up these multiple-quantum coherences depends on the strength of the dipole–dipole couplings; i.e. on the distances between the nuclei contributing to the multiple quantum coherence. The preparation time τ also governs the order of the highest coherence excited, Δm_{max}. For a random or uniform distribution of spins, Δm_{max} increases with increasing τ in a monotonic fashion. If the spins form isolated clusters, however, Δm_{max} is simply equal to the cluster size, and the multiple quantum count will reach a plateau as a function of τ. Using this technique, Baum *et al.* were able to show that a sample of amorphous Si containing ca. 8 at% H had discrete cluster units of 6 ± 1 hydrogen atoms.[655] Systematic investigations carried out by Reimer and coworkers reveal further that the cluster size depends critically upon the temperature of deposition and can be influenced by dopants, with phosphorus increasing and boron decreasing the cluster sizes.[655,657] (see Fig. 69). Larger amounts of carbon present in the sample destroy the hydrogen clusters, resulting in the formation of hydrogenated carbon atoms with sp^3 hybridization.[658] Thus, multiple-quantum NMR provides a powerful complementary technique to dipolar spin-echo NMR for the characterization of dipole couplings. This is true especially if well-defined clusters exist, whose sizes can then be determined by multiple-quantum coherence counting.

12.1.2.2. *Spin-lattice relaxation by molecular hydrogen.* Besides rigid, Si-bonded hydrogen, many NMR studies reveal the presence of molecular H_2, which is considered to be trapped within microvoids.[659–684] At room temperature its corresponding NMR signal is motionally narrowed and contributes to the narrow component of the ^1H NMR spectrum. Contrary to the assertion by

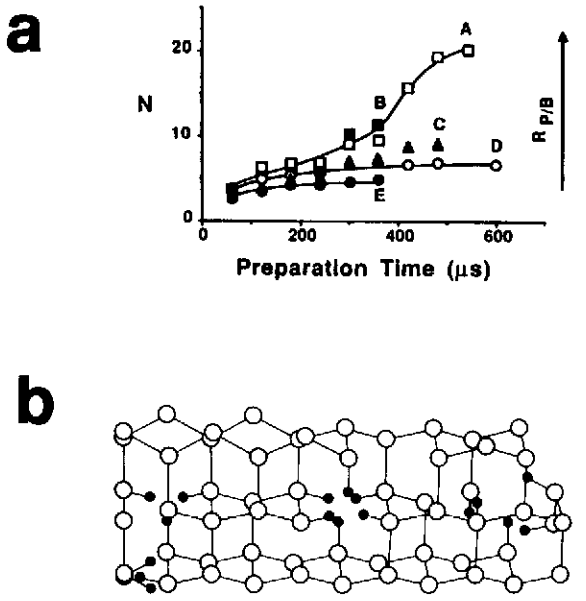

FIG. 69. (a) Effect of dopant incorporation on the hydrogen clusters in a-Si:H samples. The highest observable multiple-quantum coherence is plotted against the preparation time. (A) P-doping; (B) P- and B-doping (10:1 atomic ratio); (C) P- and B-doping (1:1 atomic ratio); (D) no doping; (E) P- and B-doping (1:10 atomic ratio). Reproduced with permission from Ref. 657. (b) Possible arrangement of hydrogen atoms in hydrogenated a-Si; consistent with the experimental observation of $\Delta m_{max} = 6$. Reproduced with permission from Refs 655 and 657.

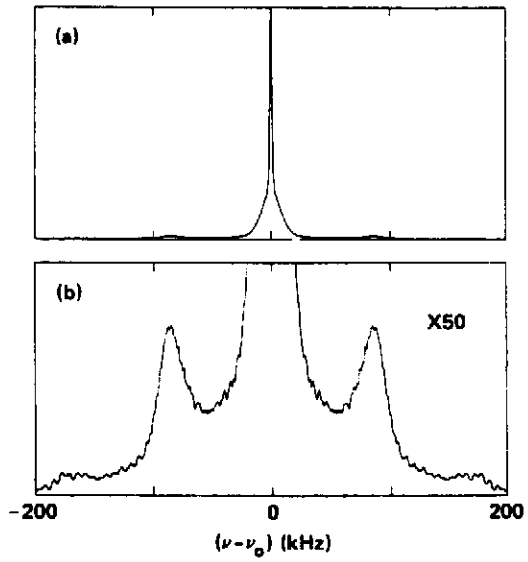

FIG. 70. ^1H NMR evidence for molecular H_2 in a-Si:H, as evident by the Pake doublet observed at 1.43 K. Reproduced with permission from Ref. 665. Top: complete spectrum; bottom: vertically expanded spectrum.

Lamotte,[659] molecular H_2 usually represents a minor constituent (10–20% of the total H content or less) in un-annealed a-Si:H. To freeze out the H_2 motion, extremely low temperatures are required. Under such conditions, H_2 manifests itself in the spectrum as a Pake doublet with a 175 kHz splitting (see Fig. 70),[663–665] although it is not clear whether this "freezing-out" effect represents orientational ordering or a slow relaxation phenomenon.[672–674] In addition, molecular H_2 species are easily detected and quantitated by either ^1H (or ^2H) spin-lattice relaxation time (T_1) measurements, or ^2H wideline quadrupole echo NMR studies. Using either of these three techniques it has been shown that annealing a-Si:H samples to temperatures above 500°C produces a significant increase in the molecular hydrogen fraction.

Variable temperature spin-lattice relaxation measurements are a particularly powerful means of probing and characterizing molecular H_2 species in a-Si samples. Most plasma-deposited a-Si:H films show a ^1H T_1 minimum in the temperature region between 25 and 55 K. Figure 71 shows such a typical result. The relaxation rate maximum and its frequency dependence suggest a molecular reorientation process with a motional correlation time in the range of ω_0^{-1}, i.e. in the MHz region at this temperature. This relaxation process, first observed by Carlos and Taylor[668] is attributed to the reorientation of the H_2 molecule.[667] Since only a small fraction of such H_2 relaxation centers are present, the large majority of hydrogen atoms are relaxed via spin diffusion. Proof for this mechanism comes from the sensitivity of T_1 to the process of *ortho–para*-H_2 conversion and to the concentration of hydrogen atoms present. In general, the spin-lattice relaxation rate T_1^{-1} can be calculated by:[638,675]

$$T_1^{-1} = T_1^{-1}(\mathrm{SD}) + T_1^{-1}(\mathrm{O}) \tag{59}$$

where $T_1^{-1}(\mathrm{SD})$ is the rate contribution due to spin diffusion, whereas $T_1^{-1}(\mathrm{O})$ comprises relaxation from other sources (e.g. paramagnetic relaxation from dangling bonds). Especially near the T_1 minimum, the contribution $T_1^{-1}(\mathrm{SD})$ dominates. Considering the effect of finite spin diffusion rates, one can write:

$$T_1(\mathrm{SD}) = \mathrm{A}T_1(\mathrm{H_2}) + \mathrm{B}. \tag{59a}$$

The constant A is given by the ratio of the spin heat capacities for H_2 and H, respectively:

$$\mathrm{A} = 1/2(n_{\mathrm{H}}/n_{\mathrm{H_2}}) \qquad \text{(assuming 75 mol.\% } o\text{-H}_2\text{)} \tag{59b}$$

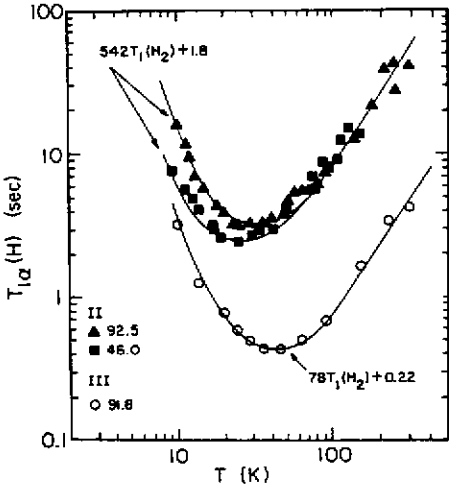

FIG. 71. Molecular hydrogen related T_1 data for two representative a-Si:H samples (labeled II and III, respectively). Included are corresponding fits to eq. (59a) with the parameters shown. Reproduced with permission from Ref. 675.

In the above expressions, n_H is the total concentration of bonded hydrogen, and n_{H_2} and $T_1(H_2)$ are the concentration and spin-lattice relaxation time of the *ortho*-hydrogen molecules relaxing to the lattice. The constant B characterizes the limiting relaxation time, due to spin-diffusion forming a kinetic bottleneck. This "bottleneck relaxation rate" is given by:

$$B^{-1} = 4\pi D_H b_H \cdot \tfrac{3}{4} n_{H_2} \tag{59c}$$

where D is the spin-diffusion constant (on the order of 10^{-12} cm^2/s) and b_H corresponds to a characteristic distance between H_2 and its nearest H neighbor. (A similar expression holds for the relaxation of ^{2}H in a-Si:D.) Since the quantity $T_1^{-1}(H_2)$ is an intrinsic property of the *ortho*-hydrogen molecule and can be calculated independently, expressions (59a, b and c) can be used to determine n_{H_2} and the spin diffusion constant D_H. It should be noted that not all a-Si:H samples give relaxation rate maxima in this temperature region. The diversity of ^{1}H relaxation behavior simply reflects the fact that the concentration of H_2 in the microvoids in these samples is variable and subject to preparation conditions.

12.1.2.3. *Deuterium NMR studies of a-Si:D.* The use of SiD_4 and D_2 in the vapor deposition atmosphere leads to incorporation of deuterium into a-Si, hence providing the opportunity of obtaining complementary structural information by ^{2}H NMR. In all of such studies, the Si-bonded deuterium gives rise to a typical axially symmetric powder pattern (see Fig. 8b). From the splitting,[670] $e^2qQ/h = 8$ kHz is determined and shows little dependence on temperature. In addition to this dominant species (typically > 90% of the deuterium present), which comprises deuterium atoms within both DI and CL region, various other lineshape components, all of which are associated with molecular HD, D_2 or "weakly bound" deuterium are present:[683] In the temperature range $4 \leqslant T \leqslant 70$ K a characteristic 27 kHz broad central line appears, which can be made to disappear upon annealing at 350 K. Also, sharper central lineshape components, attributable to D_2 molecules that are less motionally hindered, are observed. Finally, samples with very high D concentrations (above 20 at%) show a characteristic powder pattern with an apparent e^2qQ/h of 29.3 kHz. This lineshape component has a very short T_1 and can be amplified selectively by rapid pulsing; it is assigned to the powder pattern of rapidly rotating SiD_3 groups.[684] Even at 1.6 K this motion appears to be rapid on the NMR timescale. Based on these findings, it has been suggested that these "silyl rotors" either extend out of the bonded silicon network into microvoids or that they are bonded to surfaces of microcrystalline inclusions. Figure 72 shows a typical ^{2}H NMR spectrum, summarizing the various contributions to the ^{2}H NMR lineshapes.

12.1.3. *Isovalent Substitution in a-Si:H*

12.1.3.1. *Amorphous hydrogenated germanium and Ge–Si alloys.* A variety of studies on germanium-containing systems, prepared analogously by decomposition of GeH_4 have been carried out; mainly using deuterium NMR.[685–690] These germanium-containing films generally show a less well defined rigid ^{2}H signal with a somewhat reduced quadrupole coupling constant ($\sim$80 kHz); furthermore a large fraction ($\sim 2/3$) of the D is present in the form of molecular species. Below 50 K *para*-D_2 gives rise to a resolvable powder pattern with a coupling constant $e^2qQ/h = 101$ kHz. "Germyl rotors" (GeD_3 groups) have not been detected so far.

12.1.3.2. *Fluorinated amorphous silicon.*[691–698] Fluorine is thought of as playing a similar role as hydrogen in a-Si, neutralizing dangling bonds and thereby removing defect states from the band gap. In contrast to the ^{1}H spectrum in a-Si:H, the ^{19}F NMR spectra of fluorinated a-Si are motionally averaged at room temperature.[697] This mobility arises from a large fraction of molecular SiF_4 present in these films, in addition to analogous DI and CL phases.[697] Direct evidence for SiF_4 is obtained from low-temperature (4.2 K) studies, which show the structured spectra and oscillatory FID components typical of four-spin systems.[694] A more detailed study indicates that in order to explain the experimental NMR spectra satisfactorily, an additional resonance, assigned to SiF_3 species must be invoked.[697]

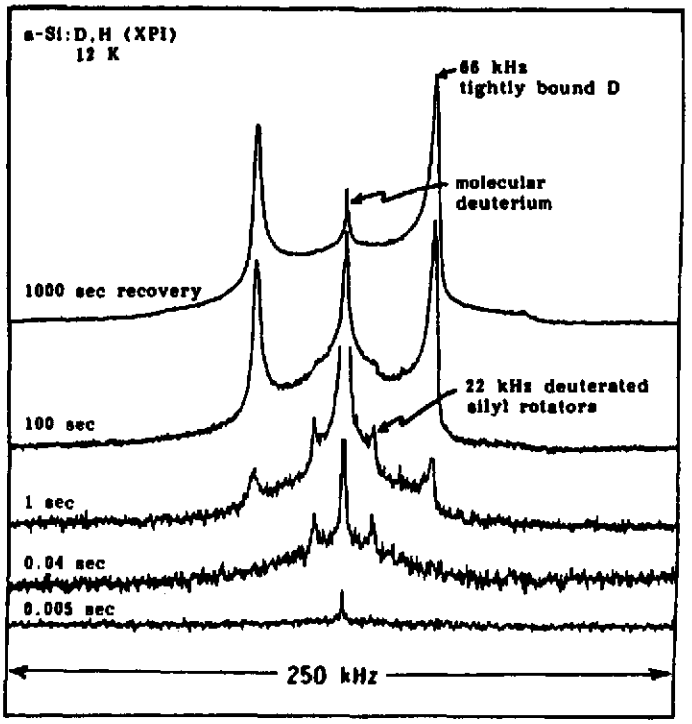

FIG. 72. ^{2}H NMR results for an a-Si:D, H sample. Variable recovery delays (indicated on the left side of the figure) have been used for selective amplification of the various lineshape components present. Reproduced with permission from Ref. 684.

12.1.3.3. *Amorphous hydrogenated Si, C:H alloys and a-C:H.* Co-deposition of SiH_4, CH_4, and H_2 affords amorphous hydrogenated silicon carbide, which is of comparable interest to a-Si:H for electric and photovoltaic applications. A variety of NMR studies have been carried out to study the hybridization state of carbon in these alloys and how carbon in a-Si:H changes the hydrogen distribution.[699-703] Multiple quantum NMR studies show that the well-defined cluster sizes seen in certain a-Si:H samples are eliminated.[658] ^{13}C NMR experiments have indicated the presence of both sp^2- and sp^3-hybridized carbons, with a ratio dependent on sample preparation conditions. In part, such discrepancies arise from the use of cross-polarization, which is inadequate to detect carbon atoms remote from hydrogen. To attain a quantitative understanding of the structure on the basis of ^{13}C NMR it is therefore important to abstain from cross-polarization and study simple Bloch decays instead, allowing enough time between pulses for spin-lattice relaxation. Such experiments have been carried out by Reimer and coworkers.[658,699] By studying the effect of ^{1}H decoupling they have further shown that it is possible to differentiate between protonated and non-protonated C-atoms. This is so because the protonated C-atoms are subject to strong ^{1}H–^{13}C dipole–dipole couplings which broaden their resonances beyond detectability in the absence of ^{1}H irradiation. Taking advantage of this effect, Petrich *et al.* could show that the majority of the sp^3 C-atoms are protonated, whereas the majority of the sp^2 C-atoms are non-protonated.[658,699]

Films of amorphous hydrogenated carbon (a-C:H) are prepared by radio-frequency plasma decomposition of hydrocarbons in a similar fashion to that used for a-Si:H. These materials are of interest because of their hardness, transparency, high resistivity and chemical inertness. In principle, ^{13}C NMR can be used to investigate the carbon hybridization state,[704-712] although some of the earlier studies undertaken with the cross-polarization technique are probably not quantitative for the reasons discussed above. The bandgap of a-C:H deposited near room temperature is ca. 3 eV, but this

can be lowered substantially by increasing the deposition temperature. Solid state NMR (^{1}H and ^{13}C-MAS without CP) has been used to investigate if this trend in band gap can be attributed to systematic changes of either hydrogen content, or carbon hybridization state. No correlation was found, suggesting that the observed effect is due to changes in the bulk density of these materials with deposition temperature.[712] From these studies, the fraction of diamond-like (unhydrogenated sp^3) carbon is estimated at 10–30 at%.

12.1.4. *Local Structure of Dopants in Hydrogenated Amorphous Silicon.* a-Si:H can be doped n- or p-type by the addition of PH_3 or B_2H_6 to SiH_4 during vapor phase deposition,[713] hence giving rise to potential device applications principally in the same fashion as crystalline silicon. P and B dopants in crystalline silicon are known to reside in substitutional four-coordinated sites. The fact that the doping efficiency in a-Si:H is, by contrast to c-Si, much reduced, suggests that the local bonding structures of the dopants present in a-Si:H are fundamentally different. In particular, three-coordinated PSi_3 and BSi_3 units, which are coordinatively saturated, are possibly present and found to be doping-inactive. Thus, the local coordination of the dopants is an important question. Furthermore, the spatial distribution of dopant atoms in relation to each other and the hydrogen species is of interest. Finally, in multiply doped ("compensated") samples, the spatial relationship between different dopants is a key issue. Much of the knowledge acquired in this field so far has been the result of well-designed selective solid state NMR experiments bearing in mind the specific spin dynamics in these materials.

Figure 73 shows the ^{31}P NMR spectra of several lightly doped (0.16–1.8 mol.% P) a-Si:H samples. Two distinct contributions are present: a component around −175 ppm is assigned to three-coordinated P atoms (P^{III}), whereas a shoulder at −70 ppm is attributed to four-coordinate P atoms (P^{IV}).[714] The assignments are confirmed by the chemical shifts of suitable model compounds: for $P(Si(CH_3)_3)_3$ and $PH(Si(CH_3)_3)_2$ $\delta_{iso} = -251$ ppm and −237 ppm, respectively, in the liquid state,[715] and the six chemically inequivalent three-coordinate P atoms in crystalline SiP give MAS-NMR peaks at −143, −152, −232, −235 (double intensity), and −239 ppm.[716] As a model for P^{IV} species one may take the ^{31}P resonance in P-doped polycrystalline silicon, for which the center of gravity lies around −70 ppm.[717] Several other studies have failed to detect the P^{IV} resonance, particularly in more heavily doped samples.[718–720] This discrepancy may be due to the reported metastability of this phosphorus site, which can be brought to disappearance by light-soaking and restored by dark annealing.[725]

Further selective experiments have served to characterize the detailed nearest-neighbor coordinations of these two phosphorus sites. 180° pulses fail to refocus the transverse magnetization associated with P^{IV}, indicating that this resonance is homogeneously broadened by dipole–dipole couplings with

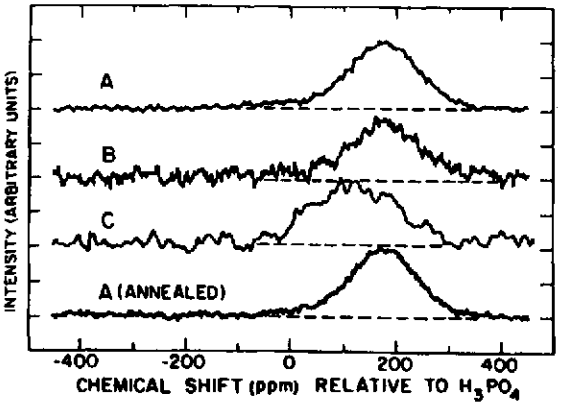

FIG. 73. ^{31}P wideline NMR spectra of several lightly doped a-Si:H, P samples A, B, and C contain 1.8, 0.33, and 0.16 mol.% P, as determined by ion microprobe analysis. Reproduced with permission from Ref. 714.

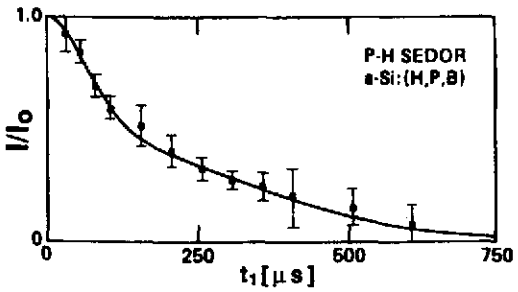

FIG. 74. ^{1}H–^{31}P SEDOR decay of an a-Si:H, B, P sample prepared by glow discharge deposition. The sample contains ca. 13 at% H, and 2 at% B and P respectively. The theoretical curve is discussed in the text. Reproduced with permission from Ref. 720.

nearby ^{1}H.[714] By contrast, the P^{III} species not only give rise to well-defined spin echoes, but the intensity of these spin echoes is apparently completely unaffected by the ^{1}H spins. The ^{31}P spin echo decay function for these P^{III} spins can be explained solely on the basis of ^{31}P–^{31}P interactions among randomly distributed ^{31}P spins. The weakness of the ^{1}H–P^{III} interactions is confirmed by SEDOR experiments, which indicate that neither singly doped nor compensated a-Si samples have any appreciable P–H bonding. A simple analysis of the experimental SEDOR curve is shown in Fig. 74. The experimental data can be fitted assuming a bimodal 1:1 distribution of P–H nearest approaches of 2.6 and 4.1 Å, respectively.[720] All of these results indicate that the P^{III} species reside in the DI phase. This is interesting in view of the fact that, according to ^{1}H NMR results, P-doping actually reduces the DI/CL ratio.

Boron doping has been studied to a lesser extent. Field-dependent ^{11}B wideline NMR spectra reveal clear second-order quadrupole effects, hence suggesting that all of the B atoms detected are three-coordinated.[718] ^{1}H–^{11}B SEDOR experiments reveal fundamental structural differences between a singly doped a-Si:B, H and a compensated a-Si:B, P, H sample (see Fig. 75).[720] While no strong B–H interactions can be detected in the compensated sample, singly-doped a-Si:(B, H) gives rise to a dramatically accelerated SEDOR decay, consistent with 40% of the B atoms having a B–H single bond at 1.6 Å. Finally, the ^{11}B–^{31}P SEDOR experiment indicates that the relative B–P distribution in the compensated sample is non-random and involves a fair amount of mutual B–P clustering. 40% of the boron atoms are P-bonded in this sample, with an approximate B–P distance of ca. 2.1 Å.

12.1.5. *Amorphous Si–N and B–N Based Films.* Plasma deposited silicon nitride is a common passivation material for integrated circuits. The thermal stability can be improved by fluorination, resulting in thin films of a-SiN_xH_y:F. ^{1}H NMR studies of these films reveal a hydrogen distribution that is distinctly different from a-Si:H,[728] and ^{29}Si NMR using selective decoupling experiments with and without MAS reveals a strong propensity for N–H vs Si–H bonding.[729] The fluorinated materials contain clustered silicon–fluorine and nitrogen–hydrogen regions within an amorphous silicon–nitrogen matrix.[730,731] In contrast, hydrogenated boron nitride films behave quite differently. Here, the analysis of dipolar couplings suggests that the hydrogen atoms are essentially randomly distributed.[732]

12.2. *Amorphous Phosphorus and Arsenic*

Both phosphorus and arsenic can be easily prepared in the amorphous state. Preliminary structural investigations by ^{31}P NMR and ^{75}As NQR have been carried out. In the case of amorphous phosphorus, the techniques used (T_1, T_2, FID) were found to be rather insensitive to structural detail, and a broad similarity of spectroscopic behavior to that observed for black crystalline P remains the only conclusion.[733] The nuclear electric quadrupole coupling constant of amorphous As was

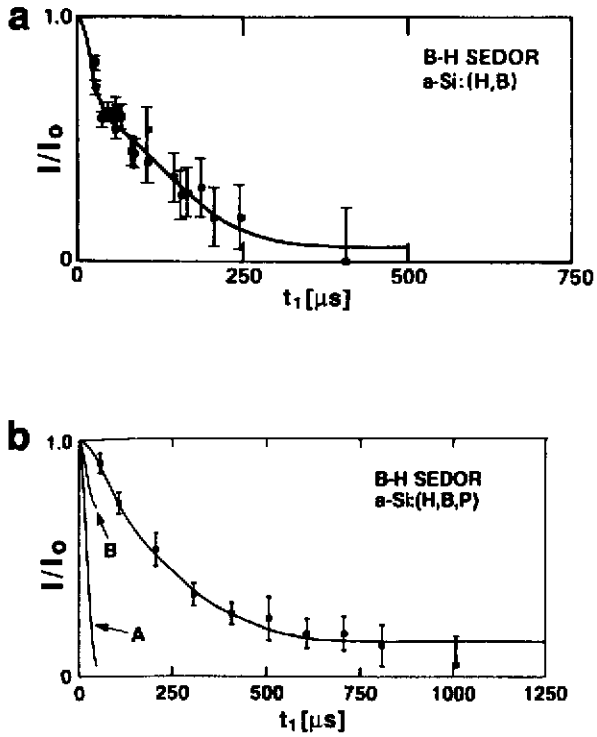

FIG. 75. ^{1}H–^{11}B SEDOR decay for hydrogenated a-Si, doped with boron. (a) Singly doped sample, containing ca. 0.5 at% B. The rapid initial decay is attributed to B atoms bonded to H. (b) Compensated sample, containing ca. 2 at% B and P, respectively. Curve A assumes that each B atom is bonded to an H atom, and curve B assumes a random distribution of B and H. Neither of these assumptions reproduce the data. Phenomenological two-Gaussian fits are shown as solid curves. Reproduced with permission from Ref. 720.

measured by pulsed NQR and found to be substantially larger (63.5 MHz) than for rhombohedral and orthorhombic arsenic (23.5 and 46.3 MHz); this was qualitatively attributed to a higher degree of sp hybridization. Due to disorder in the nearest neighbor geometries, a wide spread of quadrupole couplings exists.[734]

12.3. *Amorphous III–V Semiconductors*

It is possible to prepare the III–V semiconductors GaAs and GaP in the amorphous state by either radio frequency sputtering or by molecular beam epitaxy. These systems can be essentially considered as heteropolar analogs of amorphous silicon. For such heteropolar structures, the generation of random networks via bond-switching as described above for a-Si will necessarily lead to homopolar III–III and V–V bonds. With the objective of detecting and possibly quantitating such "chemical disorder", $^{69,71}Ga$ and ^{75}As NMR studies have been carried out.[735,736] The spectra obtained are dominated by the interaction of the nuclear electric quadrupole moments of these isotopes with electric field gradients, causing second-order lineshape perturbations. Since, unfortunately, these field gradients cannot be calculated with the desirable degree of accuracy, the question of chemical disordering has remained unanswered in these systems. Conclusive evidence for these phenomena is, however, obtained by dipolar NMR spectroscopy on II–IV–V_2 chalcopyrite glasses, discussed in the section below.

12.4. *Pnictide Glasses*

It has been known for some time that $CdGeAs_2$, $CdGeP_2$, and a variety of other P- and As-based semiconductors with the chalcopyrite stoichiometry can be prepared in the glassy state by rapid melt-quenching.[737] Most strikingly, these glasses have consistently higher densities than the corresponding crystalline compounds, hence suggesting that there are marked structural differences between these two states of matter.[738] In spite of this unusual feature there have been virtually no attempts at direct structural characterization of these glasses to date. Crystalline $CdGeAs_2$ and $CdGeP_2$ are strictly chemically ordered with As^{3-} and P^{3-} ions occupying exclusively the anionic sites of the tetragonal chalcopyrite structure.[739] Figure 76 compares the ^{113}Cd MAS-NMR spectra of glassy $CdGeP_2$ with those of related crystalline compounds. Evidently, the well-ordered Cd environments in the crystalline CdP_2 and $CdGeP_2$ are not preserved upon going to the glassy states, where only an extremely wide chemical shift distribution is seen. The chemical dissimilarity is confirmed further by a marked upfield shift of the resonances for the glassy material.

The chemical bond distribution in glassy $CdGeP_2$ has been examined in detail by various dipolar NMR approaches. Figure 77 shows the comparison of the experimental ^{31}P spin echo decay data with simulations for a chemically ordered chalcopyrite structure, a random distribution of P atoms over all the lattice sites, and an additive superposition of both. The results confirm unambiguously the occurrence of P–P bonds in glassy $CdGeP_2$, albeit at a sub-statistical level. At the same time, ^{31}P–^{113}Cd SEDOR NMR results (not shown here) suggest that the average number of Cd–P bonds is lower than in the crystalline state, and corresponds more or less to that expected for a statistical distribution of atoms.[740,741]

Systematic dipolar NMR studies of various compositions in the system $CdGeAs_{2-x}P_x$ confirm that the ^{31}P–^{31}P dipolar couplings in the glasses are consistently stronger than in their crystalline counterparts. From the data it can be concluded that chemical disorder involving the formation of

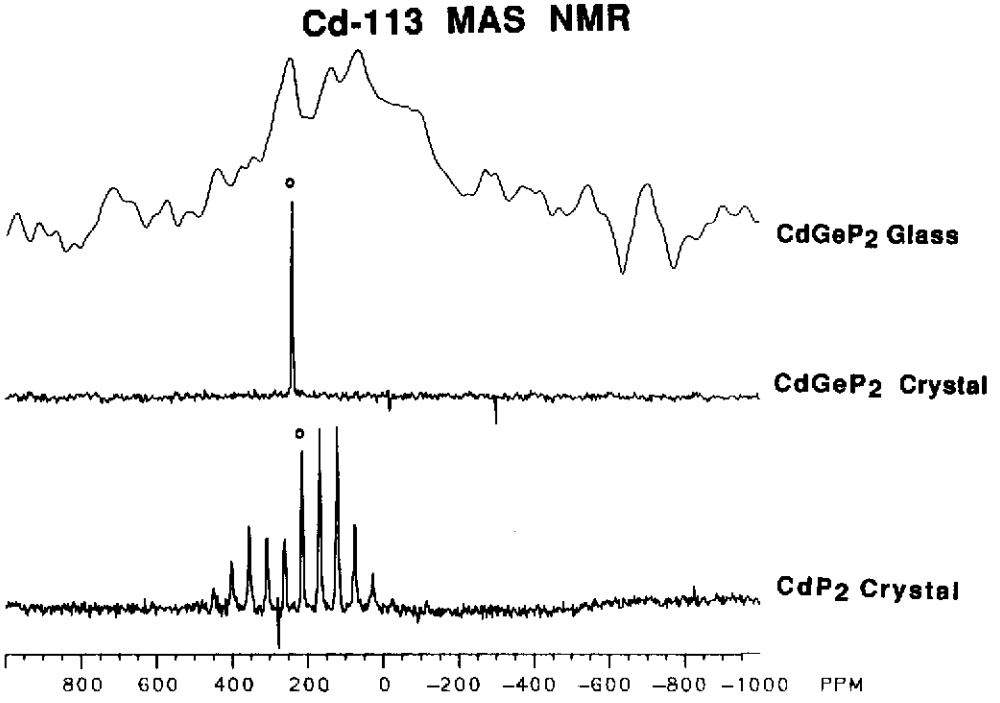

FIG. 76. Comparison of the ^{113}Cd MAS-NMR spectra for glassy $CdGeP_2$ and model compounds.

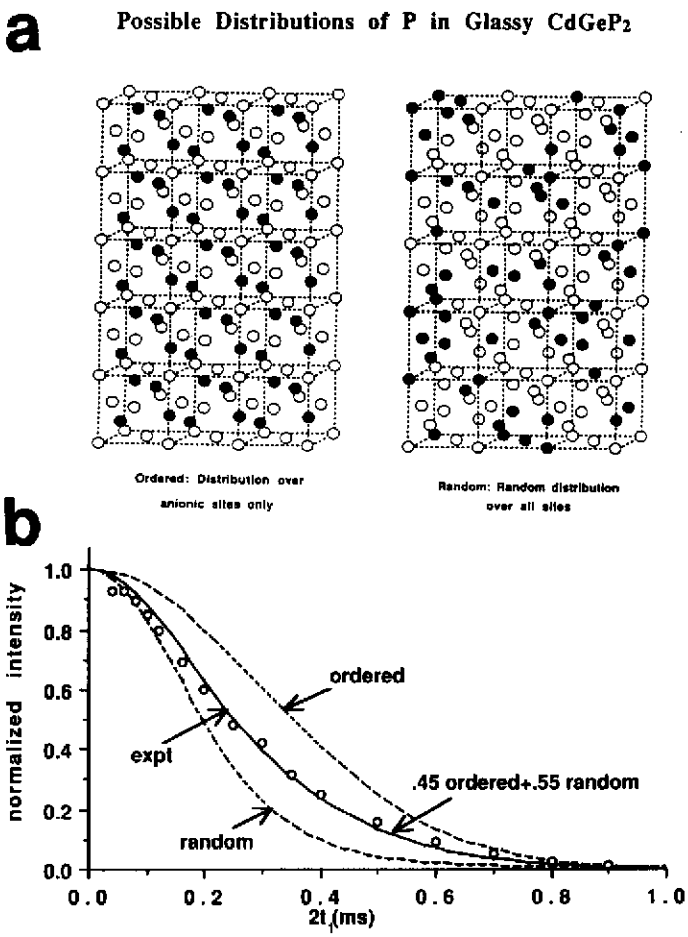

FIG. 77. (a) Possible distributions of P in glassy $CdGeP_2$. (b) Dipolar NMR spectroscopy of glassy $CdGeP_2$. ^{31}P spin echo decay. Included is a comparison of the experimental data with data calculated based on a chemically ordered and a random distribution of P atoms as shown in (a). The best fit to the data turns out to be a superposition of both models.

homopolar P–P bonds exists within the entire compositional region.[741] As discussed above, the presence of such homopolar bonds is entirely consistent with a continuous random network simulated by introducing bond switches into the chalcopyrite structure.

Disparity between glassy and crystalline structures is also evident in the ^{113}Cd spin echo NMR studies of compositions in the system $CdGe_xAs_2$ ($0 \leqslant x \leqslant 1$).[742] Here, the spin echo decays of glassy $CdAs_2$ and $CdGeAs_2$ are substantially more rapid than those of their crystalline counterparts, and rather resemble that observed for crystalline Cd_3As_2.[742] The suggestion that the structure of these glasses is characterized by the presence of Cd_3As_2 and As domains is consistent with the metastable eutectic observed in the Cd–As system at 61.5% As.[743] In excellent agreement with this prediction, most recent DSC and X-ray studies have revealed that glassy $CdAs_2$ undergoes either a glass→glass transition or a primary crystallization step to form Cd_3As_2 and As, before converting into the equilibrium phase $CdAs_2$.[744]

13. METALLIC GLASSES

13.1. *Overview*

Amorphous metals or metallic glasses are an interesting novel class of solid state materials, which can be formed by rapid quenching of certain elemental compositions from the molten or gaseous state ("splat cooling", melt-spinning, ultra-high-vacuum deposition). The lack of long-range periodicity in these systems results in materials with unique mechanical, electronic and magnetic properties that are of great interest to both materials scientists and theoretical physicists. NMR studies of these systems have focused on three central topics: (1) the characterization of the electronic structure and the charge transfer properties via Knight shift and spin-lattice relaxation studies, (2) NMR spin-echo mapping of the magnetic hyperfine field distributions at the nuclear sites in materials displaying cooperative magnetic behavior, and (3) elucidation of spatial structure and local atomic arrangements via selective measurement of dipole–dipole and nuclear electric quadrupole interactions. Although both electronic and magnetic structure constitute an essential part of the structural description of amorphous metals, space limitations demand here that the subsequent discussion will concentrate on topic (3). The key question here has been whether metallic glasses can be appropriately described as dense random packings of hard spheres (DRP model), or whether they show reproducible atomic correlations characteristic of chemical or short-range ordering.

Unfortunately, chemical shift effects in amorphous metals are dominated by nuclear hyperfine field distributions, or s-electron spin densities, and thus contain essentially no structural information. Therefore, the structural characterization by NMR hyperfine interactions is limited to interpreting nuclear electric quadrupole and magnetic dipole–dipole couplings. Although the systems studied are chemically rather diverse, several features have emerged in the NMR characterization that appear to be rather common for the large majority of metallic glasses studied to date.[745–747]

(I) Results on quadrupolar nuclei show generally quite well-defined quadrupolar splittings, indicating that the distributions of electric field gradients in these glasses are fairly narrow. This result argues strongly against the DRP model for most systems, as the latter would generally predict much wider EFG distributions. Rather the NMR results support the existence of short range order, which usually seems to mimick the short range order present in compositionally related crystalline model compounds.

(II) As in other types of glasses, the line width of the signal (in Hz) increases linearly with the strength of the applied magnetic field. This indicates that the lineshape is influenced by a distribution of Knight shifts. The detailed dependence of the line width $\Delta\nu$ as a function of field strength (or frequency ν_0) has been measured for a variety of systems. In general one expects a behavior according to:

$$(\Delta\nu)^2 = (\Delta\nu)_d^2 + a^2\nu_0^2. \tag{60}$$

The field independent linewidth $\Delta\nu_d$ is obtained from such data by extrapolation to zero field strength (resonance frequency). By assuming a Gaussian lineshape, the dipolar second moment M_{2d} is calculated according to

$$M_{2d} = 4\pi^2(\Delta\nu_d/2.36)^2 \tag{61}$$

if $\Delta\nu_d$ is defined as the full width at half height. This number should only be affected by dipole–dipole interactions, and thus should be analyzable in terms of eq. (16) for testing hypothetical atomic distribution functions. Unfortunately, this method does not allow one to differentiate between homo- and heterodipolar interactions, and the error in the extrapolation is large. Possibly more information might be obtained by using more selective experiments based on spin echo decay and SEDOR. No such applications to metallic glasses have been reported to date.

(III) NMR measurements of magnetic hyperfine field distributions in ferromagnetic samples differ strongly from those in applied field studies. The spectra in such alloys arise from the interaction of the constituent nuclear magnetic moments with magnetic hyperfine fields at the nuclear sites; thus no external magnetic field is necessary. Since in the amorphous state, a distribution of magnetic hyperfine fields is always present, one generally observes quite wide lines, sometimes extending over tens of MHz.

Spectra this broad require the use of the spin-echo mapping technique discussed earlier (Section 4). Structural information from such experiments has been deduced predominantly from careful studies of compositional dependences and from comparison with crystalline model compounds. Generally, the assumption is made that the hyperfine field distribution is in some way a reflection of the short-range order environment, although the detailed nature of this relationship is not well-known.

A further serious complication in the interpretation of zero-field spectra arises from the strong enhancement factor of both the local magnetic excitation field and the NMR signal received in ferromagnetic materials. While enhanced signals are generally desirable for sensitivity reasons, the enhancement factor is, unfortunately, orientationally dependent. Thus, in cases where a high magnetic field anisotropy exists, the nuclei in domain walls parallel to the polarization direction of the applied B_1 field contribute most of the signal. If, on the other hand, the magnetic anisotropy is weak, the range of nuclear orientations contributing to the NMR lineshapes will depend greatly on the applied rf field strength. It is clear, then, that this behavior results in considerable complications affecting peak assignments, interpretations, and quantitative NMR studies in such systems. These complications can be avoided by applying an external saturating field, resulting in a loss of the enhancement factor. rf field strength dependent lineshapes are a particularly common feature for cobalt based amorphous alloys.

For compounds with more than one NMR active isotope it must be borne in mind that zero-field spectra yield no a priori information about the assignment of a certain spectral feature to a particular nuclear isotope. In general, such assignments would have to come from isotopic substitution studies or general chemical considerations. A final complication arises for nuclei with large nuclear electric quadrupole moments. In this case, the observed resonance arises from the combined effect of hyperfine magnetic fields and nuclear electric quadrupolar interactions, and the analysis and interpretation of such spectra is naturally quite difficult.

Following this overview, specific systems will be discussed below. The types of systems investigated to date include: amorphous metallic hydrides, glassy metal–metalloid systems (mainly transition metal borides and phosphides) and amorphous alloys consisting exclusively of metals.

13.2. *Amorphous Metal Hydrides*

A number of NMR studies have been carried out on amorphous hydrides with compositions $TiCuH_x$,[748–751] Zr_2PdH_x,[752–755] Zr_3RhH_x,[756] $Pd_{80}Cu_7Si_{13}H_x$[757] and $(Zr_{0.5}Ni_{0.5})_{0.98}P_{0.02}H_x$.[758, 759] The bulk of the work has concentrated on the electronic structure as revealed by Knight shift and spin-lattice relaxation measurements, and on the characterization of hydrogen mobility by variable temperature and frequency ^1H and ^2H lineshape and spin-lattice relaxation measurements. As a general result, it is found that the hydrogen in these amorphous phases has much higher mobility than in their crystalline counterparts. Thus, the ^1H and ^2H NMR spectra are motionally averaged at room temperature, and cryogenic temperatures (77 K) are necessary to reach the rigid lattice limit. The structure of amorphous $TiCuH_{1.4}$ has also been discussed on the basis of such low-temperature ^1H second moments.[751] More explicit and far-ranging simulations, together with model compound work are required to develop this application further in the future.

13.3. *Amorphous Metal–Metalloid Systems*

Transition metal boride and phosphide systems constitute the largest known class of metallic glasses. The region of glass formation usually extends from ca. 10 to 30 at% phosphorus or boron. Both ^{31}P and ^{11}B NMR have been used extensively in order to characterize the dipole–dipole couplings, chemical shift distributions and the distributions of nuclear electric quadrupole couplings in these systems.

13.3.1. *Iron Borides.* Magnetic amorphous alloys $Fe_{1-x}B_x$ ($0.12 \leqslant x \leqslant 0.25$) are prepared by quenching the corresponding melts on rapidly spinning metal disks ("melt-spinning"). The NMR spectra of these materials are very broad and have to be recorded by the zero-field spin echo mapping method. Isotopic enrichment studies show that ^{57}Fe contributes very little to the observed natural abundance NMR

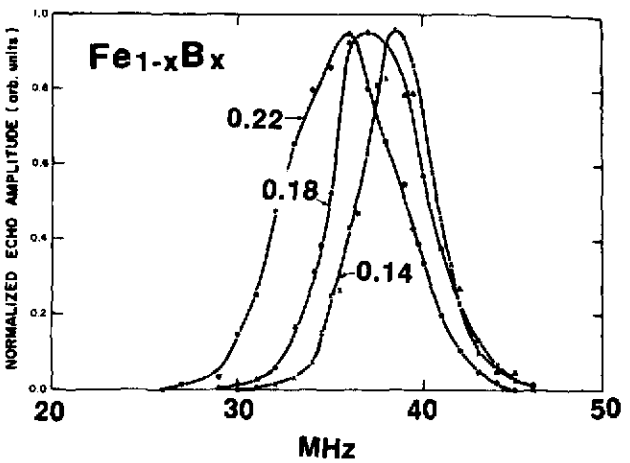

FIG. 78. Normalized NMR zero-field spin echo amplitude in glassy $Fe_{1-x}B_x$ alloys vs resonance frequency in MHz. The spectra are attributed mainly to ^{11}B nuclei. Results are shown for three compositions x, as indicated in the figure. Reproduced with permission from Ref. 761.

lineshapes.[760] Since the nuclear electric quadrupole moment of ^{11}B is small, the lineshapes are entirely governed by the magnetic hyperfine field distributions at the boron sites. Figure 78 shows the compositional dependence of the spectra.[761] At low x, a broad bell-shaped curve centered around 39 MHz is observed. As the B content is increased, the lineshape broadens considerably, as sites exposed to lower hyperfine fields are successively occupied by additional boron atoms. Concomitantly, the average hyperfine field decreases resulting in a peak maximum at ca. 35 MHz at $x=0.23$. With respect to this compositional dependence of the magnetic hyperfine field there seems to be general confluence between the results of Hines *et al.*[761] on the one hand and Pokatilov[762] on the other. In contrast Zhao *et al.* have reported substantially different results.[763]

Extensive attention has been paid to the crystallization behavior of Fe,B alloys upon annealing.[764–767] At annealing temperatures below 390°C α-Fe crystallizes, as revealed by the appearance of a sharp resonance at 46.7 MHz. The broad resonance remains initially, but shifts to lower frequency as expected for a glass that is now richer in boron. Heating above 420°C results in crystallization of the Fe_3B phase, yielding well-defined sharp signals.

The above studies have been extended to multicomponent alloys (containing Co, Mn, Si), however, the complexity of the results obtained in these systems makes any interpretation difficult at this stage.[768, 769]

Iron phosphides have been studied to a lesser extent. Investigations have concentrated on alloys with the composition $Fe_{75}P_{15}C_{10}$.[768, 770] The hyperfine field distribution in this ferromagnetic material was mapped out and, in conjunction with isotopic enrichment studies, the contributions due to ^{31}P and ^{57}Fe were separated.[770]

13.3.2. *Cobalt Borides and Phosphides.* Ferromagnetic amorphous $Co_{1-x}B_x$ alloys can be prepared over the compositional range $0.17 \leqslant x \leqslant 0.30$ by the melt-spinning technique. The zero-field spectrum of a-Co_3B extends from 50 to 200 MHz, reflecting an enormous range of magnetic hyperfine fields experienced by the ^{59}Co nuclei.[771] Since the quadrupolar interaction is moderately weak, the spectrum is dominated by the distribution of magnetic hyperfine fields. It must be borne in mind, however, that due to the effect of anisotropic magnetic enhancement factors, the spectra are not inherently quantitative and depend significantly on the applied radio frequency field strength.[772, 773] These complications can be avoided in studies using applied saturating fields.[773] Using this technique, Böhner *et al.* showed that the mean hyperfine field at the Co nuclei decreases monotonically with increasing x.[773] A similar decrease has been observed for amorphous Co–Si alloys.[774] ^{59}Co

signals have also been recorded and analyzed for a variety of compositionally more complex Co–boride alloys containing other atoms such as Fe, Mn, and Ni,[775–777] as well as more complex Si-substituted ones.[778–781]

Amorphous Co–P alloys are generally prepared by chemical or electrochemical deposition. In zero field the ^{59}Co nuclei resonate around 200 MHz,[782–786] with a gradual decrease in the average resonance frequency as the phosphorus content increases.[782] As for the Co–B system, the lineshapes are affected by anisotropic domain wall enhancement factors and have to be carried out in weak applied saturating fields.[772,785]

13.3.3. *Nickel Borides and Phosphides.* Amorphous specimens with compositions $Ni_{1-x}B_x$ ($0.18 \leqslant x \leqslant 0.40$) have been studied by a variety of NMR techniques.[787–790] These materials are Pauli paramagnets and their NMR spectra are dominated by the ^{11}B nuclear electric quadrupolar interaction. As predicted theoretically from first order perturbation theory, the quadrupolar interaction splits the line into three components, corresponding to the central transition and two satellite lines, respectively (see Fig. 8, left side). The general peak patterns observed in glassy Ni_3B and Ni_4B_3 closely resemble those observed in their respective crystalline counterparts.[789,790] This close correspondence and the observation of satellite transitions *per se*, argue strongly in favor of well-defined short range order in these samples, and are in stark contrast to predictions made on the basis of the DRP model. For the latter case one would expect that there would be a wide distribution of quadrupole couplings and hence that the satellite transitions would be unobservable. In spite of the close general agreement between the ^{11}B NMR spectra of c-Ni_3B and amorphous Ni–B glass with

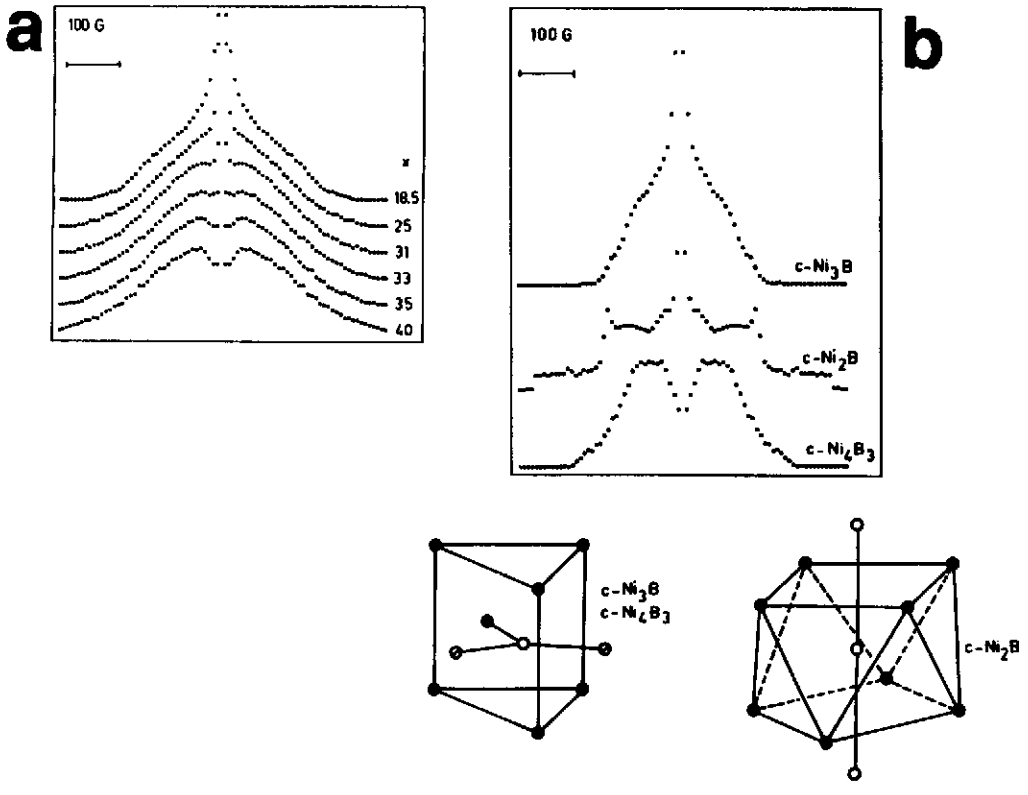

FIG. 79. ^{11}B NMR spectra in the binary nickel–boron system. (a) ^{11}B NMR spectra in amorphous $Ni_{100-x}B_x$ alloys as a function of x. (b) ^{11}B NMR spectra in crystalline nickel borides and the boron coordinations in them. Reproduced with permission from Ref. 790.

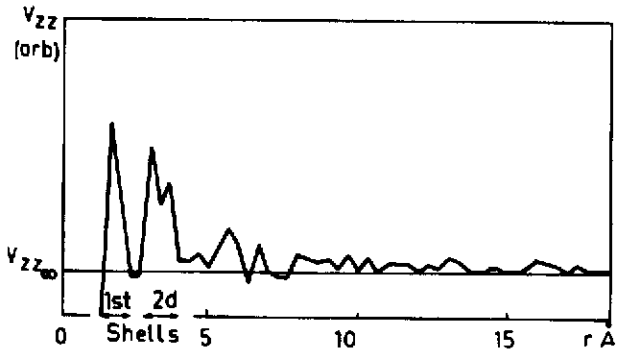

FIG. 80. The principal component of the electric field gradient tensor, V_{zz}, as calculated by a point-charge model as a function of the distance from the central boron atoms up to which the calculation is performed. $V_{zz}(\infty)$ is computed up to 40 Å distance. Reproduced with permission from Ref. 790.

similar compositions (see composite Fig. 79), the average nuclear quadrupole coupling constant e^2qQ/h is significantly larger in the glasses than in the crystalline compound. This is explained, in conjunction with Fig. 80, on the basis of electric field gradient calculations by the point charge model. Figure 80 illustrates the result of such a calculation for crystalline Ni_3B inside a sphere of radius r around a central B atom, as a function of distance. This figure shows that the V_{zz} due to nearest or next-nearest neighbor atoms (within one or two atomic distances) is significantly larger than the net $V_{zz}(\infty)$ calculated from all contributions up to very large distances (40 Å). The figure implies that in crystalline Ni_3B the shells at higher distances make a significant contribution to V_{zz}. As shown by Fig. 80 the contributions of these further removed atoms tend to reduce the net field gradient. In contrast, for glasses one expects that only atoms that are nearest (or possibly next-nearest) neighbors will contribute substantially to V_{zz}, because due to the disordered state, the distribution of atoms at higher distances will be approximately spherical. Hence there is no such diminishing effect on the field gradient in the glasses, resulting in somewhat stronger overall quadrupole coupling. These model compound studies are important as they illustrate that long-range effects can make quadrupole coupling constants between crystalline compounds and compositionally analogous glasses substantially different, even if the short range order is the same.

Some of the most widely studied systems are the amorphous alloys derived from the binary Ni_{1-x}–P_x system.[791–802] Glasses can be formed over a compositional range of approximately $0.12 \leqslant x \leqslant 0.27$.

Due to the absence of a nuclear electric quadrupole moment, the interpretation of the ^{31}P NMR spectra has focused on dipole–dipole coupling information as extracted from the zero-field intercepts of field-dependent M_2 measurements.[792, 794, 796] From the values obtained it is generally concluded that no direct phosphorus–phosphorus contacts occur in these alloys. These results support Polk's structural hypothesis stating that in amorphous metal–metalloid alloys the metal component adopts a DRP structure, while the metalloid component occupies interstitial sites present in such packings.[803] This basic model was refined later by Gaskell, who assumed a random packing of well-defined metalloid coordination polyhedra, surrounded by six metal atoms in a trigonal prismatic environment.[804] It should be noted, however, that the error of the M_2 measurement itself and the extrapolation to zero field strength could be substantial (especially because the line shapes deviate visibly from Gaussian shapes), and thus a measurement of M_{2d} by the spin-echo method would be more desirable. Furthermore, explicit simulations of the M_{2d} distributions expected from the Polk model could lend further support to the conclusions.

A variety of ternary Ni–P–X systems have been investigated (especially with X = Pt, Pd). P–P avoidance appears to be one of the common conclusions, but the emphasis of these studies has been on subtle changes in the electronic structure upon metal substitution.[795–800]

A detailed analysis of dipole–dipole interactions has been published for the ternary Ni–Cu–P system.[794] Here, the zero-field second moment is dominated by the heteronuclear direct dipole–dipole coupling between ^{31}P and $^{63,65}Cu$ nuclear spins. The extrapolated zero-frequency second moment for ^{31}P appears to agree with the value calculated for a model in which Cu and Ni form a DRP structure. This agreement may be fortuitous, however, as eq. (16c) would not be applicable if the $^{63,65}Cu$ nuclei experience strong quadrupolar interactions. In the latter case (which seems likely for a random structure), the fact that the Cu are no longer strictly quantized in the magnetic field, leads to the theoretical prediction that the second moment should be higher by a factor 1.8 than that calculated from eq. (16c).[805,806] Thus, the magnitude of the nuclear quadrupolar coupling constant needs to be determined from ^{63}Cu or ^{65}Cu NMR (or NQR) experiments.

The NMR investigations on the binary Ni–P and Ni–B systems have also been extended to the ternary systems Ni–P–B[807–810] and Ni–Si–B.[807] The dipolar analysis for non-spin-$\frac{1}{2}$ nuclei such as ^{11}B is more complicated. Field dependent M_2 measurements along the lines of eq. (16) will fail to yield dipolar second moments because at low fields, second-order quadrupolar broadening will appear. Thus, the ^{11}B–^{11}B dipolar interaction has to be extracted from spin-echo experiments. Furthermore, the theoretical expression that has to be used in lieu of eq. (16) depends on the presence and strength of nuclear electric quadrupolar interactions, and on the extent to which the quadrupole splittings render the nuclei inequivalent.[811] A preliminary discussion of structural models based on ^{11}B spin-echo decays has been given.[812]

13.3.4. *Other Metal–Metalloid Systems.* More complex systems that have been studied, with a primary emphasis on electronic structure and/or magnetic hyperfine field distributions include Mo–B,[747] Mo–Ru–B,[747] Mn–B,[813] Fe–Mn–P–B,[814] Fe–Ni–Mn–B–Si,[815] Fe–Ir–B,[816] Fe–V–B,[817b] Fe–B–C,[817a] Fe–Co–Mn–B–Si,[780,781] Fe–Co–B–Si,[779,818] and Fe–Co–Ni–Si–B–C.[778]

13.4. *Amorphous Intermetallic Systems*

The feasibility of NMR studies on amorphous strictly intermetallic systems was first demonstrated in 1980 for the system $Eu_{80}Au_{20}$. The ^{151}Eu NMR spectrum, obtained by spin-echo mapping, ranges from ca. 70–270 MHz, and its width arises from the combined effect of a very strong, dominant nuclear electric quadrupolar interaction, and a magnetic hyperfine field distribution.[819] Since that study, the structure of a number of intermetallic systems (magnetic and non-magnetic) has been investigated, predominantly by field-dependent cw line width measurements and studies of quadrupolar interactions. Again, the existence of short range order (as opposed to the DRP model) has been a key question in these studies. To date, the experimental results obtained for the majority of systems support the view that chemical order does exist, and that the DRP model is not applicable. While ^{71}Ga NMR spectra of a-La_3Ga show that there is a quadrupolar interaction in the glassy state (as contrasted to the cubic crystalline phase), the distribution of nuclear electric quadrupole coupling constants required to simulate the experimental spectrum (which resembles that of Fig. 8a for a spin 3/2 nucleus perturbed in first-order by the quadrupolar interaction) is rather narrow.[747] Similar conclusions can be drawn from the ^{27}Al NMR spectra of melt-spun glasses in the system $Ca_{1-x}Al_x$ ($0.15 \leqslant x \leqslant 0.45$).[820,821] These spectra are also dominated by first-order quadrupolar interactions, giving rise to well-observable satellites. Such structured spectra and narrow EFG distributions are not expected for a dense random packing of spheres. Rather, such an arrangement would generate large local variations in electric field gradients, and hence would broaden any first-order quadrupolar satellites beyond detection. Surprisingly, in the amorphous Ca–Al system, there appears to be no compositional lineshape trend. This indicates either that the chemical environment is uniformly similar in all of the samples investigated or that low-field ^{27}Al NMR is not sufficiently sensitive to specific details of the short range order of aluminium. Further studies at higher field strengths are required to clarify this point.

A number of other studies have been carried out, addressing the short range order of amorphous zirconium-based alloys, such as the systems Be–Nb–Zr,[822–824] Be–Mo–Zr,[823,824] V–Zr,[825]

Tm–Zr,[826] and Cu–Zr.[827] Due to the unfavorable NMR properties of the ^{91}Zr isotope, most of the structural information has relied on the isotopes introduced with the other metal constituents. This makes it more difficult to compare the various individual systems with each other. In Be–Zr–Nb alloys the authors attempt to analyze extrapolated ^{9}Be second moment at zero applied magnetic field, in terms of ^{9}Be–^{93}Nb dipolar interactions.[822] Various other Co-based alloys have been investigated.[827–832] As for all Co-based alloys, the NMR spectra are characterized by wide hyperfine field distributions.

14. CONCLUSIONS AND OUTLOOK

During the past ten years, research devoted to the synthesis of new types of glasses and their structural characterization has accelerated with a breath-taking pace. As illustrated by Fig. 1, the use of NMR spectroscopy is taking an active part in this growth. Powerful new techniques, most notably MAS—NMR in combination with high-field and Fourier transform spectroscopy, are today providing information at a detailed level not thought achieveable only ten years ago.

To date, the bulk of the published work has concentrated on the experimental facts concerning nearest- and next-nearest neighbor environments, which constitute the short-range order in glasses. The quest for a more fundamental understanding of these facts on a thermodynamic basis has already triggered several *in situ* high-temperature NMR studies of molten phases; and increased emphasis in this direction can be foreseen.

Understanding the short-range-order, however, is only a first step towards the understanding of a glass. In future efforts, the attention will be increasingly directed towards understanding ordering/disordering phenomena on larger length scales (10–20 Å). Since NMR chemical shifts are rather insensitive to such long range effects, the accurate measurement and modelling of internuclear dipolar interactions will become increasingly important. One can therefore anticipate that selective averaging experiments other than MAS, which carry dipolar coupling information (spin echo, SEDOR, correlation spectroscopy, and multiple-quantum NMR) will become more and more important. As discussed in this article, the beginnings of such applications have been made.

Perhaps most important for the future of this field is the fact that solid state NMR spectroscopy has remained a vital and attractive research area in its own right. The continued influx of new solid state NMR methodology and techniques into this area is very likely to assure that structural investigations of glasses will remain a challenging and an intellectually stimulating research subject.

Acknowledgements—I am grateful to the past and present members in my research group, Kesha Banks, Mark Beckert, Nandini Das, Delphine Davis, Mark Drake, Robert Flesher, Deanna Franke, David Gaughen, Christopher Hudalla, David Lathrop, Tim Luong, Carri Lyda, Ester Martinez, Robert Maxwell, John McArthur, Kelly L. Moran, Michael Morgen, Brian Nadel, David Schmidt, Robert Shibao, Melissa St. Rose, Thomas Tepe, Michael Tullius, Maria Vasquez-Valdez, Juan-Carlos Wallace, and Emily Wothe for their many contributions, from which this effort has benefitted. This review contains excerpts from the doctoral dissertations of David A. Lathrop, Kelly L. Moran, Deanna R. Franke, Robert S. Maxwell, and Robert K. Shibao. I would further like to thank my collaborators, Drs John H. Kennedy, Zh. Zhang, and G. D. Stucky (U.C. Santa Barbara), Drs A. Pradel and M. Ribes (Universite de Montpellier), Drs Richard C. Flagan and Edward M. Stolper (California Institute of Technology) and Dr J. P. Yesinowski (Michigan State University) for their contributions to joint work that is cited and discussed here. Thanks are also due to Beth Kuchinsky and Chuck Huber for organizing many of the less accessible references cited here to ensure completeness in this review to the maximum extent possible. Our research is currently supported by the National Science Foundation, grant # DMR 8913738, and by the Donors of the Petroleum Research Fund, administered by the American Chemical Society. This financial support is most gratefully acknowledged.

REFERENCES

1. J. HATTON, B. V. ROLLIN and E. F. W. SEYMOUR, *Phys. Rev.* **83**, 672 (1951).
2. H. E. WEAVER, Jr., *Phys. Rev.* **89**, 923 (1953).
3. G. R. HOLZMAN, J. H. ANDERSON and W. KOTH, *Phys. Rev.* **98**, 542 (1955).
4. G. R. HOLZMAN, P. C. LAUTERBUR, J. H. ANDERSON and W. KOTH, *J. Chem. Phys.* **25**, 172 (1956).
5. A. H. SILVER and P. J. BRAY, *J. Chem. Phys.* **29**, 984 (1958).

6. A. R. GRIMMER, P. STARKE and W. WIEKER, *Z. Chem.* **22**, 44 (1982).
7. E. LIPPMAA, A. SAMOSON, M. MÄGI, R. TEEÄÄR, J. SCHRAML and J. GÖTZ, *J. Noncryst. Solids* **50**, 215 (1982).
8. W. SCHILLER, D. MÜLLER and G. SCHELER, *Z. Chem.* **22**, 44 (1982).
9. S. SCHRAMM and E. OLDFIELD, *J. Chem. Soc., Chem. Commun.* 980 (1982).
10. S. G. BISHOP and P. J. BRAY, *J. Chem. Phys.* **48**, 1709 (1968).
11. F. KRÄMER, W. MÜLLER-WARMUTH and J. SCHEERER, *Z. Naturforsch.* **28a**, 1338 (1973).
12. E. GÖBEL, H. OLYSCHLÄGER, W. MÜLLER-WARMUTH and H. DUTZ, *J. Magn. Reson.* **36**, 371 (1979); and references therein.
13. C. P. SLICHTER, *Principles of Magnetic Resonance*, Harper & Row (1963).
14. A. ABRAGAM, *The Principles of Nuclear Magnetism*, Clarendon Press, Oxford (1961).
15. B. C. GERSTEIN and C. R. DYBOWSKI, *Transient Techniques in NMR of Solids*, Academic Press, New York (1985).
16. C. A. FYFE, *Solid State NMR for Chemists*, CRC Press, Guelph, Ontario (1984).
17. E. FUKUSHIMA and S. B. W. ROEDER, *Experimental Pulse NMR. A Nuts and Bolts Approach*, Addison-Wesley, Reading, MA (1981).
18. U. HAEBERLEN, *High Resolution NMR in Solids*, Academic Press, New York (1976).
19. M. MEHRING, *Principles of High Resolution NMR in Solids*, Springer-Verlag, Heidelberg (1983).
20. H. W. SPIESS, *NMR-Basic Principles and Progress*, Eds. P. DIEHL, E. FLUCK and R. KOSFELD, Vol. 15, p. 55, Springer-Verlag, Berlin (1978).
21. T. M. DUNCAN and C. R. DYBOWSKI, *Surf. Sci. Rep.* **1**, 157 (1981).
22. F. A. BOVEY, *Nuclear Magnetic Resonance Spectroscopy*, Academic Press Inc., New York (1988).
23. P. J. BRAY and A. H. SILVER, *Modern Aspects of the Vitreous State*, Ed. J. D. MACKENZIE, p. 92, Butterworth, London (1960).
24. W. MÜLLER-WARMUTH, *Glastech. Ber.* **38**, 121 (1965); *ibid.* **38**, 405 (1965).
25. P. J. BRAY, *Interaction of Radiation with Solids*, p. 25, Plenum Press, New York (1967).
26. P. J. BRAY, *Silikattechnik* **19**, 350 (1968); *ibid.* **19**, 307 (1968).
27. P. J. BRAY, *Proc. 10th Int. Congr. Glass*, p. 13, Kyoto Ceramic Society of Japan (1974).
28. P. J. BRAY, *Fiz. Khim., Stekla*, **1**, 490 (1975).
29. P. J. BRAY, *Phys. Noncryst. Solids, 4th Int. Conf.* Ed. G. H. FRISCHAT p. 65 (1977).
30. W. MÜLLER-WARMUTH, *Nuclear Magnetic Resonance in Solids*, Ed. VAN GERVEN, p. 131, Plenum Press (1977).
31. G. E. JELLISSON and P. J. BRAY, *Borate Glasses, Structure, Properties*, Applications, Eds. L. D. PYE, V. D. FRECHETTE and N. J. KREIDL, p. 353 (1978).
32. P. J. BRAY, *Borate Glasses, Structure, Properties, Applications*, Eds. L. D. PYE, V. D. FRECHETTE and N. J. KREIDL, p. 321 (1978).
33. H. R. KHAN and K. LÜDERS, *Phys. Status Solidi B* **108**, 9 (1981).
34. W. MÜLLER-WARMUTH and H. ECKERT, *Phys. Rep.* **88**, 91 (1982).
35. P. J. BRAY, F. BUCHOLTZ, A. E. GEISSBERGER and I. A. HARRIS, *Nucl. Instrum. Methods* **199**, 1 (1982).
36. P. J. BRAY, A. E. GEISSBERGER, F. BUCHOLTZ and I. A. HARRIS, *J. Noncryst. Solids* **52**, 45 (1982).
37. P. J. BRAY and W. J. DELL, *J. Phys. C9*, **43**, 131 (1982).
38. J. DURAND and P. PANISSOD, *J. Magn. Mater.* **31–34**, 1567 (1983).
39. P. PANISSOD, *Hyperfine Int.* **24–26**, 607 (1985).
40. P. J. BRAY and E. J. HOLUPKA, *J. Noncryst. Solids* **71**, 411 (1985).
41. P. J. BRAY, *J. Noncryst. Solids* **73**, 19 (1985).
42. P. J. BRAY, *J. Noncryst. Solids* **75**, 29 (1985).
43. S. R. ELLIOTT, *J. Noncryst. Solids* **76**, 79 (1985).
44. P. J. BRAY and M. L. LUI, *Structure and Bonding of Non-Crystalline Solids*, Eds. G. WALRAFEN and A. G. REVESZ, p. 285 (1986).
45. R. J. KIRKPATRICK, T. DUNN, S. SCHRAMM, K. A. SMITH, R. OESTRIKE and G. TURNER, *Structure and Bonding of Non-Crystalline Solids*, Eds. G. WALRAFEN and A. G. REVESZ, P. 303 (1986).
46. P. J. BRAY, *J. Noncryst. Solids* **95/96**, 45 (1987).
47. G. L. TURNER, R. J. KIRKPATRICK, S. H. RISBUD and E. OLDFIELD, *Am. Ceram. Soc. Bull.* **66**, 656 (1987).
48. M. DUBIEL, *Silikattechnik* **38**, 368 (1987).
49. P. J. BRAY, S. J. GRAVINA, D. H. HINTENLANG and R. V. MULKERN, *Magn. Reson. Rev.* **13**, 263 (1988).
50. J. F. STEBBINS, *Spectroscopic Methods in Mineralogy and Geology*, Ed. F. C. HAWTHORNE, p. 405, Mineralogical Society of America, Washington, DC (1988).
51. R. J. KIRKPATRICK, *Spectroscopic Methods in Mineralogy and Geology*, Ed. F. C. HAWTHORNE, p. 341, Mineralogical Society of America, Washington, DC (1988).
52. G. L. MARSHALL, R. K. HARRIS, D. APPERLEY and R. YEUNG, *Sci. Ceram.* **14**, 347 (1988).
53. S. W. MARTIN, *Mater. Chem. Phys.* **23**, 225 (1989).
54. R. DUPREE, *Exp. Tech. Physik* **36**, 315 (1989).
55. R. DUPREE and D. HOLLAND, *Glasses Glass Ceram.*, Ed., M. H. LEWIS, p. 1, Chapman and Hall, London, (1989).
56. H. ECKERT, *Angew. Chem.* **101**, 1763 (1989).
57. J. F. STEBBINS and I. FARNAN, *Science* **245**, 257 (1989).
58. A. R. GRIMMER, *Exp. Tech. Physik* **36**, 81 (1988).

59. S. R. ELLIOTT, *J. Noncryst. Solids* **123**, 149 (1990).
60. P. E. STALLWORTH and P. J. BRAY, *Glass Sci. Technol.* **4**, 77 (1990).
61. P. J. BRAY, J. F. EMERSON, D. LEE, S. A. FELLER, D. L. BAIN and D. A. FEIL, *J. Noncryst. Solids* **129**, 240 (1991).
62. R. ZALLEN, *The Physics of Amorphous Solids*, John Wiley, New York (1983).
63. H. SCHOLZE, *Glas, Natur, Struktur, Eigenschaften*, Vieweg-Verlag Braunschweig (1965).
64. W. VOGEL, *Glaschemie*, VEB Deutscher Verlag für Grundstoff-Industrie, Leipzig (1979).
65. R. DOREMUS, *Glass Science*, John Wiley, NY (1973).
66. N. SOGA, *J. Noncryst. Solids* **123**, 363 (1990).
67. W. W. ZACHARIASEN, *J. Am. Ceram. Soc.* **54**, 3841 (1938).
68. G. S. CARGILL, *J. Appl. Phys.* **41**, 2248 (1970).
69. M. H. COHEN and D. TURNBULL, *Nature (Lond.)* **203**, 964 (1964).
70. A. C. WRIGHT, *J. Noncryst. Solids* **123**, 129 (1990).
71. M. L. FRANKENHEIM, *Die Lehre von der Cohäsion*, Breslau (1835).
72. A. A. LEBEDEV, *Arb. Staatl. Opt. Inst. Leningrad* **2**, 10 (1921).
73. A. A. LEBEDEV, *Izv. Akad. Nauk SSSR, Otd. Mat. Estestv. Nauk, Ser. Fiz.* 381 (1937).
74. E. A. PORAI-KOSHITS, *J. Noncryst. Solids* **123**, 1 (1990).
75. K. W. ZILM and D. M. GRANT, *J. Am. Chem. Soc.* **103**, 2913 (1981).
76. J. H. VAN VLECK, *Phys. Rev.* **74**, 1168 (1948).
77. M. H. COHEN and F. REIFF, *Solid State Physics*, Eds. SEITZ and TURNBULL, Vol. 5, p. 321, Academic Press, NY (1958).
78. J. F. BAUGHER, P. C. TAYLOR, T. OJA and P. J. BRAY, *J. Chem. Phys.* **50**, 4914 (1969).
79. J. T. CHENG, J. C. EDWARDS and P. D. ELLIS, *J. Phys. Chem.* **94**, 553 (1990).
80. W. P. POWER, R. E. WASYLISHEN, S. MOOIBROEK, B. A. PETTIT and W. DANCHURA, *J. Phys. Chem.* **94**, 591 (1990).
81. C. H. TOWNES and B. P. DAILEY, *J. Chem. Phys.* **17**, 782 (1949).
82. H. S. GUTOWSKY and G. E. PAKE, *J. Chem. Phys.* **18**, 162 (1950).
83. N. BLOEMBERGEN, E. M. PURCELL and R. V. POUND, *Phys. Rev.* **73**, 679 (1948).
84. E. R. ANDREW, A. BRADBURY and R. G. EADES, *Nature* **183**, 1802 (1959).
85. I. J. LOWE, *Phys. Rev. Lett.* **2**, 285 (1959).
86. J. HERZFELD and A. E. BERGER, *J. Chem. Phys.* **73**, 6021 (1980).
87. M. M. MARICQ and J. S. WAUGH, *J. Chem. Phys.* **70**, 3300 (1979).
88. A. SAMOSON, E. KUNDLA and E. LIPPMAA, *J. Magn. Reson.* **49**, 350 (1982).
89. A. SAMOSON, E. LIPPMAA and A. PINES, *Mol. Phys.* **65**, 1013 (1988).
90. B. F. CHMELKA, K. T. MUELLER, A. PINES, J. F. STEBBINS, Y. WU and J. W. ZWANZIGER, *Nature* **339**, 42 (1989).
91. M. ENGELSBERG and R. E. NORBERG, *Phys. Rev. B* **5**, 3395 (1972).
92. N. BODEN, M. GIBB, Y. K. LEVINE and M. MORTIMER, *J. Magn. Reson.* **16**, 471 (1974).
93. J. A. REIMER and M. T. DUNCAN, *Phys. Rev. B* **27**, 4895 (1983).
94. D. E. KAPLAN and E. L. HAHN, *J. Phys. Radium* **19**, 821 (1958).
95. S. E. SHORE, J. P. ANSERMET, C. P. SLICHTER and J. H. SINFELT, *Phys. Rev. Lett.* **58**, 953 (1987).
96. P. K. WANG, C. P. SLICHTER and J. H. SINFELT, *Phys. Rev. Lett.* **53**, 82 (1984).
97. T. GULLION and J. S. SCHAEFER, *J. Magn. Reson.* **81**, 196 (1989).
98. M. H. LEVITT, T. G. OAS and R. G. GRIFFIN, *Isr. J. Chem.* **28**, 271 (1988).
99. T. G. OAS, M. H. LEVITT and R. G. GRIFFIN, *J. Chem. Phys.* **89**, 692 (1988).
100. A. PINES, M. G. GIBBY and J. S. WAUGH, *J. Chem. Phys.* **59**, 569 (1973).
101. S. R. HARTMANN and E. L. HAHN, *Phys. Rev.* **128**, 2042 (1962).
102. H. KESSLER, M. GEHRKE and C. GRIESINGER, *Angew. Chem., Int. Ed. Engl.* **27**, 490 (1988).
103. A. SAMOSON and E. LIPPMAA, *Phys. Rev. B* **28**, 6567 (1983).
104. A. P. M. KENTGENS, J. J. M. LEMMENS, F. M. M. GEURTS and W. S. VEEMAN, *J. Magn. Reson.* **71**, 62 (1987).
105. B. D. MOSEL, W. MÜLLER-WARMUTH and H. DUTZ, *Phys. Chem. Glasses* **15**, 154 (1974).
106. I. A. HARRIS and P. J. BRAY, *Phys. Chem. Glasses* **21**, 156 (1980).
107. A. NAVROTSKY, K. L. GEISINGER, P. MCMILLAN and G. V. GIBBS, *Phys. Chem. Miner.* **11**, 284 (1985); and references therein.
108. J. M. THOMAS, J. KLINOWSKI, S. RAMDAS, B. K. HUNTER and D. T. B. TENNAKOON, *Chem. Phys. Lett.* **102**, 158 (1983).
109. G. ENGELHARDT and R. RADEGLIA, *Chem. Phys. Lett.* **108**, 271 (1984).
110. J. V. SMITH and C. SCOTT BLACKWELL, *Nature* **303**, 223 (1983).
111. R. DUPREE and R. F. PETTIFER, *Nature* **308**, 523 (1984).
112. U. STERNBERG, *Mol. Phys.* **63**, 249 (1988).
113. R. F. PETTIFER, R. DUPREE, I. FARNAN and U. STERNBERG, *J. Noncryst. Solids* **106**, 408 (1988).
114. L. F. GLADDEN, T. A. CARPENTER and S. R. ELLIOTT, *Phil. Mag.* **B53**, L81 (1986).
115. R. AUJLA, R. DUPREE, I. FARNAN and D. HOLLAND, *Diffus. Defect Data* **53–54**, 99 (1987).
116. C. J. BRINKER, R. J. KIRKPATRICK, D. R. TALLANT, B. C. BUNKER and B. MONTEZ, *J. Noncryst. Solids* **99**, 418 (1988).
117. R. L. MOZZI and B. E. WARREN, *J. Appl. Cryst.* **2**, 164 (1969).
118. S. L. CHAN, L. F. GLADDEN and S. R. ELLIOTT, *J. Noncryst. Solids* **106**, 413 (1988).

119. H. Graetsch, A. Mosset and H. Gies, *J. Noncryst. Solids* **119**, 173 (1990).
120. A. E. Geissberger and P. J. Bray, *J. Noncryst. Solids* **54**, 121 (1983).
121. A. R. Grimmer, *Chem. Phys. Lett.* **119**, 416 (1985).
122. E. Lippmaa, M. Mägi, A. Samoson, G. Engelhardt and A. R. Grimmer, *J. Am. Chem. Soc.* **102**, 4889 (1980).
123. M. Mägi, E. Lippmaa, A. Samoson, G. Engelhardt and A. R. Grimmer, *J. Phys. Chem.* **88**, 1518 (1984).
124. R. Dupree, D. Holland and D. S. Williams, *J. Noncryst. Solids* **68**, 399 (1984).
125. A. R. Grimmer, M. Mägi, M. Hähnert, H. Stade, A. Samoson, W. Wieker and E. Lippmaa, *Phys. Chem. Glasses* **25**, 105 (1984).
126. C. M. Schramm, B. H. W. S. DeJong and V. E. Parziale, *J. Am. Chem. Soc.* **106**, 4396 (1984).
127. J. B. Murdoch, J. F. Stebbins and I. S. E. Carmichael, *Am. Miner.* **70**, 332 (1985).
128. J. F. Stebbins, *Nature* **330**, 465 (1987).
129. J. F. Stebbins, *J. Noncryst. Solids* **106**, 359 (1988).
130. J. F. Emerson, P. E. Stallworth and P. J. Bray, *J. Noncryst. Solids* **113**, 253 (1989).
131. E. Schneider, J. F. Stebbins and A. Pines, *J. Noncryst. Solids* **89**, 371 (1987).
132. W. Hater, W. Müller-Warmuth, M. Meier and G. H. Frischat, *J. Noncryst. Solids* **113**, 210 (1989).
133. W. Hater, W. Müller-Warmuth and G. H. Frischat, *Glastech Ber.* **62**, 328 (1989).
134. R. Dupree, D. Holland and M. G. Mortuza, *J. Noncryst. Solids* **116**, 148 (1990).
135. R. Dupree, D. Holland and D. S. Williams, *J. Noncryst. Solids* **81**, 185 (1986).
136. C. N. R. Rao, J. M. Thomas, J. Klinowski, U. Selvaraj, K. J. Rao, G. R. Millard and S. Ramdas, *Angew. Chem., Int. Ed. Engl.* **24**, 61 (1985).
137. U. Selvaray, K. J. Rao, C. N. R. Rao, J. Klinowski and J. M. Thomas, *Chem. Phys. Lett.* **114**, 24 (1985).
138. A. R. Grimmer and W. Müller, *Monatsh. Chem.* **117**, 799 (1986).
139. R. Dupree, D. Holland and D. S. Williams, *J. Phys. Colloq. C8* **46**, 119 (1985).
140. A. R. Grimmer, B. Thomas, G. Seifert and P. Sarv, *Magn. Reson. Chem.* **28**, S97 (1990).
141. H. Maekawa, T. Maekawa, K. Kawamura and T. Yokokawa, *J. Noncryst. Solids* **127**, 53 (1991).
142. M. E. Brandriss and J. F. Stebbins, *Geochim. Cosmochim. Acta* **52**, 2659 (1988).
143. C. T. G. Knight, R. J. Kirkpatrick and E. Oldfield, *J. Noncryst. Solids* **116**, 140 (1990).
144. R. Dupree, N. Ford and D. Holland, *Phys. Chem. Glasses* **28**, 78 (1987).
145. T. Fujiu and M. Ogino, *J. Noncryst. Solids* **64**, 287 (1984).
146. A. R. Grimmer, D. Hoebbel, J. Götz and M. Mägi, *Z. Anorg. Allg. Chem.* **547**, 45 (1987).
147. M. Leventhal and P. J. Bray, *Phys. Chem. Glasses* **6**, 113 (1965).
148. M. Nofz, K. Forkel, F. G. Wihsmann and H. G. Bartel, *Phys. Chem. Glasses* **30**, 46 (1989).
149. F. Ehrentreich, M. Nofz and H. G. Bartel, *Z. Chem.* **30**, 187 (1990).
150. E. Hallas, U. Haubenreisser, M. Hähnert and D. Müller, *Glastechn. Ber.* **56**, 63 (1983).
151. R. J. Kirkpatrick, R. Oestrike, C. A. Weiss, Jr, K. A. Smith and E. Oldfield, *Am. Miner.* **71**, 705 (1986).
152. G. Engelhardt, M. Nofz, K. Forkel, F. G. Wishmann, M. Mägi, A. Samoson and E. Lippmaa, *Phys. Chem. Glasses* **26**, 157 (1985).
153. W. Loewenstein, *Am. Miner.* **39**, 92 (1954).
154. E. D. Lacy, *Phys. Chem. Glasses* **4**, 234 (1963).
155. W. Müller-Warmuth, W. Poch and G. W. Schulz, *Glastechn. Ber.* **39**, 415 (1966).
156. G. W. Schulz, W. Müller-Warmuth, W. Poch and G. Scheerer, *Glastechn. Ber.* **41**, 435 (1968).
157. C. I. Merzbacher, B. L. Sherriff, J. S. Hartman and W. B. White, *J. Noncryst. Solids* **124**, 194 (1990).
158. E. Hallas and M. Hähnert, *Z. Chem.* **26**, 188 (1986).
159. M. Nofz, G. Engelhardt, F. G. Wihsmann, K. Forkel, M. Mägi and E. Lippmaa, *Z. Chem.* **26**, 221 (1986).
160. K. L. Geisinger, R. Oestrike, A. Navrotsky, G. L. Turner and R. J. Kirkpatrick, *Geochim. Cosmochim. Acta* **52**, 2405 (1988).
161. B. H. W. S. DeJong, C. M. Schramm and V. E. Parziale, *Geochim. Cosmochim. Acta* **48**, 2619 (1984).
162. R. Oestrike and R. J. Kirkpatrick, *Am. Mineral.* **73**, 534 (1988).
163. B. H. W. S. DeJong, C. M. Schramm and V. E. Parziale, *Geochim. Cosmochim. Acta* **47**, 1223 (1983).
164. H. Dutz and G. W. Schulz, *Glastechn. Ber.* **42**, 89 (1969).
165. D. G. Fraser and N. J. Clayden, *Chem. Geol.* **62**, 43 (1987).
166. R. Oestrike, W. H. Yang, R. J. Kirkpatrick, R. L. Hervig, A. Navrotsky and B. Montez, *Geochim. Cosmochim. Acta* **51**, 2199 (1987).
167. J. B. Murdoch, J. F. Stebbins and I. S. E. Carmichael, *Am. Miner.* **70**, 332 (1985).
168. E. Hallas and M. Hähnert, *Cryst. Res. Techn.* **20**, K25 (1985).
169. (a) J. E. Shelby and J. T. Kohli, *J. Am. Ceram. Soc.* **73**, 39 (1990); (b) S. C. Kohn, R. Dupree, M. G. Mortuza and C. M. B. Henderson, *Am. Miner.* **76**, 309 (1991).
170. S. H. Risbud, R. J. Kirkpatrick, A. P. Taglialavore and B. Montez, *J. Am. Ceram. Soc.* **70**, C-10 (1987).
171. (a) A. Yasumori, M. Iwasaki, H. Kawazoe, M. Yamane and Y. Nakamura, *Phys. Chem. Glasses* **31**, 1 (1990); (b) U. Selvaraj, S. Komarneni and R. Roy, *J. Am. Ceram. Soc.* **73**, 3663 (1990).
172. S. L. Hietala, D. M. Smith, C. J. Brinker, A. J. Hurd, A. H. Carim and N. Dando, *J. Am. Ceram. Soc.* **73**, 2815 (1990).
173. D. Müller, P. Starke, M. Jank, K. P. Wendtland and H. Bremer, *Z. Anorg. Allg. Chem.* **517**, 167 (1984).
174. J. M. Thomas, J. Klinowski, P. A. Wright and R. Roy, *Angew. Chem., Int. Ed. Engl.* **22**, 614 (1983).
175. S. Komarneni, R. Roy, C. A. Fyfe, G. J. Kennedy and H. Strobl, *J. Am. Ceram. Soc.* **69**, C42 (1986).

176. L. B. WELSH, J. P. GILSON and M. J. GATTUSO, *Appl. Catal.* **15**, 327 (1985).
177. H. HAMDAN and J. KLINOWSKI, *Chem. Phys. Lett.* **158**, 447 (1989).
178. T. M. DUNCAN, D. C. DOUGLASS, R. CSENCSITS and K. L. WALKER, *J. Appl. Phys.* **60**, 130 (1986).
179. S. YONEMORI, A. MASUI and M. NOSHIRO, *Yogyo Kyokai Shi* **94**, 863 (1986).
180. R. E. LOEHMANN, *J. Noncryst. Solids* **42**, 433 (1980); *ibid.* **56**, 123 (1983).
181. R. S. AUJILA, G. LENG-WARD, M. H. LEWIS, E. F. W. SEYMOUR, G. A. STYLES and G. W. WEST, *Phil. Mag.* **B54**, L51 (1986).
182. W. HATER, W. MÜLLER-WARMUTH, B. STEFFESTHUN and G. H. FRISCHAT, *Glastechn. Ber.* **63**, 32 (1990).
183. F. K. CHI, *Ceram. Eng. Sci. Proc.* **4**, 704 (1983).
184. J. HOMENY and G. G. NELSON, *J. Am. Ceram. Soc.* **71**, 386 (1988).
185. J. LIPOWITZ, H. A. FREEMAN, R. T. CHEN and E. R. PRACK, *Adv. Ceram. Mater.* **2**, 121 (1987).
186. V. S. R. MURTY, M. H. LEWIS, M. E. SMITH and R. DUPREE, *Mater. Lett.* **8**, 263 (1989).
187. H. ZHANG and C. G. PANTANO, *J. Am. Ceram. Soc.* **73**, 958 (1990).
188. I. FARNAN and J. F. STEBBINS, *J. Noncryst. Solids* **124**, 207 (1990).
189a. I. FARNAN and J. F. STEBBINS, *J. Am. Chem. Soc.* **112**, 32 (1990).
189b. S. SHIMOKAWA, H. MAEKAWA, E. YAMADA, T. MAEKAWA, Y. NAKAMURA and T. YOKOKAWA, *Chem. Lett.* 617 (1990).
190. J. F. STEBBINS, J. B. MURDOCH, E. SCHNEIDER, I. S. E. CARMICHAEL and A. PINES, *Nature* **314**, 250 (1985).
191. S. B. LIU, A. PINES, M. BRANDRISS and J. F. STEBBINS, *Phys. Chem. Miner.* **15**, 155 (1987).
192. S. B. LIU, J. F. STEBBINS, E. SCHNEIDER and A. PINES, *Geochim. Cosmochim. Acta* **52**, 527 (1988).
193. J. F. STEBBINS, D. R. SPEARING and I. FARNAN, *J. Noncryst. Solids* **110**, 1 (1989).
194. M. GRIMSDITCH, *Phys. Rev. Lett.* **52**, 2379 (1984).
195. R. A. B. DEVINE, R. DUPREE, I. FARNAN and J. J. CAPPONI *Phys. Rev.* **B35**, 2560 (1987).
196. P. MCMILLAN, B. PIRIOU and R. COUTY, *J. Chem. Phys.* **81**, 4234 (1981).
197. N. L. ROSS and E. P. MEAGHER, *Am. Miner* **69**, 1145 (1984).
198. C. A. ANGELL, C. A. SCAMEHORN, C. C. PHIFER, R. R. KADIYALA and P. A. CHEESEMAN, *Phys. Chem. Miner.* **15**, 221 (1988).
199. A. R. GRIMMER, F. VON LAMPE and M. MÄGI, *Chem. Phys. Lett.* **132**, 549 (1986).
200. I. L. MUDRAKOVSKII, V. M. MASTIKHIN, V. P. SHMACHKOVA and N. S. KOTSARENKO, *Chem. Phys. Lett.* **120**, 424 (1985).
201. J. F. STEBBINS and M. KANZAKI, *Science* **251**, 294 (1990).
202. X. XUE, J. F. STEBBINS, M. KANZAKI, P. F. MCMILLAN and B. POE, *Am. Miner.* **76**, 8 (1991).
203. X. XUE, J. F. STEBBINS, M. KANZAKI and R. G. TRØNNES, *Science* **245**, 962 (1989).
204. J. F. STEBBINS and P. MCMILLAN, *Am. Miner.* **74**, 965 (1989).
205. E. OHTANI, F. TAULELLE and C. A. ANGELL, *Nature* **314**, 78 (1985).
206. J. F. STEBBINS and D. SYKES, *Am. Miner.* **75**, 965 (1990).
207. R. F. BARTHOLOMEW, *Treatise Mater. Sci. Techn.* **22**, 75 (1982).
208. E. M. STOLPER, *Contrib. Miner. Petrol.* **81**, 1 (1982).
209. E. M. STOLPER, *Geochim. Cosmochim. Acta* **46**, 209 (1982).
210. R. F. BARTHOLOMEW and J. W. H. SCHREURS, *J. Noncryst. Solids* **38–39**, 679 (1980).
211. P. S. BELTON, *J. Chem. Tech. Biotechn.* **29**, 19 (1979).
212. N. I. BEZMEN, V. O. ZAVEL'SKII, YU. P. DIKOV and M. B. EPEL'BAUM, *Dokl. Akad. Nauk SSSR* **311**, 458 (1990).
213. N. I. BEZMEN, V. A. ZARIKOV, V. O. ZAVEL'SKII, S. K. KOSHEMCHUK and N. I. SUK, *Geokhimya* 640 (1990).
214. V. O. ZAVEL'SKII and N. I. BEZMEN, *Geokhimya* 1120 (1990).
215. F. MEYER and W. SPALTHOFF, *Glastechn. Ber.* **34**, 184 (1961).
216. W. MÜLLER-WARMUTH, G. W. SCHULZ, N. NEUROTH, F. MEYER and E. DEEG, *Z. Naturforsch.* **20A**, 902 (1965).
217. P. J. BRAY and E. J. HOLUPKA, *J. Noncryst. Solids* **67**, 119 (1984).
218. H. ECKERT, J. P. YESINOWSKI and E. M. STOLPER, *Solid State Ionics* **32/33**, 298 (1989).
219. H. ECKERT, J. P. YESINOWSKI, L. A. SILVER and E. M. STOLPER, *J. Phys. Chem.* **92**, 2055 (1988).
220. J. P. YESINOWSKI and H. ECKERT, *J. Am. Chem. Soc.* **109**, 6274 (1987).
221. B. BERGLUND and R. W. VAUGHAN, *J. Chem. Phys.* **73**, 2037 (1980).
222. J. P. YESINOWSKI, H. ECKERT and G. R. ROSSMAN, *J. Am. Chem. Soc.* **110**, 1367 (1988).
223. C. M. ROHLFING, L. C. ALLEN and R. DITCHFIELD, *J. Chem. Phys.* **79**, 4958 (1983); and references therein.
224. H. ECKERT, J. P. YESINOWSKI, E. M. STOLPER, T. R. STANTON and J. HOLLOWAY, *J. Noncryst. Solids* **93**, 93 (1987).
225. S. C. KOHN, R. DUPREE and M. E. SMITH, *Nature* **337**, 539 (1989).
226. I. FARNAN, S. C. KOHN and R. DUPREE, *Geochim. Cosmochim. Acta* **51**, 2869 (1987).
227. S. C. KOHN, R. DUPREE and M. E. SMITH, *Geochim. Cosmochim. Acta* **53**, 2925 (1989).
228. W. H. A. YANG and R. J. KIRKPATRICK, *Geochim. Cosmochim. Acta* **53**, 805 (1989).
229. W. H. A. YANG and R. J. KIRKPATRICK, *Am. Miner.* **75**, 1009 (1990).
230. L. C. KLEIN, *Ann. Rev. Mater. Sci.* **15**, 227 (1985); and references therein.
231. R. A. ASSINK and B. D. KAY, *J. Noncryst. Solids* **107**, 35 (1988).
232. L. W. KELTS, N. J. EFFINGER and S. M. MELPOLDER, *J. Noncryst. Solids* **83**, 353 (1986).
233. R. A. ASSINK and B. D. KAY, *J. Noncryst. Solids* **99**, 359 (1988).

234. F. ORCEL and L. HENCH, *J. Noncryst. Solids* **79**, 177 (1986).
235. A. H. BOONSTRA, T. N. M. BERNARDS and J. J. T. SMITS, *J. Noncryst. Solids* **109**, 141 (1989).
236. I. ARTAKI, S. SINHA, A. D. IRWIN and J. JONAS, *J. Noncryst. Solids* **72**, 391 (1985).
237. W. BEIER, A. A. GÖKTAS, G. H. FRISCHAT, C. WIES, K. MEISE-GRESCH and W. MÜLLER-WARMUTH, *Phys. Chem. Glasses* **30**, 69 (1989).
238. YANG HUI, DING ZISHANG, JIANG ZHONGHUA and XU XIAOPING, *J. Noncryst. Solids* **112**, 449 (1989).
239. G. E. MACIEL and D. W. SINDORF, *J. Am. Chem. Soc.* **102**, 7606 (1980).
240. T. H. WALTER, G. L. TURNER and E. OLDFIELD, *J. Magn. Reson.* **76**, 106 (1988).
241. C. E. BRONNIMAN, R. C. ZEIGLER and G. E. MACIEL, *J. Am. Chem. Soc.* **110**, 2023 (1988).
242. H. ROSENBERGER, G. SCHELER, H. BÜRGER and M. JACOB, *Colloids Surfaces* **12**, 53 (1984).
243. H. ROSENBERGER, H. BÜRGER, H. SCHÜTZ, G. SCHELER and G. MAENZ, *Z. Phys. Chem.* **153**, 27 (1987).
244. A. J. VEGA and G. W. SCHERER, *J. Noncryst. Solids* **111**, 153 (1989).
245. B. H. W. S. DEJONG, R. JANSSEN and W. S. VEEMAN, *J. Noncryst. Solids* **123**, 170 (1990).
246. A. R. GRIMMER, H. ROSENBERGER, H. BÜRGER and W. VOGEL, *J. Noncryst. Solids* **99**, 371 (1988).
247. R. H. GLASER, G. L. WILKES and C. E. BRONNIMAN, *J. Noncryst. Solids* **113**, 73 (1989).
248. C. WIES, K. MEISE-GRESCH, W. MÜLLER-WARMUTH, W. BEIER, A. A. GÖKTAS and G. H. FRISCHAT, *Phys. Chem. Glasses* **31**, 138 (1990).
249. J. S. HARTMANN, R. L. MILLARD and E. R. VANCE, *J. Noncryst. Solids* **108**, 49 (1989).
250. A. D. IRWIN, J. S. HOLMGREN and J. JONAS, *J. Noncryst. Solids* **101**, 249 (1988).
251. M. A. VILLEGAS, J. SANZ and J. M. FERNANDEZ NAVARRO, *J. Noncryst. Solids* **122**, 171 (1990).
252. C. WIES, K. MEISE-GRESCH, W. MÜLLER-WARMUTH, W. BEIER, U. WELLBROCK and G. H. FRISCHAT, *J. Noncryst. Solids* **116**, 161 (1989).
253. R. DUPREE, D. HOLLAND, M. G. MORTUZA, M. SMITH, A. CHEN and P. F. JAMES, *Magn. Reson. Chem.* **28**, S89 (1990).
254. S. P. SZU, L. C. KLEIN and M. GREENBLATT, *J. Noncryst. Solids* **121**, 90 (1990).
255. J. KROGH-MOE, *J. Noncryst. Solids* **1**, 269 (1969); and references therein.
256. J. KROGH-MOE, *Phys. Chem. Glasses* **3**, 1 (1962).
257. T. A. SIDOROV and N. N. SOBOLEV, *Opt. Spectrosc. U.S.S.R.* **4**, 9 (1958).
258. A. C. HANNON, R. N. SINCLAIR, J. A. BLACKMAN, A. C. WRIGHT and F. L. GALEENER, *J. Noncryst. Solids* **106**, 116 (1988).
259. D. KLINE, P. J. BRAY and H. M. KRIZ, *J. Chem. Phys.* **48**, 5277 (1968).
260. S. E. SVANSON and R. JOHANSSON, *Acta Chem. Scand.* **23**, 628 (1969).
261. S. E. SVANSON and R. JOHANSSON, *Acta Chem. Scand.* **23**, 635 (1969).
262. H. M. KRIZ and P. J. BRAY, *J. Noncryst. Solids* **6**, 27 (1971).
263. G. E. JELLISON Jr, L. W., PANEK, P. J. BRAY and G. B. ROUSE, *J. Chem. Phys.* **66**, 802 (1977).
264. P. C. TAYLOR and E. J. FRIEBELE, *J. Noncryst. Solids* **16**, 375 (1974).
265. L. C. SNYDER, G. E. PETERSON and C. R. KURKJIAN, *J. Chem. Phys.* **64**, 1569 (1976).
266. J. A. TOSSELL and P. LAZZARETTI, *J. Noncryst. Solids* **99**, 267 (1988).
267. J. A. TOSSELL, *J. Noncryst. Solids* **120**, 12 (1990).
268. D. LEE, S. J. GRAVINA and P. J. BRAY, *Z. Naturforsch.* **45a**, 268 (1990).
269. S. J. GRAVINA and P. J. BRAY, *J. Magn. Reson.* **89**, 515 (1990).
270. S. J. GRAVINA, P. J. BRAY and G. L. PETERSEN, *J. Noncryst. Solids* **123**, 165 (1990).
271. P. C. TAYLOR and P. J. BRAY, *J. Magn. Reson.* **2**, 305 (1970).
272. J. F. BAUGHER, H. M. KRIZ, P. C. TAYLOR and P. J. BRAY, *J. Magn. Reson.* **3**, 415 (1970).
273. P. C. TAYLOR and P. J. BRAY *Am. Ceram. Soc. Bull.* **51**, 234 (1972).
274. G. E. PETERSON, C. R. KURKJIAN and A. CARNEVALE, *J. Noncryst. Solids* **21**, 283 (1976).
275. G. E. PETERSON, C. R. KURKJIAN and L. C. SNYDER, *J. Noncryst. Solids* **21**, 301 (1976).
276. G. E. PETERSON, C. R. KURKJIAN and A. CARNEVALE, *Phys. Chem. Glasses* **16**, 63 (1975).
277. G. E. PETERSON, A. CARNEVALE and C. R. KURKJIAN, *J. Noncryst. Solids* **23**, 243 (1977).
278. G. E. JELLISON Jr., P. J. BRAY and P. C. TAYLOR, *Phys. Chem. Glasses* **17**, 35 (1976).
279. P. W. FRANCE and M. WADSWORTH, *J. Magn. Reson.* **49**, 48 (1982).
280. G. E. JELLISON, Jr and P. J. BRAY, *Solid State Commun.* **19**, 517 (1976).
281. S. E. SVANSON, E. FORSLIND and J. KROGH-MOE, *J. Phys. Chem.* **66**, 174 (1962).
282. P. J. BRAY and J. G. O' KEEFE, *Phys. Chem. Glasses* **4**, 37 (1963).
283. P. J. BRAY, M. LEVENTHAL and H. O. HOOPER, *Phys. Chem. Glasses* **4**, 47 (1963).
284. S. GREENBLATT and P. J. BRAY, *Am. Ceram. Soc. Bull.* **44**, 343 (1965).
285. D. KLINE and P. J. BRAY, *Phys. Chem. Glasses* **7**, 41 (1966).
286. S. G. BISHOP and P. J. BRAY, *Phys. Chem. Glasses* **7**, 73 (1966).
287. Y. B. KIM, S. U. KIM and M. J. PARK, *J. Korean Phys. Soc.* **19**, 230 (1986).
288. S. GREENBLATT and P. J. BRAY, *Phys. Chem. Glasses* **8**, 213 (1967).
289. S. GREENBLATT and P. J. BRAY, *Phys. Chem. Glasses* **8**, 190 (1967).
290. J. F. BAUGHER and P. J. BRAY, *Phys. Chem. Glasses* **10**, 77 (1969).
291. W. MÜLLER-WARMUTH, W. POCH and G. SIELAFF, *Glastechn. Ber.* **43**, 5 (1970).
292. H. M. KRIZ, M. J. PARK and P. J. BRAY, *Phys. Chem. Glasses* **12**, 45 (1971).
293. C. RHEE and P. J. BRAY, *Phys. Chem. Glasses* **12**, 165 (1971).

294. C. RHEE, *J. Korean Phys. Soc.* **4**, 51 (1971).
295. M. J. PARK and P. J. BRAY, *Phys. Chem. Glasses* **13**, 50 (1972).
296. J. F. BAUGHER and P. J. BRAY, *Phys. Chem. Glasses* **13**, 63 (1972).
297. K. S. KIM and P. J. BRAY, *J. Nonmetals* **2**, 95 (1974).
298. K. S. KIM and P. J. BRAY, *Phys. Chem. Glasses* **15**, 47 (1974).
299. R. N. PLETNEV, A. D. GALAKTIONOV and A. A. FOTIEV, *Izv. Akad. Nauk SSSR Neorg. Mater.* **10**, 133 (1974).
300. R. GRESCH, W. MÜLLER-WARMUTH and H. DUTZ, *J. Noncryst. Solids* **21**, 31 (1976).
301. G. E. JELLISON, Jr, S. A. FELLER and P. J. BRAY, *Phys. Chem. Glasses* **19**, 52 (1978).
302. M. J. PARK, K. S. KIM and P. J. BRAY, *Phys. Chem. Glasses* **20**, 31 (1979).
303. Y. H. YUN and P. J. BRAY, *J. Noncryst. Solids* **44**, 227 (1981).
304. M. J. PARK and P. J. BRAY, *J. Korean Phys. Soc.* **14**, 67 (1981).
305. S. K. SONG, J. W. KHANG, S. J. CHUNG and M. J. PARK, *J. Korean Phys. Soc.* **14**, 59 (1981).
306. S. SIMON and A. NICULA, *Solid State Commun.* **39**, 1251 (1981).
307. R. GÖRING, H. BÜRGER, H. NASS and B. SCHNABEL, *Phys. Status Solidi* **A68**, K29 (1981).
308. R. J. ARAUJO and J. W. H. SCHREURS, *Phys. Chem. Glasses* **23**, 108 (1982).
309. S. A. FELLER, W. J. DELL and P. J. BRAY, *J. Noncryst. Solids* **51**, 21 (1982).
310. G. CHIODELLI, A. MAGISTRIS, M. VILLA and J. L. BJORKSTAM, *J. Noncryst. Solids* **51**, 143 (1982).
311. I. ARDELEAN, M. COLDEA and O. COZAR, *Nucl. Instrum. Methods* **199**, 189 (1982).
312. A. MAGISTRIS, G. CHIODELLI and M. VILLA, *J. Power Sources* **9**, 379 (1983).
313. S. SIMON and A. NICULA, *J. Noncryst. Solids* **57**, 23 (1983).
314. F. BUCHOLTZ and P. J. BRAY, *J. Noncryst. Solids* **54**, 43 (1983).
315. J. W. KHANG, *Nonmunjip-Chju Taehak* **16**, 187 (1983).
316. I. A. HARRIS, Jr and P. J. BRAY, *Phys. Chem. Glasses* **25**, 69 (1984).
317. I. A. HARRIS, Jr and P. J. BRAY, *Phys. Chem. Glasses* **25**, 44 (1984).
318. F. TIAN, X. WU, L. PAN and X. WU, *Wuli Xuaebao* **38**, 326 (1987).
319. YU. F. ZHURAVLEV, A. D. DMITRIEV, R. N. PLETNEV and V. K. SLEPUKHIN, *Fiz. Khim. Stekla* **13**, 135 (1987).
320. D. J. CHA, Y. K. KIM, S. J. MOON, H. I. KYE, H. T. KIM, H. J. LEE and S. J. CHUNG, *Sae Mulli* **28**, 593 (1988).
321. Y. TANG, Z. JIANG and X. SONG, *J. Noncryst. Solids* **112**, 131 (1989).
322. J. ZHONG and P. J. BRAY, *J. Noncryst. Solids* **111**, 67 (1989).
323. S. K. SONG and M. J. PARK, *Sae Mulli* **29**, 619 (1989).
324. Y. TANG, Z. JIANG and X. J. SONG, *J. Noncryst. Solids* **112**, 131 (1989).
325. S. HAYASHI and K. HAYAMIZU, *J. Noncryst. Solids* **111**, 214 (1989).
326. P. MUSTARELLI, S. SCOTTI, M. VILLA and P. R. GANDHI, *Solid State Ionics* **39**, 217 (1990).
327. M. S. SHIM, S. R. KOO, D. S. BYUN, Y. J. KIM, S. J. CHUNG, H. T. KIM and D. J. CHA, *Sae Mulli* **30**, 58 (1990).
328. L. PAN, T. FENG and X. ZHANG, *Guisuanyan Xuebao* **17**, 385 (1990).
329. S. XU and X. WU, *Guisuanyan Tongbao* **9**, 1 (1990).
330. S. PRABHAKAR, K. J. RAO and C. N. R. RAO, *Proc. R Soc. London Ser. A* **429**, 1 (1990).
331. J. BISCOE and B. E. WARREN, *J. Am. Ceram. Soc.* **21**, 287 (1938).
332. J. E. SHELBY, *J. Am. Ceram. Soc.* **66**, 225 (1983).
333. S. W. MARTIN, *J. Noncryst. Solids* **66**, 429 (1984).
334. M. D. INGRAM, *J. Am. Ceram. Soc.* **63**, 248 (1980).
335. A. H. DIETZEL, *Phys. Chem. Glasses* **24**, 172 (1983).
336. C. JÄGER and U. HAUBENREISSER, *Phys. Chem. Glasses* **26**, 152 (1985).
337. I. YASUI, H. HASEGAWA and Y. SAITO, *J. Noncryst. Solids* **106**, 30 (1988).
338a. L. W. PANEK and P. J. BRAY, *J. Chem. Phys.* **66**, 3822 (1977).
338b. R. K. MOMII and N. H. NACHTRIEB, *J. Phys. Chem.* **72**, 3416 (1968).
339. J. KROGH-MOE, *Phys. Chem. Glasses* **6**, 46 (1965).
340. G. E. JELLISON, Jr and P. J. BRAY, *J. Noncryst. Solids* **29**, 187 (1978).
341. P. J. BRAY, S. A. FELLER, G. E. JELLISON, Jr and Y. H. YUN, *J. Noncryst. Solids* **38/39**, 93 (1980).
342. S. A. FELLER, W. J. DELL and P. J. BRAY, *J. Noncryst. Solids* **51**, 21 (1982).
343. G. E. JELLISON, Jr, S. A. FELLER and P. J. BRAY, *J. Magn. Reson.* **27**, 121 (1977).
344. R. DUPREE, D. HOLLAND and D. S. WILLIAMS, *Phys. Chem. Glasses* **26**, 50 (1985).
345. R. OESTRIKE, A. NAVROTSKY, G. L. TURNER, B. MONTEZ and R. J. KIRKPATRICK, *Am. Miner.* **72**, 788 (1987).
346. M. HÄHNERT and E. HALLAS, *Rev. Chim. Miner.* **24**, 221 (1987).
347. M. HÄHNERT and E. HALLAS, *Z. Chem.* **26**, 144 (1986).
348. E. HALLAS, K. GERTH and M. HÄHNERT, *Z. Chem.* **27**, 270 (1987).
349. R. OESTRIKE, A. NAVROTSKY, G. L. TURNER, B. MONTEZ and R. J. KIRKPATRICK, *Am. Miner.* **72**, 788 (1987).
350. H. BÜRGER, L. HORN, W. JÄCKEL and W. VOGEL, *Silicattechnik* **32**, 177 (1981).
351. J. E. DICKINSON, Jr, B. H. W. S. DEJONG and C. M. SCHRAMM, *J. Noncryst. Solids* **102**, 1965 (1988).
352. P. J. BRAY, D. KLINE and W. POCH, *Glastechn. Ber.* **39**, 175 (1966).
353. (a) A. H. SILVER, *J. Chem. Phys.* **32**, 959 (1960); (b) D. W. JONES, R. S. MATTHEWS, K. RUDDLESDEN and D. J. WILLIAMS, *J. Am. Ceram. Soc.* **51**, 664 (1968).
354. M. P. TABBEY and J. R. HENDRICKSON, *J. Noncryst. Solids* **38/39**, 51 (1980).
355. M. RUBINSTEIN, *Phys. Rev.* **B14**, 2778 (1976).
356. S. XU, L. PAN, F. TIAN and X. WU, *Wuli Xuebao* **37**, 1866 (1988).

357. A. R. GRIMMER and G. HERMS, *Z. Chem.* **26**, 452 (1986).
358. S. XU, L. PAN and X. WU, *Bopuxue Zashi* **7**, 115 (1990).
359. J. SZEFTEL and H. ALLOUL, *Phys. Rev. Lett.* **34**, 657 (1975).
360. M. RUBINSTEIN, H. A. RESING, T. L. REINECKE and K. L. NGAI, *Phys. Rev. Lett.* **34**, 1444 (1975).
361. M. RUBINSTEIN and H. A. RESING, *Phys. Rev.* **B13**, 959 (1976).
362. J. SZEFTEL and H. ALLOUL, *J. Noncryst. Solids* **29**, 253 (1978).
363. T. L. REINECKE and K. L. NGAI, *Phys. Rev.* **B12**, 3476 (1975).
364. T. MINAMI, Y. TAKUMA and M. TANAKA, *J. Electrochem. Soc.* **124**, 1659 (1977).
365. J. P. MALUGANI, A. WASNIEWSKI, M. DOREAU and G. ROBERT, *Mater. Res. Bull.* **13**, 427 (1978).
366. D. EHRT, C. FUCHS and W. VOGEL, *Silikattechnik* **35**, 6 (1984).
367. R. K. SANDWICH, R. J. SCHELLER and K. H. MADER, *SPIE* **171**, 161 (1979).
368. W. K. TREDWAY and S. H. RISBUD, *Non-Oxide Technical and Engineering Ceramics*, Ed. S. HAMPSHIRE, p. 203, Elsevier Appl. Science Publ. (1987).
369. A. R. GRIMMER and G. U. WOLF, *Eur. J. Solid State Inorg. Chem.* **28**, 221 (1991).
370. J. R. VAN WAZER, *J. Am. Chem. Soc.* **72**, 644 (1950).
371. H. OLYSCHLÄGER, PhD Dissertation, Münster (1977).
372. G. L. TURNER, K. A. SMITH, R. J. KIRKPATRICK and E. OLDFIELD, *J. Magn. Reson.* **70**, 408 (1986).
373. S. PRABHAKAR, K. J. RAO and C. N. R. RAO, *Chem. Phys. Lett.* **139**, 96 (1987).
374. A. K. CHEETHAM, N. J. CLAYDEN, C. M. DOBSON and R. J. JAKEMAN, *J. Chem. Soc., Chem. Commun.* 195 (1986).
375. T. M. DUNCAN and D. C. DOUGLASS, *Chem. Phys.* **87**, 339 (1984).
376. A. R. GRIMMER and U. HAUBENREISSER, *Chem. Phys. Lett.* **99**, 487 (1983).
377. D. ELWELL, D. KUMAR and D. WILLIAMS, *Nature* **188**, 1103 (1960).
378. E. L. KRIVOVYAZOV, V. F. CHUVAEV and B. F. DZHURINSKII, *Izv. Akad. Nauk. SSSR, Neorg. Mater.* **13**, 574 (1977).
379. M. VILLA, G. CHIODELLI and M. SCAGLIOTTI, *Solid State Ionics* **18/19**, 382 (1986).
380. U. BÄRENWALD, M. DUBIEL, W. MATZ, D. EHRT and W. VOGEL, *J. Noncryst. Solids* **103**, 311 (1988).
381. S. PRABHAKAR and K. J. RAO, *J. Solid State Chem.* **91**, 186 (1991).
382. R. BROW, R. KIRKPATRICK and G. TURNER, *J. Noncryst. Solids* **116**, 39 (1990).
383. S. HAYASHI and K. HAYAMIZU, *J. Solid State Chem.* **80**, 195 (1989).
384. M. C. R. SHASTRY and K. J. RAO, *Pramana* **32**, 811 (1989).
385. B. C. BUNKER, D. R. TALLANT, C. A. BALFE, R. J. KIRKPATRICK, G. L. TURNER and M. R. REIDMEYER, *J. Am. Ceram. Soc.* **70**, 675 (1987).
386. M. DUBIEL and D. EHRT, *Phys. Status Solidi (a)* **100**, 415 (1987).
387. J. P. FLETCHER, S. H. RISBUD and R. J. KIRKPATRICK, *J. Mater. Res.* **5**, 835 (1990).
388. J. P. FLETCHER, S. H. RISBUD, S. HAYASHI and R. J. KIRKPATRICK, *Diffus. Defect Data* **53–54**, 493 (1987).
389. M. POLLAK-STACHUROVA, W. BOROWNICKI and M. SZUSTAKOWSKI, *Acta Phys. Pol.* **34**, 141 (1968).
390. N. N. GUROVA, V. A. VOPILOV, V. M. BUZNIK and L. N. URUSOVSKAYA, *Fiz. Khim. Stekla* **15**, 687 (1989).
391. V. A. VOPILOV, E. A. VOPILOV, V. M. BUZNIK, V. L. BOGDANOV, V. D. KHALILEV and G. S. GABRIELYAN, *Fiz. Khim. Stekla* **12**, 242 (1986).
392. P. W. FRANCE and H. O. HOOPER, *J. Phys. Chem. Solids* **31**, 1307 (1970).
393. G. F. LYNCH, M. SAYER, S. L. SEGEL and G. ROSENBLATT, *J. Appl. Phys.* **42**, 2587 (1971).
394. J. F. LANDSBERGER and P. J. BRAY, *J. Chem. Phys.* **53**, 2757 (1970).
395. G. F. LYNCH and M. SAYER, *J. Phys. C., Solid State Phys.* **6**, 3661 (1973).
396. L. W. PANEK, G. J. EXARHOS, P. J. BRAY and W. M. RISEN, *J. Noncryst. Solids* **24**, 51 (1977).
397. L. KOLDITZ and E. WAHNER, *Z. Anorg. Allg. Chem.* **400**, 161 (1973).
398. D. MÜLLER, G. BERGER, I. GRUNZE, G. LADWIG, E. HALLAS and U. HAUBENREISSER, *Phys. Chem. Glasses* **24**, 37 (1983).
399. A. V. DMITRIEV, YU, F. ZHURAVLEV, R. N. PLETNEV and V. K. SLEPUKHIM, *Fiz. Khim. Stekla* **12**, 636 (1986).
400. R. K. BROW, R. J. KIRKPATRICK and G. L. TURNER, *J. Am. Ceram. Soc.* **73**, 2293 (1990).
401. B. O. MYSEN, F. J. RYERSON and D. VIRGO, *Am. Miner.* **66**, 106 (1981).
402. W. H. YANG, R. J. KIRKPATRICK and G. TURNER, *J. Am. Ceram. Soc.* **69**, C222 (1986).
403. R. DUPREE, D. HOLLAND and M. G. MORTUZA, *Nature* **328**, 416 (1987).
404. R. DUPREE, D. HOLLAND, M. G. MORTUZA and M. W. G. LOCKYER, *J. Noncryst. Solids* **106**, 403 (1988).
405. R. DUPREE, D. HOLLAND and M. G. MORTUZA, *Phys. Chem. Glasses* **29**, 18 (1988).
406. R. DUPREE, D. HOLLAND, M. G. MORTUZA, J. A. COLLINS and M. W. G. LOCKYER, *J. Noncryst. Solids* **112**, 111 (1989).
407. T. SEKIYA, N. MOCHIDA, A. OHTSUKA and K. UCHIDA, *Nippon Seramikkusu Kyokai Gakujutsu Ronbushi* **96**, 571 (1988).
408. T. L. WEEDING, B. H. W. S. DEJONG, W. S. VEEMAN and B. G. AITKEN, *Nature* **318**, 352 (1985).
409. T. M. DUNCAN, D. C. DOUGLASS, K. L. WALKER and R. CSENCSITS, *J. Appl. Phys.* **58**, 197 (1985).
410. S. G. KOSINSKI, D. M. KROL, T. M. DUNCAN, D. C. DOUGLASS, J. B. MCCHESNEY and J. R. SIMPSON, *J. Noncryst. Solids* **105**, 45 (1988).
411. M. VILLA, K. R. CARDUNER and G. CHIODELLI, *J. Solid State Chem.* **69**, 19 (1987).
412. M. VILLA, K. R. CARDUNER and G. CHIODELLI, *Phys. Chem. Glasses* **28**, 131 (1987).
413. M. VILLA, M. SCAGLIOTTI and G. CHIODELLI, *J. Noncryst. Solids* **94**, 101 (1987).

414. A. M. BONDAR', E. S. KUTUKOVA and Z. M. SYRITSKAYA, *Izv. Akad. Nauk SSSR* **11**, 916 (1975).
415. TIAN FENG and PAN LINZHANG, *J. Noncryst. Solids* **112**, 142 (1989).
416. Y. H. YUN and P. J. BRAY, *J Noncryst. Solids* **30**, 54 (1978).
417. W. CUI and J. QIN, *Bopuxue Zazhi* **4**, 67 (1987).
418. P. BEEKENKAMP and G. E. G. HARDEMAN, *Verres Refract.* **20**, 419 (1966).
419. J. SCHEERER, W. MÜLLER-WARMUTH and H. DUTZ, *Glastechn. Ber.* **46**, 109 (1972).
420. K. OOKA and T. KISHII, *J. Noncryst. Solids* **3**, 344 (1970).
421. M. E. MILBERG, J. G. O'KEEFE, R. A. VERHELST and H. O. HOOPER, *Phys. Chem. Glasses* **13**, 79 (1972).
422. S. P. ZHDANOV and G. SHMIDEL, *Fiz. Khim. Stekla* **1**, 452 (1975).
423. S. P. ZHDANOV, I. KERGER and E. V. KOROMAL'DI, *Dokl. Akad. Nauk SSSR* **204**, 622 (1972).
424. S. P. ZHDANOV, *Dokl. Akad. Nauk SSSR* **217**, 581 (1974).
425. M. P. BRUNGS and E. R. MCCARTNEY, *Phys. Chem. Glasses* **16**, 48 (1975).
426. Y. H. YUN and P. J. BRAY, *J. Noncryst. Solids* **27**, 363 (1978).
427. A. I. ZVYAGIN, *Inorg. Mater. USSR* **7**, 312 (1971).
428. K. KOBAYASHI, *J. Am. Ceram. Soc.* **62**, 440 (1979).
429. K. KOBAYASHI and H. OKUMA, *J. Am. Ceram. Soc.* **59**, 354 (1976).
430. J. C. BRETHOUS, A. LEVASSEUR, G. VILLENEUVE, P. ECHEGUT, P. HAGENMULLER and M. COUZI, *J. Solid State Chem.* **39**, 199 (1981).
431. Y. H. YUN, S. A. FELLER and P. J. BRAY, *J. Noncryst. Solids* **33**, 273 (1979).
432. S. Z. XIAO, *J. Noncryst. Solids* **45**, 29 (1981).
433. W. J. DELL, P. J. BRAY and S. Z. XIAO, *J. Noncryst. Solids* **58**, 1 (1983).
434. S. XIAO and Q. MENG, *J. Noncryst. Solids* **80**, 195 (1986).
435. S. XIAO and Q. GUO, *J. Noncryst. Solids* **52**, 171 (1982).
436. H. DOWEIDAR, M. S. MEIKHAIL and D. HOLLAND, *J. Noncryst. Solids* **101**, 280 (1988).
437. J. ZHONG, X. WU, M. L. LIU and P. J. BRAY, *J. Noncryst. Solids* **107**, 81 (1988).
438. T. TEMPLETON and R. K. MACCRONE, *J. Noncryst. Solids* **56**, 387 (1983).
439. L. ZHOU, G. LI and J. ZHONG, *Huadong Huagong Xueyuan Xuebao* **15**, 688 (1989).
440. Z. JIANG and T. YONGXING, *Guangxue Xuebao* **8**, 75 (1988).
441. Y. J. KIM, S. J. MOON, M. J. GANG, S. Y. KIM, S. K. HONG, S. J. CHUNG and D. J. CHA, *Sae Mulli* **28**, 599 (1988).
442. H. T. KIM, M. J. PARK and S. J. CHUNG, *Sae Mulli* **27**, 257 (1987).
443. S. XIAO and Q. GUO, *Guisuanyan Xuebao* **17**, 385 (1990).
444. X. WU, *Bopuxue Zazhi* **1**, 437 (1984).
445. B. C. BUNKER, D. R. TALLANT, R. J. KIRKPATRICK and G. L. TURNER, *Phys. Chem. Glasses* **31**, 30 (1990).
446. R. GÖRING, K. KNEIPP and H. NASS, *Phys. Status Solidi A* **72**, 623 (1982).
447. K. S. KIM, P. J. BRAY and S. MERRIN, *J. Chem. Phys.* **64**, 4459 (1976).
448. T. S. PETROVSKAYA, P. S. KALININ, R. S. SHEVELEVITCH and V. I. VERESHCHAGIA, *Fiz. Khim. Stekla* **10**, 150 (1984).
449. R. V. MULKERN, S. J. CHUNG, P. J. BRAY, G. D. CHRYSSIKOS, D. E. TURCOTTE and W. M. RISEN, *J. Noncryst. Solids* **85**, 69 (1986).
450. G. L. TURNER, K. A. SMITH, R. J. KIRKPATRICK and E. OLDFIELD, *J. Magn. Reson.* **67**, 544 (1986).
451. J. ZHONG and P. J. BRAY, *J. Noncryst. Solids* **94**, 122 (1987).
452. T. YOKO, M. FUHITA, F. MIYAJI and S. SAKKA, *Chem. Express* **5**, 549 (1990).
453. J. M. ROJO, J. SANZ, J. M. REAU and B. TANGUY, *J. Noncryst. Solids* **116**, 167 (1990).
454. I. P. ALEKSANDROVA and L. R. BATSANOVA, *Zh Strukt. Khim.* **13**, 232 (1972).
455. D .E. O'REILLY and E. M. PETERSON, *J. Chem. Phys.* **62**, 2512 (1975).
456. W. J. DELL, R. V. MULKERN, P. J. BRAY, M. J. WEBER and S. A. BRAWER, *Phys. Rev. B* **31**, 2624 (1985).
457. E. I. ARDASHNIKOVA, M. P. BORZENKOVA, A. V. NOVOSELOVE, L. R. BATSANOVA and V. F. CHUBAEV, *Izv. Akad. Nauk SSSR Neorg. Mater.* **11**, 2169 (1975).
458. A. ABRAGAM and J. WINTER, *Compt. Rend. Acad. Sci.* **249**, 1633 (1959).
459. M. MEHRING, G. SINNING and A. PINES, *Z. Physik* **B24**, 73 (1976).
460. M. POULAIN, M. POULAIN and J. BRUN, *Mater. Res. Bull.* **10**, 243 (1975).
461. P. J. BRAY and R. V. MULKERN, *J. Noncryst. Solids* **80**, 181 (1986).
462. D. R. MCFARLANE, J. O. BROWNE, T. J. BASTOW and G. W. WEST, *J. Noncryst. Solids* **108**, 289 (1989).
463. R. S. AUJILA, R. DUPREE, D. HOLLAND and A. P. KEMP, *Mater. Sci. Forum* **19–20**, 147 (1987).
464. (a) I. FARNAN, R. DUPREE, Y. JEONG, G. E. THOMPSON, G. C. WOOD and A. J. FORTY, *Thin Solid Films* **173**, 209 (1989); (b). R. DUPREE, I. FARNAN, A. J. FORTY, S. El-MASHRI and L. BOTTYAN, *J. Physique* **C8**, 113 (1985).
465. R. DUPREE, D. HOLLAND and D. S. WILLIAMS, *Phil. Mag. B* **50**, L13 (1984).
466. (a) P. C. TAYLOR, *Mater. Res. Soc. Bull.* 36 (1987); (b). A. M. ANDRIESH, *J. Noncryst. Solids* **77/78**, 1219 (1985).
467. (a) S. A. DEMBOVSKII and E. A. CHECHETKINA, *J. Noncryst. Solids* **85**, 364 (1986). (b). J. BICERANBO and S. R. OVSHINSKY, *J. Noncryst. Solids* **74**, 75 (1985).
468. P. BOOLCHAND, *Hyperfine Interact.* **27**, 3 (1986).
469. J. C. PHILLIPS, *J. Noncryst. Solids* **43**, 37 (1981); *ibid.* **34**, 153 (1979).
470. M. TENHOVER, M. A. HAZLE and R. K. GRASSELLI, *Phys. Rev. B* **29**, 6732 (1984).
471. A. KOMA, O. MIZUNO and S. TANAKA, *Phys. Status Solidi B* **46**, 225 (1971).
472. A. KOMA and S. TANAKA, *J. Noncryst. Solids* **8–10**, 251 (1972).

473. J. SZEFTEL, *Phil. Mag. B* **43**, 549 (1981).
474. S. UEDA and T. SHIMIZU, *Phys. Status Solidi B* **95**, 279 (1979).
475. S. UEDA and T. SHIMIZU, *Phys. Status Solidi B* **88**, K1 (1978).
476. S. G. BISHOP, P. C. TAYLOR and D. L. MITCHELL, *J. Noncryst. Solids* **8–10**, 106 (1972).
477. S. G. BISHOP and P. C. TAYLOR, *Phys. Rev. B* **7**, 5177 (1973).
478. S. G. BISHOP and P. C. TAYLOR, *Solid State Commun.* **11**, 1323 (1972).
479. G. E. JELLISON, Jr, and S. G. BISHOP, *Phys. Rev. Lett.* **40**. 1204 (1978).
480. V. A. ANANICHEV, A. N. KUDRYAVTSEV, L. A. BAIDAKOV and L. N. BLINOV, *Fiz. Khim. Stekla* **10**, 93 (1984).
481. L. A. BAIDAKOV, *Tr. Politekhn. Inst.* (373), 4.
482. L. A. BAIDAKOV and V. A. SHCHERBAKOV, *Izv. Akad. Nauk SSSR, Neorg. Mater.* **5**, 1882 (1969).
483. L. A. BAIDAKOV, and A. N. KATRUZOV and H. M. EL-LABANI, *Vestn. Leningr. Univ. Fiz. Khim.* 147 (1978).
484. S. K. NOVOSELOV and L. A. BAIDAKOV, *Vestn. Leningr. Univ. Fiz. Khim.* 140 (1976).
485. L. A. BAIDAKOV and V. A. TSAREV, *Fiz. Khim. Stekla* **1**, 456 (1975).
486. L. A. BAIDAKOV, A. N. KATRUZOV and KH. M. EL LABANI, *Izv. Akad. Nauk SSSR, Neorg. Mater.* **14**, 1810 (1978).
487. L. A. BAIDAKOV, A. N. KUDRYAVTSEV and S. K. NOVOSELOV, *Izv. Akad. Nauk SSSR, Neorg. Mater.* **9**, 1640 (1973).
488. L. A. BAIDAKOV and A. N. KUDRYAVTSEV, *Vestn. Leningr. Univ. Fiz. Khim.* **3**, 114 (1973).
489. L. A. BAIDAKOV, S. K. NOVOSELOV and E. O. OSMANOV, *Vestn. Leningr. Univ. Fiz. Khim.* **2**, 101 (1973).
490. V. S. TSAREV and L. A. BAIDAKOV, *Izv. Akad. Nauk SSSR, Neorg. Mater.* **8**, 1388 (1972).
491. H. ECKERT and W. MÜLLER-WARMUTH, *J. Noncryst. Solids* **70**, 199 (1985).
492. D. ADLER, M. H. COHEN, E. A. FAGEN and J. C. THOMPSON, *J. Noncryst. Solids* **3**, 402 (1970).
493. D. BROWN, D. S. MOORE and E. F. W. SEYMOUR, *J. Noncryst. Solids* **8–10**, 256 (1972).
494. S. D. SENTURIA, C. R. HEWES and D. ADLER, *J. Appl. Phys.* **41**, 430 (1970).
495. L. F. GLADDEN and S. R. ELLIOTT, *J. Noncryst. Solids* **97/98**, 1175 (1987).
496. V. I. SVERGUN, YA. KH. GRINBERG, V. M. KUSNETS and T. A. BABUSHKINA, *Izv. Akad. Nauk SSSR, Ser. Khim.* 1448 (1970).
497. J. R. HENDRICKSON and S. G. BISHOP, *Solid State Commun.* **17**, 301 (1975).
498. H. U. HÜRTER, B. KREBS, H. ECKERT and W. MÜLLER-WARMUTH, *Inorg. Chem.* **24**, 1282 (1985).
499. S. W. MARTIN, *J. Am. Ceram. Soc.* **73**, 3481 (1990).
500. B. KREBS, *Angew. Chem.* **95**, 113 (1983).
501. O. M. UY and J. DROWART, *High Temp. Sci.* **2**, 293 (1970).
502. M. TENHOVER, R. S. HENDERSON, D. LUKCO, M. A. HAZLE and R. K. GRASSELLI, *Solid State Commun.* **51**, 455 (1984).
503. J. E. GRIFFITHS, M. MALYI, G. P. ESPINOSA and J. P. REMEIKA, *Phys. Rev. B* **30**, 6978 (1984).
504. M. TENHOVER, M. A. HAZLE and R. K. GRASSELLI, *Phys. Rev. B* **29**, 6732 (1984).
505. M. TENHOVER, R. D. BOYER, R. S. HENDERSON, T. E. HAMMOND and G. A. SHREVE, *Solid State Commun.* **65**, 1517 (1988).
506. K. L. MORAN, R. K. SHIBAO and H. ECKERT, *Hyperfine Interact.* **62**, 55 (1990).
507. H. ECKERT, Z. ZHANG and J. H. KENNEDY, *J. Noncryst. Solids* **107**, 271 (1989).
508. M. TENHOVER, personal communication.
509. M. TENHOVER, R. S. HENDERSON, M. A. HAZLE, D. LUKCO and R. K. GRASSELLI, *Design of New Materials*, Eds. D. L. COCKE and A. CLEARFIELD, p. 329, Plenum Publishing Corp. (1987).
510. Z. U. BORISOVA, *Glassy Semiconductors*, p. 70, Plenum Press, NY (1981).
511. Z. U. BORISOVA, B. E. KASATKIN and E. I. KIM, *Izv. Akad. Nauk SSSR, Neorg. Mater.* **9**, 822 (1973).
512. R. BLACHNIK and A. HOPPE, *J. Noncryst. Solids* **34**, 191 (1979).
513. Y. MONTEIL and H. VINCENT, *J. Inorg. Nucl. Chem.* **37**, 2053 (1975); *Z. Anorg. Allg. Chem.* **428**, 259 (1977).
514. F. HEYDER and D. LINKE, *Z. Chem.* **13**, 480 (1973).
515. Y. MONTEIL and A. VINCENT, *Can. J. Chem.* **52**, 2190 (1974).
516. E. I. KIM, A. P. CHERNOV, S. A. DEMBOVSKII and Z. U. BORISOVA, *Izv. Akad. Nauk SSSR, Neorg. Mater.* **12**, 1021 (1976).
517. D. L. PRICE, M. MISAWA, S. SUSMAN, T. I. MORRISON, G. K. SHENOY and M. GRIMSDITCH, *J. Noncryst. Solids* **66**, 443 (1984).
518. M. ARAI, R. W. JOHNSON, D. L. PRICE, S. SUSMAN, M. GAY and J. E. ENDERBY, *J. Noncryst. Solids* **83**, 80 (1986).
519. A. KUMAR, L. K. MALHOTRA and K. L. CHOPRA, *J. Noncryst. Solids* **92**, 51 (1987).
520. D. LATHROP and H. ECKERT, *J. Noncryst. Solids* **106**, 417 (1988).
521. D. LATHROP and H. ECKERT, *J. Phys. Chem.* **93**, 7895 (1989).
522. D. LATHROP and H. ECKERT, *J. Am. Chem. Soc.* **111**, 3536 (1989).
523. H. ECKERT, D. FRANKE, D. LATHROP, R. MAXWELL and M. TULLIUS, *Mater. Res. Soc. Symp. Proc.* **172**, 193 (1990).
524. D. LATHROP and H. ECKERT, *Phys. Rev. B*, **43**, 7279 (1991).
525. D. LATHROP and H. ECKERT, *J. Am. Chem. Soc.* **112**, 9017 (1990).
526. M. F. THORPE, *J. Noncryst. Solids* **76**, 109 (1985).
527. D. LATHROP, M. TULLIUS, T. TEPE and H. ECKERT, *J. Noncryst. Solids*, in press (1991).
528. T. TEPE, D. LATHROP and H. ECKERT, in preparation.

529. M. TULLIUS, D. LATHROP and H. ECKERT, *J. Phys. Chem.* **94**, 2145 (1990).
530. M. C. DEMARCQ, *Phosphorus Sulfur* **33**, 127 (1987).
531. M. C. DEMARCQ, *J. Phys. Chem.* **94**, 7330 (1990).
532. H. ECKERT, C. S. LIANG and G. D. STUCKY, *J. Phys. Chem.* **93**, 452 (1989).
533. T. BJORHOLM, *Chem. Phys. Lett.* **143**, 259 (1988).
534. T. BJORHOLM and H. JACOBSEN, *J. Am. Chem. Soc.* **113**, 27 (1991).
535. R. K. HARRIS, P. J. WILKES, P. T. WOOD and J. D. WOOLLINS, *J. Chem. Soc. Dalton Trans.* 809 (1989).
536. M. G. GIBBY, A. PINES, W. K. RHIM and J. S. WAUGH, *J. Chem. Phys.* **56**, 991 (1972).
537. M. RUBINSTEIN and P. C. TAYLOR, *Phys. Rev. B* **9**, 4258 (1974).
538. Z. M. SALEH, G. A. WILLIAMS and P. C. TAYLOR, *J. Noncryst. Solids* **114**, 58 (1989).
539. I. P. PEN'KOV and I. A. SAFIN, *Dokl. Akad. Nauk SSSR* **156**, 139 (1964).
540. Z. M. SALEH, G. A. WILLIAMS and P. C. TAYLOR, *Phys. Rev. B* **40**, 10557 (1989).
541. D. J. TREACY, S. G. GREENBAUM, U. STROM and P. C. TAYLOR, *J. Noncryst. Solids* **59/60**, 847 (1983).
542. J. H. KENNEDY, Zh. ZHANG and H. ECKERT, *J. Noncryst. Solids* **123**, 328 (1990).
543. H. ECKERT, W. MÜLLER-WARMUTH, W. HAMANN and B. KREBS, *J. Noncryst. Solids* **65**, 53 (1984).
544. D. E. HINTENLANG and P. J. BRAY, *J. Noncryst. Solids* **69**, 243 (1974).
545. M. ZAHIR, G. VILLENEUVE and R. OLAZCUAGA, *Rev. Chim. Miner.* **22**, 297 (1985).
546. Z. ZHANG, J. H. KENNEDY, J. THOMPSON, S. ANDERSON, D. LATHROP and H. ECKERT, *Appl. Phys. A* **49**, 41 (1989).
547. K. S. SUH, A. HOJJAJI, G. VILLENEUVE, M. MENETRIER and A. LEVASSEUR, *J. Noncryst. Solids* **128**, 13 (1991).
548. Z. ZHANG, J. H. KENNEDY and H. ECKERT, unpublished.
549. J. H. KENNEDY and Y. YANG, *J. Electrochem. Soc.* **133**, 2437 (1986).
550. J. H. KENNEDY and ZH. ZHANG, *J. Electrochem. Soc.* **135**, 859 (1988).
551. A. PRADEL and M. RIBES, *Solid State Ionics* **18/19**, 351 (1986).
552. H. ECKERT, ZH. ZHANG and J. H. KENNEDY, *J. Noncryst. Solids* **107**, 271 (1989).
553. H. ECKERT, J. H. KENNEDY, A. PRADEL and M. RIBES, *J. Noncryst. Solids* **113**, 287 (1989).
554. A. PRADEL, M. RIBES and H. ECKERT, to be published.
555. J. P. MALUGANI and G. ROBERT, *Solid State Ionics* **1**, 519 (1980).
556. ZH. ZHANG and J. H. KENNEDY, *Solid State Ionics* **38**, 217 (1990).
557. H. ECKERT, ZH. ZHANG and J. H. KENNEDY, *Chem. Mater.* **2**, 273 (1990).
558. J. H. KENNEDY and ZH. ZHANG, *J. Electrochem. Soc.* **136**, 2441 (1989).
559. H. ECKERT, ZH. ZHANG and J. H. KENNEDY, *Mater. Res. Soc. Symp. Proc.* **135**, 259 (1989).
560. J. H. KENNEDY, C. S. SCHAUPP, H. ECKERT and M. RIBES, *Solid State Ionics* **45**, 21 (1991).
561. D. RAVAINE and J. L. SOUQUET, *Phys. Chem. Glasses* **18**, 27 (1977).
562. (a) K. FUNKE, *Z. Phys. Chem. Neue Folge* **154**, 251 (1987).
562. (b) K. FUNKE and D. WILMER, *Europhys. Lett.* **12**, 363 (1990).
563. (a) R. KOHLRAUSCH, *Ann. Phys. (Leipzig)* **12**, 393 (1847).
563. (b) G. WILLIAMS and D. C. WATTS, *Trans. Faraday Soc.* **66**, 80 (1970).
564. P. J. BRAY, D. E. HINTENLANG, R. V. MULKERN, S. G. GREENBAUM, D. C. TRAN and M. DREXHAGE, *J. Noncryst. Solids* **56**, 27 (1983).
565. D. RAVAINE, W. G. PERERA and M. MINIER, *J. Physique C9* **43**, 407 (1982).
566. H. W. SUN, H. AOMI, R. M. REAU, J. SENEGAS and M. POULAIN, *Mater. Sci. Forum* **6**, 793 (1985).
567. J. M. REAU, J. SENEGAS, H. AOMI, P. HAGENMULLER and M. POULAIN, *J. Solid State Chem.* **60**, 159 (1985).
568. J. SENEGAS, J. M. REAU, H. AOMI, P. HAGENMULLER and M. POULAIN, *J. Noncryst. Solids* **85**, 315 (1986).
569. J. SENEGAS and S. H. PULCINELLI, *J. Fluorine Chem.* **38**, 375 (1988).
570. J. SENEGAS and S. H. PULCINELLI, *J. Fluorine Chem.* **42**, 31 (1989).
571. Y. KAWAMOTO, J. FUJIWARA and C. ICHIMURA, *J. Noncryst. Solids* **111**, 245 (1989).
572. Y. KAWAMOTO and J. FUJIWARA, *Phys. Chem. Glasses* **31**, 117 (1990).
573. V. A. VOPILOV, M. G. ISOZIMOVA, V. M. BUZNIK, V. L. BOGDANOV, V. D. KHALILEV and N. A. ARUTYUNUYAN, *Fiz. Khim. Stekla* **12**, 238 (1986).
574. V. A. VOPILOV, V. M. BUZNIK, V. L. BOGDANOV, M. A. ORLOVA and V. D. KHALILEV, *Fiz. Khim. Stekla* **11**, 610 (1985).
575. V. A. VOPILOV, V. M. BUZNIK, A. N. MATSULEV, V. L. BOGDANOV, A. K. KARAPETYAN and V. D. KHALILEV, *Fiz. Khim. Stekla* **11**, 162 (1985).
576. A. UHLHERR, D. R. MACFARLANE and T. J. BASTOW, *J. Noncryst. Solids* **123**, 42 (1990).
577. A. AVOGADRO, S. MANZINI and M. VILLA, *Fast Ion Transport in Solids*, Eds. VASHISHTA, MUNDY and SHENOY, p. 723, Elsevier (1979).
578. A. AVOGADRO, F. TABAK, M. CORTI and F. BORSA, *Phys. Rev. B* **41**, 6137 (1990).
579. S. W. MARTIN, H. J. BISCHOF, M. MALI, J. ROOS and D. BRINKMANN, *Solid State Ionics* **18/19**, 421 (1986).
580. M. VILLA, G. CHIODELLI, A. MAGISTRIS and G. LICHERI, *J. Chem. Phys.* **85**, 2392 (1986).
581. G. CHIODELLI, A. MAGISTRIS, M. VILLA and J. L. BJORKSTAM, *J. Noncryst. Solids* **51**, 143 (1982).
582. S. H. CHUNG, K. R. JEFFREY, J. R. STEVENS and L. BÖRJESSON, *Phys. Rev. B* **41**, 6154 (1990).
583. J. ROOS, D. BRINKMANN, M. MALI, A. PRADEL and M. RIBES, *Solid State Ionics* **28–30**, 710 (1988).
584. M. VILLA and G. C. FARRINGTON, *Phil. Mag. B* **56**, 147 (1987).
585. S. H. CHUNG, K. R. JEFFREY, J. R. STEVENS and L. BÖRJESSON, *Solid State Ionics* **40/41**, 279 (1990).

586. S. E. SVANSON and R. JOHANSSON, *Acta Chem. Scand.* **24**, 755 (1970).
587. W. MÜLLER-WARMUTH and E. SCHICK, *Noncryst. Solids*, Ed. G. H. FRISCHAT, p. 453, *Trans Tech. Publ.* (1977).
588. J. OLIVIER-FOURCADE, C. CAMBIE, E. PHILIPPOT and P. BERNIER, *J. Solid State Chem.* **45**, 212 (1982).
589. P. HEITJANS, B. BADER, H. J. STÖCKMANN, K. DÖRR, G. KIESE, H. ACKERMANN, P. FREILÄNDER, W. MÜLLER-WARMUTH and K. MEISE-GRESCH, *Hyperfine Interact.* **15/16**, 597 (1983).
590. P. HEITJANS, B. BADER, K. DÖRR, H. J. STÖCKMANN, G. KIESE, H. ACKERMANN, P. FREILÄNDER and W. MÜLLER-WARMUTH, *J. Physique C9* **43**, 143 (1982).
591. A. SCHIRMER, P. HEITJANS, H. ACKERMANN, B. BADER, P. FREILÄNDER and H. J. STÖCKMANN, *Solid State Ionics* **28–30**, 717 (1988).
592. J. R. HENDRICKSON and P. J. BRAY, *J. Chem. Phys.* **61**, 2754 (1974); *J. Magn. Reson.* **9**, 341 (1973). *Phys. Chem. Glasses* **13**, 43 (1972).
593. G. VILLENEUVE, P. ECHEGUT, J. M. REAU, A. LEVASSEUR and J. C. BRETHOUS, *J. Solid State Chem.* **30**, 275 (1979).
594. A. E. GEISSBERGER, F. BUCHOLTZ and P. J. BRAY, *J. Noncryst. Solids* **49**, 117 (1982).
595. T. ASAI, S. SUGIMOTO, S. KAWAI, S. OKADA and J. YAMAKI, *Mater. Res. Bull.* **24**, 75 (1989).
596. S. J. VISCO, P. SPELLANE and J. H. KENNEDY, *J. Electrochem. Soc.* **132**, 751 (1985).
597. S. J. VISCO, P. SPELLANE and J. H. KENNEDY, *J. Electrochem. Soc.* **132**, 1766 (1985).
598. J. SENEGAS and J. OLIVIER-FOURCADE, *J. Phys. Chem. Solids* **44**, 1033 (1983).
599. A. PRADEL, M. RIBES and M. MAURIN, *Solid State Ionics* **28–30**, 762 (1988).
600. M. GRÜNE, H. MEIERKORD, W. MÜLLER-WARMUTH, P. ZUM HEBEL, B. KREBS and M. WULFF, *Ber. Bunsenges Phys. Chem.* **93**, 1313 (1989).
601. H. JAIN, G. BALZER-JÖLLENBECK and O. KANERT, *J. Am. Ceram. Soc.* **68**, C24 (1985).
602. G. BALZER-JÖLLENBECK, O. KANERT, H. JAIN and K. L. NGAI, *Phys. Rev. B* **39**, 6071 (1989).
603. K. L. NGAI, J. N. MUNDY, H. JAIN, O. KANERT and G. BALZER-JÖLLENBECK, *Phys. Rev. B* **39**, 6169 (1989).
604. C. RHEE and P. J. BRAY, *Phys. Chem. Glasses* **12**, 156 (1971).
605. L. W. PANEK, G. J. EXARHOS, P. J. BRAY and W. M. RISEN, *J. Noncryst. Solids* **24**, 51 (1977).
606. H. A. RESING, *J. Chem. Phys.* **43**, 669 (1965).
607. J. L. BJORKSTAM, J. LISTERUD, M. VILLA and C. I. MASSARA, *J. Magn. Reson.* **65**, 383 (1985).
608. S. W. MARTIN, *Mater. Chem. Phys.* **23**, 225 (1989).
609. W. SCHIRMACHER and A. SCHIRMER, *Solid State Ionics* **28–30**, 134 (1988).
610. K. L. NGAI, *Solid State Ionics* **5**, 27 (1981).
611. C. A. ANGELL and S. W. MARTIN, *Mater. Res. Soc. Symp. Proc.* **135**, 73 (1989).
612. K. L. FUNKE, *Solid State Ionics* **28–30**, 100 (1988).
613. K. L. FUNKE and R. HOPPE, *ISSI Lett.* **1**, 3 (1990).
614. K. L. FUNKE, *Mater. Res. Soc. Symp. Proc.* **210**, 97 (1991).
615. K. L. FUNKE and R. HOPPE, *Solid State Ionics* **40/41**, 200 (1990).
616. G. BALZER-JÖLLENBECK, O. KANERT, J. STEINERT and H. JAIN, *Solid State Commun.* **65**, 303 (1988).
617. S. R. ELLIOTT, *Adv. Phys.* **38**, 1 (1989).
618. J. A. REIMER, P. D. MURPHY, B. C. GERSTEIN and J. C. KNIGHT, *J. Chem. Phys.* **74**, 1501 (1981).
619. F. R. JEFFREY, P. DUBOIS MURPHY and B. C. GERSTEIN, *Phys. Rev. B* **23**, 2099 (1981).
620. B. LAMOTTE, A. ROUSSEAU and A. CHENEVAS-PAULE, *J. Physique C4* **42**, 839 (1981).
621. S. HAYASHI, K. HAYAMIZU, S. YAMASAKI, A. MATSUDA and K. TANAKA, *Jpn. J. Appl. Phys.* **25**, L313 (1986).
622. N. ZUMBULYADIS, *J. Chem. Phys.* **86**, 1162 (1987).
623. S. HAYASHI, K. HAYAMIZU, S. YAMASAKI, A. MATSUDA and K. TANAKA, *J. Appl. Phys.* **60**, 1839 (1986).
624. S. HAYASHI, K. HAYAMIZU, S. YAMASAKI, A. MATSUDA and K. TANAKA, *J. Appl. Phys.* **56**, 2658 (1984).
625. S. HAYASHI, K. HAYAMIZU, S. YAMASAKI, A. MATSUDA and K. TANAKA, *Phys. Rev. B* **35**, 4581 (1987).
626. W. L. SHAO, J. SHINAR, S. MITRA, B. C. GERSTEIN, F. LI, J. FORTNER and J. S. LANNIN, *J. Noncryst. Solids* **114**, 232 (1989).
627. W. L. SHAO, J. SHINAR, B. C. GERSTEIN, F. LI and J. S. LANNIN, *Phys. Rev. B* **41**, 9491 (1990).
628. D. E. POLK, *J. Noncryst. Solids* **5**, 365 (1971).
629. D. E. POLK and D. S. BOUDREUX, *Phys. Rev. Lett.* **31**, 92 (1973).
630. P. STEINHARDT, R. ALBEN and D. WEAIRE, *J. Noncryst. Solids* **15**, 199 (1974).
631. F. WOOTEN, K. WINER and D. WEAIRE, *Phys. Rev. Lett.* **54**, 1392 (1985).
632. F. WOOTEN and D. WEAIRE, *J. Noncryst. Solids* **64**, 325 (1984).
633. J. WEICHERT, D. WEAIRE and F. WOOTEN, *J. Noncryst. Solids* **122**, 241 (1990).
634. J. A. REIMER, R. W. VAUGHAN and J. C. KNIGHTS, *Phys. Rev. Lett.* **44**, 193 (1980).
635. J. A. REIMER, R. W. VAUGHAN and J. C. KNIGHTS, *Solid State Commun.* **37**, 161 (1981).
636. J. C. KNIGHTS, R. A. LUJAN, M. P. ROSENBLUM, R. A. STREET, D. K. BIEGELSEN and J. A. REIMER, *Appl. Phys. Lett.* **38**, 331 (1981).
637. W. E. CARLOS and P. C. TAYLOR, *Phys. Rev. Lett.* **45**, 358 (1980).
638. W. E. CARLOS and P. C. TAYLOR, *Phys. Rev. B* **26**, 3605 (1982).
639. J. A. REIMER, R. W. VAUGHAN and J. C. KNIGHTS, *Phys. Rev. B* **24**, 3360 (1981).
640. W. E. CARLOS and P. C. TAYLOR, *J. Phys. Soc. Jpn* **49**, 1193 (1980).
641. W. E. CARLOS and P. C. TAYLOR, *J. Physique C4* **42**, 725 (1981).
642. F. R. JEFFREY and M. E. LOWRY, *J. Appl. Phys.* **52**, 5529 (1981).

643. M. LOWRY, F. R. JEFFREY, R. G. BARNES and D. R. TORGESON, *Solid State Commun.* **38**, 113 (1981).
644. S. UEDA, M. KUMEDA and T. SHIMIZU, *Jpn. J. Appl. Phys.* **20**, L399 (1981).
645. S. UEDA, A. CHAYAHARA, T. IMURA, U. OSAKA, M. KUMEDA and T. SHIMIZU, *Jpn. J. Appl. Phys.* **25**, 1148 (1986).
646. B. A. SCOTT, J. A. REIMER and P. A. LONGEWAY, *J. Appl. Phys.* **54**, 6853 (1983).
647. M. KUMEDA, H. KOMATSU, T. SHIMIZU, N. FUKUDA and N. KITAGAWA, *Jpn. J. Appl. Phys.* **24**, L495 (1985).
648. J. B. BOYCE and M. J. THOMPSON, *J. Noncryst. Solids* **66**, 127 (1984).
649. T. SHIMIZU, *J. Noncryst. Solids* **59/60**, 117 (1983).
650. M. KUMEDA, S. NAKANISHI and T. SHIMIZU, *Solid State Commun.* **67**, 585 (1988).
651. M. KUMEDA, S. NAKANISHI and T. SHIMIZU, *Jpn. J. Appl. Phys.* **26**, L1915 (1987).
652. J. B. BOYCE, *NATO ASI Ser., Ser. B* **136**, 101 (1986).
653. N. ZUMBULYADIS, *Phys. Rev. B* **33**, 6495 (1986).
654. K. K. GLEASON, J. BAUM, A. N. GARROWAY, A. PINES and J. A. REIMER, *Mater. Res. Soc. Symp. Proc.* **70**, 83 (1986).
655. J. BAUM, K. K. GLEASON, A. PINES, A. N. GARROWAY and J. A. REIMER, *Phys. Rev. Lett.* **56**, 1377 (1986).
656. K. K. GLEASON, M. A. PETRICH, and J. A. REIMER, *Mater. Res. Soc. Symp. Proc.* **95**, 171 (1987).
657. K. K. GLEASON, M. A. PETRICH and J. A. REIMER, *Phys. Rev. B* **36**, 3259 (1987).
658. M. A. PETRICH, K. K. GLEASON and J. A. REIMER, *Phys. Rev. B* **36**, 9722 (1987).
659. B. LAMOTTE, *Phys. Rev. Lett.* **53**, 576 (1984).
660. W. E. CARLOS, J. A. REIMER and P. C. TAYLOR, *Phys. Rev. Lett.* **54**, 1205 (1985).
661. B. LAMOTTE, *Phys. Rev. Lett.* **54**, 1206 (1985).
662. M. KUMEDA and T. SHIMIZU, *Solid State Commun.* **58**, 455 (1986).
663. J. B. BOYCE, M. STUTZMANN and S. E. READY, *J. Noncryst. Solids* **77/78**, 265 (1985).
664. J. B. BOYCE, S. E. READY, M. STUTZMANN and R. E. NORBERG, *J. Noncryst. Solids* **114**, 211 (1989).
665. J. B. BOYCE and M. STUTZMANN, *Phys. Rev. Lett.* **54**, 562 (1985).
666. D. J. LEOPOLD, J. B. BOYCE, P. A. FEDDERS and R. E. NORBERG, *Phys. Rev. B* **26**, 6053 (1982).
667. M. CONRADI and R. E. NORBERG, *Phys. Rev. B* **24**, 3385 (1981).
668. W. E. CARLOS and P. C. TAYLOR, *Phys. Rev. B* **25**, 1435 (1982).
669. J. A. REIMER, R. W. VAUGHAN and J. C. KNIGHTS, *Phys. Rev. B* **23**, 2567 (1981).
670. D. J. LEOPOLD, B. S. COUGHLAN, P. A. FEDDERS, R. E. NORBERG, J. B. BOYCE and J. C. KNIGHTS, *J. Noncryst. Solids* **66**, 121 (1984).
671. E. D. VANDERHEIDEN, W. D. OHLSEN and P. C. TAYLOR, *J. Noncryst. Solids* **66**, 115 (1984).
672. P. A. FEDDERS, R. FISCH, and R. E. NORBERG, *Phys. Rev. B* **31**, 6887 (1985).
673. P. A. FEDDERS, *Phys. Rev. B* **36**, 2107 (1987).
674. S. LEE, *Phys. Rev. B* **34**, 78 (1986).
675. D. J. LEOPOLD, P. A. FEDDERS, R. E. NORBERG, J. B. BOYCE and J. C. KNIGHTS, *Phys. Rev. B* **31**, 5642 (1985).
676. S. E. READY, J. B. BOYCE and C. C. TSAI, *Mater. Res. Soc. Symp. Proc.* **118**, 103 (1988).
677. J. B. BOYCE, M. STUTZMANN and S. E. READY, *Phys. Rev. B* **32**, 6062 (1985).
678. V. P. BORK, P. A. FEDDERS, R. E. NORBERG, D. J. LEOPOLD, K. D. MACKENZIE and W. PAUL, *J. Noncryst. Solids* **77/78**, 715 (1985).
679. V. P. BORK, P. A. FEDDERS, R. E. NORBERG, D. J. LEOPOLD, K. D. MACKENZIE and W. PAUL, *NATO ASI Ser., Ser. B* **136**, 101 (1986).
680. D. J. LEOPOLD, P. A. FEDDERS, R. E. NORBERG, J. B. BOYCE and J. C. KNIGHTS, *Bull. Magn. Reson.* **5**, 129 (1983).
681. V. P. BORK, P. A. FEDDERS, D. J. LEOPOLD and R. E. NORBERG, *Mater. Res. Soc. Symp. Proc.* **70**, 89 (1986).
682. P. A. FEDDERS, V. P. BORK, D. J. LEOPOLD, R. E. NORBERG, J. B. BOYCE and J. C. KNIGHTS, *J. Noncryst. Solids* **97/98**, 357 (1987).
683. V. P. BORK, P. A. FEDDERS, D. J. LEOPOLD, R. E. NORBERG, J. B. BOYCE and J. C. KNIGHTS, *Phys. Rev. B* **36**, 9351 (1987).
684. P. SANTOS-FILHO, J. BODART, P. A. FEDDERS and R. E. NORBERG, *Solar Cells* **27**, 385 (1989).
685. P. SANTOS-FILHO, M. P. VOLZ, R. L. COREY, Y. W. KIM, P. A. FEDDERS, R. E. NORBERG, W. TURNER and W. PAUL, *J. Noncryst. Solids* **114**, 235 (1989).
686. M. STUTZMANN, R. A. STREET, C. C. TSAI, J. B. BOYCE, and S. E. READY, *J. Appl. Phys.* **66**, 569 (1989).
687. M. P. VOLZ, P. A. FEDDERS and R. E. NORBERG, *J. Noncryst. Solids* **114**, 546 (1989).
688. M. KUMEDA, Y. TSUJIMURA, Y. YONEZAWA, A. MORIMOTO and T. SHIMIZU, *Solid State Commun.* **55**, 409 (1985).
689. J. A. REIMER, B. A. SCOTT, D. J. WOLFORD and J. NIJS, *Appl. Phys. Lett.* **46**, 369 (1985).
690. W. A. TURNER, S. J. JONES, D. PANG, B. F. BATEMAN, J. H. CHEN, Y. M. LI, F. C. MARCQUES, A. E. WETSEL, P. WICKBOLDT, W. PAUL, J. BODART, R. E. NORBERG, I. EL ZAWAWI and M. L. THEYE, *J. Appl. Phys.* **67**, 7430 (1990).
691. V. P. BORK, P. A. FEDDERS, R. E. NORBERG, D. J. LEOPOLD, K. D. MACKENZIE and W. PAUL, *Mater. Res. Soc. Symp. Proc.* **70**, 307 (1986).
692. S. UEDA, K. NAKAZAWA, M. KUMEDA and T. SHIMIZU, *Solid State Commun.* **42**, 261 (1982).
693. S. UEDA, M. KUMEDA and T. SHIMIZU, *J. Physique C4* **42**, 729 (1981).
694. M. KUMEDA, Y. YONEZAWA and T. SHIMIZU, *Jpn. J. Appl. Phys.* **23**, L540 (1984).

695. T. SHIMIZU, K. NAKAZAWA, M. KUMEDA and S. UEDA, *Jpn. J. Appl. Phys.* **21**, L351 (1982).
696. T. SHIMIZU, M. KUMEDA, H. KOMATSU and Y. YONEZAWA, *J. Noncryst. Solids* **77/78**, 719 (1985).
697. M. KUMEDA, Y. TAKAHASI and T. SHIMIZU, *Phys. Rev. B* **36**, 2713 (1987).
698. S. UEDA, M. KUMEDA and T. SHIMIZU, *Jpn. J. Appl. Phys.* **20**, L399 (1981).
699. M. A. PETRICH and J. A. REIMER, *Mater. Res. Soc. Symp. Proc.* **95**, 329 (1987).
700. K. NAKAZAWA, S. UEDA, M. KUMEDA, A. MORIMOTO and T. SHIMIZU, *Jpn. J. Appl. Phys.* **21**, L176 (1982).
701. M. A. PETRICH, K. K. GLEASON and J. A. REIMER, *Phys. Rev. B* **36**, 9722 (1987).
702. K. YAMAMOTO, Y. ICHIKAWA, N. FUKADA, T. NAKAYAMA and Y. TAWADA, *Thin Solid Films* **173**, 253 (1989).
703. M. KUMEDA, S. NAKANISHI and T. SHIMIZU, *J. Noncryst. Solids* **114**, 516 (1989).
704. J. A. REIMER, R. W. VAUGHAN, J. C. KNIGHTS and R. A. LUJAN, *J. Vac. Sci. Techn.* **19**, 53 (1981).
705. S. KAPLAN and A. DILKS, *Thin Solid Films* **84**, 419 (1981).
706. S. KAPLAN, F. JANSEN and M. MACHONKIN, *Appl. Phys. Lett.* **47**, 750 (1980).
707. K. YAMAMOTO, Y. ICHIKAWA, T. NAKAYAMA and T. TAWADA, *Jpn. J. Appl. Phys.* **27**, 1415 (1988).
708. R. H. JARMAN, G. J. RAY, R. W. STANDLEY and G. W. ZAJAC, *Appl. Phys. Lett.* **49**, 1065 (1986).
709. R. H. JARMAN and G. J. RAY, *J. Chem. Soc., Chem. Commun.* 1153 (1985).
710. F. JANSEN, M. MACHONKIN, S. KAPLAN and S. HARK, *J. Vac. Sci. Techn.* **A3**, 605 (1985).
711. A. GRILL, B. S. MEYERSON, V. V. PATEL, J. A. REIMER and M. PETRICH, *J. Appl. Phys.* **61**, 2874 (1987).
712. K. C. BUSTILLO, M. A. PETRICH and J. A. REIMER, *Chem. Mater.* **2**, 202 (1990).
713. W. E. SPEAR and P. G. LECOMBER, *Solid State Commun.* **17**, 1193 (1975).
714. J. A. REIMER and T. M. DUNCAN, *Phys. Rev. B* **27**, 4895 (1983).
715. M. M. CRUTCHFIELD, C. H. DUNGAN, J. H. LETCHER, V. MARK and J. R. VAN WAZER, *Topics in Phosphorus Chemistry*, Eds. M. GRAYSON and E. J. GRIFFITH, Vol. 5, Wiley, New York (1967).
716. D. FRANKE, R. S. MAXWELL and H. ECKERT, *Solid State NMR*, in press.
717. M. J. MCCARTHY, B. S. MEYERSON and J. A. REIMER, *J. Appl. Phys.* **62**, 3665 (1987).
718. S. HAYASHI, K. HAYAMIZU, S. YAMASAKI, A. MATSUDA and K. TANAKA, *Jpn. J. Appl. Phys.* **26**, L2041 (1987).
719. S. HAYASHI, K. HAYAMIZU, S. YAMASAKA, A. MATSUDA and K. TANAKA, *Phys. Rev. B* **38**, 31 (1988).
720. J. B. BOYCE and S. E. READY, *Phys. Rev. B* **38**, 11008 (1988)
721. S. E. READY, J. B. BOYCE and C. C. TSAI, *AIP Conf. Proc.* **157**, 229 (1987).
722. J. B. BOYCE, S. E. READY and C. C. TSAI, *J. Noncryst. Solids* **97/98**, 345 (1987).
723. S. E. READY and J. B. BOYCE, *Mater. Res. Soc. Symp. Proc.* **95**, 153 (1987).
724. J. A. REIMER, M. J. MCCARTHY, K. K. GLEASON and P. W. MORRISON, Jr, *Mater. Res. Soc. Symp. Proc.* **95**, 209 (1987).
725. M. J. MCCARTHY and J. A. REIMER, *Phys. Rev. B* **36**, 4525 (1987).
726. S. G. GREENBAUM, W. E. CARLOS and P. C. TAYLOR, *Solid State Commun.* **43**, 663 (1982).
727. S. G. GREENBAUM, W. E. CARLOS and P. C. TAYLOR, *Physica* **117/118B**, 886 (1983).
728. M. KUMEDA, S. NAKANISHI and T. SHIMIZU, *Solid State Commun.* **67**, 585 (1988).
729. M. A. PETRICH, R. E. LIVENGOOD, J. A. REIMER and D. W. HESS, *Mater. Res. Soc. Symp. Proc.* **70**, 337 (1986).
730. M. A. PETRICH, R. E. LIVENGOOD, D. W. HESS and J. A. REIMER, *Mater. Res. Soc. Symp. Proc.* **118**, 67 (1988).
731. R. E. LIVENGOOD, M. A. PETRICH, D. W. HESS and J. A. REIMER, *J. Appl. Phys.* **63**, 2651 (1988).
732. T. M. DUNCAN, R. A. LEVY, P. K. GALLAGHER and M. W. WALSH, Jr, *J. Appl. Phys.* **64**, 2990 (1988).
733. G. E. JELLISON, Jr, *Solid State Commun.* **30**, 481 (1979).
734. G. E. JELLISON, Jr, G. L. PETERSEN and P. C. TAYLOR, *Phys. Rev. Lett.* **42**, 1413 (1979).
735. S. G. GREENBAUM, R. A. MARINO, K. J. ADAMIC and C. CASE, *J. Noncryst. Solids* **77/78**, 1285 (1985).
736. S. G. GREENBAUM, D. J. TREACY, B. V. SHANABROOK, J. COMAS and S. G. BISHOP, *J. Noncryst. Solids* **66**, 133 (1984).
737. A. A. VAIPOLIN, E. O. OSMANOV and YU. RUD, *Sov. Phys. Solid State* **7**, 1833 (1966).
738. N. A. GORYUNOVA, G. S. KUZMENKO and E. O. OSMANOV, *Mater. Sci. Eng.* **7**, 54 (1971).
739. H. PFISTER, *Acta Cryst.* **11**, 221 (1958).
740. D. FRANKE, R. MAXWELL, D. LATHROP and H. ECKERT, *J. Am. Chem. Soc.* **13**, 4822 (1991).
741. D. FRANKE, K. BANKS and H. ECKERT, *Phys. Rev. B*, in press (1992).
742. D. FRANKE and H. ECKERT, *J. Phys. Chem.* **95**, 331 (1991).
743. D. D. THORNBURG, *Thin Solid Films* **45**, 95 (1977).
744. (a) K. S. HONG, Y. BERTA and R. F. SPEYER, *J. Am. Ceram. Soc.* **73**, 1351 (1990); (b). S. MAHADEVAN and A. GIRIDHAR, *J. Noncryst. Solids* **128**, 8 (1991).
745. P. PANISSOD, *J. Phys. Colloq. C8* **46**, 241 (1985).
746. P. PANISSOD, *Helv. Phys. Acta* **58**, 60 (1985).
747. P. PANISSOD, D. ALIAGA GUERRA, A. AMAMOU, J. DURAND, W. L. JOHNSON, W. L. CARTER and S. J. POON, *Phys. Rev. Lett.* **44**, 1465 (1980).
748. R. C. BOWMAN, Jr and A. J. MAELAND, *Phys. Rev. B* **24**, 2328 (1981).
749. M. P. VOLZ, V. P. BORK, P. A. FEDDERS, R. E. NORBERG, R. C. BOWMAN Jr, A. J. MAELAND and J. S. CANTRELL, *Mater. Sci. Eng.* **97**, 427 (1988).
750. M. P. VOLZ, V. P. BORK, P. A. FEDDERS, R. E. NORBERG, R. C. BOWMAN, Jr, A. J. MAELAND and J. S. CANTRELL, *Mater. Res. Soc. Symp. Proc.* **80**, 187 (1987).
751. R. C. BOWMAN, Jr, A. J. MAELAND and W. K. RHIM, *Phys. Rev. B* **26**, 6362 (1982).

752. V. P. BORK, P. A. FEDDERS, R. E. NORBERG, R. C. BOWMAN, Jr and E. L. VENTURINI, *NATO ASI Ser. B* **136**, 236 (1986).
753. R. C. BOWMAN, Jr, A. ATTALLA, A. J. MAELAND and W. L. JOHNSON, *Solid State Commun.* **47**, 779 (1983).
754. R. C. BOWMAN, Jr, M. J. ROSKER and W. L. JOHNSON, *J. Noncryst. Solids* **53**, 105 (1982).
755. R. C. BOWMAN, Jr, W. L. JOHNSON, A. J. MAELAND and W. K. RHIM, *Phys. Lett.* **94A**, 181 (1983).
756. R. C. BOWMAN, Jr, J. S. CANTRELL, K. SAMWER, J. TEBBE, E. L. VENTURINI and J. J. RUSH, *Phys. Rev. B* **37**, 8575 (1988).
757. H. K. SCHONE, E. F. W. SEYMOUR and G. A. STYLES, *J. Physique Coll. C8* **46**, 675 (1985).
758. I. FURO, I. BAKONYI, K. TOMPA, A. LOPVAS, I. HEINMAA, M. ALLA, E. LIPPMAA and H. SCHONE, *Mater. Sci. Eng.* **99**, 305 (1988).
759. H. E. SCHONE, H. C. HOKE, A. JOHNSON, I. BAKONYI, K. TOMPA and A. LOVAS, *Mater. Sci. Eng.* **97**, 433 (1988).
760. V. S. POKATILOV, *Fiz. Metal Metalloved.* **60**, 1160 (1985).
761. J. C. FORD, J. I. BUDNICK, W. A. HINES and R. HASEGAWA, *J. Appl. Phys.* **55**, 2286 (1984).
762. V. S. POKATILOV, *Sov. Phys. Doklady.* **29**, 234 (1984).
763. ZHAO JIAN-GAO, SHEN BAO-GEN, ZHAN WHEN-SHAN and CHEM JIN-CHANG, *J. Magn. Magn. Mater.* **50**, 119 (1985).
764. (a) V. S. POKATILOV, *Fiz. Metal. Metalloved.* **57**, 723 (1984); (b). V. S. POKATILOV, N. B. DYAKOVNOVA and A. N. MINCHEV, *Metallofiz.* **12**, 117 (1990).
765. T. V. DOLIDZE, A. F. SHEVAKIN and G. V. TSAGAREYSHVILI, *Fiz. Metall. Metalloved.* **67**, 423 (1989).
766. Y. D. ZHANG, J. I. BUDNICK, J. C. FORD, W. A. HINES, F. H. SANCHEZ and R. HASEGAWA, *J. Appl. Phys.* **61**, 3231 (1987).
767. F. H. SANCHEZ, Y. D. ZHANG and J. I. BUDNICK, *Phys. Rev. B* **38**, 8508 (1988).
768. J. FUSY and P. PAREJA, *J. Noncryst. Solids* **104**, 153 (1988).
769. L. RESSLER, B. BORGMEIER, K. ERDMANN and M. ROSENBERG, *Hyperfine Interact.* **51**, 1031 (1989).
770. K. RAJ, J. DURAND, J. I. BUDNICK, C. C. TSUEI and S. SKALSKI, *Solid State Commun.* **24**, 189 (1977).
771. J. DURAND, B. LEMIUS, R. HASEGAWA, D. ALIAGA-GUERRA and P. PANISSOD, *J. Magn. Magn. Mater.* **15–18**, 1373 (1980).
772. P. PANISSOD, A. QUACHAOU, J. DURAND and R. HASEGAWA, *Nucl. Instrum. Methods* **199**, 231 (1982).
773. W. BOËHNER, H. LUETGEMEIER and W. ZINN, *J. Magn. Magn. Mater.* **62**, 152 (1986).
774. M. MISAWA, Y. TANAKA, H. NAGAI and A. TSUJIMURA, *J. Phys. Colloq. C8* **49**, 1373 (1988).
775. M. MISAWA, Y. TANAKA, J. HAGAI and A. TSUJIMURA, *J. Noncryst. Solids* **117/118**, 344 (1990).
776. E. JEDRYKA, F. NESTERUK, M. WOJCIK and P. DUAHJ, *Acta Phys. Pol.* **A72**, 169 (1987).
777. J. PAVLOVSKY, M. ROTTER, B. SEDLAK, L. LESTAK, M. BARTOS, I. PROCHAZKA and M. FINGER, *Hyperfine Interact.* **22**, 181 (1985).
778. V. V. KOTOV, V. V. POLOTNJUK, A. M. SHALAEV and V. M. SHKAPA, *Hyperfine Interact.* **59**, 305 (1990).
779. J. C. FORD, W. A. HINES, J. I. BUDNICK, A. PAOLUZI, D. M. PEASE, L. T. KABACOFF and C. U. MODZELEWSKI, *J. Appl. Phys.* **53**, 2288 (1982).
780. R. KRISHNAN, K. LEDANG, P. VEILLET and V. R. V. RAMANAN, *J. Appl. Phys.* **57**, 1394 (1985).
781. R. KRISHNAN, K. LEDANG, V. R. V. RAMANAN and P. VEILLET, *J. Magn. Magn. Mater.* **54–57**, 263 (1986).
782. R. S. ISKHAKOV, G. I. FISH, V. K. MAL'TSEV and R. G. KHLEBOPROS, *Fiz. Metall. Metalloved.* **58**, 1214 (1984).
783. V. K. MAL'TSEV, G. I. FISH and V. I. TSIFRINOVICH, *Fiz. Metall. Metalloved.* **52**, 439 (1981).
784. V. K. MAL'TSEV, G. I. FISH and V. I. TSIFRINOVICH, *Sov. Phys. Solid State* **23**, 667 (1981).
785. H. LÜTGEMEIER, M. W. PIEPER and G. DIETZ, *J. Magn. Magn. Mater.* **41**, 145 (1984).
786. K. RAJ, J. DURAND, J. I. BUDNICK and S. SKALSKI, *J. Appl. Phys.* **49**, 1671 (1978).
787. I. BAKONYI, P. PANISSOD, J. DURAND and R. HASEGAWA, *J. Noncryst. Solids* **61/62**, 1189 (1984).
788. I. BAKONYI, P. PANISSOD and R. HASEGAWA, *J. Appl. Phys.* **53**, 7771 (1982).
789. P. PANISSOD, I. BAKONYI and R. HASEGAWA, *J. Magn. Magn. Mater.* **31–34**, 1523 (1983).
790. P. PANISSOD, I. BAKONYI and R. HASEGAWA, *Phys. Rev. B* **28**, 2374 (1983).
791. I. BAKONYI, L. K. VARGA, A. LOVAS, E. TOTH-KADAR and A. SOLYOM, *J. Magn. Magn. Mater.* **50**, 111 (1985).
792. L. H. BENNETT, H. E. SCHONE and P. GUSTAFSON, *Phys. Rev. B* **18**, 2027 (1978).
793. W. A. HINES, C. U. MODZELEWSKI, R. N. PAOLINO and R. HASEGAWA, *Solid State Commun.* **39**, 699 (1981).
794. I. BAKONYI, L. TAKACS and K. TOMPA, *Phys. Status Solidi B* **103**, 489 (1981).
795. I. BAKONYI, H. EBERT, W. SOCHER, J. VOITLÄNDER, F. FURA, P. BANKI, A. LOVAS and U. MIZUTANI, *Mater. Sci. Eng.* **99**, 301 (1988).
796. R. HASEGAWA, W. A. HINES, L. E. KABACOFF and P. DUWEZ, *Solid State Commun.* **20**, 1035 (1976).
797. W. A. HINES, K. GLOVER, W. G. CLARK, L. T. KABACOFF, C. U. MODZELEWSKI, R. HASEGAWA and P. DUWEZ, *Phys. Rev. B* **21**, 3771 (1980).
798. I. BAKONYI, H. EBERT, J. VOITLÄNDER, K. TOMPA, A. LOVAS, G. KONCZOS, P. BANKI and H. E. SCHONE, *J. Appl. Phys.* **61**, 3664 (1987).
799. W. A. HINES, L. T. KABACOFF, R. HASEGAWA and P. DUWEZ, *J. Appl. Phys.* **49**, 1724 (1978).
800. W. A. HINES, C. U. MODZELEWSKI, R. N. PAOLINO and H. S. CHEN, *J. Appl. Phys.* **52**, 1814 (1981).
801. I. BAKONYI, P. PANISSOD and K. TOMPA, *Phys. Status Solidi B* **111**, 59 (1982).
802. D. S. LASHMORE, L. H. BENNETT, H. E. SCHONE, P. GUSTAFSON and R. E. WATSON, *Phys. Rev. Lett.* **48**, 1760 (1982).
803. D. E. POLK, *Scr. Metall.* **4**, 117 (1970).

804. P. H. GASKELL, *J. Noncryst. Solids* **32**, 207 (1979).
805. D. L. VANDERHART, H. S. GUTOWSKY and T. C. FARRAR, *J. Am. Chem. Soc.* **89**, 5056 (1967).
806. G. M. SHELDRICK, *J. Chem. Soc., Chem. Commun.* 751 (1967).
807. I. BAKONYI, P. PANISSOD, M. MILJAK and E. BABIC, *J. Magn. Magn. Mater.* **58**, 97 (1986).
808. D. ALIAGA GUERRA, P. PANISSOD and J. DURAND, *Solid State Commun.* **28**, 745 (1978).
809. I. BAKONYI, P. BANKI, K. TOMPA, H. EBERT, W. SOCHER and J. VOITLÄNDER, *Hyperfine Interact.* **51**, 1019 (1989).
810. A. AMAMOU, D. ALIAGA GUERRA, P. PANISSOD, G. KRILL and R. KUENTZLER, *J. Phys. Colloq. C8* **41**, 396 (1980).
811. K. KAMBE and J. F. OLLOM, *J. Phys. Soc. Jpn.* **11**, 50 (1956).
812. I. BAKONYI, K. TOMPA, E. TOTH-KADAR and A. LOVAS, *Magn. Reson. Relat. Phenom., 20th Congr. Ampere*, Eds. E. KUNDLA, E. LIPPMAA and T. SALUVERE, p. 347, Springer-Verlag, Berlin (1979).
813. K. B. VLASOV, V. I. TIMOSHCHUK and V. V. SERIKOV, *Fiz. Metal. Metalloved.* **67**, 712 (1989).
814. A. QUACHAOU, P. PANISSOD and J. DURAND, *J. Magn. Magn. Mater.* **31–34**, 1525 (1983).
815. R. KRISHNAN, K. LEDANG and P. VEILLET, *J. Appl. Phys.* **63**, 2992 (1988).
816. M. TRHLIK, B. SEDLAK, S. KAPUSTA, P. CIZEK, M. FINGER, J. KONICEK, E. KISDI-KOSZO, A. LOVAS, M. VOBECKY and J. KOVAC, *Hyperfine Ineract.* **50**, 793 (1989).
817. (a) V. S. POKATILOV, *Metallofiz.* **12**, 121 (1990); (b). V. S. POKATILOV, *Dokl. Akad. Nauk SSSR* **290**, 345 (1986).
818. V. S. POKATILOV, YU, A. GRATSIANOV and B. N. KULAGIN, *Dokl. Akad. Nauk SSSR* **251**, 92 (1980).
819. J. M. FRIEDT, M. MAURER, J. P. SANCHEZ, A. BERRADA, A. QUACHAOU, P. PANISSOD and J. DURAND, *J. Phys. Colloq. C8* **41**, 638 (1980).
820. W. A. HINES, P. MILLER, A. PAOLUZI, C. L. TSAI and B. C. GIESSEN, *J. Appl. Phys.* **53**, 7789 (1982).
821. W. A. HINES, A. PAOLUSI, J. I. BUDNICK, W. G. CLARK and C. L. TSAI, *J. Noncryst. Solids* **61/62**, 1255 (1984).
822. J. GOEBBELS, K. LÜDERS, H. C. FREYHARDT and J. REICHELT, *Physica* **108B**, 1223 (1981).
823. H. C. FREYHARDT, J. GOEBBELS, K. LÜDERS and J. REICHELT, *Phys. Status Solidi B* **102**, K137 (1980).
824. J. GOEBBELS, K. LÜDERS, H. C. FREYHARDT and J. REICHELT, *Nucl. Instrum. Methods.* **199**, 203 (1982).
825. I. BAKONYI, K. S. HAN and H. E. SCHONE, *Phys. Status Solidi B* **131**, 249 (1985).
826. (a) H. J. EIFERT, B. ELSCHNER and K. H. J. BUSCHOW, *Phys. Rev. B* **25**, 7441 (1982); (b). B. A. ALEKSASHIN, S. V. VERKHOVSKII, K. N. MIKHALEV and K. A. OKULOVA, *Fiz. Metall. Metalloved.* **68**, 408 (1989).
827. H. LERCHNER and M. ROSENBERG, *Hyperfine Interact.* **39**, 51 (1988).
828. B. P. VOZNYUK, R. GONTARZ, J. DUBOWNIK, YU. V. KUDRYAVTSEV and N. A. LESNIK, *Sov. Phys. Solid State* **32**, 409 (1990).
829. J. DUBOWNIK, YU. V. KUDRYAVTSEV and R. GONTARZ, *Acta Phys. Pol.* **A76**, 331 (1989).
830. K. LEDANG, P. VEILLET, R. KRISHNAN and G. SURAN, *J. Magn. Magn. Mater.* **15–18**, 1399 (1980).
831. K. LEDANG, P. VEILLET, H. SAKAKIMA and R. KRISHNAN, *J. Physique Colloq. C8* **49**, 1713 (1988).
832. H. NABIL, M. PIECUCH, J. DURAND and G. MARCHAL, *J. Phys. Colloq. C8* **46**, 229 (1985).